

A KINETIC STUDY OF LABILE
METAL COMPLEXES -
A MODEL ENZYME SYSTEM

by

George R. Cayley

A thesis submitted in part fulfilment of
the requirements for the degree of
Doctor of Philosophy

University Chemical Laboratory,
Canterbury, 1969-72.

ACKNOWLEDGMENTS

I should like to thank my Supervisor, Dr. David Hague, for his guidance, encouragement and helpful criticism during the last three years.

I should also like to express my thanks to all the members of the "Fast Reactions" research group, in particular Dr. Brian Robinson and Mr. Stephen Martin for their helpful criticism, and to Dr. J.A. Creighton and Dr. J.H.S. Green of the National Physical Laboratory, Teddington for use of the laser Raman spectrometers.

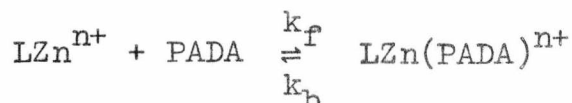
I am grateful to the Science Research Council for the award of a Studentship during the period 1969-72.

Finally, I should like to thank the technical and secretarial staff at the Chemical Laboratories, in particular Mrs. Joanna Teverson for the excellent typing and printing of this thesis.

ABSTRACT

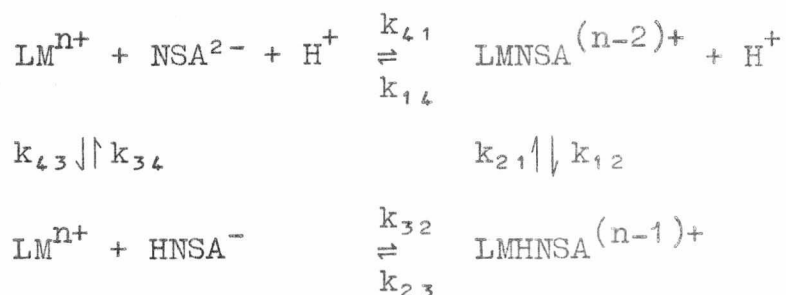
The mixed ligand (ternary) complexes considered in this thesis are intended to represent an enzyme-metal-substrate system. Both zinc(II) and magnesium(II) occur widely in hydrolytic enzymes and in these enzymes ternary complex formation is often important. In this work an attempt has been made to compare the kinetics of ternary complex formation for magnesium and zinc and to investigate the modifying nature of bound ligands on the kinetics of complex formation.

The following reactions have been investigated in aqueous solution:



where PADA is the neutral bidentate ligand pyridine-2-azo-p-dimethylaniline and L is one of the following ligands: diethylenetriamine (dien), triethylenetetramine (trien), 2,2',2'' triaminotriethylamine (tren), nitrilotriacetate (NTA^{3-}), cystein (cyst^{2-}), iminodiacetate (IDA^{2-}), ethylenediamine-diacetate (EDDA^{2-}) and tripolyphosphate (TP^{5-}). The reaction between aquo zinc and PADA has also been investigated. The reaction between 5-nitrosalicylic acid (NSA) and the ZnL complexes where L represents uramil NN diacetate (UDA^{3-}) and N,N'-bis(2-aminoethyl)-1,3-propanediamine(2-3-2 tet) and the ligands used for the PADA work except cysteine have been investigated. No evidence for ternary complex formation was found for the reaction between Zntren^{2+} and PADA or NSA. The reactions of aquomagnesium, magnesium-NTA, -UDA, -adenosine-5'-triphosphate (ATP^{2-}) and -TP with NSA have also been investigated.

The kinetics of the reaction of NSA with metal ions are consistent with a two path mechanism involving the addition of the metal species to either the NSA dianion or the mono-protonated species.



The temperature-jump relaxation method was used to measure the formation and dissociation rate constants over a range of temperature, and the activation enthalpies (ΔH^\ddagger) and entropies (ΔS^\ddagger) associated with these rate constants have been determined.

The pKs of NSA have been determined spectrophotometrically as have the stability constants of LZn(PADA) and LM(NSA) for the majority of the above systems.

In general, the formation rate constants and the associated activation parameters for the magnesium systems are consistent with a diffusion-controlled pre-equilibrium step involving the formation of an outer sphere complex and the rate limiting dissociation of a water molecule from the inner coordination sphere of the metal. The data for the zinc systems are not consistent with such a mechanism. Here the rate at which the ligand enters the inner-sphere of the metal and the rate of closure of the chelate ring are thought to be important. The results are discussed in terms of the number and types of group bound to the metal in the ligand, L, and hence the stereochemistry of the ML complex.

The stereochemistry of a number of zinc amines has been investigated using an empirical correlation between the zinc-nitrogen stretching frequency and the coordination number. The frequency of the principal Zn-N stretching mode at about 450 cm^{-1} , as determined by the laser Raman method, is reported for complexes of zinc containing the ligands ethylenediamine, diethylenetriamine, triethylenetetramine, 2,2',2''-triaminotriethylamine, tris(2-dimethyl(aminoethyl)-amine, N,N'-dimethylethylenediamine and N,N'-bis(2-aminoethyl)-1,3-propanediamine(2-3-2 tet). The correlation between the frequency of the Zn-N stretching mode seems to be independent of the phase, the nature of the other groups in the inner coordination sphere of the metal and the other groups bound to the coordinating nitrogen.

It has been suggested that the reason why Co(II) can be substituted into a number of Zn(II) metalloenzymes without complete loss of activity is due to the ability of Co(II) like Zn(II) to adopt a number of different configurations of its inner coordination sphere. Although no concrete conclusions may be drawn from a comparison of the kinetics of ternary complex formation of Co(II) and Zn(II) species it is interesting to note the similar pattern found for the formation rate constants of Co(II) and Zn(II) species with PADA.

CONTENTS

	<u>Page</u>
<u>CHAPTER 1. Introduction.</u>	
1.1 The role of metal ions in enzyme systems.	1
1.2 Mechanisms of metal complex formation.	7
1.3 Measurement of fast reactions.	13
1.4 Choice of a temperature-jump system.	17
<u>CHAPTER 2. Apparatus and general experimental procedures.</u>	
2.1 Introduction.	20
2.2 Chemicals.	20
2.3 Purification of chemicals and preparation of stock solutions.	24
2.4 Temperature-jump apparatus.	27
2.5 Calibration of temperature rise in T-jump cell.	31
2.6 pH measurement.	35
2.7 Spectrophotometers.	36
2.8 Thermostatting.	36
2.9 General experimental procedure.	36
2.10 Treatment of data.	39
<u>CHAPTER 3. The coordination number of Zinc.</u>	
3.1 Introduction.	41
3.2 Laser Raman Spectroscopy.	
3.2.1. Introduction.	43
3.2.2. Apparatus and Experimental details.	44
3.3 Conductivity measurements.	55
3.4 Thermodynamics of metal complex formation.	55
3.5 The stereochemistry of Zinc-ammines.	
3.5.1. Zinc tren.	60
3.5.2. Zinc(en)n.	61
3.5.3. Zinc dien.	62
3.5.4. Zinc trien.	65
3.5.5. Zn 2,3,2-tet.	66

	<u>Page</u>	
3.6	The stereochemistry of oxygen containing Zinc complexes.	
3.6.1.	Zinc nitrilotriacetate.	67
3.6.2.	Zinc iminodiacetate.	69
3.6.3.	Zinc N,N'ethylenediaminediacetate.	69
3.6.4.	Zinc cysteine.	70
3.6.5.	Zinc tripolyphosphate.	70
<u>CHAPTER 4.</u>	<u>Equilibrium and kinetic studies of the Zinc(II) PADA system.</u>	
4.1	Introduction.	72
4.2	Spectroscopic determination of stability constants.	73
4.2.1.	Derivation of optical density expression.	73
4.2.2.	Experimental conditions.	74
4.2.3.	Analysis of data.	76
4.2.4.	Index to plots.	76
4.2.5.	Results.	76
4.3	Kinetic studies.	86
4.3.1.	Experimental conditions.	86
4.3.2.	Results.	86
4.3.3.	Index to plots.	87
4.3.4.	Tables of results.	87
4.4	Discussion.	107
<u>CHAPTER 5.</u>	<u>Complex formation and dissociation involving Mg(II) and 5-nitrosalicylic acid.</u>	
5.1	Introduction.	110
5.2	Determination of K_1 .	112
5.3	Determination of K_2 .	
5.4	Stability constants of Magnesium-NSA complexes.	
5.4.1.	Determination of K_3 at 25°C	119
5.4.2.	Conditions used.	121
5.4.3.	Results.	121
5.5	Choice of conditions for the kinetics.	
5.5.1.	Ligand : metal ratio.	125
5.5.2.	Choice of buffer.	125
5.5.3.	Choice of metal concentrations and pH range.	126

	<u>Page</u>
5.6	Experimental data. 127
5.7	Interpretation of data. 127
5.7.1.	Proposed mechanism. 127
5.7.2.	Derivation of the relaxation expression for the proposed mechanism. 141
5.7.3.	Calculation of rate constants. 143
5.8	Results. 144
5.9	Preliminary investigation of the reaction between the aquo magnesium ion and 8-hydroxyquinoline-5-sulphonic acid (OXS). 149
5.9.1.	pK_1 of OXS at 25°C. 149
5.9.2.	Kinetics at 25°C. 149
5.10	Discussion. 150
<u>CHAPTER 6.</u>	<u>Complex formation and dissociation involving Zn(II) species and 5-nitrosalicylic acid.</u>
6.1	Introduction. 155
6.2	Stability constants of Zinc NSA complexes. 155
6.2.1.	Determination of K_3 at 25°C. 155
6.2.2.	Conditions used. 156
6.2.3.	Results. 157
6.3	Kinetics of the Zn(II) species with NSA. 157
6.3.1.	Choice of conditions. 157
6.3.2.	Choice of buffer. 166
6.4	Kinetic data. 170
6.5	Results. 170
6.6	Discussion. 201
<u>CHAPTER 7.</u>	<u>General Discussion.</u>
7.1	Outer-sphere complex formation. 205
7.2	Hydroxy complexes of zinc. 206
7.3	Comparison of the kinetic data for zinc and magnesium. 210
7.4	Comparison of Zinc(II) with the divalent metal ions of the first transition metal series. 212

	<u>Page</u>
<u>APPENDIX 1.</u> Computer Program GRC1. "Equilibrium concentrations for ZnL systems".	215
<u>APPENDIX 2.</u> Computer Program GRC4. "Iterative calculation of K from spectrophotometric data".	217
<u>APPENDIX 3.</u> Computer Program GRC2. "Least squares for kinetic data".	220
<u>APPENDIX 4.</u> Determination of K_3 for M-NSA systems.	222
<u>APPENDIX 5.</u> pK determination from two solutions.	223
<u>APPENDIX 6.</u> Optical density expression for the stability constant of $[ZntetOH]^+$ with NSA^{2-} .	224
<u>APPENDIX 7.</u> Computer Program GRC5. "Least squares for kinetic data NSA".	225
<u>APPENDIX 8.</u> Relaxation expression for the reaction of $Zntet^{2+}$ with NSA^{2-} .	227
<u>REFERENCES.</u>	229

CHAPTER 1

Introduction

1.1 The role of metal ions in enzyme systems

It has been shown⁽¹⁾ that the activity of several enzymes is dependent upon the presence of a particular metal ion. The experimentally observed differences in the strength of the interaction between metal ions and enzymatic proteins leads to a convenient classification of metal-enzymes into two types.

1. "Metalloenzymes", in which the metal ions are bound firmly enough to remain associated with the protein throughout the various enzyme isolation procedures. Metal exchange is usually extremely slow, although the metal can often be removed by the addition of an excess of a chelating agent, e.g. EDTA, 1,10 phenanthroline.

2. "Metal-activated enzymes", where the metal is loosely bound and often dissociates from the protein on isolation of the enzyme.

The metals involved in this work, magnesium and zinc, are usually associated with types 2 and 1 respectively.

The absolute requirement of an enzyme for a particular metal ion can usually be attributed to the ability of the metal to perform one or more of the following functions:-

(i) to act as a bridge between the enzyme and the substrate, e.g. zinc in carbonic anhydrase (CA)⁽²⁾;

(ii) to produce a conformational change in the enzyme although the metal is not necessarily at the active site, e.g. magnesium in yeast enolase⁽³⁾;

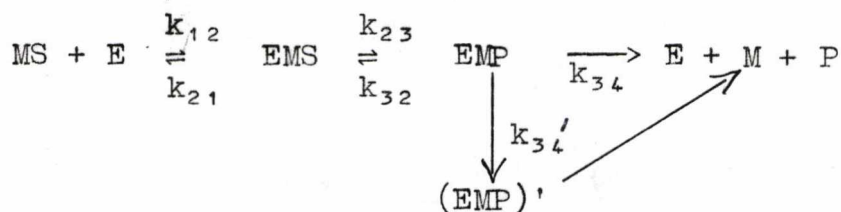
(iii) to polarise a bond and hence assist in hydrolysis, e.g. zinc in carboxypeptidase A (CPA)⁽⁴⁾;

(iv) to assist in electron transfer reactions, e.g. Mo in xanthine oxidase⁽⁵⁾.

Whilst both magnesium and zinc occur widely in enzyme systems, the functions they perform, and hence the type of enzyme in which they occur, differ considerably. This can, perhaps, be explained by their different Lewis acid strengths ($\text{Ca} < \text{Mg} < \text{Mn} < \text{Fe} < \text{Co} < \text{Zn} < \text{Ni} < \text{Cu}$) and by their different affinities for various donor atoms (e.g. magnesium binds to oxygen centres in preference to nitrogen and sulphur whilst zinc prefers sulphur and nitrogen centres⁽⁶⁾). This is well illustrated by phosphate transfer enzymes where magnesium is invariably the metal associated with the native enzyme. Many metals, including Mg, Mn, Co, Ni and Zn, bind to ATP and catalyse its non-enzymatic hydrolysis to approximately the same extent. However, in the enzyme Mg and Mn act as activators but Co and Zn are inhibitors so there must be a different mechanism governing the enzymatic and non-enzymatic hydrolyses. It has been suggested⁽⁷⁾ that there is a basic nitrogen group in the vicinity of the metal binding site in the enzyme which is essential for catalysis. For Co, Ni and Zn, this nitrogen group apparently binds to the metal, thus causing inhibition; with magnesium and manganese, with their low affinity for nitrogen donors, no such binding occurs.

It is very difficult to predict which metal will be the most efficient activator for a particular enzyme even when a great deal is known about the behaviour of the metal ion in model systems. It appears that the rate of complex formation and dissociation are as important as the stability of the

enzyme-metal-substrate complex. For example, magnesium and calcium form complexes of similar stability⁽⁹⁾ but there is quite often a mutual antagonism between them in biological systems⁽¹⁰⁾. Thus, in the enzyme myosin ATPase, calcium is much more effective than magnesium in catalysing the hydrolysis of ATP whilst, on the other hand, it sometimes happens that magnesium cannot be replaced by calcium. This can, perhaps, be explained by considering a mechanism of this type



where E represents the enzyme, M the metal, P the product and S the substrate. The lifetime of the EMP intermediate will be much less for calcium than for magnesium (since calcium complexes dissociate more rapidly than magnesium complexes) and hence product formation will be more rapid if the reaction follows the upper pathway. If, however, the intermediate (EMP)' is essential for product formation, only for magnesium (where k_{34}' can compete with k_{32}) can this reaction path be followed and thus calcium effectively acts as an inhibitor to product formation.

Zinc is often found in hydrolytic enzymes, where its function appears to be to polarise a bond in the vicinity of the bond which is to be hydrolysed and hence to aid the hydrolysis. Thus, in CPA X-ray studies⁽⁴⁾ have shown the zinc atom to be in a position where it can polarise the carbonyl bond thus making the carbonyl carbon atom more susceptible to nucleophilic attack (see fig. 1.1.1).

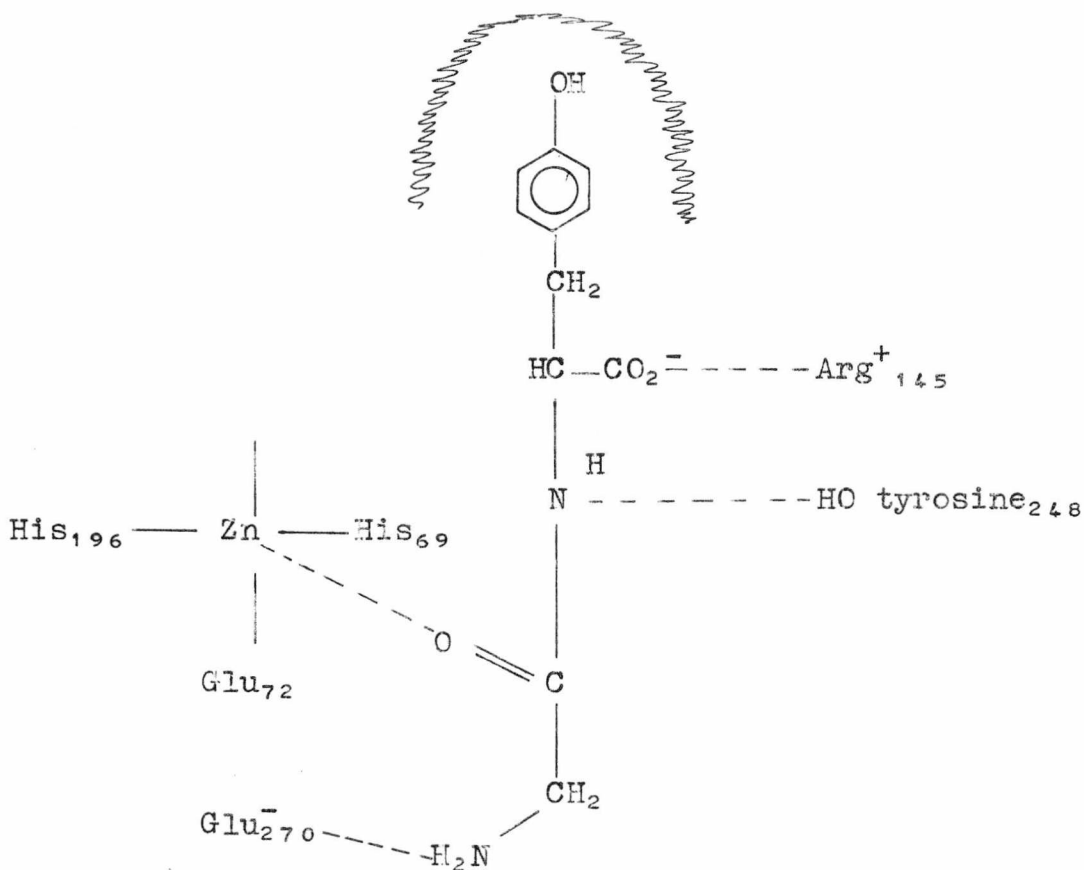


Fig. 1.1.1. The active site of CPA.

That the metal in CPA appears to act as a Lewis acid in the hydrolysis of peptides is suggested by the fact that the replacement of the native zinc by some other transition metals causes little change in the enzyme activity (Table 1.1.1).

TABLE 1.1.1. Metal ion specificity of Carboxypeptidase A.

<u>Metal ion</u>	<u>Peptidase activity %</u>	<u>Esterase activity %</u>
Zn	100	100
Co	160	95
Ni	106	87
Mn	8	35

The appearance of zinc as the naturally occurring metal in this enzyme can probably be explained by the unusual stability order of transition metals with the apo-enzyme



which is contrary to the Irving-Williams series⁽¹¹⁾. The visible spectrum of the cobalt(II) enzyme⁽¹²⁾ suggests that the metal is situated in a distorted tetrahedral environment, and perhaps this condition of low symmetry enhances the stability of the zinc enzyme.

It has been observed for other zinc enzymes (e.g. carbonic anhydrase, alkaline phosphatase and liver alcohol dehydrogenase) that the metal has an unusual coordination number and Vallee and Williams⁽¹³⁾ have suggested that the reason that Co(II), but not Ni(II), can often replace zinc in enzymes is that it, too, can readily accept distorted geometries whilst Ni(II) adopts more regular geometries in its model complexes. Investigation of the visible spectrum of Co(II) CA⁽¹⁴⁾ shows that the metal occupies a tetrahedral site at low pH but at higher pH the metal becomes penta-coordinate with a correspondingly enhanced activity. A possible mechanism for the hydration of carbon dioxide, fig. 1.1.2, involves the transfer of a hydroxyl group from the metal ion to the carbon dioxide molecule. It is therefore not surprising that the activity of the metalloenzyme is directly related to the ease of hydrolysis of the water molecules bound to the metal, Table 1.1.2. (Although this table gives an

TABLE 1.1.2. Metal ion specificity of Bovine Carbonic Anhydrase B.

<u>Metal ion</u>	<u>CO₂[†]</u>	<u>pK of aquo metal⁽¹⁵⁾</u>
Zn	100	8.7
Co	50	8.9
Ni	2	9.6
Cd	0	11.6
Mg	0	12.0

[†]Relative activities in standard assays^(16,17).

indication of the relative pK's of metal ions it must be noted that the ligands bound to the metal ion will significantly change the pK of the metal and in some instances may even change the order).

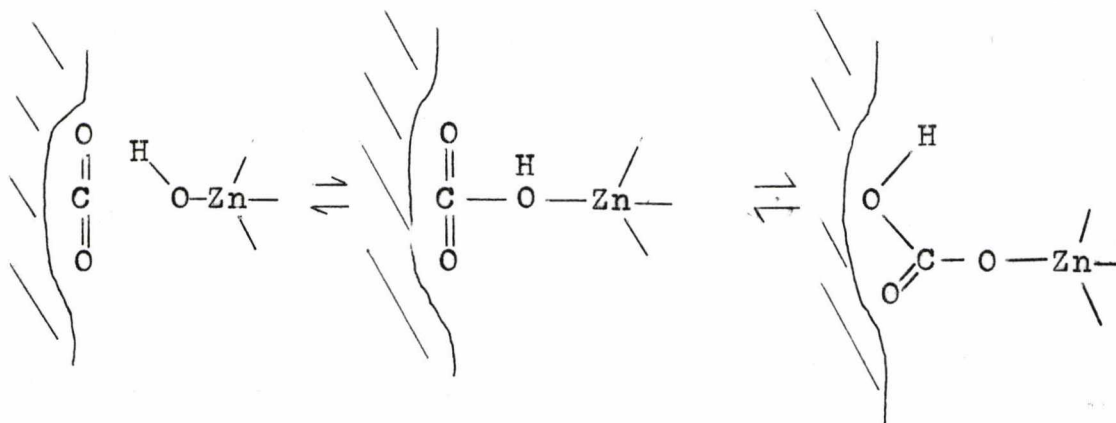


Fig. 1.1.2. Tentative scheme for the hydrolysis of CO₂ by Carbonic Anhydrase.

The low symmetry at the metal site in metal-enzymes is not peculiar to zinc. The absorption and the e.p.r. spectra of copper blue enzymes and the non-heme iron enzymes have characteristics which do not appear in the spectra of simple complexes. It is often the case for these enzymes that the addition of an extra ligand, such as cyanide, converts the spectrum into one resembling a more usual stereochemistry. Thus, the high pH spectrum of Co(II) carbonic anhydrase changes from that typical of a five-coordinate cobalt species to that of tetrahedral Co(II) on the addition of cyanide, whilst the binding of carbon dioxide, the natural substrate, and iso-electronic species such as N₃⁻, leaves the spectrum unaltered.

The unusual stereochemistry of metalloenzymes has been discussed by Vallee and Williams⁽¹³⁾ in terms of the "entatic" nature of the active site in which the metal ion is in a position similar to that of the intermediate state for its normal reactions and thus displaced from the position of minimum free energy. Thus a substrate entering the active site would find itself under attack from unusually activated groups with a correspondingly reduced activation energy.

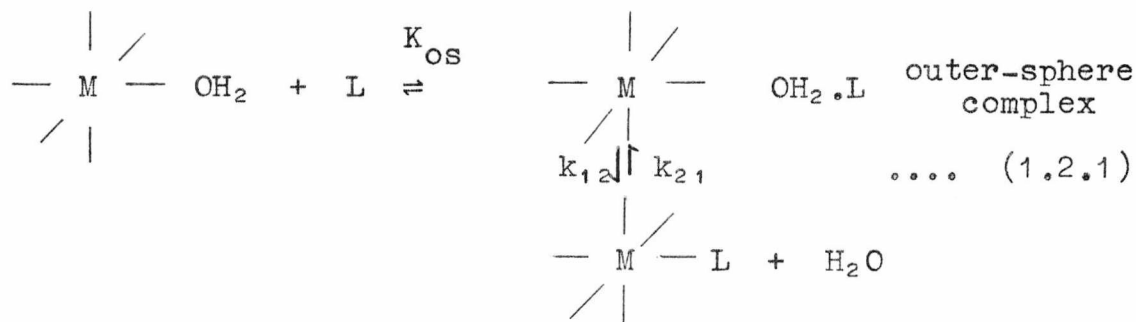
To get an intimate understanding of the mechanism of enzyme action it is necessary to understand the function of the various components of the enzyme. Because of the close interaction between the metal ion and the protein in an enzyme it is very difficult to assign the mechanistic details to either one or the other. It is therefore necessary to study simple model systems to attempt to show the influence of the protein on the metal ion and vice versa. One way of accomplishing this is by a study of ternary complex formation at a metal centre and this has been the approach in this work.

1.2 Mechanisms of metal complex formation

A great deal of work has been done to try to elucidate the mechanism of substitution reactions at metal centres. Most of the effort has been concentrated on Co(III) and other non-labile systems such as the square-planar complexes of Pt(II) and for these systems mechanisms ranging from limiting S_N1 to S_N2 have been postulated.

Metal complex formation for labile octahedral complexes is usually discussed in terms of the Eigen mechanism⁽¹⁹⁾ in which the preliminary formation of an outer-sphere complex where water molecules are retained in the inner-sphere of the metal ion is proposed. Then, as a water molecule

dissociates from the inner-sphere, its place is taken by the ligand held in the outer-sphere. This mechanism may be represented by



The formation of the outer-sphere complex is usually rapid in comparison with k_{12} and k_{21} , and may be treated as a pre-equilibrium. So, for the simplest case where L is a monodentate ligand, the observed forward rate constant is given by $K_{OS}k_{12}$, where k_{12} is the water exchange rate constant for the metal.

For metals with "closed-shell" electronic configurations it has been found⁽²⁰⁾ that there is a correlation between $\log_{10}k_{12}$ and the ionic radius of the metal ion (fig. 1.2.1),

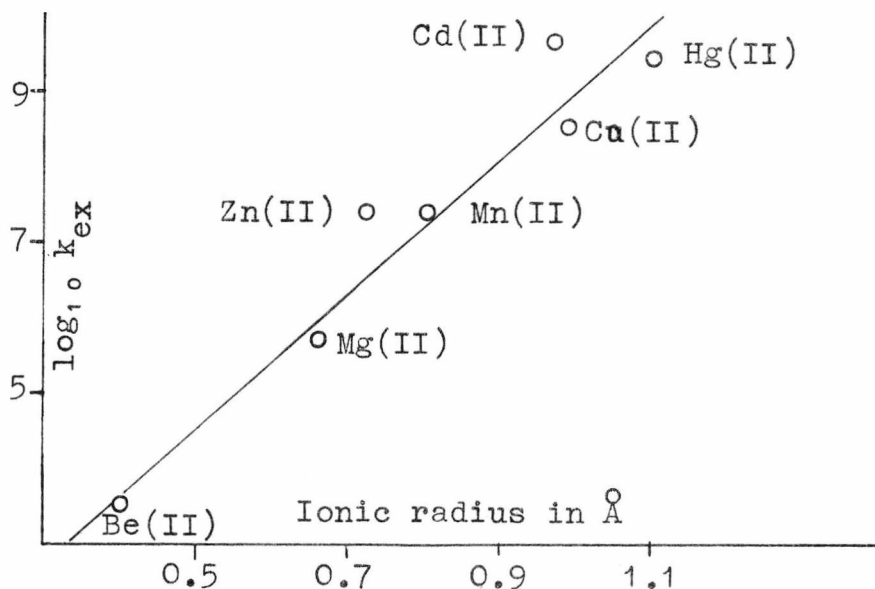


Fig. 1.2.1. Rate constants for water exchange as a function of ionic radius for "closed-shell" metals.

but this relationship does not hold for the transition metal series where ligand field effects lead to unexpectedly low water exchange rates for V(II) and Ni(II) whilst Jahn-Teller effects lead to high rates of water exchange for Cr(II) and Cu(II), see fig. 1.2.2.

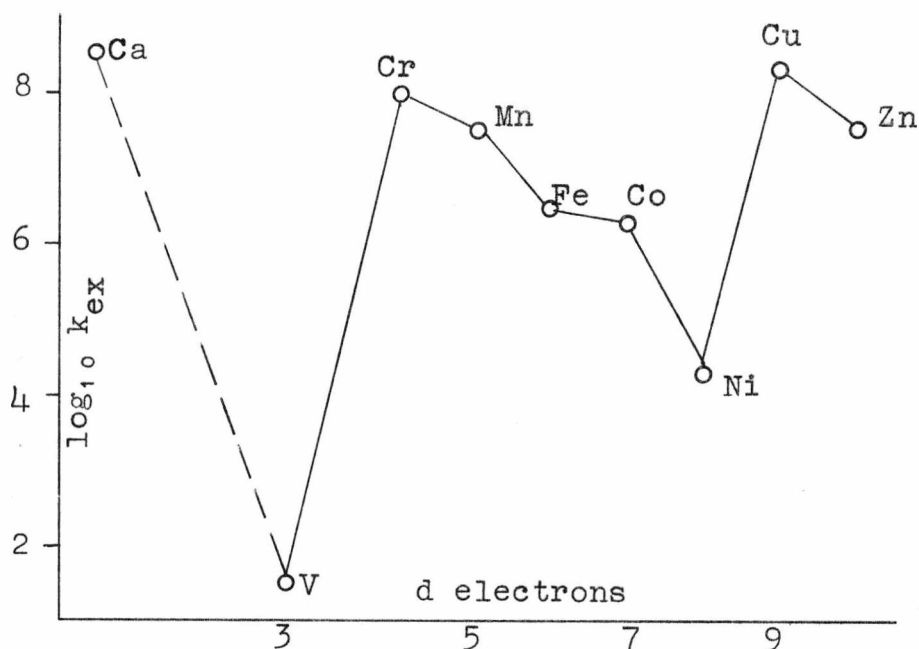
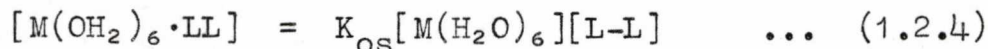


Fig. 1.2.2. Water exchange rates for the bivalent ions of the first transition metal series.

Metals have been classified into three groups according to the magnitude of their water exchange rates⁽²⁰⁾:-

1. In this group the water molecules are weakly bound to the metal owing to the low charge density at the metal surface. The rate of water exchange is comparable to the rate of formation of the outer-sphere complex and rate constants are typical of a diffusion controlled process. This group includes the alkali metals and the heavier alkaline earths, Cu^{2+} , Sr^{2+} and Ba^{2+} .

If the formation of the outer-sphere complex is fast compared to the following steps, then



and a steady-state treatment can be applied to the pentaquo species:

$$\begin{aligned} \frac{d[(H_2O)_5M-L-L]}{dt} &= -(k_{21}+k_{23})[(H_2O)_5M-L-L] + k_{32}[(H_2O)_4ML_2] \\ &+ k_{12}K_{OS}[M(H_2O)_6][L-L] = 0 \quad \dots (1.2.5) \end{aligned}$$

$$\therefore [(H_2O)_5M-L-L] = \frac{k_{12}K_{OS}}{(k_{12}+k_{23})}[M(H_2O)_6][L-L] + \frac{k_{32}}{(k_{12}+k_{23})}[(H_2O)_4ML_2] \quad \dots (1.2.6)$$

Substituting equation 1.2.6 in the rate equation gives

$$\begin{aligned} \frac{d[M(H_2O)_4L_2]}{dt} &= \frac{k_{23}k_{12}K_{OS}}{(k_{21}+k_{23})}[M(H_2O)_6][L-L] + \frac{k_{32}k_{23}}{(k_{21}+k_{23})}[M(H_2O)_4L_2] \\ &- k_{32}[M(H_2O)_4L_2] \quad \dots (1.2.7) \end{aligned}$$

$$= \frac{k_{23}k_{12}K_{OS}}{(k_{21}+k_{23})}[M(H_2O)_6][L-L] - \frac{k_{32}k_{21}}{(k_{21}+k_{23})}[M(H_2O)_4L_2] \quad \dots (1.2.8)$$

Hence the observed rate constants for formation and dissociation of ML_2 are given by, respectively,

$$k_f = \frac{k_{23}k_{12}K_{OS}}{(k_{21}+k_{23})} \quad \text{and} \quad k_b = \frac{k_{32}k_{21}}{(k_{21}+k_{23})}$$

If the ring closure step is fast compared to the dissociation of the pentaquo species, i.e. $k_{23} \gg k_{21}$, then $k_f = k_{12}K_{OS}$ and $k_b = \frac{k_{21}k_{32}}{k_{23}}$. The forward rate constant is thus identical to that found in the monodentate case whilst the decrease in k_b reflects the increased stability associated with a bidentate ligand. However, if ring closure is rate-determining (i.e. $k_{21} \gg k_{23}$) then

$$k_f = \frac{K_{OS}k_{12}k_{23}}{k_{21}} \quad \text{and} \quad k_b = k_{32}.$$

It has been suggested by Hoffmann⁽²¹⁾ that ring closure can become important when the first "arm" of the bidentate ligand forms only a weak bond with the metal ion (i.e. k_2 is comparatively large, as in the formation of nickel malonate⁽²²⁾). It has also been suggested⁽²³⁾ that the difficulty of forming a six-membered ring can lead to a ring-closure contribution in the forward rate constant although this effect is often very small⁽²⁴⁾.

Returning to the simple situation where water loss is the rate-determining step, it can be seen that it should be possible to check the reliability of the proposed mechanism by independently determining the value of the water exchange rate and the outer-sphere constant for a particular reaction. Water exchange rates have been measured for several metal species by n.m.r. techniques^(25,26), but it is very difficult to measure K_{OS} directly for labile metal systems.

The absence of values for K_{OS} has not completely precluded the testing of the theory because it has been possible to calculate values for K_{OS} using the equations of Fuoss⁽²⁷⁾, Eigen⁽²⁸⁾ and Hemmes⁽²⁹⁾. The Fuoss equation for the formation of a complex between two ions of charge $Z+$ and $Z-$ is

$$K_{OS} = \frac{4\pi N a^3}{3 \times 10^3} \exp\left(-\frac{|Z+Z-|e^2}{aDkT}\right) M^{-1} \dots (1.2.9)$$

where N = Avogadro's number

a = distance between the metal and the ligand in the complex (usually taken to be 5\AA)

e = electronic charge

D = macroscopic dielectric constant

k = Boltzman's constant

T = absolute temperature .

For a test of the Eigen mechanism it is not necessary to have an absolute value of K_{OS} since (equation 1.2.9), to a first approximation, it is independent of the nature of the ligand for given Z^+ and Z^- . A large amount of kinetic data has now been obtained, especially for Ni(II) with neutral ligands^(18,25,30), in which there is a small spread in k_f , except for polyamines where an alternative mechanism has been suggested^(30a), giving support to the proposed mechanism.

1.3 Measurement of Fast Reactions

The methods of studying fast reactions in solution have been extensively reviewed⁽³¹⁻³⁴⁾. These methods generally employ either rapid mixing or, for shorter times, the study of a system close to equilibrium. Stopped-flow is the most widely used of the rapid mixing techniques; in this method, two solutions are brought together in a mixing chamber and the mixed solution flows down an observation tube. The flow is rapidly stopped and the course of the subsequent reaction is followed by monitoring some property of the solution (e.g. optical density, conductance) as a function of time, at a fixed distance from the mixer. The upper limit of reaction rates measurable by stopped-flow is set by the mixing time, usually about 1 millisecond. To measure reactions faster than this, one has to rapidly perturb a system at equilibrium and follow the way in which the new equilibrium position is attained. Methods which use this approach are known as relaxation techniques and have been widely developed by Eigen's school at Göttingen⁽³³⁾.

There are three ways in which the system can react to the perturbation:-

1. The system exactly follows the perturbation and so only a lower limit can be assigned to the reaction rate.

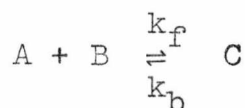
2. The system reacts so slowly that no change in the equilibrium occurs.

3. The system changes but lags behind the perturbing function giving rise to a "relaxation" effect. In this case, provided that the perturbation is small, the reaction follows an exponential path described by

$$C = C_0 e^{-t/\tau}$$

where C is concentration difference between the new equilibrium value and that at time t , C_0 is the concentration difference between the initial and final conditions, and τ is the time for C to fall to C_0/e , known as the relaxation time (see fig. 1.3.1).

Consider the reaction



Suppose the system is at equilibrium and that this system is perturbed by, say, a rapid change in temperature (as in the temperature-jump technique). Let the concentrations at the new equilibrium temperature be \bar{C}_A , \bar{C}_B and \bar{C}_C and at any time, t , be C_A , C_B and C_C . At time t the displacement from the final equilibrium will be

$$\Delta C_A = \bar{C}_A - C_A$$

$$\Delta C_B = \bar{C}_B - C_B$$

$$\Delta C_C = \bar{C}_C - C_C$$

The net forward rate is given by

$$\frac{dC_C}{dt} = k_f C_A C_B - k_b C_C \quad \dots (1.3.1)$$

which on substitution becomes

$$\frac{d(\bar{C}_C - \Delta C_C)}{dt} = k_f (\bar{C}_A - \Delta C_A) (\bar{C}_B - \Delta C_B) - k_b (\bar{C}_C - \Delta C_C) \quad \dots (1.3.2)$$

If the displacement of the equilibrium is small (i.e. $\bar{C}_A \gg \Delta C_A$ etc.) and second order terms (e.g. $\Delta C_A \Delta C_B$) are neglected, then

$$-\frac{d(\Delta C_C)}{dt} = -k_f(\bar{C}_A \Delta C_B + \bar{C}_B \Delta C_A) + k_b \Delta C_C \quad \dots (1.3.3)$$

The stoichiometric relationships

$$\Delta C_C = -\Delta C_A = -\Delta C_B$$

may be substituted into equation 1.3.3 to give

$$-\frac{d(\Delta C_C)}{dt} = [k_f(\bar{C}_A + \bar{C}_B) + k_b] \Delta C_C .$$

This is of the form $\frac{dC}{dt} = -kC$

where $C = C_0 e^{-kt}$ and

$$k = \tau^{-1} = k_f(\bar{C}_A + \bar{C}_B) + k_b .$$

Thus a plot of τ^{-1} against $(\bar{C}_A + \bar{C}_B)$ yields a straight line with the rate constants, k_f and k_b , given by the slope and intercept respectively. If $\bar{C}_A \gg \bar{C}_B$ (i.e. pseudo first order conditions are maintained) then the expression can be simplified to

$$\tau^{-1} = k_f C_A^T + k_b$$

where C_A^T is the total concentration of A.

If $\bar{C}_A \approx \bar{C}_B$, a value for the stability constant determined by some other means can be used to calculate \bar{C}_A and \bar{C}_B and then these values can be used to calculate k_f and k_b .

Relaxation expressions for more complex systems can be derived by similar methods^(33,35).

There are three methods for producing fast, single step perturbations:-

1. Methods which involve a rapid increase in temperature (temperature-jump). The temperature rise is usually produced by joule heating in the case of aqueous solutions and by the

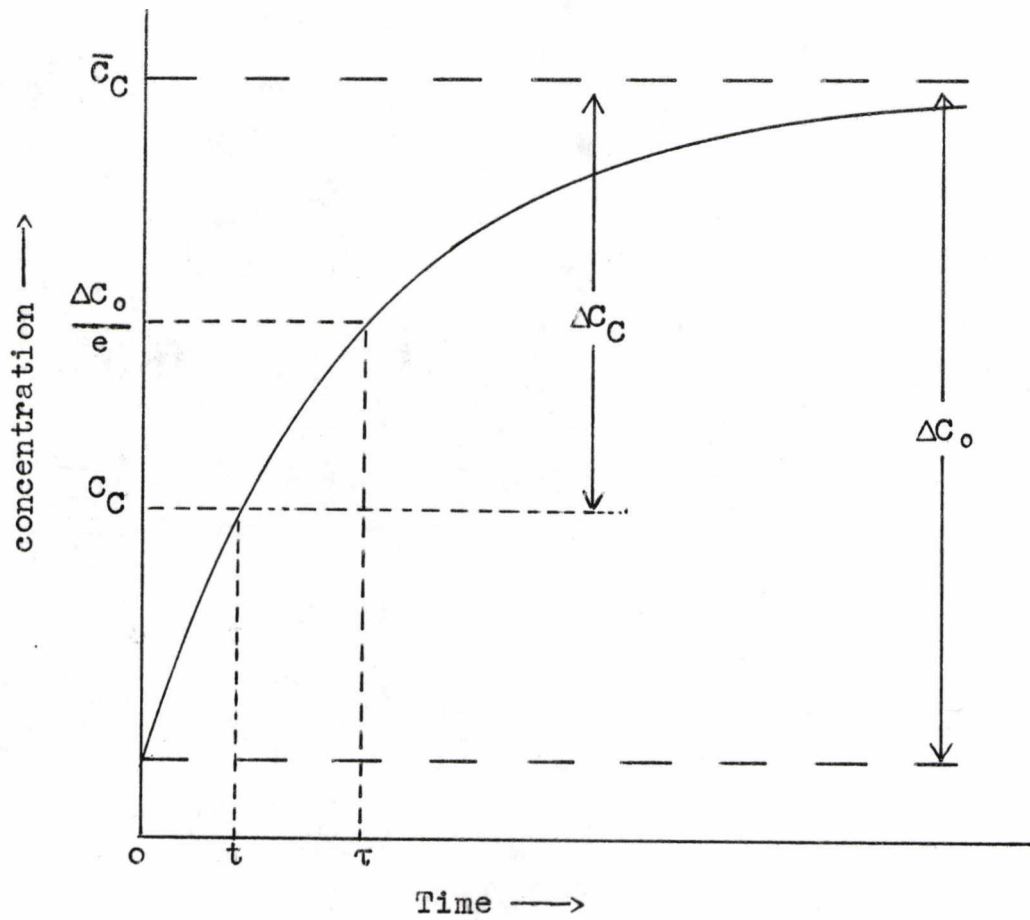


Fig. 1.3.1. Relaxation curve showing the variation of the concentration of species C with time after a single displacement from equilibrium.

absorption of microwaves or laser light for non-aqueous systems. The changes in the equilibrium concentrations which follow the temperature rise are governed by the relationship between temperature and the stability constant as represented by the van't Hoff equation

$$\left(\frac{\partial(\ln K)}{\partial T}\right)_P = \frac{\Delta H^\circ}{RT^2}$$

2. Methods involving a rapid change in pressure (pressure-jump). The corresponding equation in this case is

$$\left(\frac{\partial \ln K}{\partial P}\right)_T = -\frac{\Delta V^\circ}{RT}$$

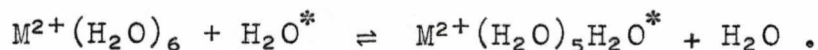
where ΔV° is the volume change for the reaction.

3. Methods involving a rapid change in the applied electric field (electric field jump). The equation governing this change is

$$\left(\frac{\partial \ln K}{\partial E}\right)_{PT} = \frac{\Delta D_0}{RT}$$

where ΔD_0 is the change in dipole moment.

Other methods for studying fast reactions include stationary methods, in which a periodic forcing function is applied across the test solution and the effect of the chemical relaxation on the periodic function is observed, and n.m.r. techniques which are particularly useful for following reactions in which there is no overall stoichiometric change, e.g.



1.4 Choice of a temperature-jump system

For the study of ternary complexes

the ligands L_1 and L_2 have to satisfy certain stringent requirements, the most important being that L_1 should not react with L_2 . In addition, the following conditions should be obeyed.

Bound Ligand L_1

1. The ligand must be soluble or form soluble metal complexes.
2. The stability constant with the metal should be large so that $[ML] \gg [ML_2], [M]$. If this is not the case, the system may still be amenable to study provided (a) that conditions can be chosen such that only one unambiguously assignable relaxation is observed and (b) that stability constants are known with sufficient accuracy to permit the calculation of the concentrations of the species present (particularly $[ML]$).
3. To investigate the effect of charge at the metal centre the ligands, L_1 , should be chosen so as to give the largest possible variation in the overall charge on ML_1 .
4. It has been suggested⁽¹³⁾ that the geometry of the metal is important in the reactions of metallo-enzymes so that ligands which impose particular conformations on the metal atom should be of interest.

Choice of ligands for zinc and magnesium

The choice of the ligands, L_1 , for zinc is complicated by the ability of zinc to form complexes of high stability since a tri- and tetra-dentate ligand tends to form a bis complex which gives rise to a second relaxation effect. The high affinity of zinc for carboxylates and amine groups, however, makes a charge variation of the metal complex from +2 to -3 relatively easy to obtain. For magnesium, however,

the dislike of the formation of metal-nitrogen bonds prevents the use of amines for the ligands, L_1 , and leaves the main binding groups as carboxylates and phosphates, thus reducing the possible charge variation.

Incoming Ligand L_2

1. The formation of the ternary complex should produce a change in the optical density of the test solution at a convenient wavelength. If a ligand, L_2 , does not give such a spectral change but does give a pH change, a suitable pH indicator can be used to produce the required spectral change. Such systems, however, are often experimentally difficult to study.
2. The stability constant of the ternary complex must be temperature dependent.
3. The stability constant for the ternary complex should be such that the optical density of the test solution is acceptable when the concentrations of L_1ML_2 and L_2 are comparable (i.e. under conditions for the largest change in optical density with temperature).
4. A series of charge types should be used if possible as a variety of charged ligands can emphasise the effect of the bound ligand on the reactivity of the metal.

CHAPTER 2

Apparatus and General Experimental Procedure

2.1 Introduction

In this chapter the equipment, experimental procedure and apparatus relating to the kinetic and equilibrium measurements are described.

2.2 Chemicals used

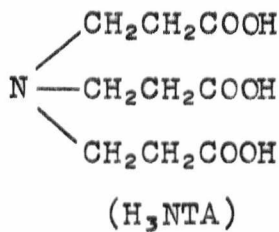
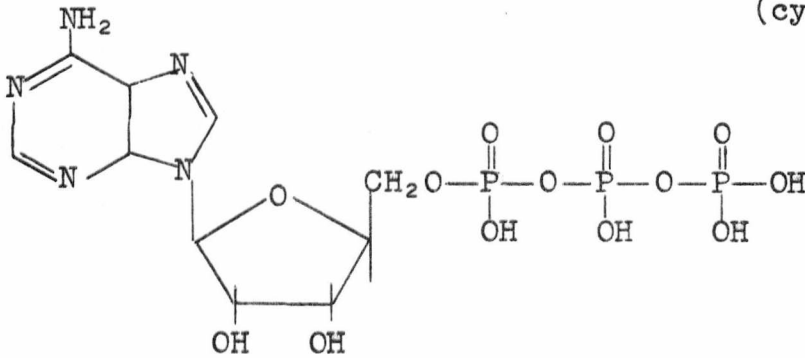
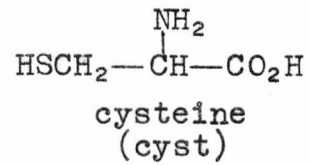
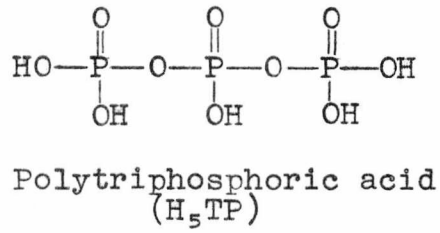
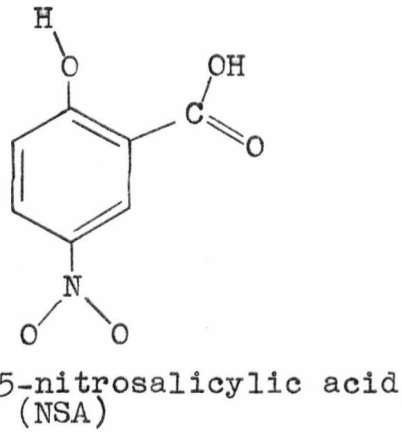
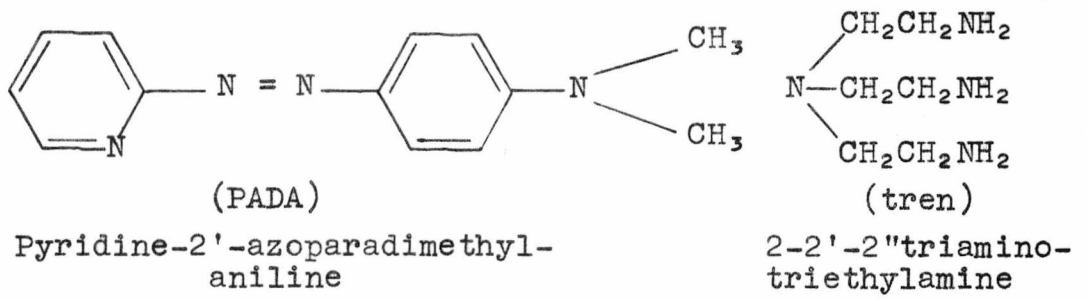
TABLE 2.2.1

<u>Chemical</u>	<u>Supplier</u>	<u>Grade</u>
Zinc oxide	Fisons	A.R.
Magnesium nitrate	B.D.H.	A.R.
Triethylenetetramine (trien)	Fluka, B.D.H.	Technical
Diethylenetriamine (dien)	Fluka	Puriss
Sym. dimethylethylenediamine (syndimeen)	Emanuel	Reagent
Ethylenediamine (en)	B.D.H.	Reagent
N,N'-bis(2-aminoethyl)-1,3-propanediamine (2-3-2 tet)	Eastman	Reagent
2,2'-2" triaminotriethylamine (tren)	By extraction (see section 2.3)	
Sodium nitrate	Fisons	A.R.
Sodium perchlorate	B.D.H.	A.R.
Nitric acid	Fisons	A.R.
Perchloric acid	Fisons	A.R.
Hydrochloric acid	B.D.H.	A.R.
Iminodiacetic acid (IDA)	Fisons	>98% pure
Cysteine (cyst)	B.D.H. Biochemicals	>98% pure
Nitrilotriacetic acid (NTA)	Fluka	Puriss
Sodium oxalate	Fisons	A.R.
Ethylenediamine N,N' diacetic acid (EDDA)	K. & K.	Reagent

Table 2.2.1 - continued

<u>Chemical</u>	<u>Supplier</u>	<u>Grade</u>
Triethylamine (E ₃ N)	Fisons	Technical
Sodium chloride	Fisons	A.R.
Triethanolamine (tea)	Fluka	Puriss
Ammonium nitrate	B.D.H.	A.R.
Sodium acetate	Fisons	A.R.
Uramil NN-diacetic acid (UDA)	Fluka	Puriss
Adenosine-5-triphosphate	Boehringer	> 98% pure
Sodium tripolyphosphate (TP)	Albright and Wilson	> 99% pure
Benzaldehyde	Fisons	A.R.
Trishydroxymethylamine (tris)	Fisons	A.R.
Borax	Fisons	A.R.
Potassium hydrogen phthalate	B.D.H.	A.R.
Barbitone	Fisons	> 98.5% pure
Pyridine-2-azo-p-dimethylaniline (PADA)	Sigmar	> 99% pure
5 nitro-salicylic acid (NSA)	Fluka	Puriss
Sodium hydroxide	Fisons	A.R.
Disodium hydrogen phosphate	B.D.H.	A.R.
Potassium dihydrogen phosphate	B.D.H.	A.R.
Cresol red	Fisons	Indicator
De-acidite FF-1P anionic exchange resin	Permutit	SRA 71 WR 0.6-1.0
8-hydroxyquinoline-5-sulphonic acid (OXS)	Hopkin & Williams	Reagent

The structure of the ligands used, which are not general laboratory reagents, are shown in figs. 2.2.1 and 2.2.2.



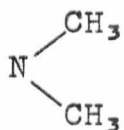
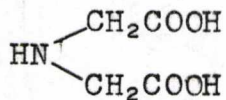
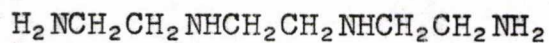
Me₆tren is like tren but with  replacing the NH₂ groups.

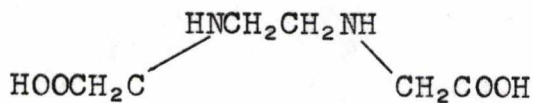
Fig. 2.2.1.



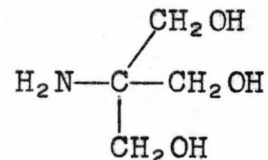
Iminodiacetic acid
(H₂IDA)



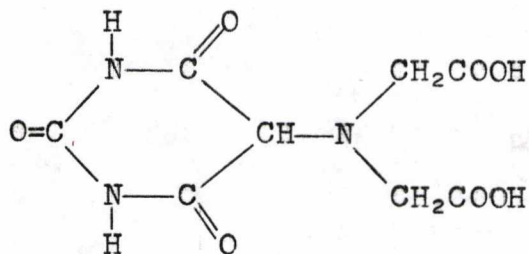
triethylenetetramine
(trien)



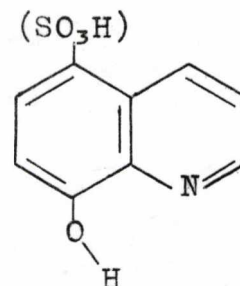
Ethylenediamine diacetic acid
(H₂EDDA)



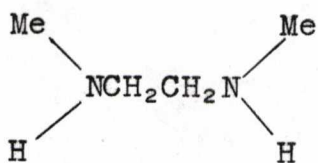
tris(hydroxymethyl)methylamine
"tris" buffer



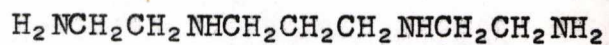
Uramil N-N diacetic acid
(H₃UDA)



8-hydroxyquinoline(5-sulphonic acid)
(oxine)



N,N'-dimethylethylene diamine
(s-diMeen)



2-3-2 tet

dien is like trien but with one less (CH₂CH₂NH).

2.3 Purification of chemicals and preparation of stock solutions

TREN: Commercial trien usually contains up to 20% of tren as impurity and this can be separated by fractional crystallisation of the two hydrochlorides from ethanolic solution.⁽³⁶⁾ 200 gm of trien was dissolved in 750 ml of ethanol and cooled to below 5°C in an ice-salt bath. Concentrated hydrochloric acid was added dropwise, with stirring, and the temperature was kept below 10°C. The white solid which precipitated was removed in fractions after the addition of each 2 ml of acid. This procedure was continued until the addition of acid caused no further precipitation. The $\text{tren} \cdot 3\text{HCl}$ was recrystallised by dissolving it in the minimum amount of hot water and precipitating the salt by the addition of alcohol. The precipitate was collected, filtered, washed with acetone and ether and finally dried in a vacuum desiccator.

The salt was converted into the free amine by passing through an exchange column of De-acidite FF-1P SR 71 anion exchange resin in the hydroxide form. The free amine was collected and standardised by titrating the three primary amino groups with a standard acid solution using bromocresol green as indicator.

TRIEN: The trien could not be prepared as above because of the problems involved in titrating it with acid using a pH indicator, and because chloride would interfere with the kinetics of the reactions to be studied. The required acid salts were, therefore, prepared as below and accurate concentrations were obtained by direct weighing.

TRIEN(HNO₃)₂ was prepared (cf. 37) by dissolving 1 mol of trien in 500 mls of ethanol and cooling to below 10°C. 1 mol of conc. nitric acid was then added slowly with stirring while maintaining a temperature of < 10°C. The white precipitate which formed was removed and discarded. Then a further mol of nitric acid was slowly added and the white precipitate was collected at a water pump. The salt was recrystallised by dissolving in the minimum amount of hot water and precipitating out with ethanol. It was filtered and dried under vacuum. The product was analysed for C, H and N and standard solutions were prepared by direct weighing.

TRIEN(HClO₄)₄ was prepared by a modification of the method of Schwarzenbach⁽³⁸⁾. To 1 mol. of trien(HNO₃)₂, prepared as above, was added 2 mols. of sodium hydroxide in the minimum amount of water. When all the trien(HNO₃)₂ had dissolved, 500 ml of 80-100 pet. ether was added and the sodium chloride which precipitated was removed. 3 mols of benzaldehyde was added to the solution and the white solid which formed was collected, recrystallised from pet. ether and dried under vacuum. M.pt. 86.2°C. [lit. value 86°C⁽³⁸⁾]. The benzaldehyde adduct was converted into the perchlorate by adding four equivalents of perchloric acid, removing the benzaldehyde by steam distillation and making up the solution to the required volume.

DIEN and 2-3-2tet: Stock solutions of these two amines were prepared by weighing the free amine directly into a volumetric flask and then making up the solution to the required volume. The resulting solutions were standardised by titrating two and four of the amine groups for dien (pK 9.9, 9.1 and 4.3)⁽³⁹⁾ and 2-3-2 tet (pK 10.3, 9.5, 7.3

and 6.0)⁽⁴⁰⁾, respectively using standard acid and bromothymol blue (pK 7.1) or bromocresol green (pK 4.7) as indicators.⁽⁴¹⁾

Metal solutions: The required zinc stock solutions were prepared by neutralising a weighed amount of zinc oxide with the required acid. The resulting solutions were standardised against EDTA using Eriochrome Black T as indicator⁽⁴²⁾. Magnesium stock solutions were prepared by dissolving weighed amounts of magnesium nitrate and titrating the resulting solutions against EDTA⁽⁴²⁾.

Na₅TP was twice recrystallised by dissolving in boiling water, filtering and precipitating out the salt by the addition of ethanol. The white solid was collected at a water pump and air dried as the hexahydrate^(43,44).

Carboxylic acids: Because of the low solubility of the carboxylic acids it was convenient to convert them into their more soluble sodium salts by the addition of stoichiometric amounts of sodium hydroxide. Solutions of UDA and cysteine were made up just prior to use because of their tendencies to dimerise to murexide and cystine respectively. The disodium salt of EDDA tends to hydrolyse in solution⁽⁴⁵⁾ and so the zinc salt of this acid was always used within four hours of preparation.

PADA: PADA is not very soluble in water but if first dissolved in a small amount of methanol, which has been shown to have no effect on the kinetics, a fairly high concentration can then be obtained on dilution with water. Solutions of PADA are stable for about a month, but those containing metal ions tend to fade over a period of about 12 hours, so metal-PADA solutions were made up just prior to use.

All other chemicals were used without further purification.

Solutions were made up using triply distilled water, the middle distillation being from alkaline permanganate.

The ligand:metal ratios for the stock solutions of ML_1 , were chosen to give maximum values of $[ML_1]:[M]$ and $[ML_1]:[M(L_1)_2]$; concentrations were calculated using computer program GR1 (see Appendix). The effect of using the wrong ligand:metal ratio is shown in fig. 2.9.1. These traces all refer to the $MgUDA^- + NSA$ system at $22^\circ C$ and pH 8.76.

The first trace shows the usual single relaxation obtained when a 1:1.0 ligand:metal ratio is used. When the $Mg:UDA^-$ ratio is increased to 1.05:1, the second trace is obtained in which the fast relaxation due to the reaction of $MgUDA^-$ with NSA becomes partially obscured by the larger, slower relaxation due to the reaction between the excess magnesium and NSA. The third trace shows the relaxation effect due to the reaction of $5 \times 10^{-4} M$ magnesium, the excess amount in the above experiments, with NSA.

2.4 Temperature-jump apparatus

The most widely used of the relaxation techniques is the temperature-jump method. The temperature-jump can be produced in one of three ways:- by the absorption of microwave or laser radiation or, more commonly, by joule heating. The main advantage of joule heating is the relatively large temperature rise which can be obtained; typically this is $5-10^\circ C$, with a rise time of only a few microseconds compared to $0.4^\circ C$ in $1\mu sec$ ⁽⁴⁶⁾ for microwave heating, and $3^\circ C$ in $300\mu sec$ ⁽⁴⁷⁾ for laser heating.

A schematic diagram of a joule heating temperature-jump apparatus is shown in fig. 2.4.1. A high voltage generator, H, is used to charge up the capacitor, C, to V volts. This voltage is then discharged through the cell containing the test solution (fig. 2.4.2) by pneumatically closing the spark gap, G. The rise time of the apparatus (i.e. the time for the voltage to fall to $1/e$ of its original value) is given by $\frac{1}{2}RC$, where C is the capacitance and R the resistance of the cell and its contents. The temperature rise in the cell is proportional to CV^2 so that, in order to realise a large temperature rise in the shortest possible time, it is necessary to use large voltages and small capacitances and to have a low cell resistance (i.e. a test solution with high ionic strength). Typical values for C and V are $0.05 \mu\text{F}$ and 20 KV, respectively.

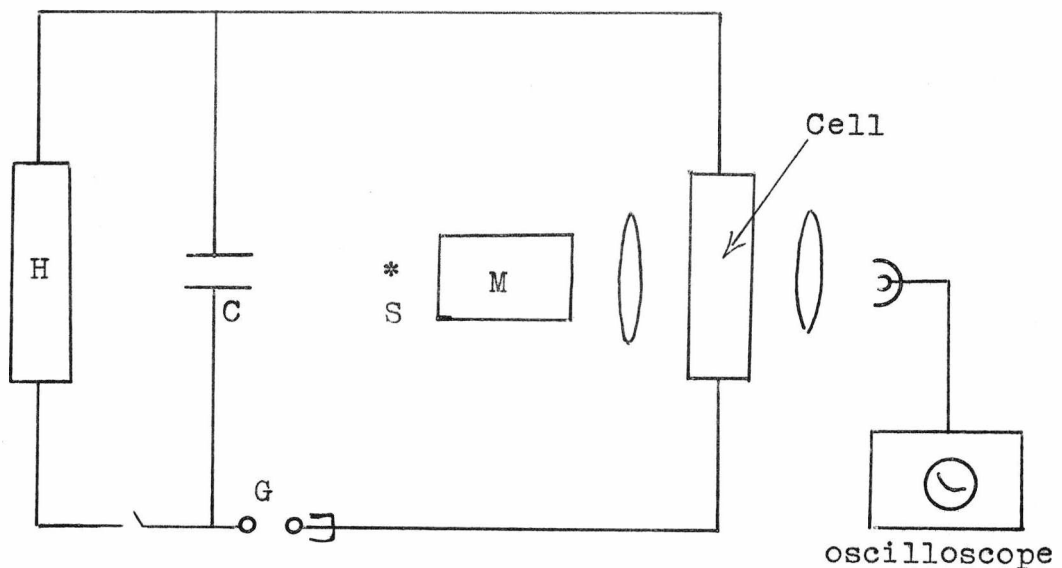


Fig. 2.4.1. Schematic diagram of a joule heating temperature-jump apparatus.

With joule heating it is usual to employ a spectrophotometric detection system since small conductance changes would tend to be swamped by the high conductance associated with the large background ionic strength. Light from the source, S, is monochromated and passed through the sample solution and then focussed onto a photomultiplier. Changes in optical density are then recorded as changes in voltage, as a function of time, on a storage oscilloscope. The components employed in the optical and detection systems are given in table 2.4.1.

The temperature-jump apparatus was constructed by Messanlagenstudienges. mbH. (Göttingen). A double beam instrument was used for the slower magnesium systems where the instability of the mercury arc lamp affected the accuracy of results obtainable on the single beam instrument described above.

TABLE 2.4.1.

Components of the optical system

<u>Component</u>	<u>Supplier</u>	<u>Type</u>
High pressure mercury arc lamp	Wotan	HBO 100W/2
Monochromators	Bausch and Lomb	33-86-01(u.v.) 33-86-02(visible)
Photomultiplier	R.C.A.	1P28
Storage Oscilloscope	Tektronix	549
Differential Preamplifier	Tektronix	1A6

This apparatus gives reproducible results throughout the $5\mu\text{sec}$ to 1sec time range. At times longer than 1 second convective mixing occurs and obscures the concentration changes. Near the lower limit of the time range and at high temperatures, cavitation effects due to pressure changes in the cell

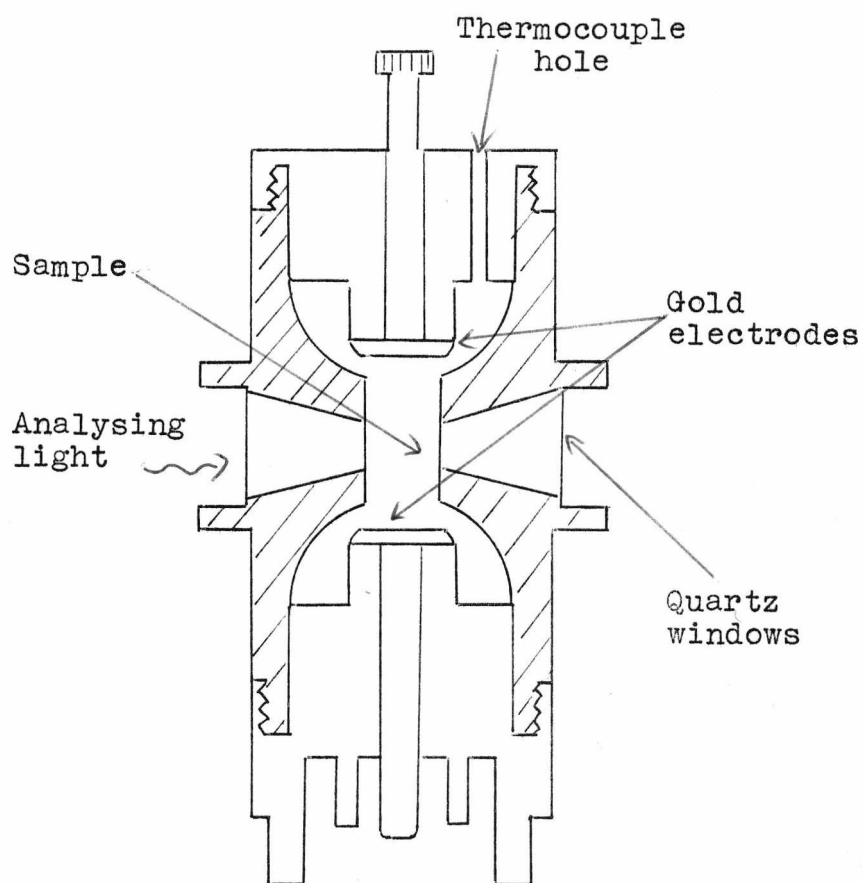


Fig. 2.4.2. Temperature-jump cell.

(accompanying the discharge) become important, although these can be considerably reduced by careful degassing of solutions.

2.5 Calibration of temperature rise in T-jump cell

For a solution which has a small optical density change, there is a linear relationship between percentage transmission and optical density; thus, the output signal from the photomultiplier is directly proportional to the perturbation.

This may be expressed as

$$OS. = 2.303 \times OV. \times \Delta OD.$$

where OS = change in photomultiplier signal in volts,
OV = offset voltage of the photomultiplier, set automatically to 4.3 volts on the double-beam instrument,
 ΔOD = change in optical density of the solution.

Hence by measuring OS as a function of the discharge voltage, for a solution for which the temperature dependence of the optical density is known, the temperature rise associated with a particular discharge voltage may be determined.

Method. A solution containing approximately $4 \times 10^{-2}M$ tris buffer, $2.5 \times 10^{-5}M$ cresol red and $0.15M$ sodium nitrate was adjusted to about pH 8.1 at $16^{\circ}C$ with nitric acid. The optical density of this solution was recorded at 562.5 nm as a function of temperature, over the range $14-30^{\circ}C$. The temperature of the solution was measured in the reference cell, which contained all the components except the cresol red, using a Comark electronic thermometer. The plot of ΔOD against temperature (fig. 2.3.1) gives a straight line of

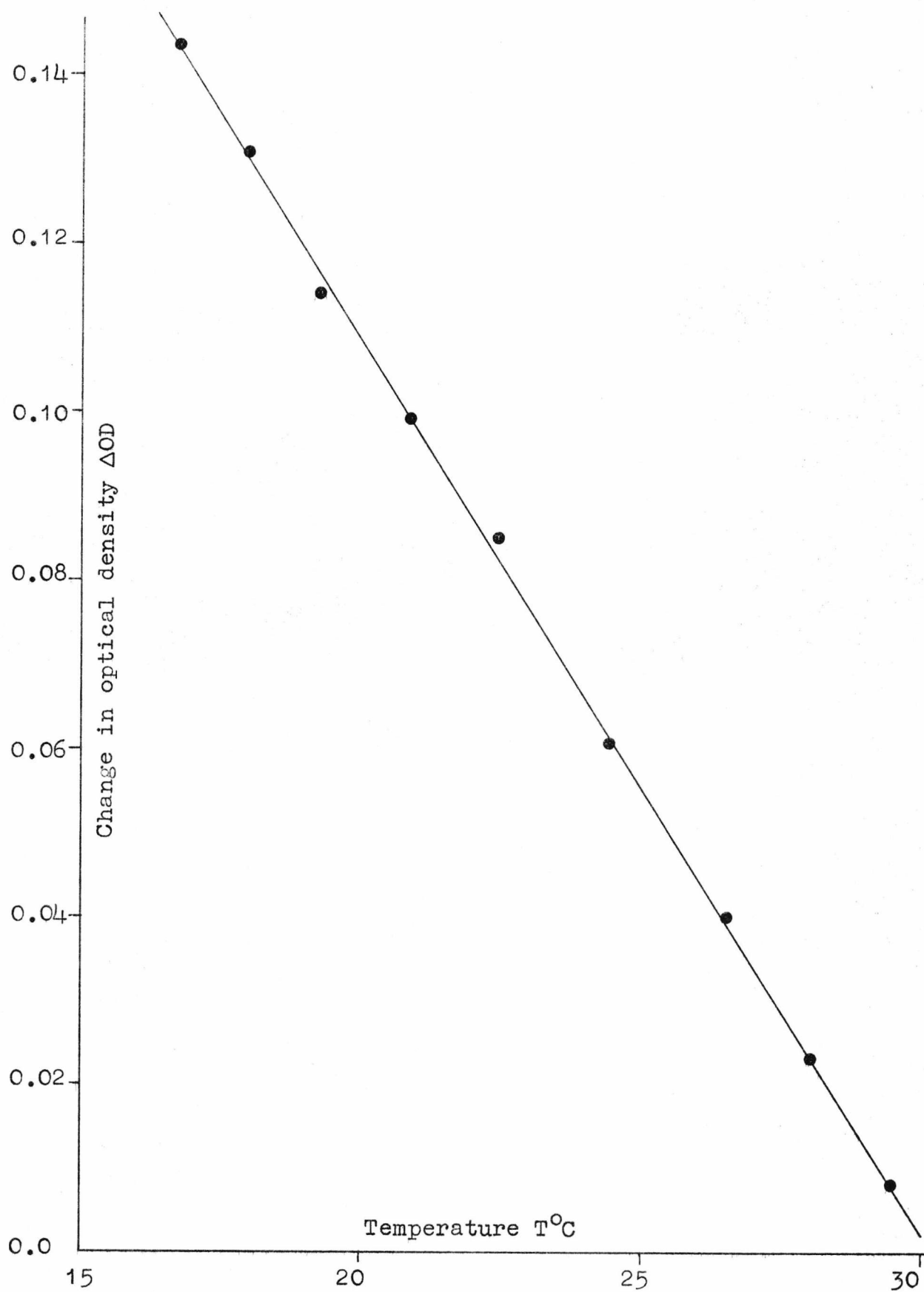


Fig. 2.5.1. Change of optical density of the cresol red solution with temperature.

slope, 0.00993 OD units/ $^{\circ}\text{C}$. The path length of the temperature-jump cell was measured using a travelling microscope.

The amplitude of the temperature-jump was then measured on a storage oscilloscope for discharge voltages between 10 and 26 KV, each voltage being repeated four times and the mean values obtained. The oscilloscope traces were photographed, enlarged and traced onto graph paper to enable accurate measurement of the amplitude change to be made. The apparatus was thermostatted throughout at 16°C so that the final temperature always came within the temperature range over which the optical density change of the indicator with temperature was found to be linear. The results are shown in table 2.5.1, and plots of temperature rise, ΔT , against V and V^2 are shown in figs. 2.5.2 and 2.5.3, respectively.

TABLE 2.5.1

Jump amplitudes and temperature rises for various discharge voltages.

<u>Discharge voltage</u> <u>(KV)</u>	<u>Change in output</u> <u>signal (MV)</u>	<u>Temperature</u> <u>rise ($\Delta T^{\circ}\text{C}$)</u>
10	78	1.12
12	115	1.66
14	161	2.34
16	201	2.92
18	264	3.79
20	323	4.68
22	407	5.80
24	472	6.83
26	545	7.88

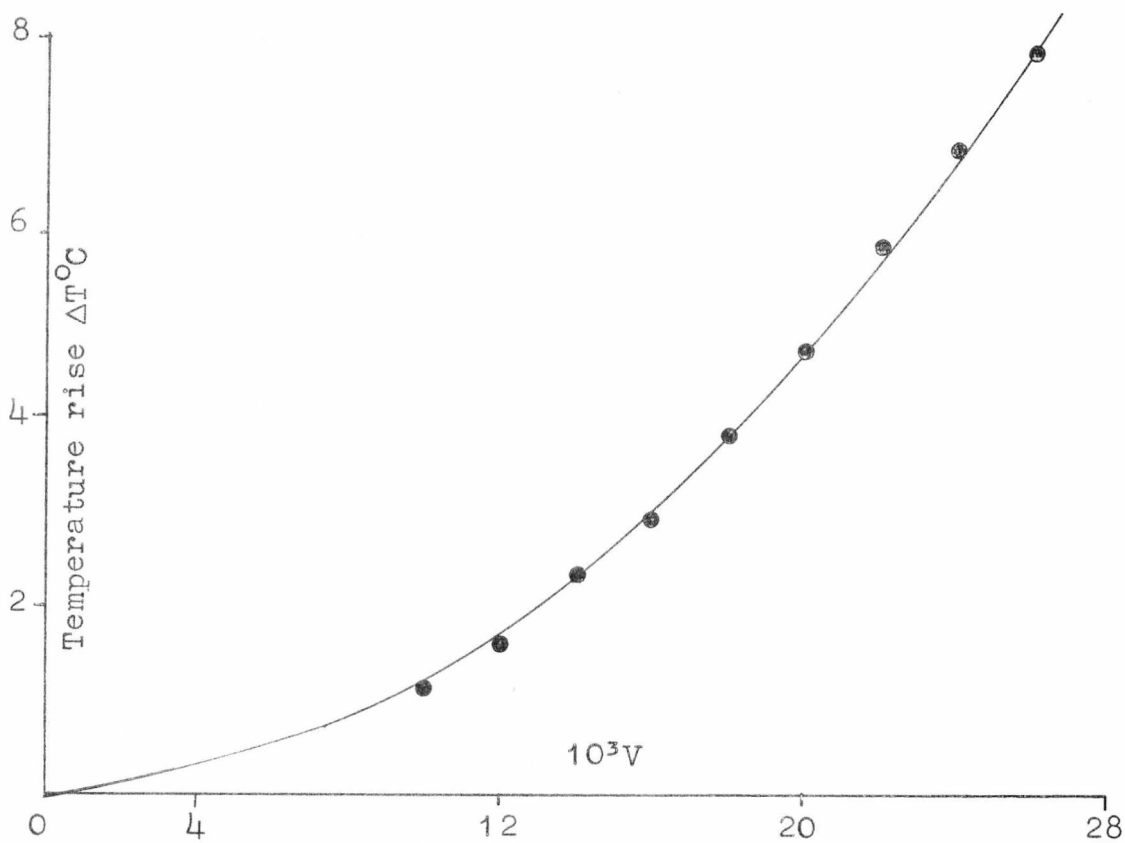


Fig. 2.5.2. Temperature rise vs. discharge voltage.

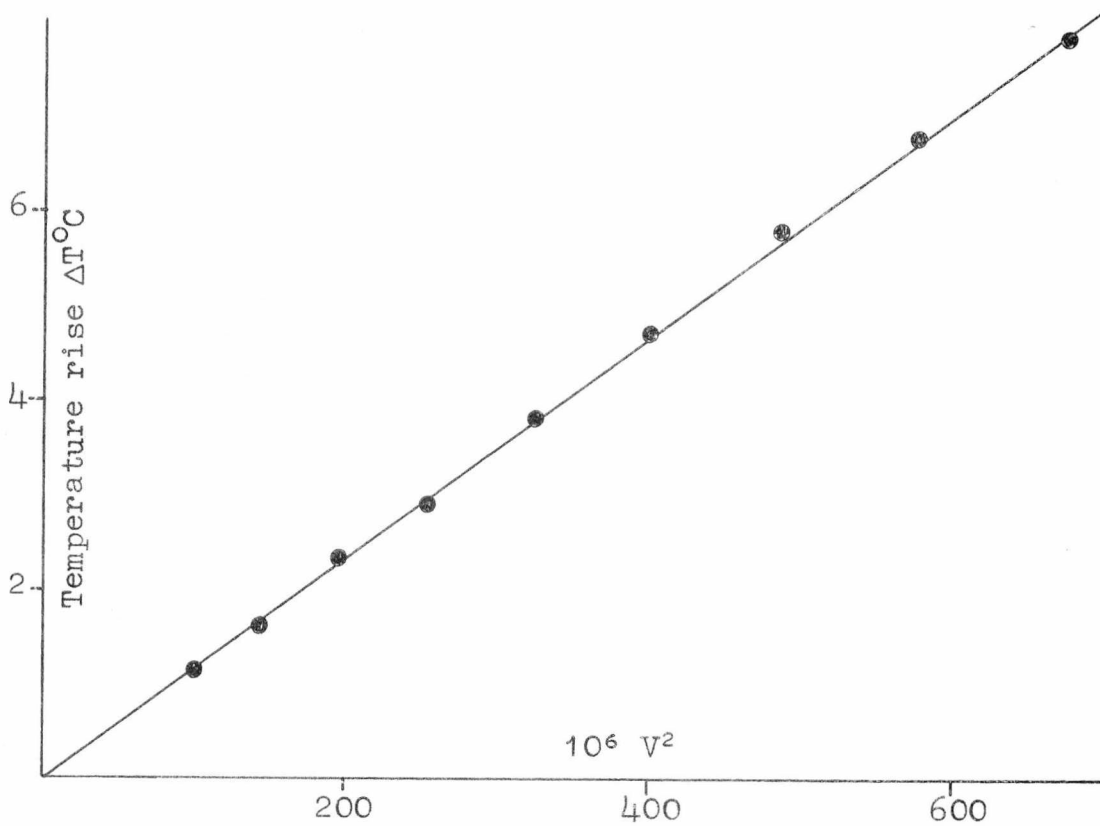


Fig. 2.5.3. Temperature rise vs. the square of the discharge voltage.

2.6 pH measurement

Three pH meters were used for this work: a Radiometer PHM4, a Radiometer PHM26 and an E.I.L. Vibron Electrometer model 33B with a C33B.2 measuring unit.

Electrodes. Because of the low solubility of potassium perchlorate it was found to be impossible to measure the pH of a perchlorate solution using a normal calomel electrode with a potassium chloride salt bridge, so reference electrodes based on lithium chloride and sodium chloride were used with the Radiometer and Vibron pH meters respectively. Details of the electrodes used are given below.

<u>Manufacturer</u>	<u>Medium</u>	<u>Glass</u>	<u>Calomel</u>
Radiometer	nitrate	G202C	K101
	perchlorate	G202C	K901
E.I.L. Vibron	nitrate	GHSN 33C	RJ 23/1
	perchlorate	GHSN 33C	RJ 23/2

For measuring the pH of small volumes of solution a type 9259/81 dual electrode was used in conjunction with the Vibron pH meter and a type GK 2321 with the Radiometers.

Experimental procedure. Before beginning a kinetic or spectrophotometric run, the electrodes were standardised against N.B.S. standard borax and phthalate buffers. Before measuring the pH of a test solution, the electrodes were standardised against the standard buffer (borax, phosphate or phthalate) closest to the pH to be measured. Between measurements, the electrodes were washed with distilled water and dried with tissue paper.

2.7 Spectrophotometers

All stability constant work was carried out on a Pye Unicam SP8000 u.v.-visible scanning spectrophotometer. For work which involved measuring small optical density changes, a Perkin-Elmer 402 u.v.-visible scanning spectrophotometer with five times scale expansion was used; where accurate fixed wavelength optical densities were required, a Hitachi Perkin-Elmer 139 spectrophotometer was used.

The linearity of the absorbance scale of the SP8000 was checked at 410 nm by taking accurately known dye concentrations and plotting the observed optical density against the optical density calculated from accurate measurements on the Hitachi spectrophotometer (fig. 2.7.1).

2.8 Thermostating

The thermostating of the spectrophotometers and the temperature-jump equipment was achieved by means of a thermistor arrangement which controlled the temperature to better than 0.05°C over the range -10 to 40°C . The pH meter baths were thermostatted using a simple relay controlled by a mercury contact thermometer, keeping the temperature constant to $\pm 0.1^{\circ}\text{C}$.

2.9 General experimental procedure

Particular care had to be taken in the preparation of solutions for high temperature runs and for those approaching the rise-time of the apparatus. Under these conditions, minute solid particles can give rise to poor traces and so all stock solutions were filtered using millipore filters (AAWP 025 00 AA 0.8μ) and solutions were degassed to

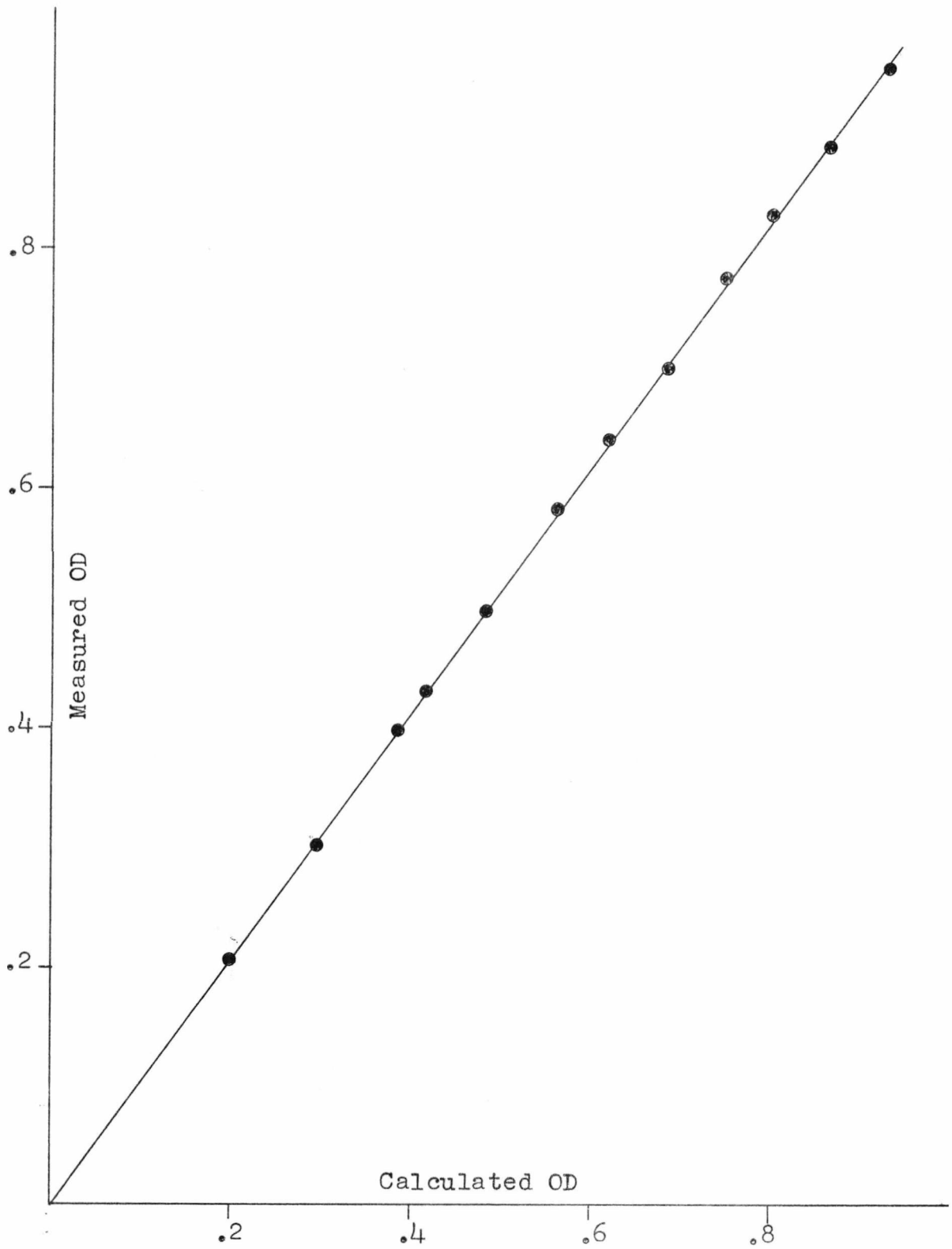
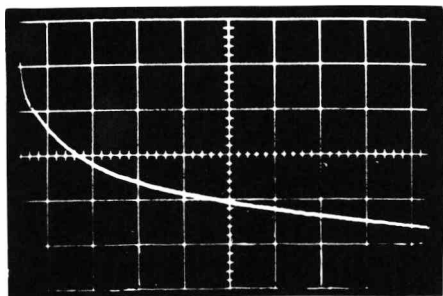
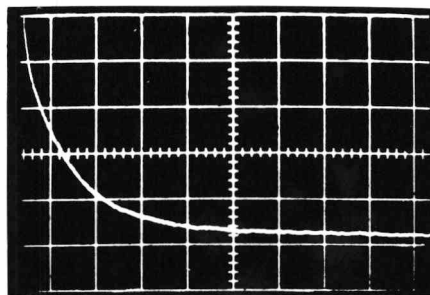


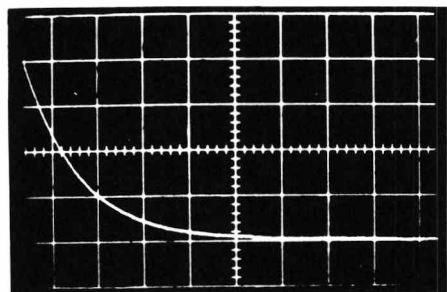
Fig. 2.7.1. Calibration of SP8000 spectrophotometer.



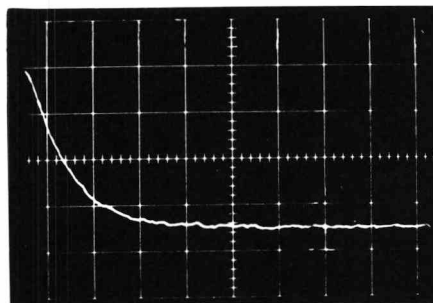
MgUDA⁻ (1.05:1) + NSA²⁻
 22°C, [Mg] = 1.05 x 10⁻²M,
 pH 8.76, time base .5 ms.



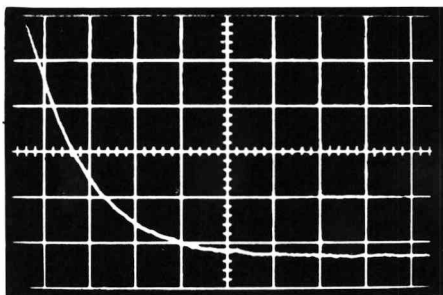
MgUDA⁻ (1:1) + NSA²⁻, 22°C,
 [Mg²⁺] = 1 x 10⁻²M,
 pH 8.76, time base .5 ms.



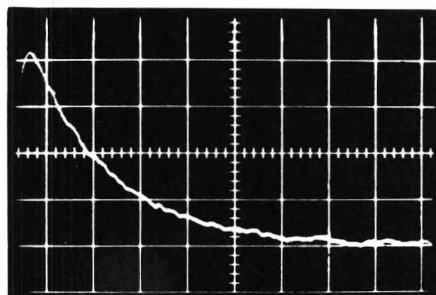
Mg(H₂O)₆²⁺ + NSA²⁻, 22°C,
 [Mg] = 5 x 10⁻⁴M,
 pH 8.76, time base 5 ms.



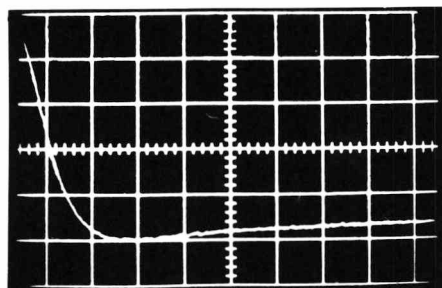
Zndien²⁺ perchlorate + NSA²⁻,
 20°C, [Zndien] = 7.2 x 10⁻³M,
 pH 7.90, time base 50 μsec.



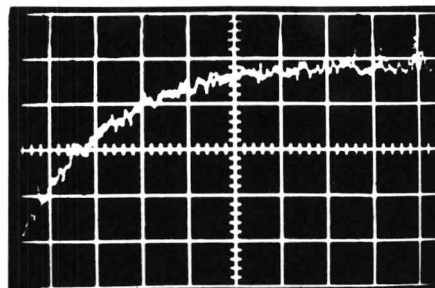
Zndien²⁺ nitrate + NSA²⁻,
 20°C, [Zndien] = 7.2x10⁻³M,
 pH 7.90, time base 50 μsec.



Zndien²⁺ chloride + NSA²⁻,
 20°C, [Zndien] = 7.2 x 10⁻³M,
 pH 7.90, time base 50 μsec.



Zn(H₂O)₆²⁺ + tris, 7°C,
 [Zn] = 1.28 x 10⁻²M,
 [tris] = 8 x 10⁻³M,
 pH 7.68, time base 5 μsec.



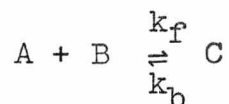
Zn(H₂O)₆²⁺ + tris, 7°C,
 [Zn] = 1.28 x 10⁻²M,
 [tris] = 8 x 10⁻³M,
 pH 7.68, time base 20 μsec.

Figure 2.9.1. Typical relaxation curves.

reduce "cavitation" effects. Degassing was achieved by inserting a syringe needle through a suba seal covering the mouth of the flask and attaching this to a vacuum line for about one minute whilst gently tapping the flask to dislodge air bubbles. The pH of the test solution was measured in a bath thermostatted at the temperature to which the kinetics refer, T_2 . The temperature-jump cell was filled from a syringe to avoid bubble formation and then placed in the thermostatted cell housing. The temperature in the cell was then measured using a chromel/alumel thermocouple, placed through the top of the cell, connected to a Comark type 1604 electronic thermometer which had been calibrated close to the initial temperature, T_1 , using an accurate mercury-in-glass thermometer. When the temperature in the cell reached T_1 , the capacitor was discharged, raising the temperature of the solution to T_2 , and the resulting relaxation trace was recorded on a storage oscilloscope and then photographed on 35 mm film using a Telford camera arrangement. This procedure was usually repeated five times for each test solution. The film was developed and the relaxation traces analysed using an exponential generator⁽⁴⁸⁾.

2.10 Treatment of data

All the systems studied were of the general form



(where both or either A and B may be involved in pre-equilibria) and so the rate constants were obtained by plotting τ^{-1} vs. $f([A] + [B])$ giving k_f and k_b as the slope and intercept respectively (see section 1.4).

The activation enthalpies for the formation and dissociation reactions were calculated using the Arrhenius equation

$$\frac{d \ln K}{d(1/T)} = - \frac{E_A}{R}$$

where the activation energy $E_A = \Delta H^\ddagger + RT$. (R is the gas constant $1.98 \text{ cal K}^{-1} \text{ mol}^{-1}$).

Thus a plot of $\log_{10} K$ vs. $1/T$ gives a straight line of slope $E_A/2.303R$, from which ΔH^\ddagger can be calculated.

The free energy of activation, ΔG^\ddagger , is obtained from transition state theory, using the equation derived by Eyring⁽⁴⁹⁾,

$$\begin{aligned} k &= \frac{kT}{h} \exp\left(-\frac{\Delta H^\ddagger}{RT}\right) \exp\left(\frac{\Delta S^\ddagger}{R}\right) \\ &= \frac{kT}{h} \exp\left(-\frac{\Delta G^\ddagger}{RT}\right) \end{aligned}$$

where k is the Boltzmann constant and h Planck's constant.

$$\text{Thus } \Delta G^\ddagger = (\log_{10} \frac{kT}{h} - \log_{10} k) 2.303 RT.$$

The activation entropy is then obtained using

$$\Delta G^\ddagger = \Delta H^\ddagger - T\Delta S^\ddagger.$$

The values of ΔG^\ddagger , ΔH^\ddagger and ΔS^\ddagger were always calculated at 298°K for the formation and dissociation reactions.

CHAPTER 3

The Coordination Number of Zinc

3.1 Introduction

It has been suggested that the wide occurrence of zinc as the native metal in metallo-enzymes is due to the ease with which it can change its geometry⁽¹³⁾. Despite Martell's suggestion that zinc generally has a coordination number of four⁽⁵⁰⁾, it has been shown by X-ray analysis that zinc can adopt coordination numbers of four, five or six, the actual number being determined by the nature of the ligands. It appears that a higher coordination number is favoured when the donor atoms are oxygen and that a lower number is favoured when they are nitrogens. Thus, for example, the maximum number of ammonia molecules which can be bound to zinc appears to be four (in the tetrahedral species $\text{Zn}(\text{NH}_3)_4^{2+}$) whereas the aquo ion ($\text{Zn}(\text{OH}_2)_6^{2+}$) contains octahedrally coordinated zinc^(6,51). The tendency of zinc to form complexes of coordination number four with nitrogen ligands is also supported by the low stability constant of the tris-ethylenediamine complex compared to those of cobalt(II) and nickel(II)⁽⁹⁾.

To enable a discussion of the kinetic results (presented in Chapters 4 and 6) it is necessary to have an indication of the coordination number of the starting complex. Because there are either experimental difficulties or because the time factor involved is so large with existing methods, it has been necessary to find a new technique for this purpose. It is a difficult problem to determine the geometry of any labile metal complex, but it is especially difficult in the case of zinc

which, because of its "closed shell" d^{10} electronic configuration, lacks suitable magnetic or spectral properties. This configuration immediately precludes the use of electron paramagnetic resonance and the diamagnetic nature of zinc systems makes it difficult to use n.m.r. techniques.

Recently, however, work has been done in which the zinc has been removed from native enzymes and replaced by cobalt(II) (52-54). This results, usually, in a less active enzyme but one which has a visible spectrum and the attendant magnetic properties of unpaired electrons. This is a useful method of examining the stereochemistry of zinc in enzymes but there is always the possibility that the two metals will be bound in slightly different positions or configurations. ^{35}Cl n.m.r. techniques have been used in an attempt to determine the number of water molecules bound to zinc in enzyme systems (55,56) but here there is the added problem that a very large excess of chloride over enzyme is required and it has been shown that the coordination number of zinc can be changed by large excesses of anions (57,58).

X-ray data on solids can obviously give unambiguous information concerning zinc stereochemistries but the structure in solution is not unequivocally the same as in the solid state. However, if the anions are bound to the metal ion in the solid state, it can be shown whether they are still bound in solution by measuring the molar conductance of the solution to determine the "ionic type" of the complex. This method cannot determine the absolute stereochemistry of the complex in solution since solvent molecules can enter the metal coordination sphere without changing the conductivity of the complex.

It has been found that in suitable cases Raman spectroscopy provides a quick and relatively easy method of determining the coordination number of zinc complexes and structural information obtained by other methods, and can be used as a check on the interpretation (section 3.2)⁽⁵⁸⁾. Another method for obtaining an indication of the coordination number of a metal complex in solution is by comparison of the thermodynamic quantities for the formation of the complex with those for the formation of analogous complexes with different metals (section 3.4).

3.2 Laser Raman Spectroscopy

3.2.1 Introduction

The medium intensity band which occurs around 450 cm^{-1} in the Raman and infra-red spectra of zinc amines has been attributed to the metal-nitrogen stretching mode by several authors^(59,60). It appears that, for octahedral complexes, the zinc-nitrogen band centre lies between 410 and 425 cm^{-1} , for five-coordinate species between 430 and 445 cm^{-1} , and for tetrahedral species between 460 and 480 cm^{-1} ⁽⁵⁸⁾. The exact position of the band seems to be independent of the number of hydrogens bound to the nitrogen; thus, for example, the isomeric amines tren and trien have zinc-nitrogen stretching frequencies of 469 and 468 cm^{-1} respectively, when the counterion is perchlorate, even though the tren complex involves a tertiary and three primary nitrogens while the trien complex has two primary and two secondary nitrogens. The metal-nitrogen frequency is also independent of the nature of the other coordinated ligands (since, for example, ZntrenBr_2 and Zntren(NCS)_2 both have bands at 440 cm^{-1}) provided that the other bound groups are not carboxylates, when there is almost

certainly coupling between the zinc-oxygen and zinc-nitrogen modes. The assignments of the zinc-nitrogen frequency are discussed in further detail in section 3.5.

The change of the zinc-nitrogen stretching frequency with coordination number can be rationalised on the basis of crowding around the central metal ion. R.J.H. Clark, in a study of titanium and vanadium halides⁽⁶¹⁾, has suggested that increasing the coordination number generally gives rise to increased bond lengths and hence lower frequency vibrations. He found that the metal halide frequency was indicative of the coordination number of the metal but independent of the nature of the bound groups (table 3.2.2.1). With a coordination number of four the metal halide band was centred around 490 cm^{-1} , and it moved to 380 cm^{-1} for six coordinate species and to 320 cm^{-1} for eight coordinate species (table 3.2.2.2).

3.2.2 Apparatus and Experimental Details

The Raman spectra of solids and concentrated solutions (usually $5 \times 10^{-1}\text{M}$) were run on a Coderg PH-1 spectrometer using excitation at 633 nm with a 150mW helium-neon laser. Spectra of dilute solutions ($5 \times 10^{-2}\text{M}$) were obtained with a Spex monochromator using the excitation at 488 nm produced by a 500mW argon laser (by courtesy of the National Physical Laboratory, Teddington). A schematic diagram of the Coderg spectrometer is shown in fig. 3.2.2.1.

The solution cell used with the Coderg spectrometer was an all-glass cell with optically ground surfaces and a path length of 2 cm while the solid samples were packed into glass bottles of 1 cm diameter. The cell containing the test substance was placed in the sample beam and the spectrum quickly

TABLE 3.2.2.1 - Effect of bound groups on the metal-chloride stretching frequency

<u>Compound</u>	<u>ν_{M-Cl} (cm⁻¹)</u>
TiCl ₄ 2.THF	371
1-4 dioxan	389
2 acetonitrile	387
2 pyridine	368
2-2' bipy	384, 366sh
0 phen	379, 356sh
VC1 ₄ 2 acetonitrile	392sh, 366s
2-2' bipy	384sh, 360s
0 phen	380sh, 361s

TABLE 3.2.2.2 - The effect of coordination number on the metal-chloride stretching frequency

<u>Compound</u>	<u>Coordination No.</u>	<u>$\nu(M-Cl)$</u>
TiCl ₄	4	490
TiCl ₄ .2L	6	~380
TiCl ₄ .2D	8	317
VC1 ₄	4	482
VC1 ₄ .2L	6	~380
VC1 ₄ .2D	8	317

where L = monodentate ligand

D = o-phenylene bis dimethylarsine

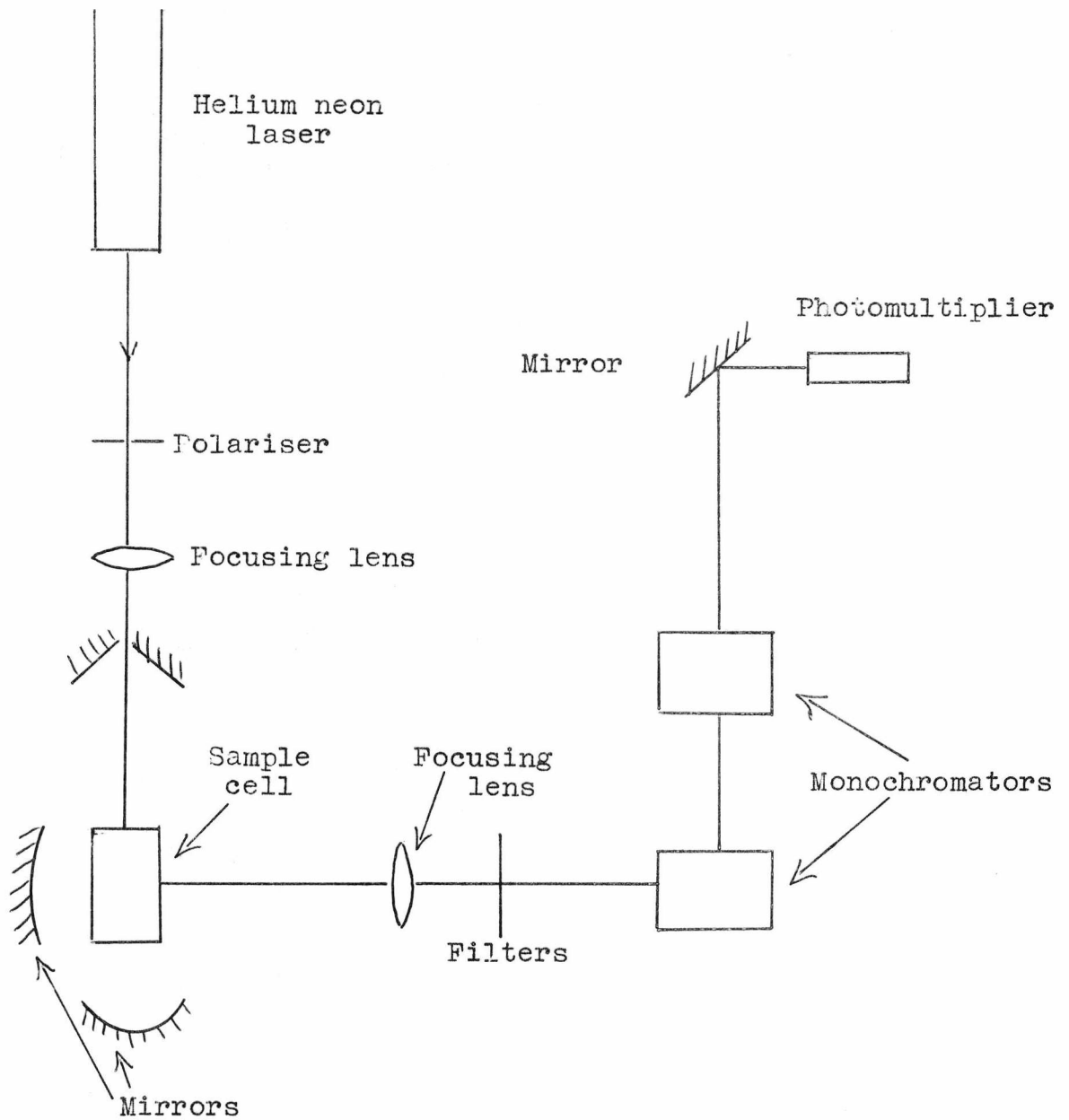


Fig. 3.2.2.1 - Schematic layout of the Coderg Raman Spectrometer.

scanned to find a strong band on which to maximise the signal to noise ratio. Then the zinc-nitrogen band was scanned two or three times, usually at 15 cm^{-1} per minute. The band centre for each spectrum was obtained by measuring from calibration marks on the chart paper. For spectra with steeply sloping baselines, the band centre was determined using a Du Pont 310 curve analyser. Spectra obtained and the positions of the band centres are shown in figs. 3.2.2.2 - 3.2.2.7 and table 3.2.2.3 respectively.

As a baseline for the Raman work, the Raman spectra have been obtained for several complexes for which X-ray data is available. The preparations of these complexes are given below.

Zntren(SCN)₂ was prepared by the method of Barclay and Bernard⁽⁶²⁾ and ZnMe₆trenBr₂ by the method of Ciampolini⁽⁶³⁾.

Zntren(ClO₄)₂.Zntren(Br)₂. 11 millimoles of tren-hydrochloride were neutralised with sodium hydroxide and the sodium chloride which was precipitated from the resulting solution by the addition of 10 ml of ethanol was filtered off. Then 10 millimoles of zinc perchlorate or bromide were added and the solution concentrated and cooled. The resulting precipitate was collected and recrystallised from water or methanol respectively, collected and dried in a vacuum desiccator.

Zn(dien)₂(ClO₄)₂ was collected as the precipitate which formed when aqueous solutions of zinc perchlorate and dien were mixed in the ratio 1:2.5. The precipitate was recrystallised from hot water and dried under vacuum.

Zn(en)₃Br₂ and Zn(sym-diMeen)₂Br₂ were prepared as in ref. 59 except that the sym-diMeen complex was recrystallised from methanol.

Fig. 3.2.2.2. Zinc Ammine Raman Spectra.

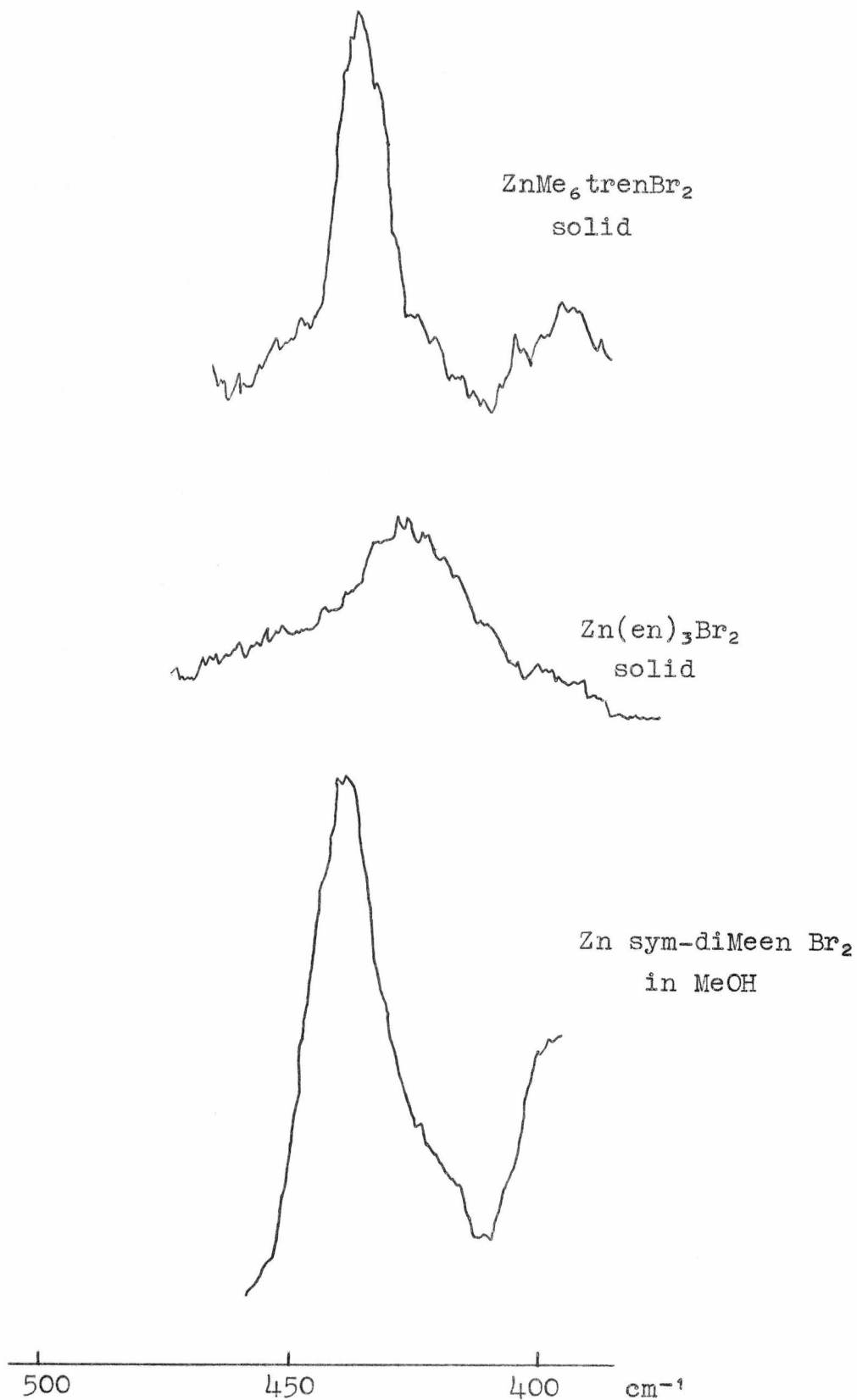


Fig. 3.2.2.3. Some Zinc tren Raman spectra.

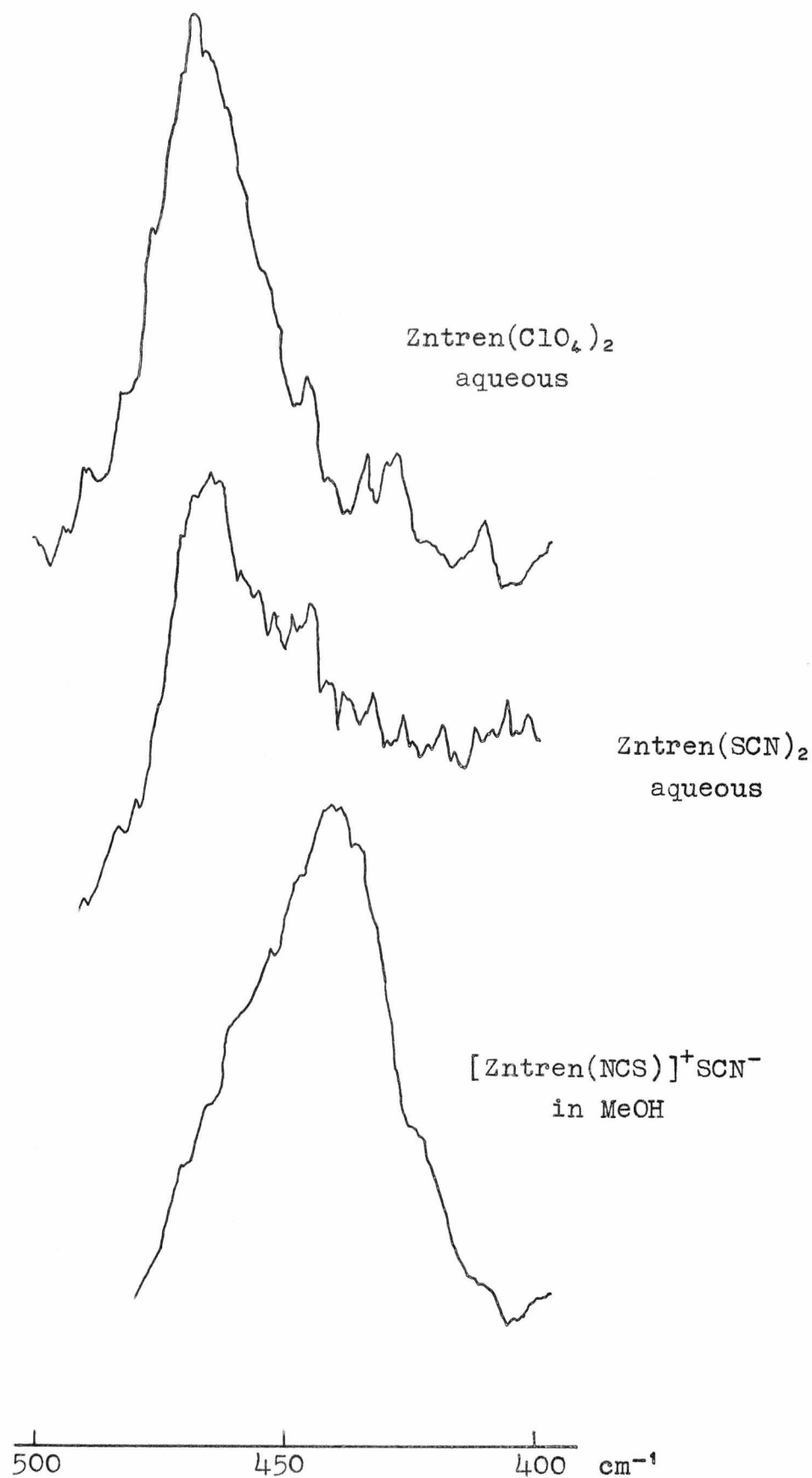


Fig. 3.2.2.4. Aqueous Raman spectra of some ZincDIEN complexes.

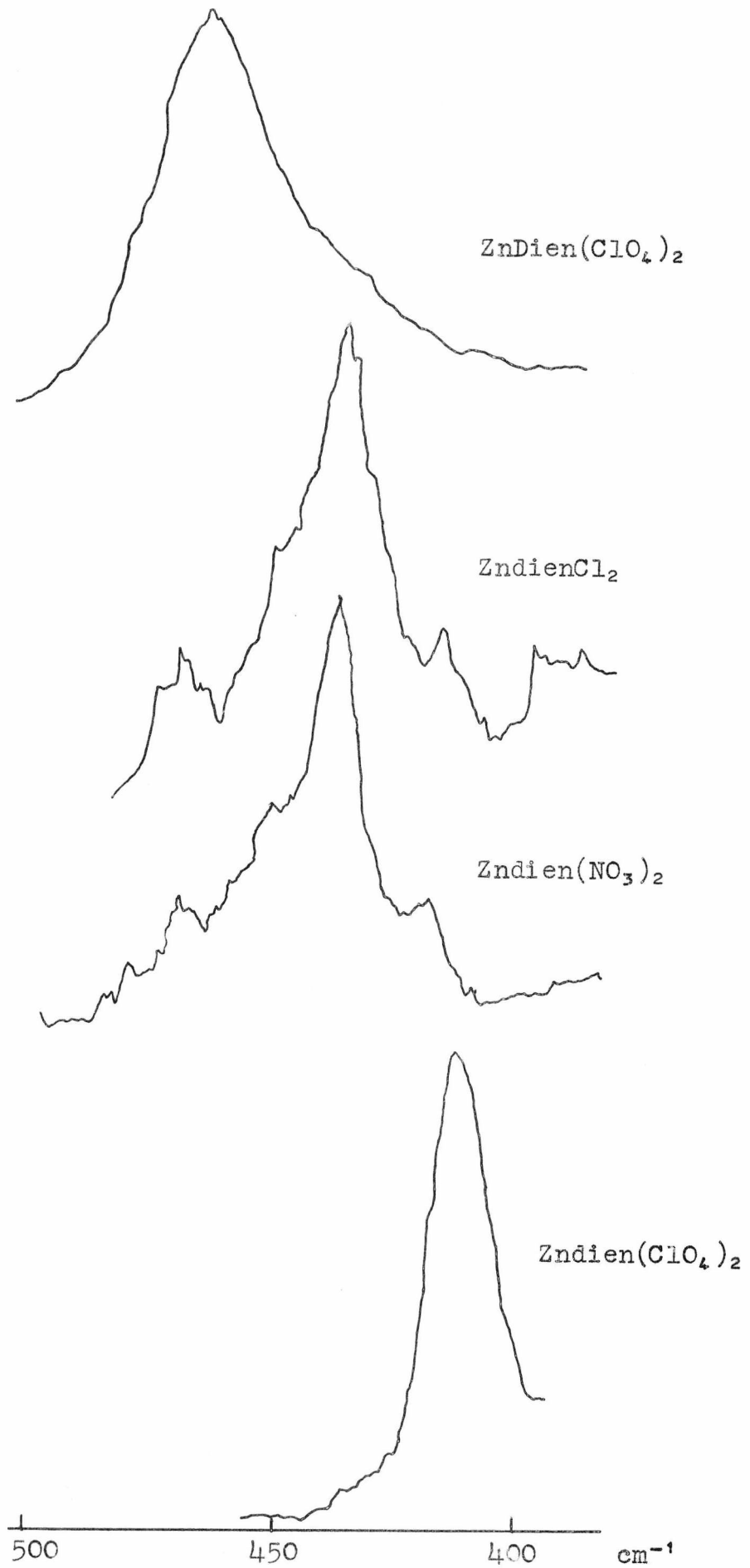


Fig. 3.2.2.5. Aqueous Raman spectra of some Zntrien complexes.

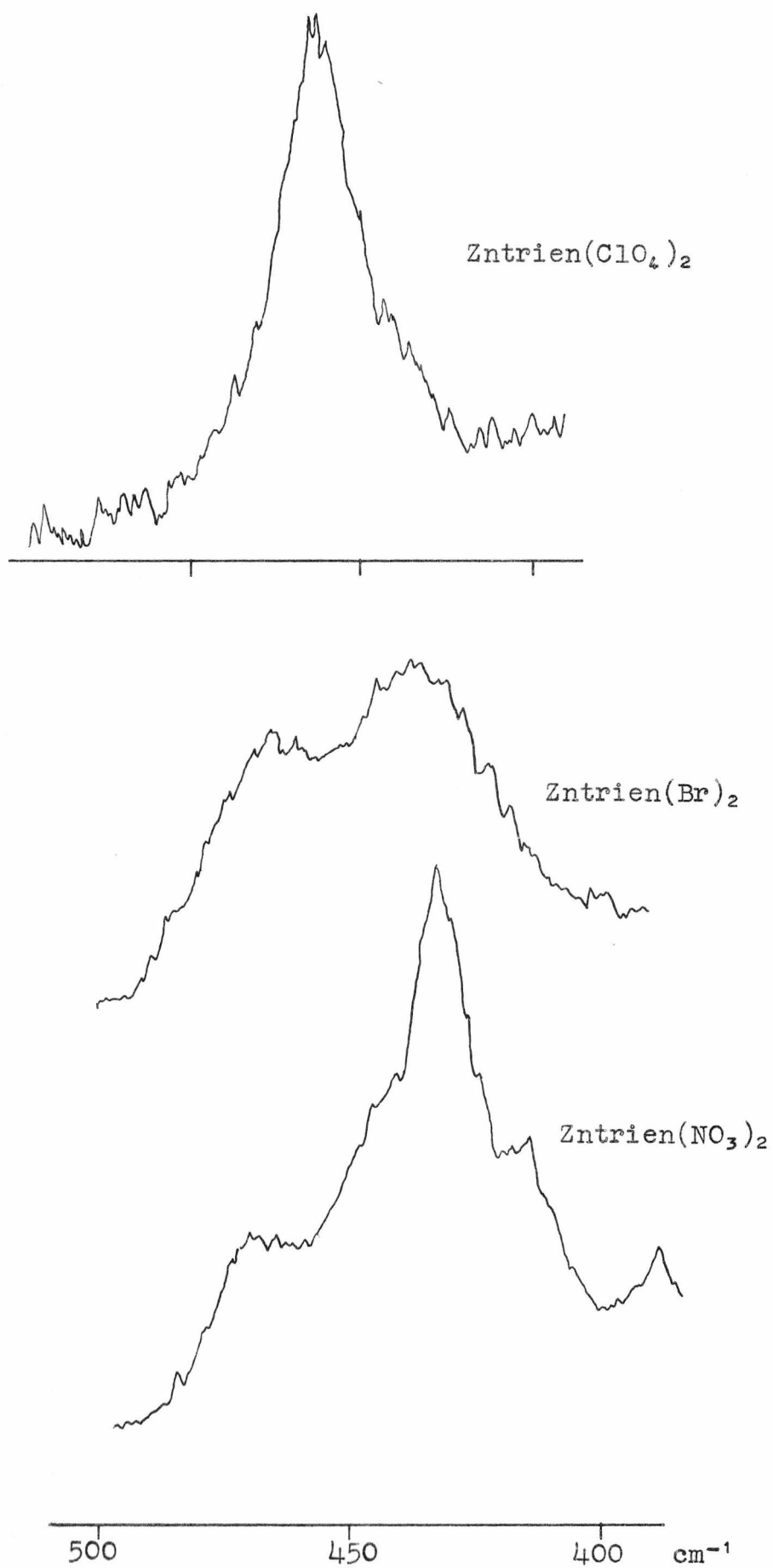


Fig. 3.2.2.6. Raman spectra of $ZnCl_2$.

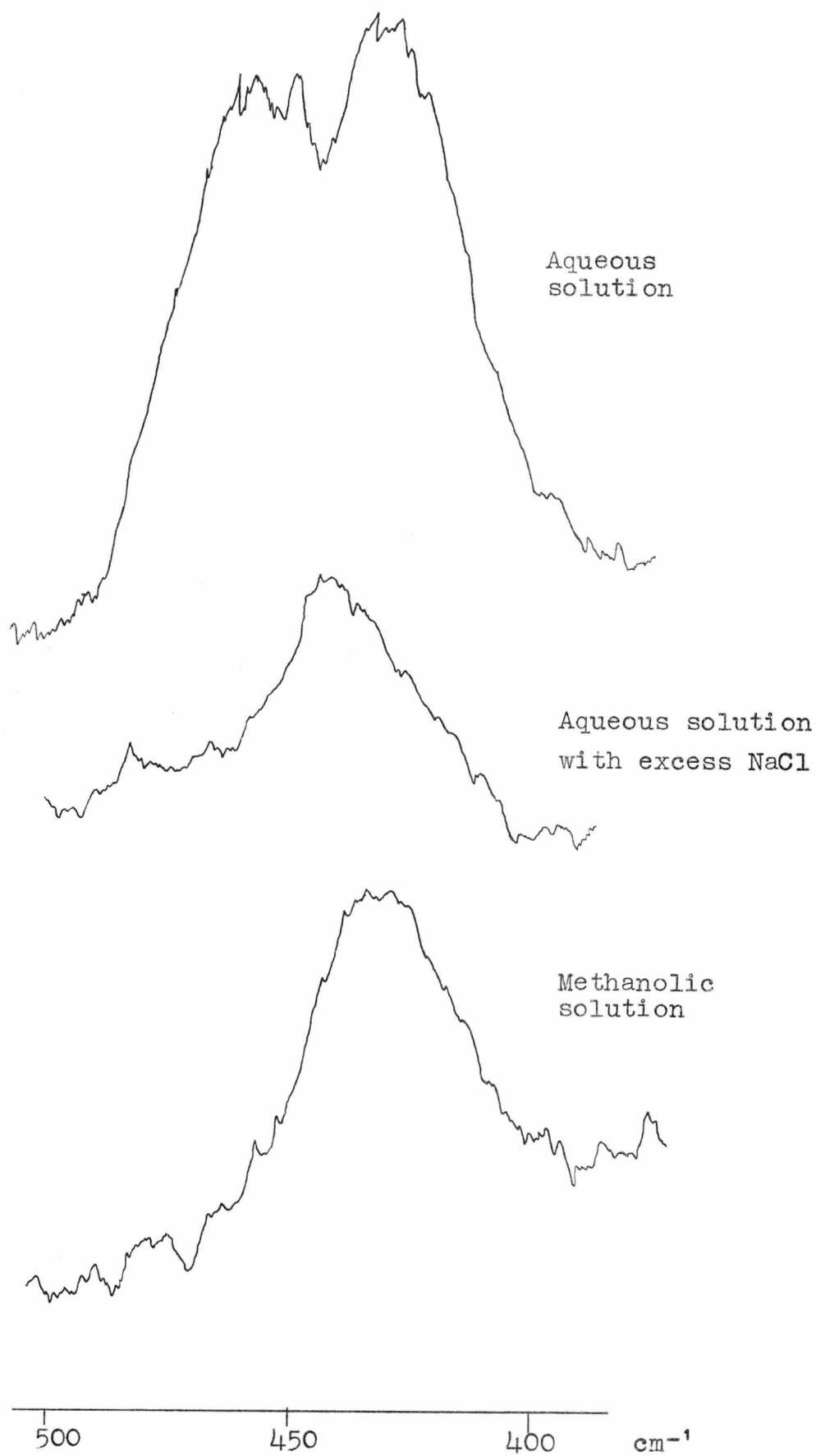


Fig. 3.2.2.7. Raman spectra of Zinc 2,3,2 Tet CO_4 at varying pH at 25°C.

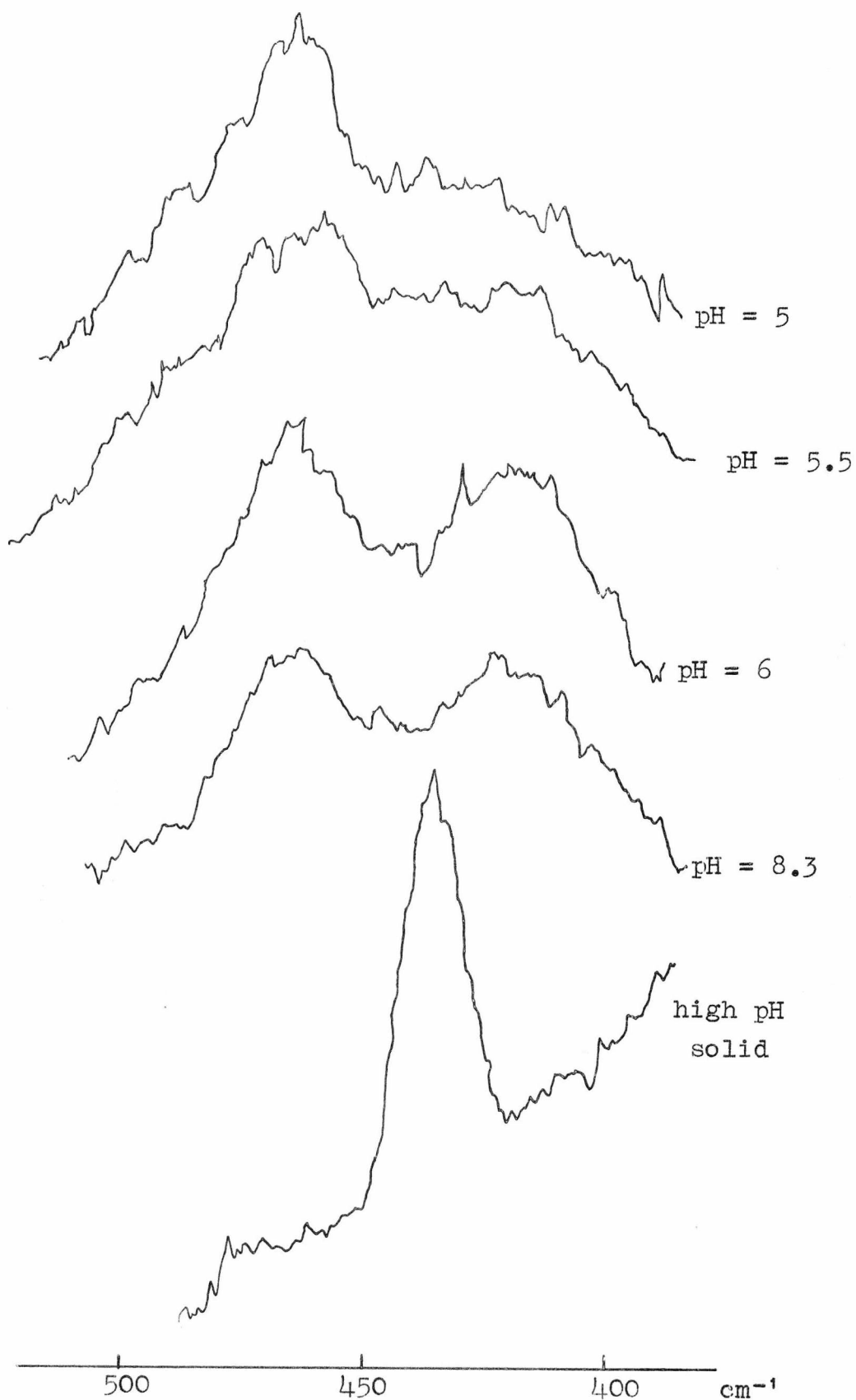


TABLE 3.2.2.3. Zn-Nitrogen Stretching Frequencies (cm⁻¹)

ZnMe ₆ trenBr ₂	solid	436
	solid	440
Zntren(NCS) ₂	MeOH	437
	aqueous	467
	solid	440
ZntrenBr ₂	aqueous (5x10 ⁻²)	473
	solid	469
Zntren(ClO ₄) ₂	aqueous	468
	solid	420
Zn(en) ₃ Cl ₂	aqueous	423
	solid	425
Zn(en) ₃ Br ₂	aqueous	425
	solid	424
Zn(dien) ₂ (ClO ₄) ₂	solid	424
	solid	421
Zn(sym-diMeen)Br ₂	aqueous	438
	aqueous	419
Zn(dien) ₂ (ClO ₄) ₂	aqueous	462
	aqueous	435
	aqueous	437
	solid	468
Zntrien(ClO ₄) ₂	MeOH	467
	aqueous	466
	MeOH	431
ZntrienCl ₂	aqueous	431, 462
	aqueous excess Cl ₂	431
	aqueous	433
Zntrien(NO ₃) ₂	aqueous	433
Zntet(ClO ₄) ₂	aqueous	465, 421
Zntet(NO ₃) ₂	aqueous	433, 410

Zntrien(ClO₄)₂ was collected from a 1:1 mixture of aqueous zinc perchlorate and trien which was left to evaporate slowly.

All the complexes were characterised by C, H and N analyses which gave reasonable agreement with the calculated values.

3.3 Conductivity Measurements

Since the time of Werner, conductivity measurements have been used in the investigation of the structure of complex salts. The "ionic type" of the unknown complex is determined by comparing its molar conductance with those of a series of electrolytes of known type. An illustration of the molar conductance for a series of Co(III) complexes is shown in fig. 3.3.1.⁽⁶⁴⁾

In this work, the conductivity of a series of zinc complexes was measured using a Wayne-Kerr B221 conductance bridge thermostatted at 25°C. The cell constant was measured using 10⁻²M potassium chloride as described in ref. 65. The solutions for the conductivity measurements were usually made up to concentrations of 10⁻²M in water or 10⁻³M in methanol, starting from the solid complexes or a suitable mixture of the components. The molar conductances of zinc nitrate and sodium tetraphenylboron were used as the reference points for 2:1 and 1:1 electrolytes, respectively. The molar conductivities of the complexes investigated are shown in table 3.3.1.

3.4 Thermodynamics of Metal Complex Formation

When a complex is formed between a multidentate ligand and a metal ion, a large redistribution of solvent molecules occurs and, associated with this, are characteristic changes

Fig. 3.3.1. The molar conductances of a series of Co(III) complexes at 25°C.

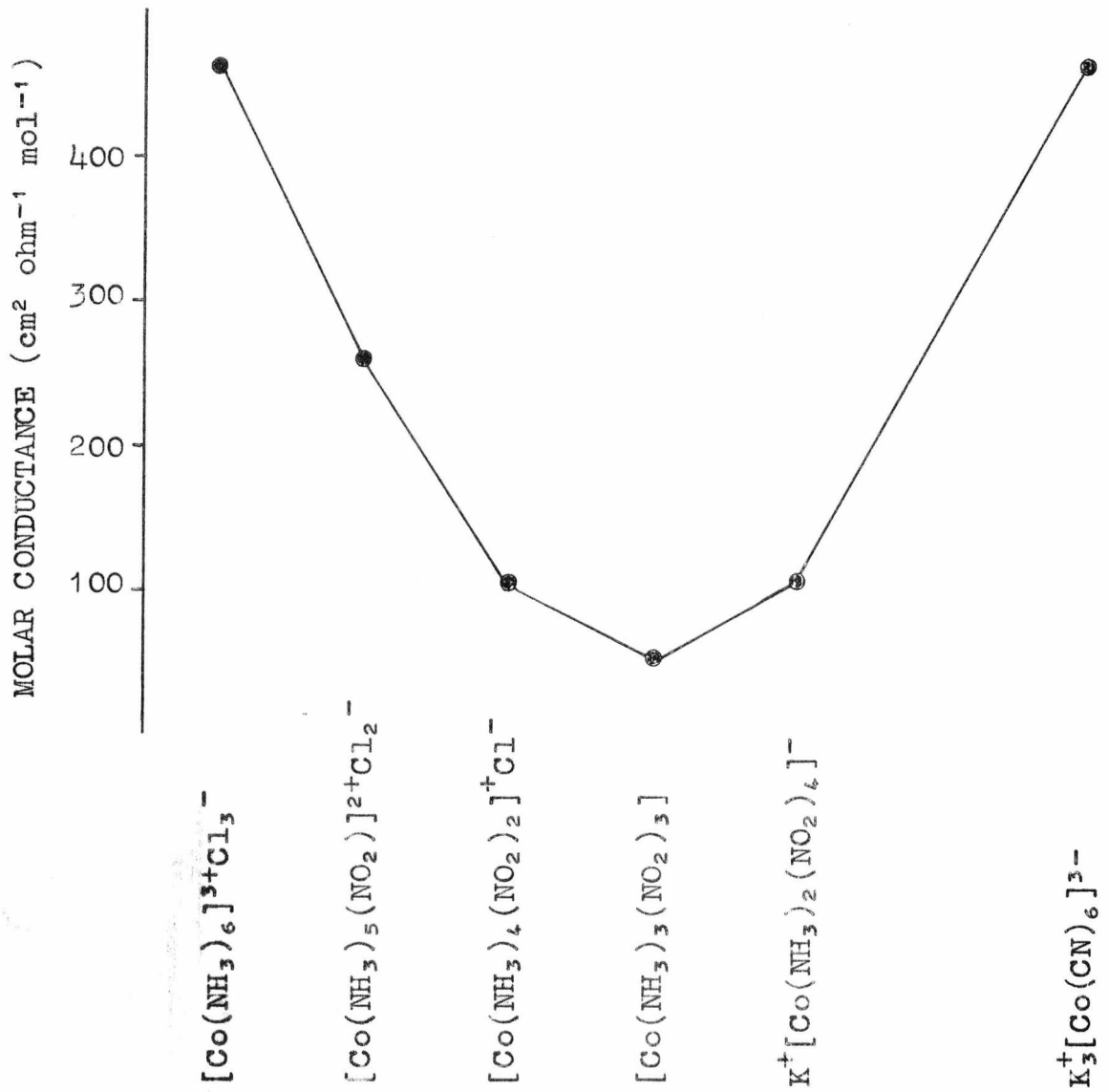


TABLE 3.3.1. Molar conductivities of Zinc complexes

<u>Compound</u>	<u>Water</u>	<u>Methanol</u>
Zn(tren)(SCN) ₂	212	100
Zn(tren)(ClO ₄) ₂	180	162
Zn(tren)Br ₂	182 ^a	101 ^a
Zn(en) ₃ Br ₂	201	97
Zn(dien) ₂ (ClO ₄) ₂	176	136
Zn(dien)(ClO ₄) ₂	214 ^a	-
Zn(trien)(ClO ₄) ₂	198	166
Zn(trien)Cl ₂	198 ^a	93 ^a
Zn(s-diMeen) ₂ Br ₂	-	72 ^b
Zn(H ₂ O) ₆ (NO ₃) ₂	202	-
NaB(Ph) ₄	63	64

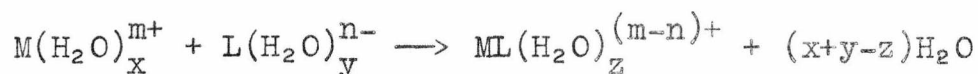
a. Measurement made on mixed components.

b. Value in nitroethane 18cm² ohm⁻¹ mol⁻¹.

Values are given in cm² ohm⁻¹ mol⁻¹ and all data refer to 25°C.

in the entropy and enthalpy of the system. These changes (especially that in entropy) can be used to diagnose the structure of the complex.

In the general case



the release of water molecules from the inner and outer coordination sphere of the metal ion and the first solvation shell of the ligand contributes in a positive sense to the overall entropy change in the system. Countering this will be negative entropy contributions caused by the loss of translational entropy of the ligand and metal ion when the complex is formed and by the hydration of the metal complex. So, for complex formation the observed overall entropy change, ΔS_{obs} , comprises four terms:

$$\Delta S_{obs} = -\bar{S}_M - \bar{S}_L + \bar{S}_{ML} + (x+y-z)\Delta S_{H_2O}$$

where \bar{S}_M , \bar{S}_L and \bar{S}_{ML} are the partial molar entropies of the metal ion, the ligand and the complex respectively and $(x+y-z)\Delta S_{H_2O}$ represents the entropy change associated with the change in hydration of the species in solution. Several workers have measured values of \bar{S}_M and the values used in the following discussion (shown in table 3.4.1) are taken from reference 66.

TABLE 3.4.1. Ionic entropies at 25°C relative to $\bar{S}_{H^+} = 0$ for the formation of the aquo metal species.

<u>Ion</u>	\bar{S}_M cal.deg ⁻¹ mol ⁻¹
Mn ²⁺	-18
Co ²⁺	-22
Ni ²⁺	-23
Cu ²⁺	-23.6
Zn ²⁺	-25.5

For complex formation between a particular ligand and a range of similar metals, e.g. the first transition series, the value of \bar{S}_L will be constant and \bar{S}_{ML} can be assumed to be constant. Thus, if the value of \bar{S}_M is subtracted from ΔS_{obs} , comparative values of $(x+y-z)\Delta S_{H_2O}$ can be obtained for the various metals. A large difference in this value from one metal to another probably indicates the release of differing numbers of water molecules on complex formation. This type of treatment must be used with great caution because the formation of, say, a tetrahedral complex from an octahedral aquo metal ion would be expected to give a large entropy change but at the same time the tetrahedral complex allows water molecules of the second coordination sphere to approach closer to the metal ion. Thus the metal ion has a greater ordering influence over these water molecules in a tetrahedral complex compared to an octahedral complex and so reduces the overall entropy change. Therefore, it is only reasonable to discuss large entropy variations.

It is more difficult to discuss coordination changes on the basis of enthalpy changes. This is because the enthalpy change associated with the replacement of a metal-water bond by a metal-ligand bond is generally small and also because there is much less regularity in ΔH values than in ΔS values when a wide variety of metal ions and ligands are considered. Recently, however, an attempt has been made by Degischer and Nancollas⁽⁶⁷⁾ to separate the enthalpy changes for complex formation into temperature dependent and temperature independent components and, from the latter, to discuss the number of bonds formed in the complex.

3.5 The stereochemistry of zinc-ammines

3.5.1 Zinctren

The structures of $\text{Zntren}(\text{NCS})_2$ (68,69) and $\text{ZnMe}_6\text{trenBr}_2$ (63,70) have been determined by X-ray methods. Both have been shown to contain five-coordinate zinc, with the ligands arranged towards the corners of a trigonal bipyramid, in which the fifth coordination position is occupied by one of the anions. In both cases the Raman spectrum of the solid shows one band centred around 440 cm^{-1} (figs. 3.2.2.2, 3.2.2.3). When $[\text{Zntren}(\text{NCS})](\text{SCN})$ is dissolved in methanol its Raman band remains at 440 cm^{-1} and the molar conductance corresponds to that for a 1:1 electrolyte (table 3.3.1; cf. ref. 63) suggesting that the zinc-containing species is again the five-coordinate ion $[\text{Zntren}(\text{NCS})]^+$. However, when the complex is dissolved in water its Raman band moves to 467 cm^{-1} while the molar conductance is that of a 2:1 electrolyte. This could be explained either by the formation of a tetrahedral species $[\text{Zntren}]^{2+}$ or by the thiocyanate being replaced by one or two water molecules; the comments of Irving and Williams⁽¹¹⁾ support the suggestion that the coordination number is reduced to four. The Raman spectrum of solid $\text{Zntren}(\text{ClO}_4)_2$ shows one band at the same frequency (467 cm^{-1}) as that formed for aqueous $\text{Zntren}(\text{NCS})_2$ and the conductivity of a methanolic solution indicates that it is a 2:1 electrolyte. The conductance and the position of the Raman band are unchanged on dissolving $\text{Zntren}(\text{ClO}_4)_2$ in water. The difference in behaviour between Zntren thiocyanate and perchlorate is reasonable in view of the different complexing abilities of the two anions. On this basis it would be expected that, in the solid state, ZntrenBr_2 contains the five-coordinate species $[\text{ZntrenBr}]^+$. The position of the Raman band

440 cm^{-1} , confirms this suggestion and it is also in agreement with the conclusions of Interrante⁽⁷¹⁾ based largely on infrared spectroscopic measurements.

The spectroscopic data on tren complexes indicates that any structural assignments made solely on the basis of thermodynamic data should be treated with great caution. From an examination of the ΔS° values obtained by Ciampolini et al. (fig. 3.5.1) for the complexes of tren with metal ions of the first transition series, it appears that the same number of water molecules are displaced on complex formation for all the metals⁽⁷²⁾. The X-ray structure determination of Nitren(SCN)₂ shows that the nickel atom is in an octahedral environment with two cis thiocyanate ions completing the inner coordination sphere.⁽⁷³⁾ This is in agreement with the assignment made by Jørgenson⁽⁷⁴⁾, based on the solution visible spectrum of this complex, in which two water molecules replace the thiocyanates. In contrast, the reflectance spectra of CotrenI₂ and Cotren(SCN)₂⁽⁷⁵⁾ show that the metal is in a five-coordinate environment and water exchange measurements on the copper complex indicate that the copper complex is also five coordinate⁽⁷⁶⁾.

3.5.2. Zn(en)_n.

The Raman spectrum of aqueous Zn(en)₃Br₂ is concentration dependent. A concentrated solution ($>5 \times 10^{-1}\text{M}$) shows only one band at 425 cm^{-1} identical with that of the solid and the complex is assumed to be octahedral. On dilution to $5 \times 10^{-2}\text{M}$, a second band appears at 467 cm^{-1} , as noted by Plane⁽⁵⁹⁾ using Zn(en)₃Cl₂. Using a stability constant of $10^{1.86}$ ⁽⁷⁷⁾ for the formation of [Zn(en)₃]²⁺, it is possible to calculate the concentrations of Zn(en)₃²⁺ and Zn(en)₂²⁺ in the $5 \times 10^{-2}\text{M}$ solution; they are $3.4 \times 10^{-2}\text{M}$ and $1.6 \times 10^{-2}\text{M}$, respectively. Thus, the

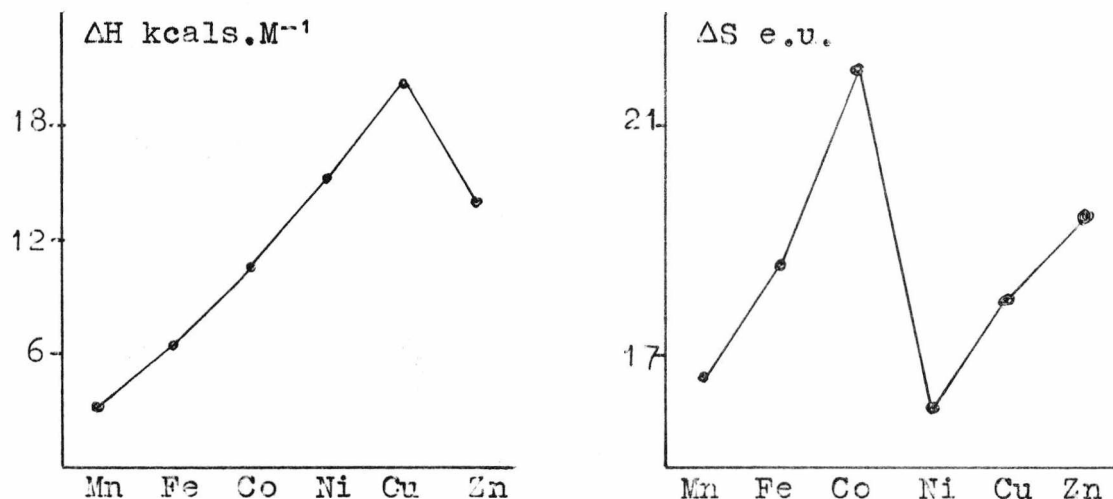


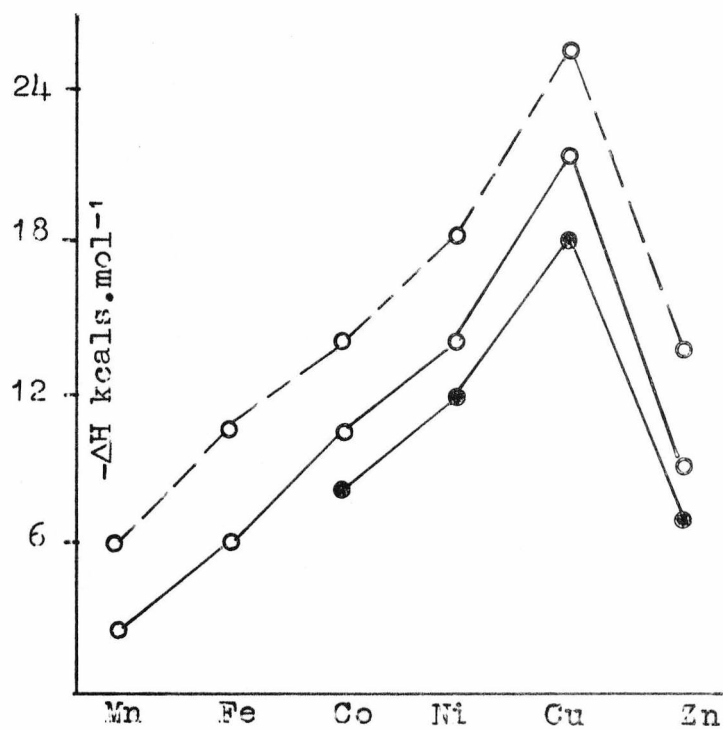
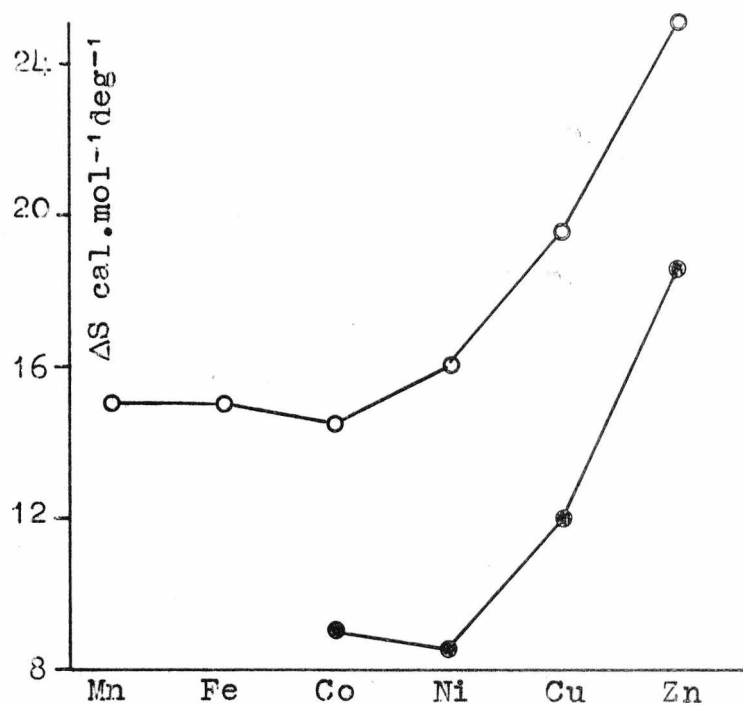
Fig. 3.5.1. Thermodynamic parameters for [Mtren]²⁺.

new band at 467 cm⁻¹ is assigned to the species Zn(en)₂²⁺, for which the thermochemical evidence of Ciampolini et al.⁽⁵⁷⁾ favours a tetrahedral geometry.

3.5.3. Zndien

The thermodynamic data of Ciampolini et al.⁽⁷⁸⁾, shown in fig. 3.5.2., indicate a particularly low heat of formation for the zinc dien complex (less than the value for the [Znen]²⁺ ion in which one less metal-nitrogen bond is formed). The authors suggest that this can be explained by the release of more than three water molecules from the inner coordination sphere of the zinc in the case of the dien complex and that the complex is tetrahedral. The variation of ΔH° along the transition metal series Mn²⁺ to Zn²⁺ runs parallel to that for the M(en)₂ complexes (fig. 3.5.2) where a tetrahedral configuration was assigned to the zinc complex⁽⁵⁷⁾.

The Raman spectra of several zinc dien species are shown in fig. 3.2.2.4. From these it can be seen that the position of the band centre is dependent on the counter-ion present.



● — [Mdien]²⁺ ○ — [Mtrien]²⁺ - - ○ - - [M(en)₂]²⁺

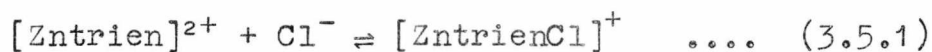
Fig. 3.5.2. Thermodynamic parameters for complex formation between some polyamines and the first row transition metals.

The spectrum of the perchlorate salt, in which the anion is thought not to bind, indicates a tetrahedral species in the solid state and solution and the conductivity measurements show that the complex is a 2:1 electrolyte. Hence the fourth coordination position must be taken up by a water molecule (see Chapter 6). The spectra of both the nitrate and chloride complexes have band centres around 440 cm^{-1} and it therefore appears that both are five-coordinate complexes. It is not possible to say whether one or both counter-ions are bound to the metal in aqueous solution from conductivity measurements since, at the concentrations used (ca 10^{-2}M), it is likely that the anions will have dissociated from the metal complex in view of the probably low stability constant for the formation of the anion complexes (see Chapter 6). However, it seems reasonable to assume that only one of the chloride anions is bound to the metal since it is possible to make solutions of at least 0.5M without precipitation and it is therefore unlikely that the complex is a non-electrolyte. Thus, in the chloride complex, the coordination shell of zinc dien must be expanded without the replacement of the water molecule while in the case of the nitrate complex there is the additional possibility that the anion acts as a bidentate ligand.

The thermodynamic parameters for the formation of metal-trien complexes (fig. 3.5.2) show a remarkable resemblance to those of the dien and bis-ethylenediamine systems. This, and the fact that there is a marked difference between the ΔS_{obs} values for the zinc and nickel complexes (the latter has been shown to be octahedral on the basis of its visible spectrum⁽⁸⁰⁾), has led Ciampolini et al. to suggest that the zinc is in a tetrahedral environment.⁽⁷⁹⁾

3.5.4 Zntrien

The Raman spectra of zinc trien with several anions is shown in fig. 3.2.2.5. The spectra are anion-dependent, that of the perchlorate being typical of a tetrahedral zinc species. The spectrum of solid ZntrienCl₂ has a main band at 431 cm⁻¹, as does that of the solution in methanol, but that of an aqueous solution has an additional band at 462 cm⁻¹ (fig. 3.2.2.6). The addition of sodium chloride to this solution leads to the disappearance of the band at 462 cm⁻¹ with a concomitant increase in the intensity of the 431 cm⁻¹ band. This can be explained in terms of the formation of a complex between [Zntrien]²⁺ and chloride which has a low stability constant. In aqueous solution the complex is partially dissociated to give a mixture of the tetrahedral [Zntrien]²⁺ species and the five-coordinate [ZntrienCl]⁺ species; the addition of sodium chloride displaces the equilibrium (3.5.1.) to the right.



In methanol the equilibrium is displaced even further to the right because the formation of complexes of low charge is favoured by the lower polarity of the solvent giving an enhanced stability to the chloride complex relative to (Zntrien)²⁺ (cf. the stability constants for [ZnCl]⁺ in water and ethanol^(81,82)). This interpretation is confirmed by the conductivity measurements of zinc trien complexes in methanol and water. These show that Zntrien(ClO₄)₂ is a 2:1 electrolyte in both solvents, while ZntrienCl₂ behaves as a 2:1 electrolyte in water and a 1:1 electrolyte in methanol. The replacement of perchlorate by nitrate as the counter-ion also gives rise to changes in the Raman spectra, indicating a change in the coordination number of the zinc from four to five.

3.5.5 Zn 2,3,2-tet

No thermodynamic data is available for the formation of metal 2,3,2-tet complexes, although the stability constants, which have been determined by Margerum et al.⁽⁸³⁾, are very similar to those of the corresponding trien complexes. Margerum suggests, on the basis of model building, that 2,3,2-tet should be able to adopt a tetrahedral configuration around metal ions with fewer steric constraints than trien and that the slightly increased stability of zinc tet compared to zinc trien is a reflection of this.

The low pH Raman spectrum of a solution of zinc tet(ClO₄)₂ is in agreement with the tetrahedral assignment but, as the pH is increased, a second band appears at lower frequency, indicating an increase in coordination number of the zinc complex (fig. 3.2.2.7). Unfortunately, at the metal concentrations necessary to obtain clear Raman spectra with the Coderg spectrometer, it was not possible to use higher pH values than 8.5 without precipitation and so the high pH spectrum could not be obtained. The solid which precipitates has a spectrum corresponding to a five coordinate species but for a complete assignment some work on lower concentration solutions using the Spex monochromator (which we do not have at Canterbury) should be very informative. As with the trien system, the use of nitrate as the counter-ion produces a change in the Raman spectrum and at intermediate pH's there are two distinct bands, indicating the presence of five- and six-coordinate species. Thus, it seems likely that the hydroxide ion as well as the nitrate ion can increase the coordination number of zinc tet.

3.6 The Stereochemistry of Oxygen-containing Zinc Complexes

Unfortunately, no structure determinations have been carried out on any of the complexes used in the kinetic experiments and the only way at present to obtain an indication of the stereochemistry of these complexes is from thermodynamic parameters.

3.6.1 Zinc Nitrilotriacetate

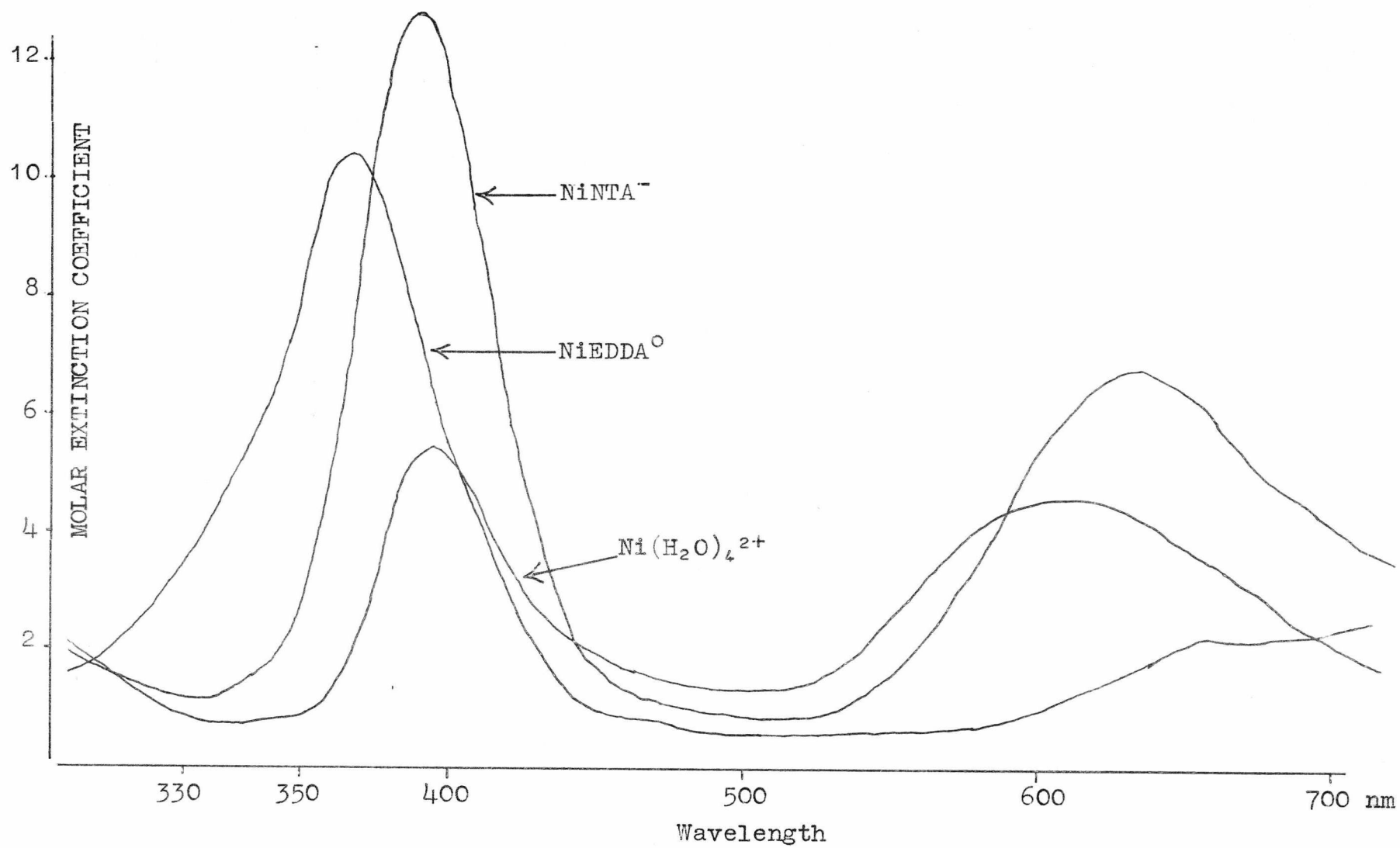
The thermodynamic table of Hull et al.⁽⁶⁶⁾, shown in table 3.6.1 for the formation of 1:1 metal-NTA complexes suggest that the manganese, nickel, zinc and probably cobalt complexes contain the same number of water molecules.

TABLE 3.6.1. Overall entropy changes for the formation of metal-NTA complexes ($\mu = 0.1M NaNO_3$)

<u>Metal ion</u>	ΔS_{obs}	$\Delta S_{obs}^{\circ} + S_M^{\circ}$
Mn	37.9	19.9
Co	47.1	25.1
Ni	44.1	21.1
Cu	53.0	29.4
Zn	46.0	20.5

It has been shown by infra-red spectroscopy that all the carboxylates and the nitrogen are bound to the metal atom for the cobalt, nickel and zinc complexes.⁽⁸⁴⁾ The visible spectrum for the nickel complexes is indicative of an octahedral complex⁽⁸⁵⁾ whilst the spectra for copper⁽⁸⁶⁾ and cobalt⁽⁸⁷⁾ suggest that there is some degree of tetragonal distortion in these complexes (this could account for the slightly larger value of $\Delta S_{obs}^{\circ} + \bar{S}_M^{\circ}$ for these complexes). It, therefore, seems reasonable to assign an octahedral configuration to the zinc complex and as the conformation of the ligand prevents it from occupying the four planar positions in the octahedron (cf. the similar ligand tren⁽⁸⁸⁾) the two water molecules completing the inner coordination sphere must occupy cis positions.

Fig. 3.6.1. Visible spectra of Ni(II) species.



3.6.2 Zinc iminodiacetate

Because of the similarity between IDA and NTA one would expect them to take up similar coordination positions on metal complex formation and this is confirmed by the thermodynamic parameters obtained by Anderegg⁽⁸⁹⁾ shown in table 3.6.2.

TABLE 3.6.2. Entropy changes for the formation of 1:1 metal IDA complexes ($\mu = 0.1M KNO_3$)

<u>Metal</u>	ΔS_{obs}	$\Delta S_{obs}^{\circ} + \Delta S_M^{\circ}$
Mg	23.5	-4.7
Co	24.6	2.6
Ni	20.0	-3.0
Cu	33.3	9.7
Zn	25.7	0.2

The visible spectra of the cobalt(II) and nickel(II) complexes suggest that both these complexes are octahedral^(85,87) and the $\Delta S_{obs} + \bar{S}_M^{\circ}$ values indicate that all the above complexes, except that of copper, have the same coordination number. The zinc complex is thus assumed to be octahedral.

3.6.3 Zinc N,N' ethylenediaminediacetate

The similarity between the $\Delta S_{obs} + \Delta S_M^{\circ}$ values for nickel(II) and zinc(II) EDDA leads to the conclusion that these two complexes have the same coordination number, table 3.6.3.

TABLE 3.6.3. Entropy changes for the formation of 1:1 metal-EDDA complexes ($\mu = 0.1M NaNO_3$)

<u>Metal</u>	ΔS_{obs}°	$\Delta S_{obs}^{\circ} + \bar{S}_M^{\circ}$
Mn	29.4	11.4
Co	32.2	10.2
Ni	28.9	5.9
Zn	31.0	5.5
Cd	25.0	10.4

Data taken from ref. 90.

The visible spectrum of NiEDDA (fig. 3.6.1) is indicative of an octahedral nickel complex and so it seems reasonable that the zinc complex is also octahedral.

3.6.4 Zinc cysteine

It has been suggested by Li and Manning⁽⁹¹⁾ that only two of the three possible donor atoms can be simultaneously bound to the zinc atom giving rise to three possible isomers for the 1:1 complex. By comparing the stability constant for zinc-cysteine ($10^{9.9}$) with those for zinc glycine ($10^{5.4}$), zinc mercaptoacetic acid ($10^{7.4}$) and zinc mercaptoethylamine ($10^{9.9}$) they came to the conclusion that the binding to zinc must be through the amine and sulphide groups. However, there is a significant decrease in the zinc stability constant when cysteine is converted into the methyl ester ($10^{8.4}$) suggesting that perhaps the carboxylate group is also involved in complex formation in the zinc cysteine complex.

3.6.5 Zinc tripolyphosphate

The thermodynamic parameters for the formation of metal-tripolyphosphate complexes⁽⁹²⁾ show much larger values of ΔS_{obs} than the values for the amino carboxylate complexes. This has been explained in terms of the loss of solvent ordering effect in changing from the divalent cation and the highly structure promoting anionic ligand, with large charges, to the less charged complex. The values of $\Delta S_{\text{obs}} + \bar{S}_M^0$ (table 3.6.5) are approximately constant with the values centred around the value for nickel.

TABLE 3.6.5. Variation of ΔS with metal ion for 1:1 tripolyphosphate complexes ($\mu = 0.1M \text{ Me}_2\text{N}_2\text{NO}_3$)

<u>Metal</u>	ΔS_{obs}	$\Delta S_{\text{obs}} + \bar{S}_M^{\circ}$
Mn	46.4	26.4
Co	51.7	26.6
Ni	52.7	29.7
Cu	59.2	35.6
Zn	59.8	34.3

On the basis of their visible spectra both the Co(II) and Ni(II) complexes have been assigned an octahedral configuration⁽⁹³⁾. The 1:1 complexes have been isolated for each of the above metals⁽⁹⁴⁾ and in every case there are twelve water molecules associated with the complex. This seems to be good evidence that the complexes have the same stereochemistry since a change would be expected to affect the number of water molecules associated with the complex. It therefore seems likely that the zinc complex is octahedral.

CHAPTER 4

Equilibrium and kinetic studies of the Zinc(II) PADA system⁽⁹⁵⁾

4.1 Introduction

PADA has been shown to bind to transition metals^(96,97) and the resulting complexes have strong absorption bands around 550 nm. The spectrum of PADA is independent of pH above pH 6, but the pKs of the aniline (pK = 2) and the pyridine nitrogens (pK ~ 4.5) give rise to pH-dependent spectra and metal binding behaviour below pH 6. As the visible spectrum of the isomeric pyridine-4-azo-p-dimethylaniline (fig. 4.1.1) is unchanged on the addition of metal ions, it seems that the orthopyridine nitrogen is essential for complex formation and as five-membered

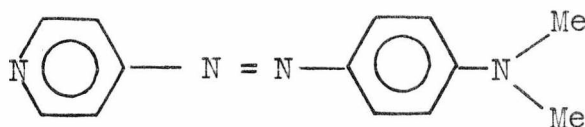


Fig. 4.1.1. Pyridine-4-azo-p-dimethylaniline.

rings are usually more stable than four, the likely configuration of the metal complex is that shown in fig. 4.1.2.

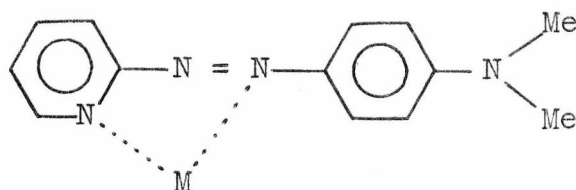


Fig. 4.1.2. Probable configuration of M-PADA complex.

The rates of formation and dissociation of some zinc complexes with PADA have been measured. The general reaction may be represented by $ZnL + D \rightleftharpoons LZnD$, from which charges and

water molecules have been omitted for the sake of clarity. The zinc species studied are $Zn(H_2O)_6^{2+}$, $ZnIDA^0$, $ZnDIEN^{2+}$, $ZnTRIEN(NO_3)_2^{2+}$, $ZnTRIEN(ClO_4)_2^{2+}$, $ZnTREN^{2+}$, $ZnTP^{3-}$, $ZnNTA^-$, $ZnEDDA^0$ and $ZnCYST^0$. The kinetics have been measured by the temperature-jump method over a range of temperatures from 4°C to 40°C. An upper temperature limit was generally imposed by the relaxation time of the system approaching the rise-time of the apparatus.

Stability constants for the ternary complexes were also measured spectroscopically at several wavelengths and for a range of temperatures.

4.2 Spectroscopic Determination of Stability Constants

The systems were all of the type $ZnL + D \rightleftharpoons LZnD$, so that

$$K = \frac{[ZnLD]}{[ZnL][D]} \quad \text{where } D = \text{PADA.}$$

Let the total concentration of PADA be C and the extinction coefficients of D and ZnLD at a particular wavelength be ϵ_L and ϵ_{ML} respectively.

$$C = [ML] + [L]$$

Then, if the effective extinction coefficient of the whole system can be represented by ϵ and since the metal does not absorb,

$$d = C\epsilon = \epsilon_{ML}[ML] + \epsilon_L[L]$$

$$\therefore \epsilon[ML] + \epsilon[L] = \epsilon_{ML}[ML] + \epsilon_L[L]$$

Rearranging and substituting for [ML] gives

$$(\epsilon - \epsilon_{ML})K[M][L] + (\epsilon - \epsilon_L)[L] = 0$$

Multiplying by C/L

$$(d - C\epsilon_{ML})K[M] + (d - C\epsilon_L) = 0$$

or

$$d - C\epsilon_{ML} + \frac{(d - C\epsilon_L)}{K[M]} = 0$$

Let $C\epsilon_L = d_0$

then $d = -\frac{1(d-d_0)}{K[M]} + C\epsilon_{ML}$

which is of the form $y = mx + c$.

Thus, if the concentration of PADA is kept constant and the metal concentration varied, to give a series of spectra as in fig. 4.2.1.1, a plot of d vs. $\frac{(d-d_0)}{[M]}$ for a fixed wavelength gives a straight line of slope $-\frac{1}{K}$ and intercept $C\epsilon_{ML}$.

4.2.2 Experimental conditions

The $[ML]$ used to obtain a wide variation of optical densities are shown in table 4.2.2.1.

TABLE 4.2.2.1. Conditions for spectrophotometric determination of stability constants.

<u>System</u>	<u>Concentration range M</u>
$Zn(OH_2)_6^{2+}$	$5 \times 10^{-4} - 5 \times 10^{-3}$
$Zndien^{2+}$	$1.2 \times 10^{-3} - 1.2 \times 10^{-2}$
$Zntrien^{2+}(NO_3)_2$	$3 \times 10^{-3} - 3 \times 10^{-2}$
$ZnIDA^0$	$1 \times 10^{-3} - 5 \times 10^{-3}$
$ZnEDDA^0$	$2.8 \times 10^{-3} - 2.4 \times 10^{-2}$
$ZnCyst^0$	$2 \times 10^{-4} - 3 \times 10^{-3}$
$ZnNTA^-$	$4 \times 10^{-3} - 5 \times 10^{-2}$
$ZnTP^{3-}$	$1 \times 10^{-3} - 1 \times 10^{-2}$

For all systems $[PADA] = 3 \times 10^{-5}M$.

For all systems the ionic strength was kept constant at 0.3.

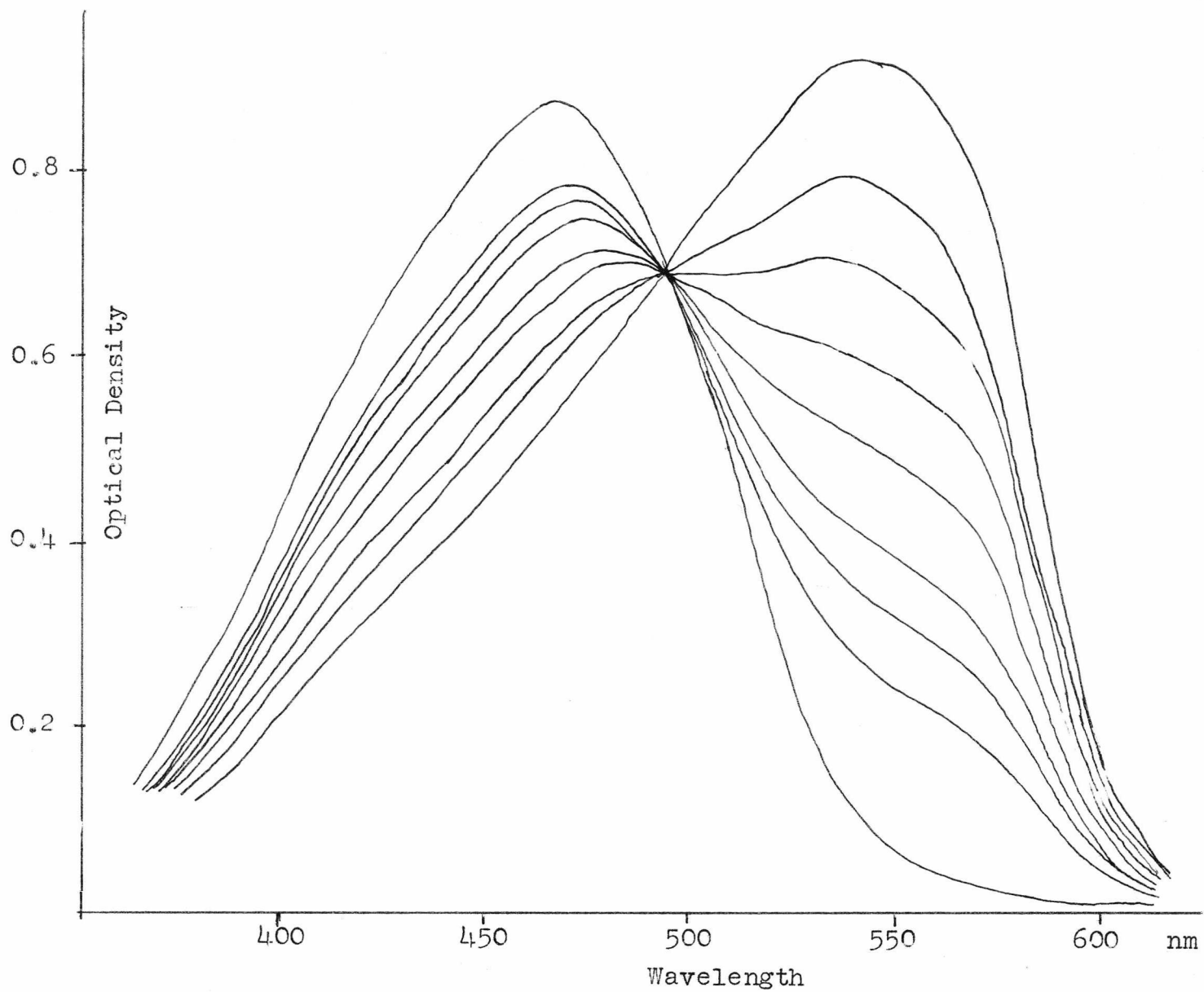


Fig. 4.2.1.1. Visible spectra of Znndien^{2+} + PADA for varying $[\text{Znndien}^{2+}]$.

4.2.3 Analysis of data

Since
$$-\log_{10} K = \frac{\Delta H^\circ}{2.303RT} - \frac{\Delta S^\circ}{2.303R}$$

a plot of $\log_{10} K$ vs. $1/T$ gives a straight line of slope $-\Delta H^\circ/2.303R$ and intercept $\Delta S^\circ/2.303R$. A typical plot of d vs. $(d-d_0)/[M]$ for each of the systems studied, together with the corresponding van't Hoff plot, is shown in figs. 4.2.3.1 - 4.2.3.8.

4.2.4 Index to plots

<u>System</u>	<u>Figure</u>
Zn(OH ₂) ₆ ²⁺	4.2.3.1
Zn(dien) ²⁺	4.2.3.2
Zntrien(NO ₃ ⁺) ₂	4.2.3.3
ZnIDA ⁰	4.2.3.4
ZnEDDA ⁰	4.2.3.5
ZnCYST ⁰	4.2.3.6
ZnNTA ⁻	4.2.3.7
ZnTP ³⁻	4.2.3.8

4.2.5 Results

The measured stability constants for the zinc PADA systems are given in the following table (4.2.5.1) together with the overall thermodynamic parameters (table 4.2.5.2).

TABLE 4.2.5.1. Stability constants for the LZn PADA systems

Zn(H ₂ O) ₆ ²⁺ + PADA					
Temp. °C	8.5	16	24	30.5	27.8
K. M ⁻¹	325	238	172	133	111
Zndien ²⁺ + PADA					
Temp. °C	6	11	16.8	24.5	33
K. M ⁻¹	242	183	154	122	93

Zntrien(NO ₃) ₂ ²⁺ + PADA						
Temp. °C	6.5	11.5	16	23.3	31.7	39.5
K. M ⁻¹	90	80	76	64	52	45
ZnIDA ⁰ + PADA						
Temp. °C	4.8	10.5	16	22.5	30	
K. M ⁻¹	370	326	282	238	209	
ZnEDDA ⁰ + PADA						
Temp. °C	5.8	11.2	16	23.5	30	
K. M ⁻¹	65	54.1	45	31.7	24.1	
Zncyst ⁰ + PADA						
Temp. °C	7	13.2	17.5	24.3	25.5	33.2
K. M ⁻¹	632	555	500	450	435	386
ZnNTA ⁻ + PADA						
Temp. °C	16.5	22.7	39.5			
K. M ⁻¹	15.4	14.6	14.1			
ZnTP ³⁻ + PADA						
Temp. °C	8	16	23.7	31	41	
K. M ⁻¹	796	680	563	464	404	

For the (Zntren)²⁺ system, no evidence of complex formation was found even for [Zntren]²⁺ = 3 x 10⁻²M and [PADA] = 3 x 10⁻⁵M.

TABLE 4.2.5.2. Thermodynamic parameters for the formation of the ZnL PADA ternary complexes.

	$-\Delta G^{\circ}$ kcal.mol ⁻¹	$-\Delta H^{\circ}$ kcal.mol ⁻¹	ΔS° e.u.
Zn(H ₂ O) ₆ ²⁺	-3.0	6.5	-11.7
Zndien ²⁺	-2.8	5.7	- 9.6
Zntrien(NO ₃) ₂ ²⁺	-2.5	3.6	- 3.8
ZnIDA ⁰	-3.3	5.4	- 7.2
ZnEDDA ⁰	-2.4	7.0	-15.3
ZnCYST ⁰	-2.8	3.2	1.3
ZnNTA ⁻	-0.8	1.2	1.2
ZnTP ³⁻	-3.5	3.6	0.5

Fig. 4.2.3.1. Optical Density Data for Zn^{2+} + PADA.

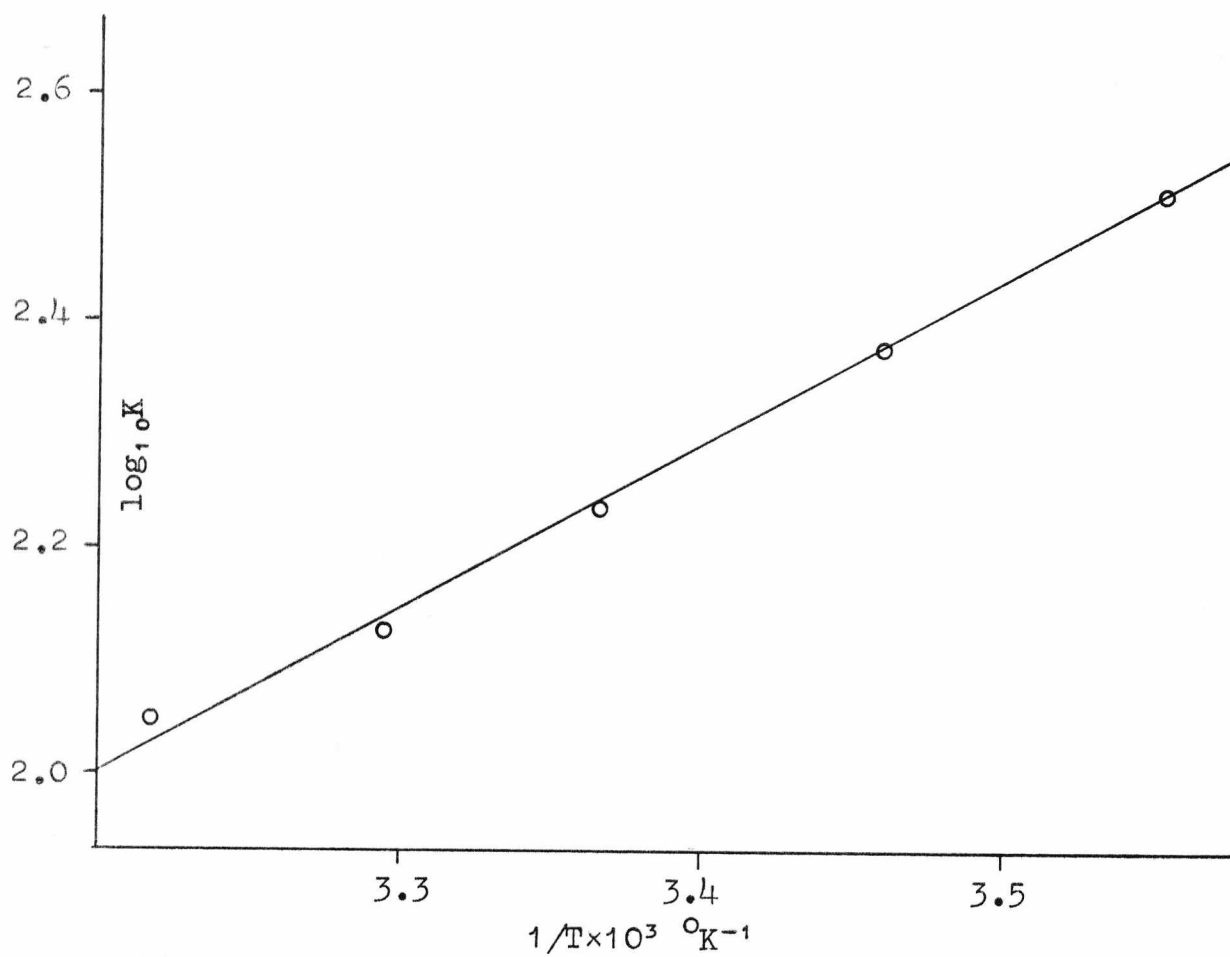
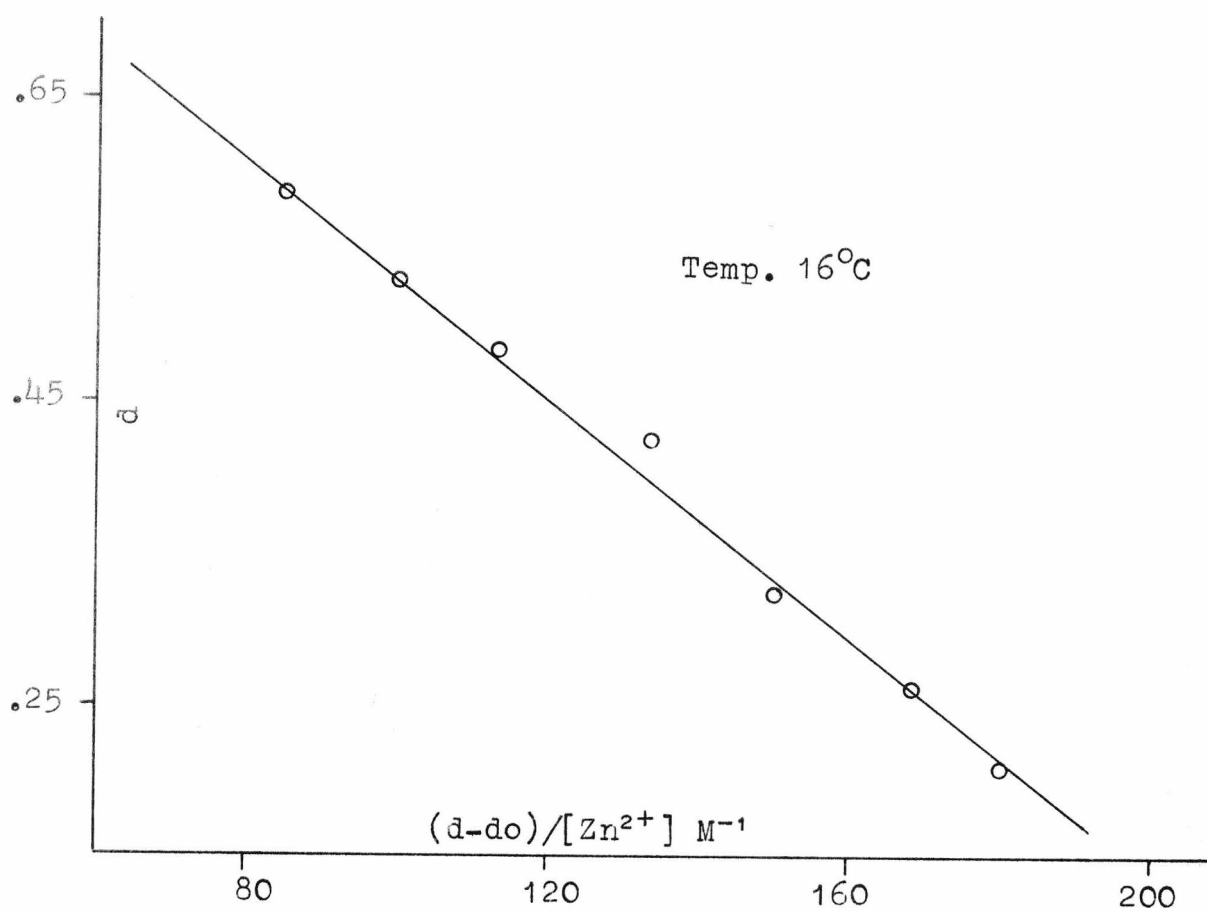


Fig. 4.2.3.2. Optical Density Data for ZnDIEN²⁺ + PADA.

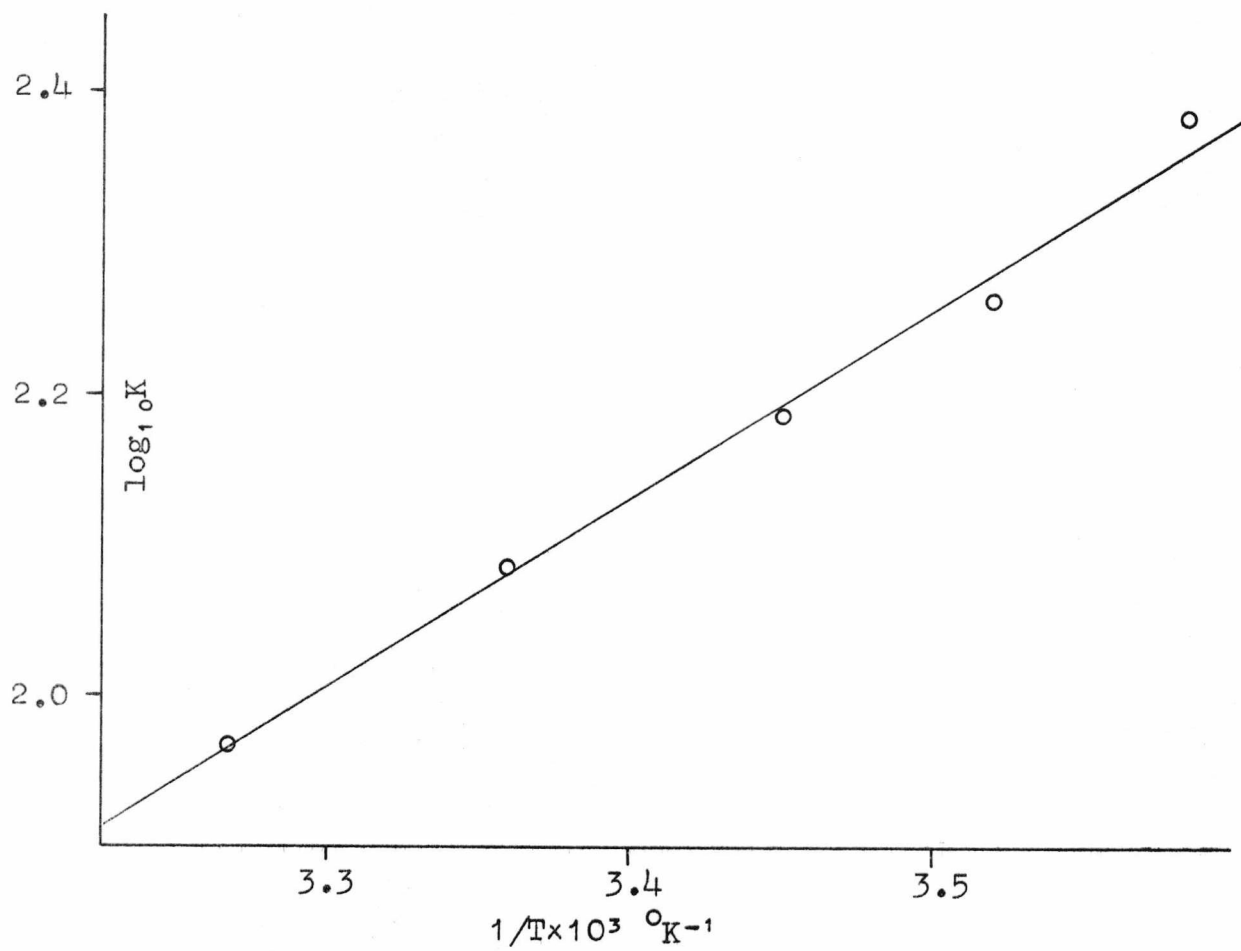
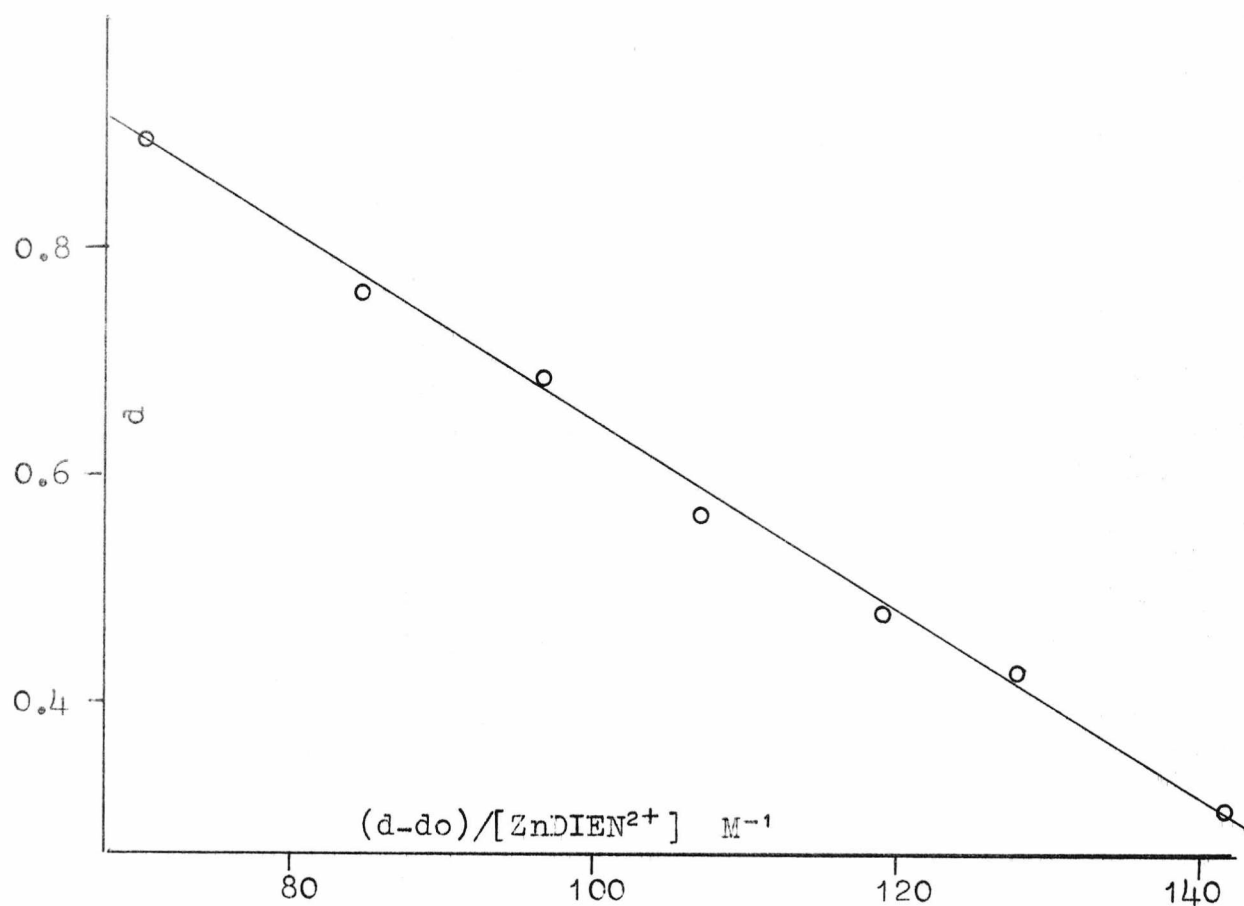


Fig. 4.2.3.3. Optical Density Data for $Zntrien^{2+}(NO_3)_2^-$ + PADA.

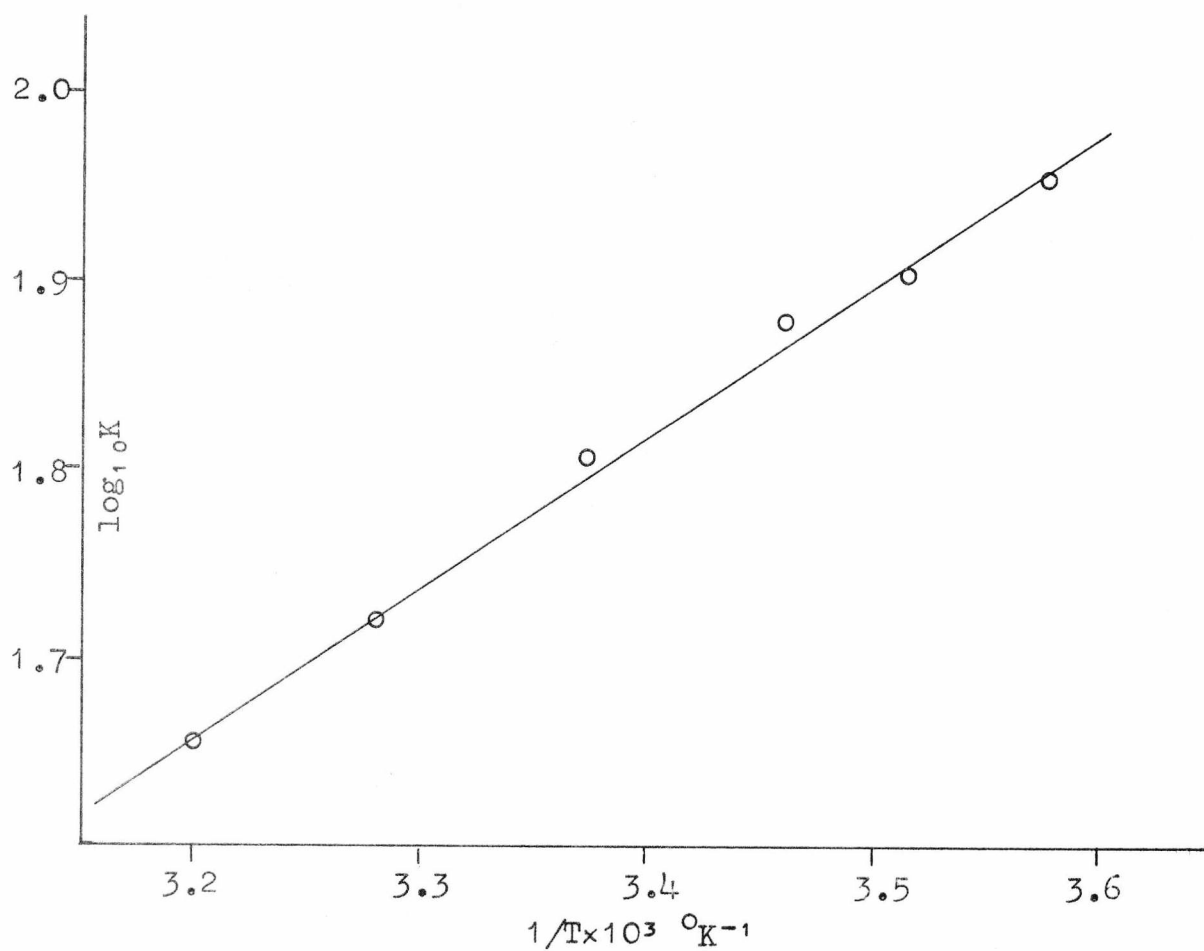
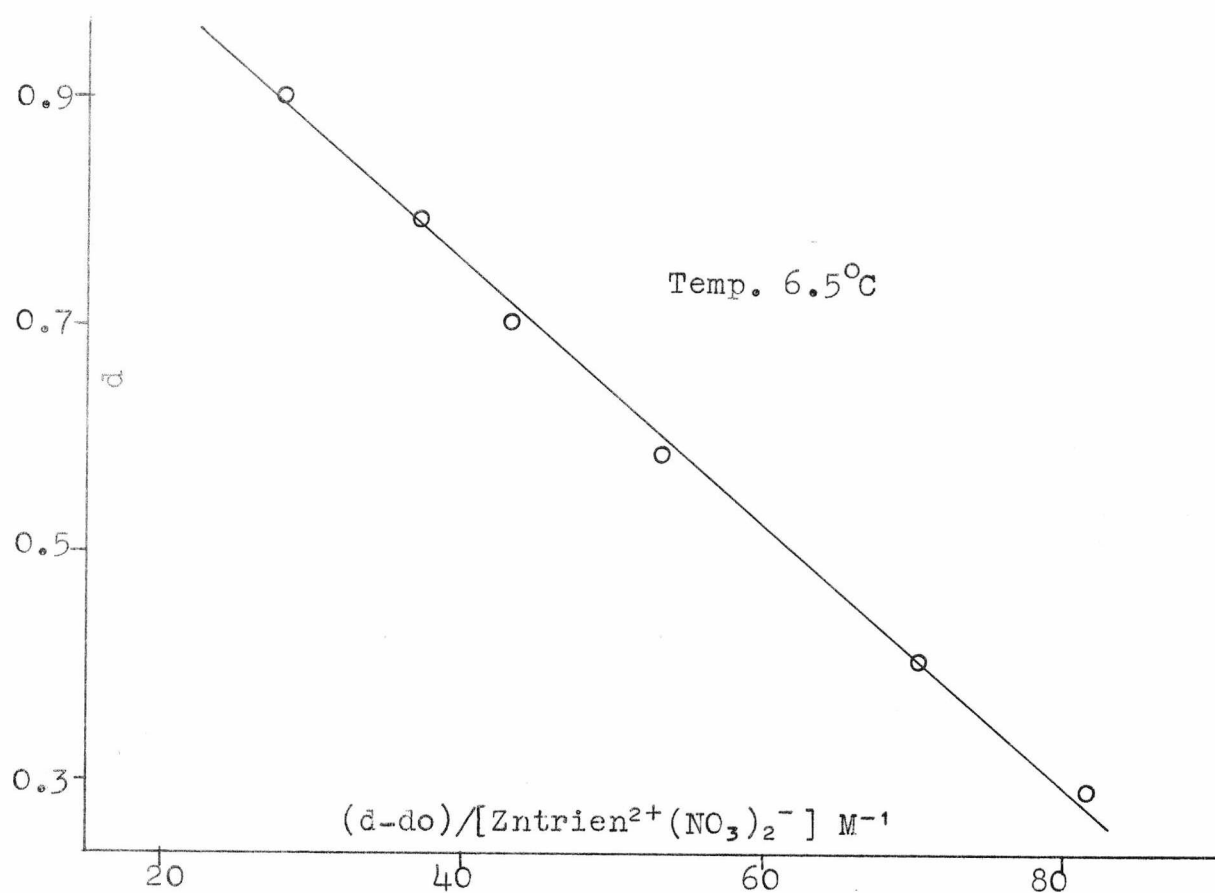


Fig. 4.2.3.4. Optical Density Data for ZnIDA^o + PADA.

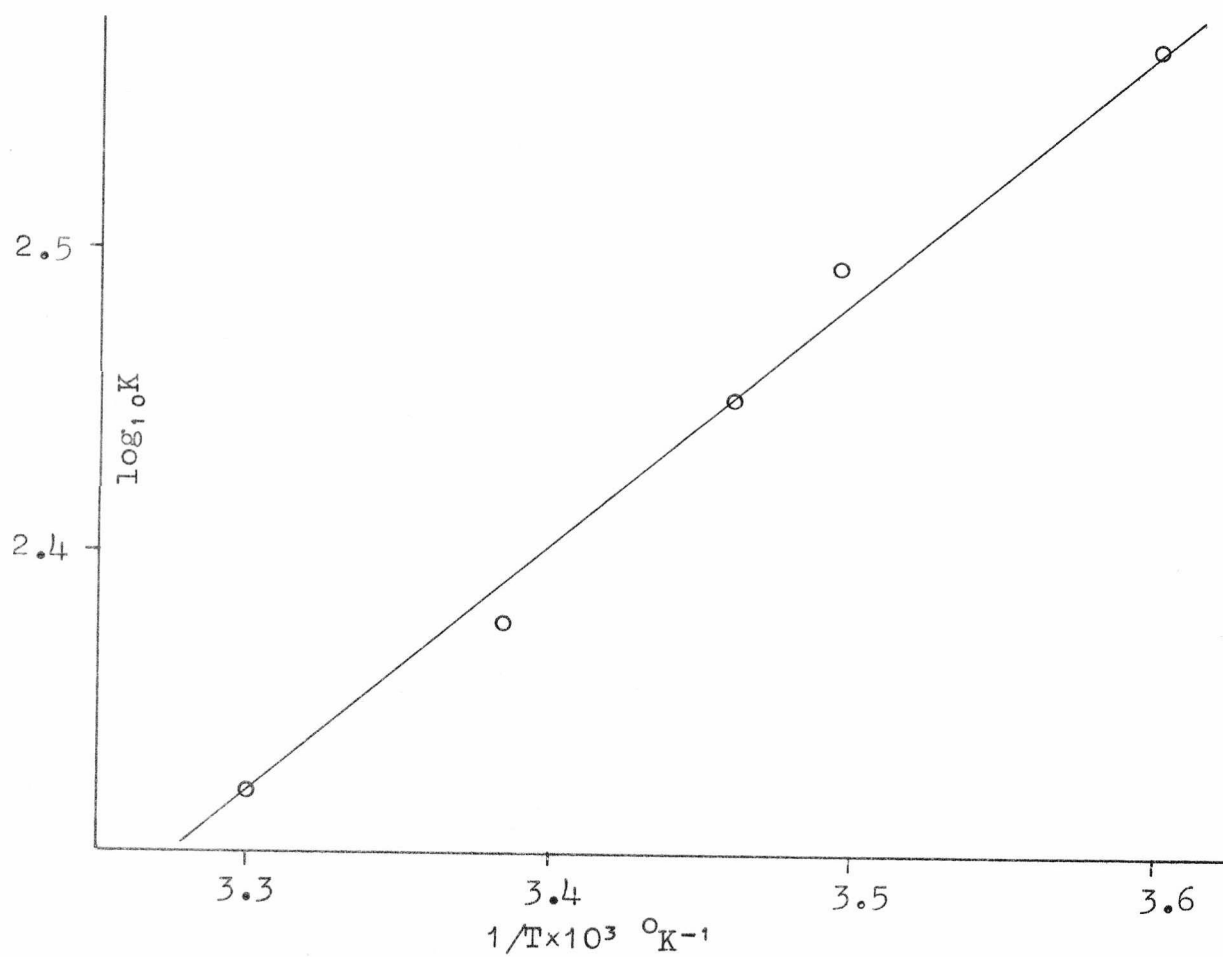
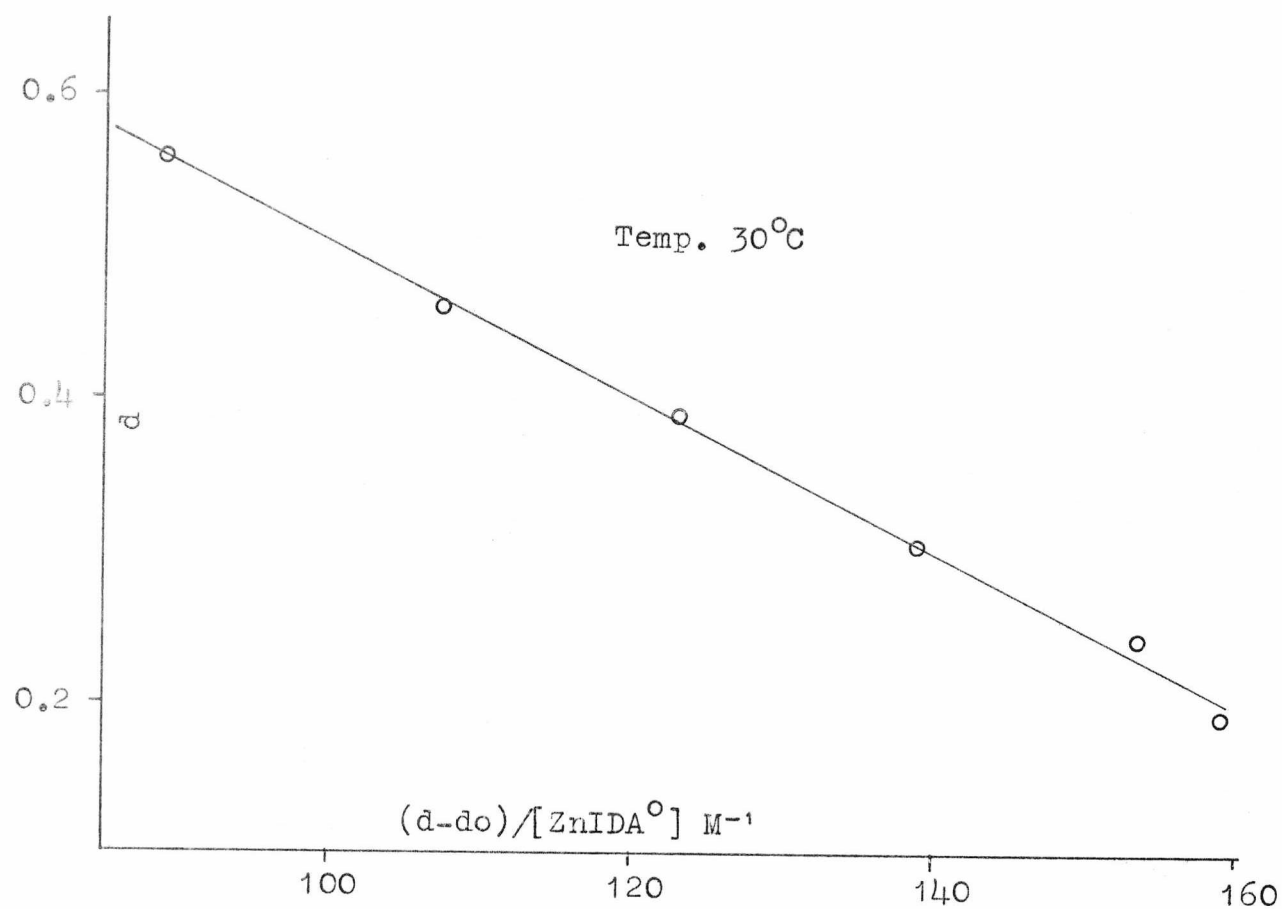


Fig. 4.2.3.5. Optical Density Data for ZnEDDA⁰ + PADA.

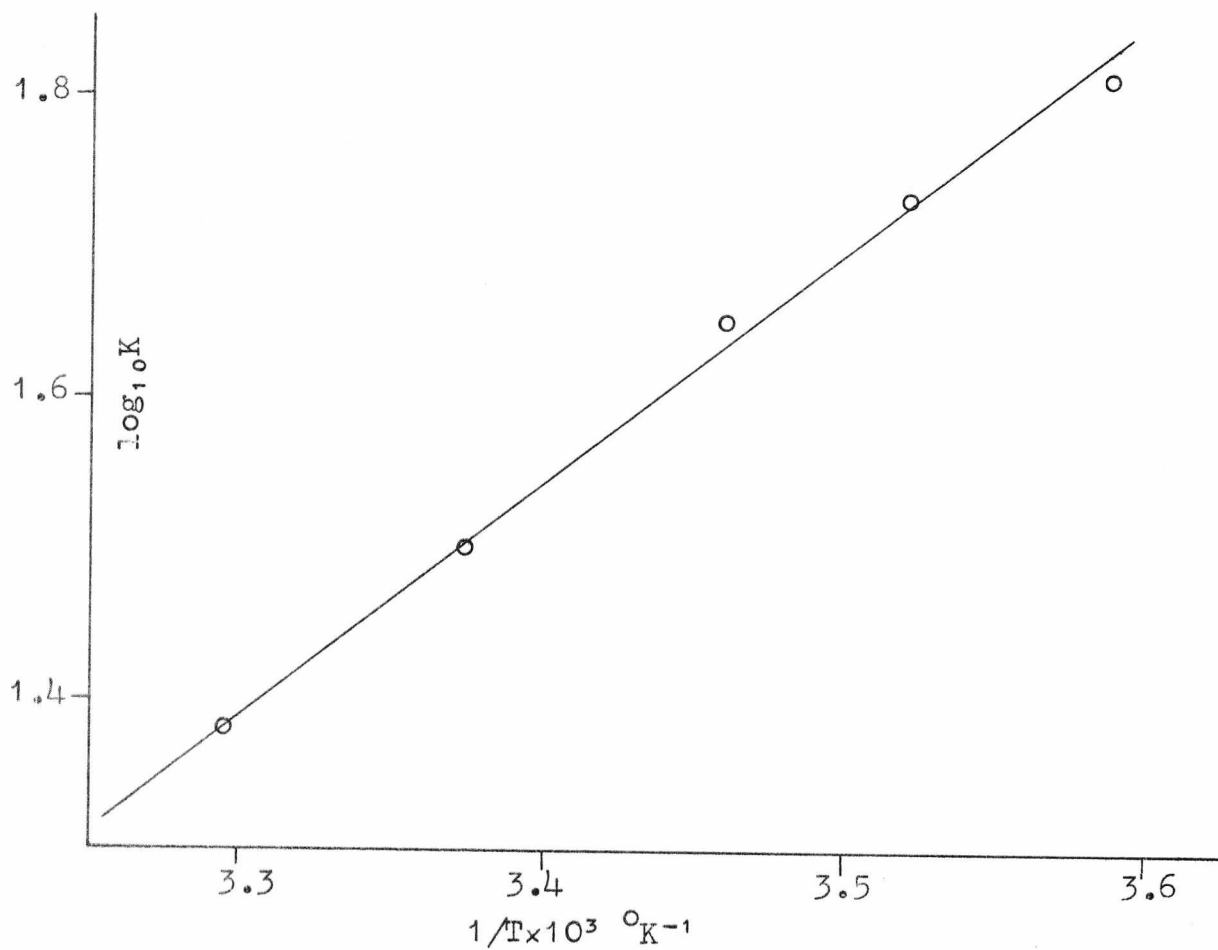
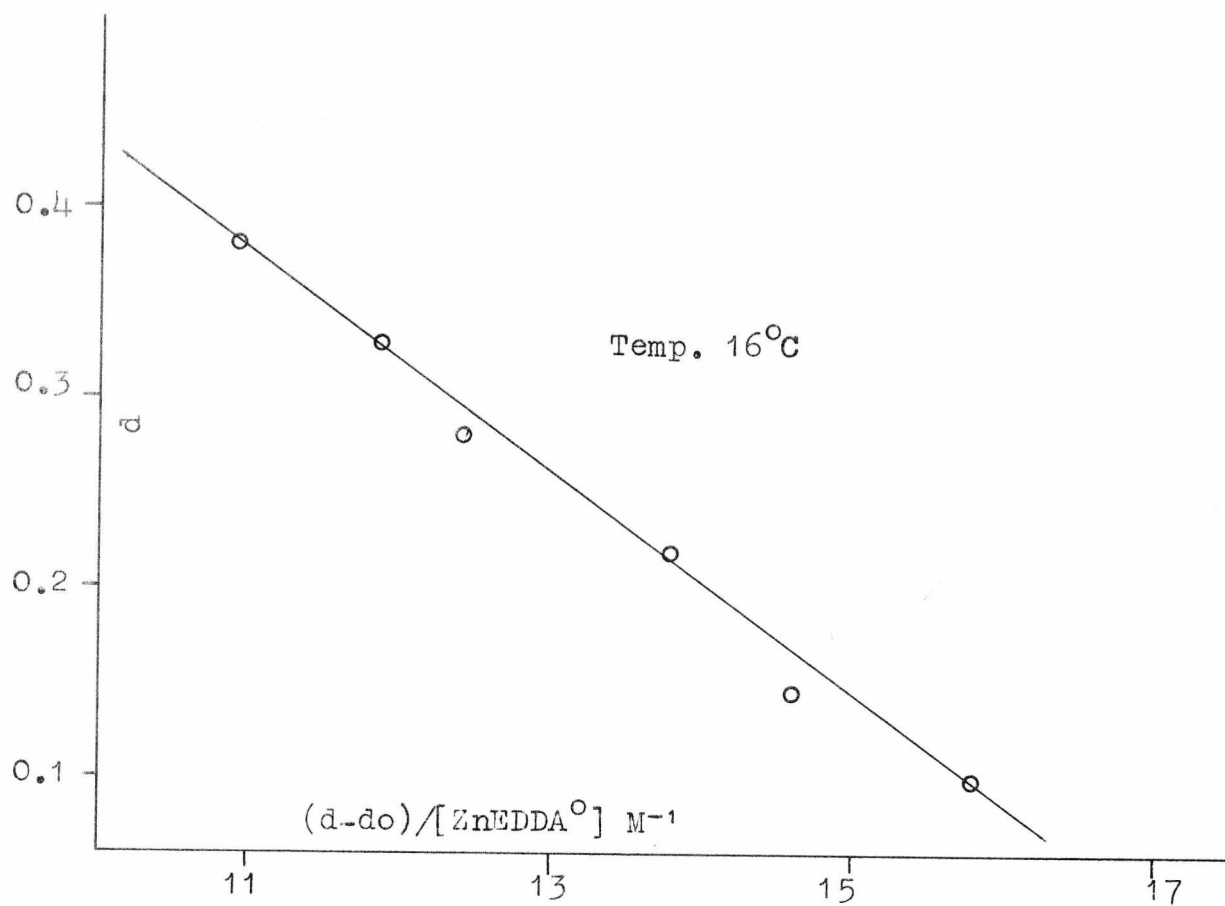


Fig. 4.2.3.6. Optical Density Data for $\text{Zncyst}^{\circ} + \text{PADA}$.

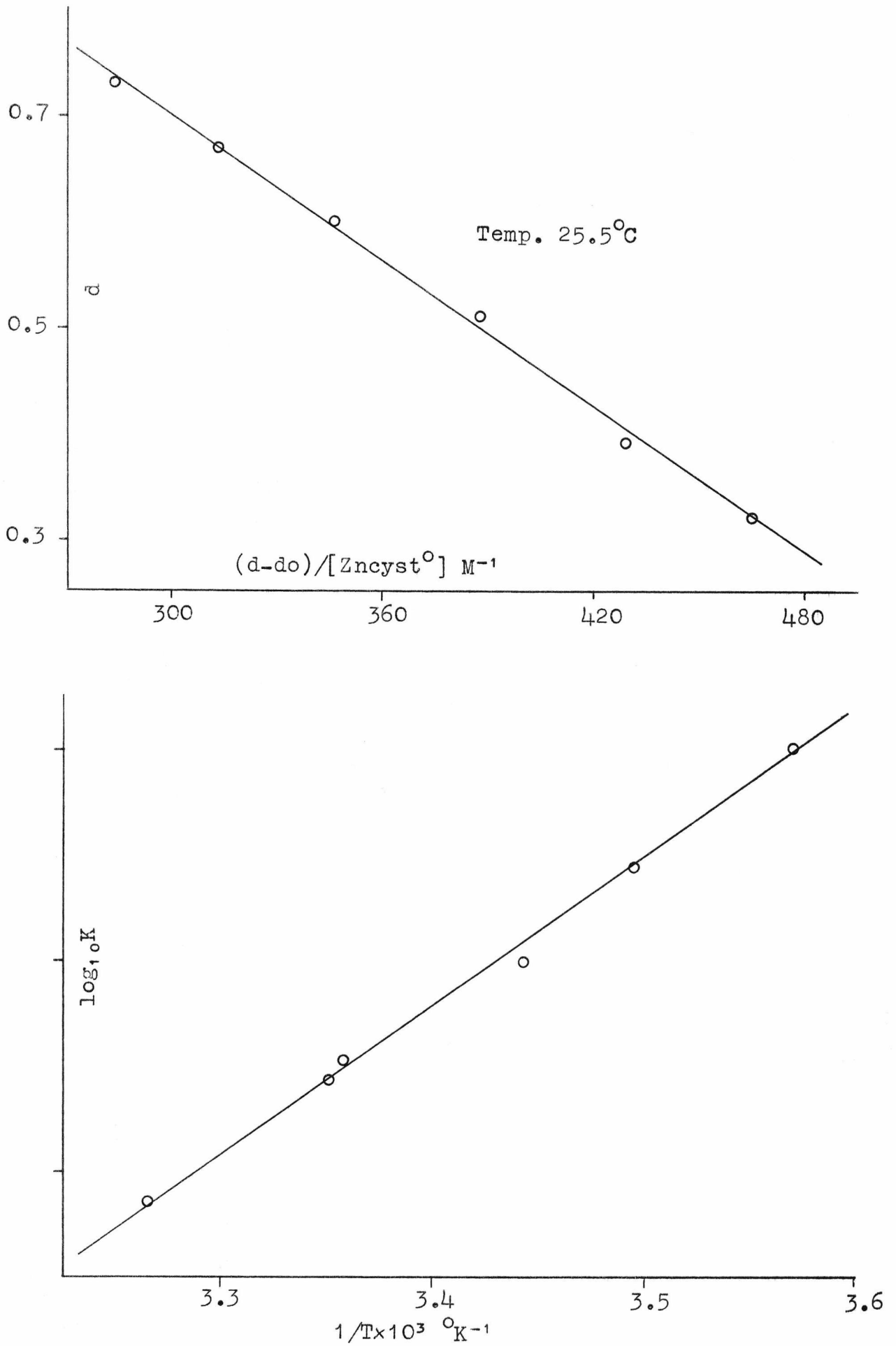


Fig. 4.2.3.7. Optical Density Data for ZnNTA⁻ + PADA.

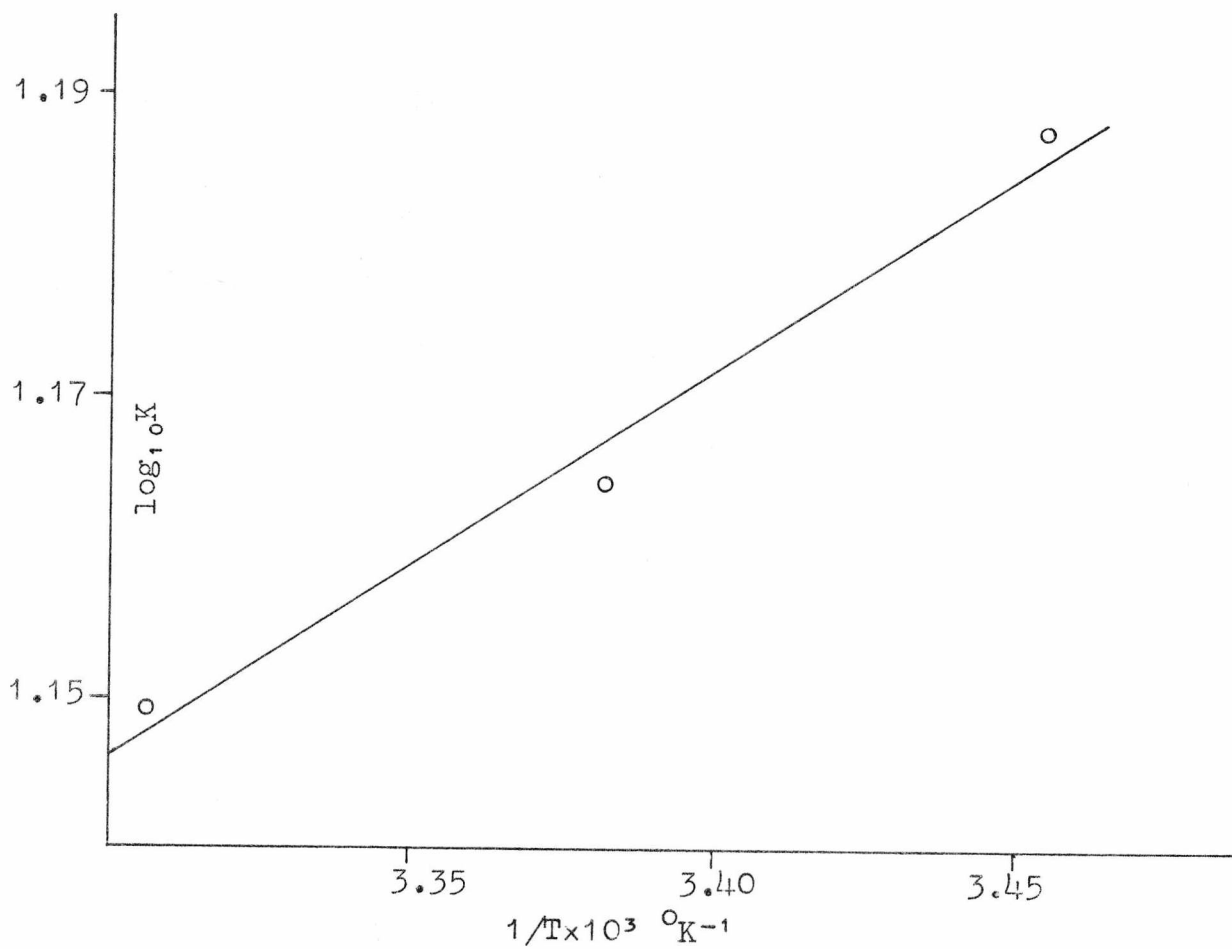
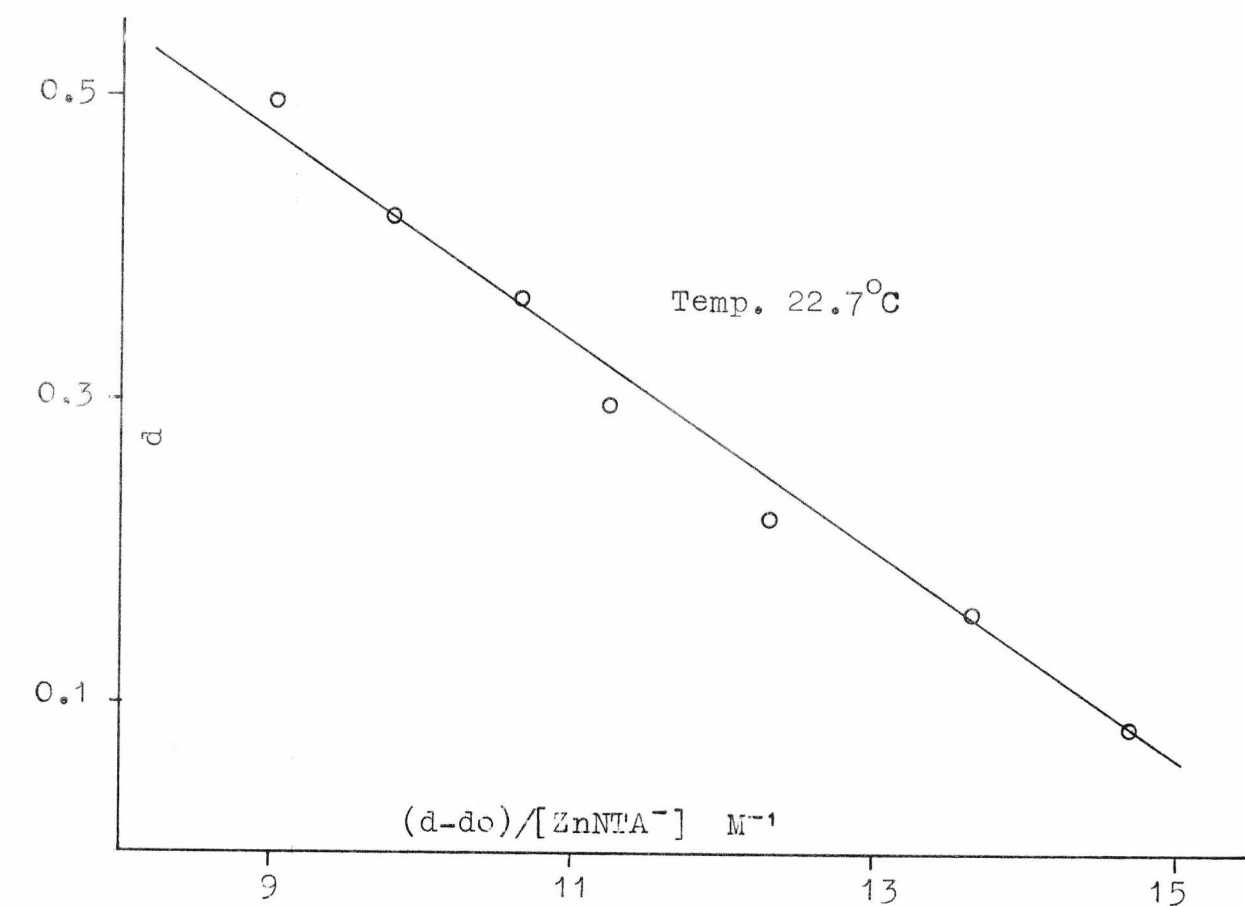
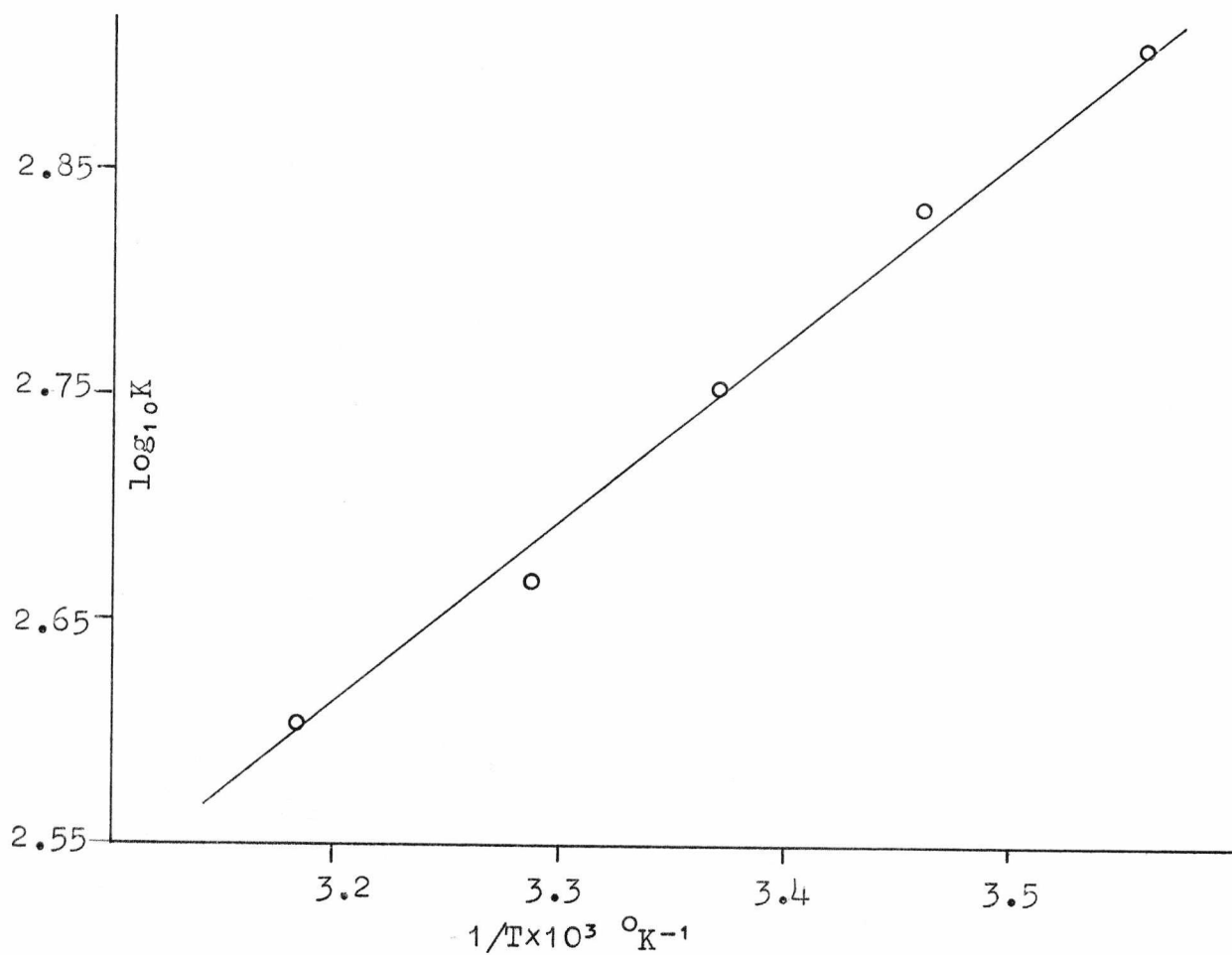
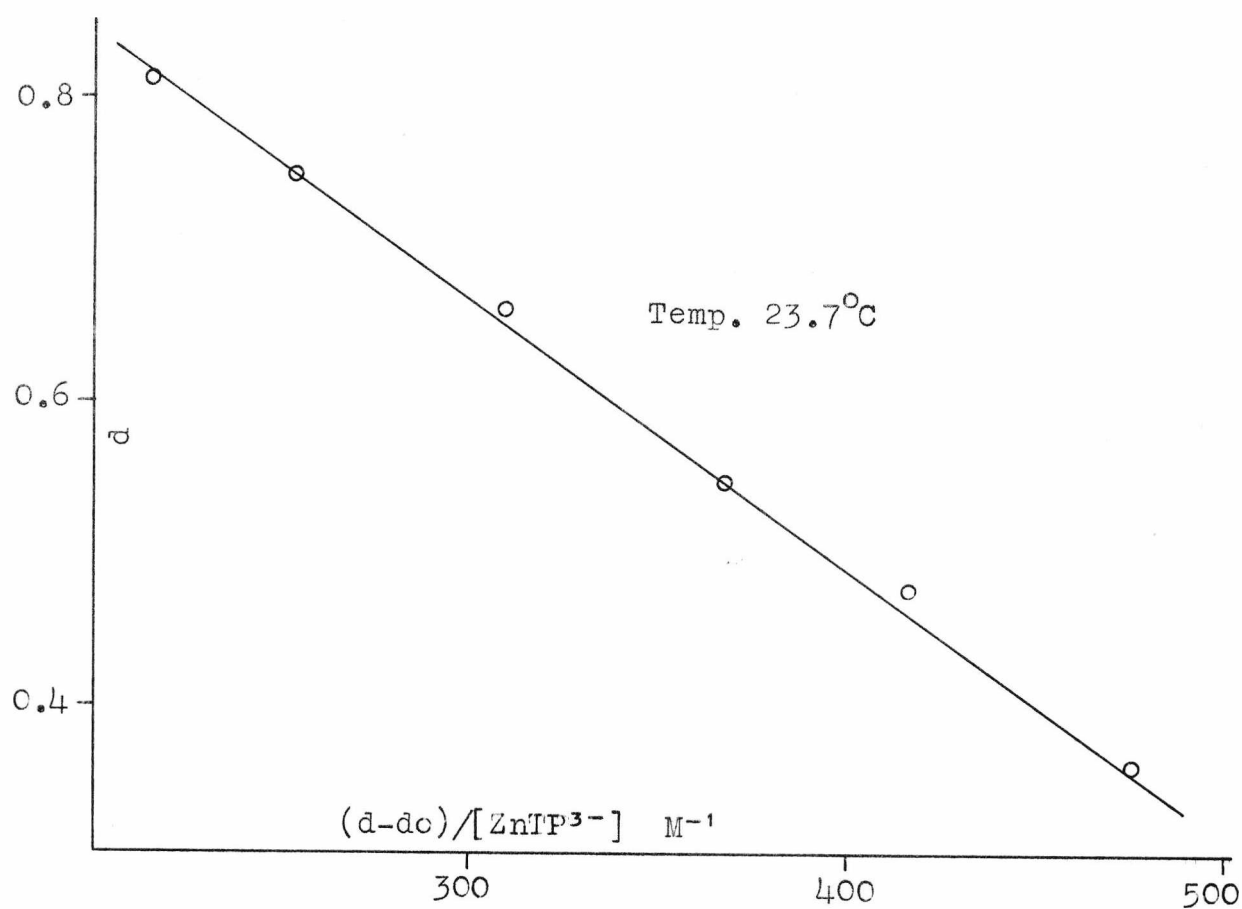


Fig. 4.2.3.8. Optical Density Data for ZnTP^{3-} + PADA.



4.3 Kinetic Studies

4.3.1 Experimental conditions

The concentrations used were the same as in the spectroscopic studies except for the Zndien^{2+} systems where much lower concentrations, $1.6-8 \times 10^{-4}\text{M}$, had to be used to obtain measurable relaxations.

Identical relaxation effects were observed at 450 nm and 550 nm but as the signal to noise ratio was much better at 550 nm all the reactions were followed at this wavelength. The relaxation time was found to be independent of the buffer and PADA concentrations.

4.3.2 Results

The experimental data have been analysed using the relaxation expression derived in section 1.3.

$$\tau^{-1} = k_f(\bar{c}_{\text{ZnL}} + \bar{c}_{\text{D}}) + k_b .$$

In all cases, except for Zndien^{2+} , $[\text{ZnL}] \gg [\text{PADA}]$ so a plot of τ^{-1} against $[\text{ZnL}]$ gives a straight line of slope k_f and intercept k_b .

Attempts were made to study the reaction between Zntren^{2+} and ZnNTA^- with PADA. The former gave no relaxation even with a concentration of Zntren^{2+} of $3 \times 10^{-2}\text{M}$ and a PADA concentration of $3 \times 10^{-5}\text{M}$. With ZnNTA^- a small effect was obtained at 6°C ($[\text{ZnNTA}]^- = 8 \times 10^{-4}\text{M}$; $[\text{PADA}] = 3 \times 10^{-5}\text{M}$) which was too fast to measure, but this enables a lower limit to be placed on the rate constants.

$$\tau^{-1} = k_f c_M + k_b \quad \text{and} \quad K = \frac{k_f}{k_b} = 20$$

$$\text{so} \quad \tau^{-1} = 20 k_b c_M + k_b \quad \tau^{-1} \geq 10^5 \text{ sec}^{-1}$$

$$\therefore \quad k_b \geq 10^5 \text{ sec}^{-1}$$

$$\text{and} \quad k_f \geq 2 \times 10^6 \text{ M}^{-1}\text{sec}^{-1} .$$

The following plots show reciprocal relaxation time, τ^{-1} , as a function of the equilibrium concentration of ZnL and $\log_{10}K$ as a function of $1/T$. The vertical lines represent the experimental scatter of relaxation times and the horizontal lines represent the mean relaxation times.

4.3.3 Index to plots

<u>System</u>	<u>Figure Number</u>	
	<u>τ^{-1} vs. [ML]</u>	<u>$\log_{10}K$ vs. $1/T$</u>
Zn(H ₂ O) ₆ ²⁺	4.3.3.1	4.3.3.2
Zndien ²⁺	4.3.3.3	-
Zntrien(ClO ₄) ₂ ²⁺ (98)	4.3.3.4	4.3.3.5
Zntrien(NO ₃) ₂ ²⁺	4.3.3.6	4.3.3.7
ZnIDA ⁰	4.3.3.8	4.3.3.9
ZnEDDA ⁰	4.3.3.10	4.3.3.11
ZnCYST ⁰	4.3.3.12	4.3.3.13
ZnTP ³⁻	4.3.3.14	4.3.3.15

4.3.4 Tables of results

Tables 4.3.4.1 and 4.3.4.2 show the experimental rate and stability constants at each temperature for all the systems studied. The figures in brackets represent the experimental errors. Tables 4.3.4.3 and 4.3.4.4 show the activation parameters and the rate constants at 25°C, the latter being taken from the Arrhenius plots. The spectrophotometric stability constants, K_{spec} , are also given.

Fig. 4.3.3.1. τ^{-1} vs. $[\text{Zn}^{2+}]$ for $\text{Zn}^{2+} + \text{PADA}$.

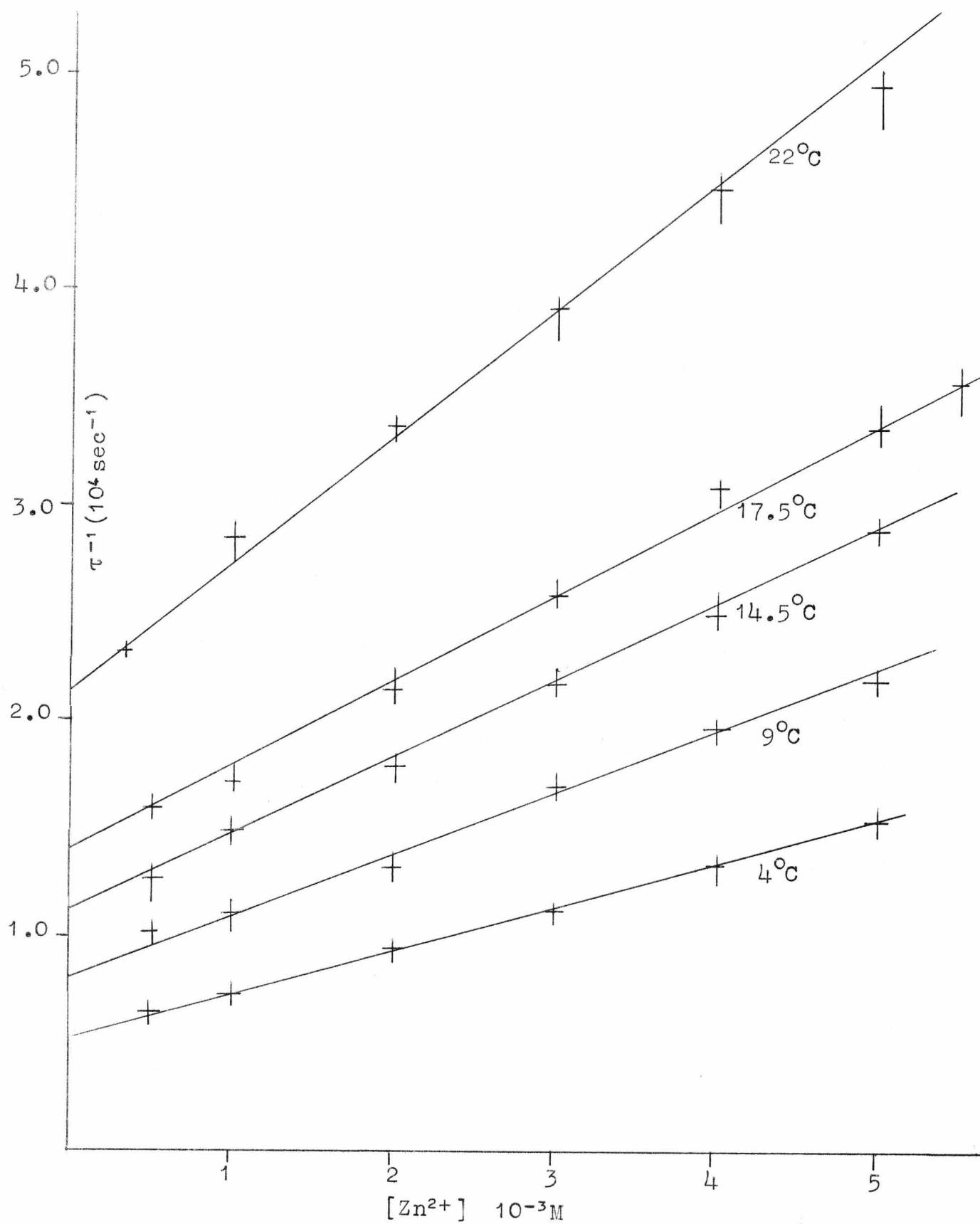


Fig. 4.3.3.2. $\log_{10} k_f$, k_b and K vs. $1/T$ for $Zn^{2+} + PADA$.

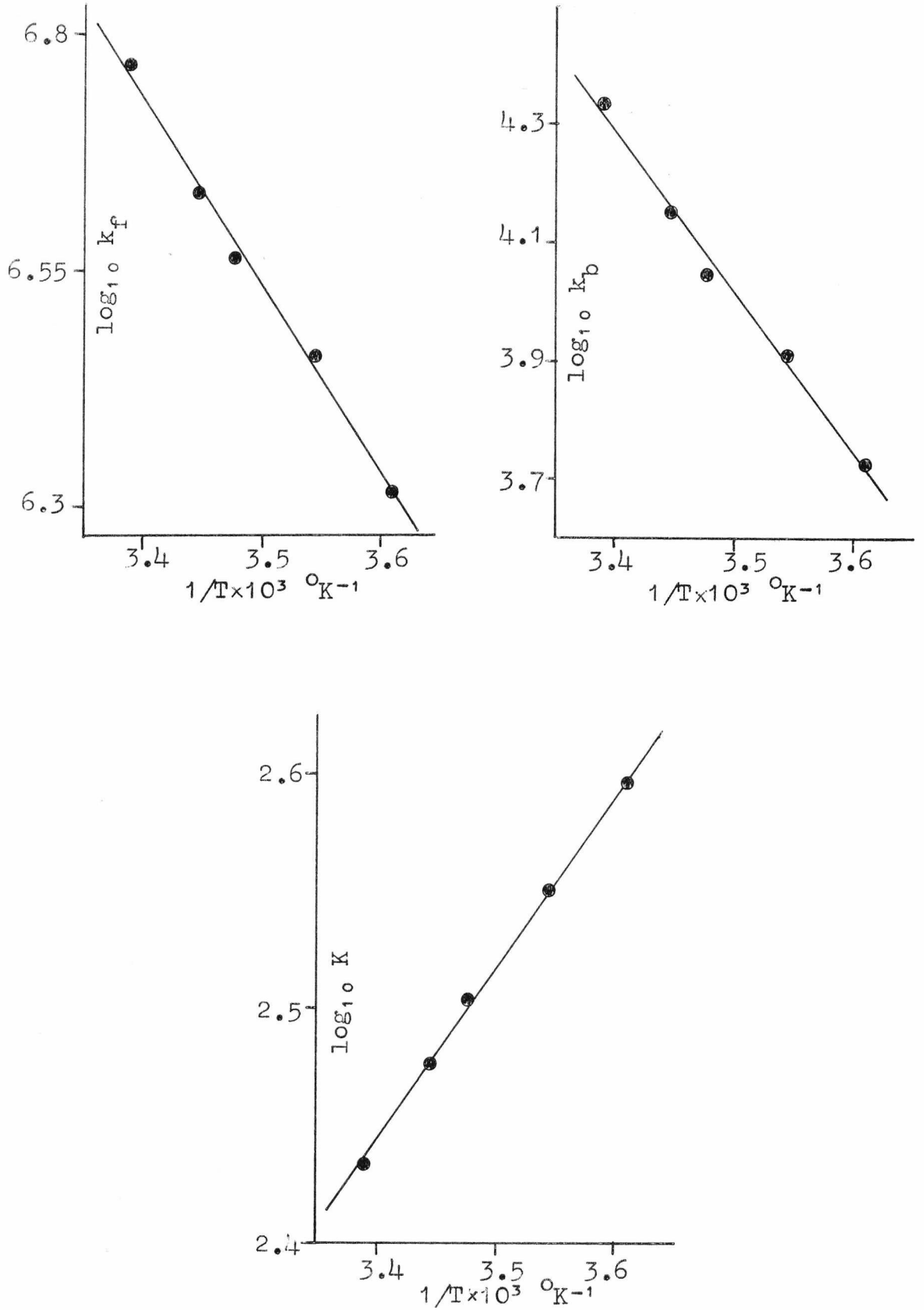


Fig. 4.3.3.3. τ^{-1} vs. concentration for Zndien^{2+} + PADA.

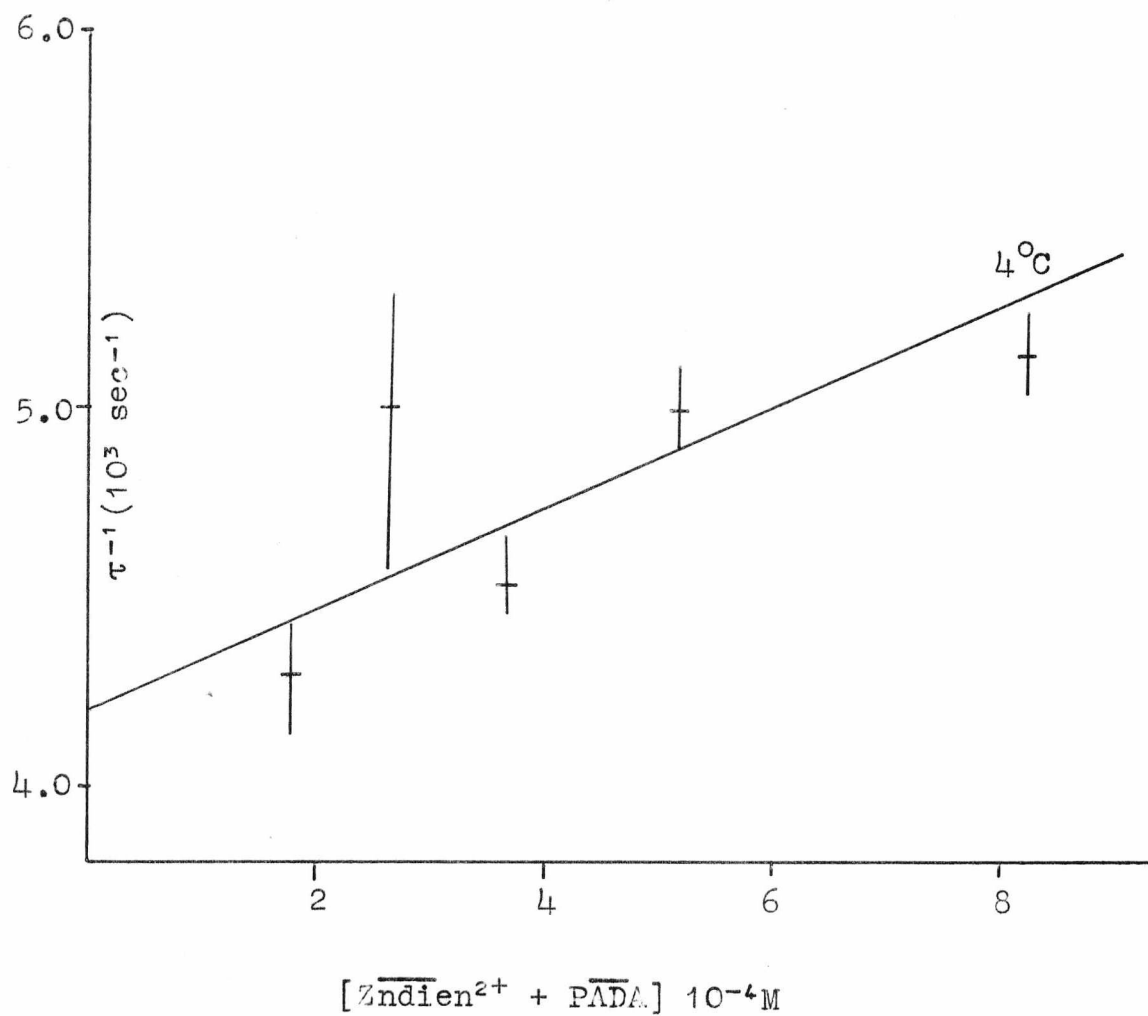


Fig. 4.3.3.4. τ^{-1} vs. $[\text{Zntrien}^{2+}(\text{ClO}_4)_2^-]$ for $\text{Zntrien}^{2+}(\text{ClO}_4)_2^-$
+ PADA.

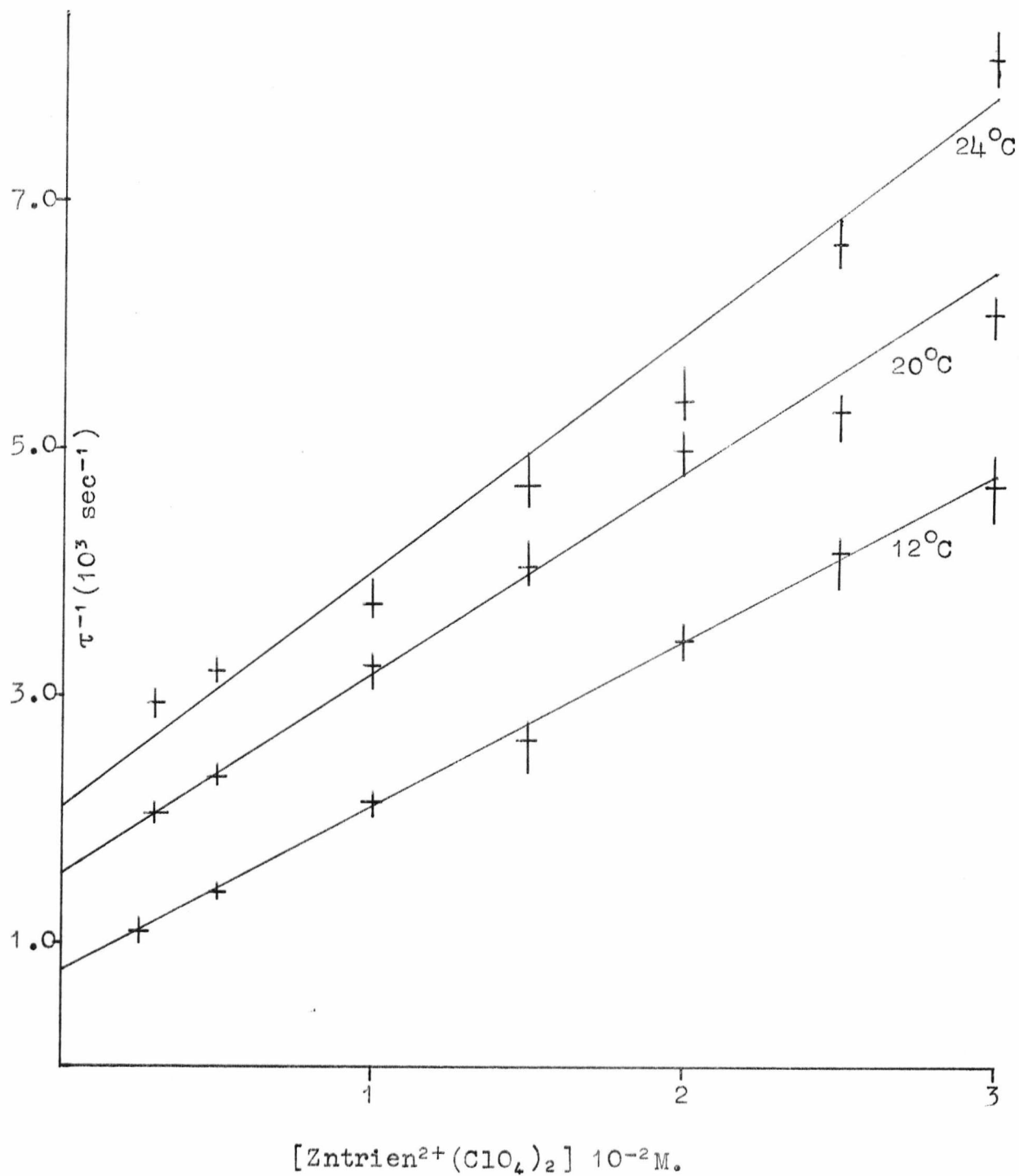


Fig. 4.3.3.5. $\log_{10} k_f, k_b$ and K vs. $1/T$ for $Zntrien^{2+}(ClO_4)_2$ + PADA.

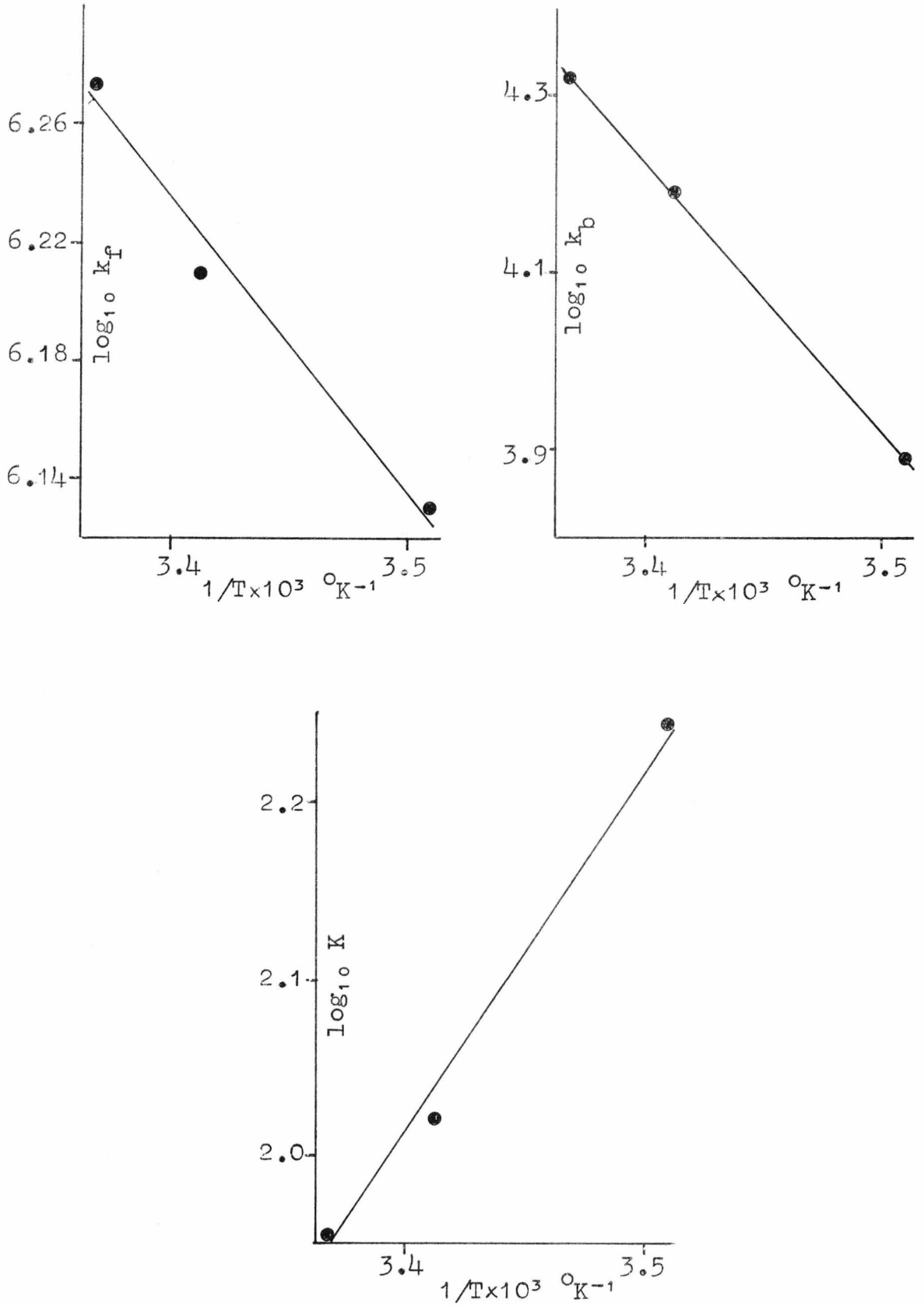


Fig. 4.3.3.6. τ^{-1} vs. $[\text{Zntrien}^{2+}(\text{NO}_3)_2^-]$ for $\text{Zntrien}^{2+}(\text{NO}_3)_2^-$ + PADA.

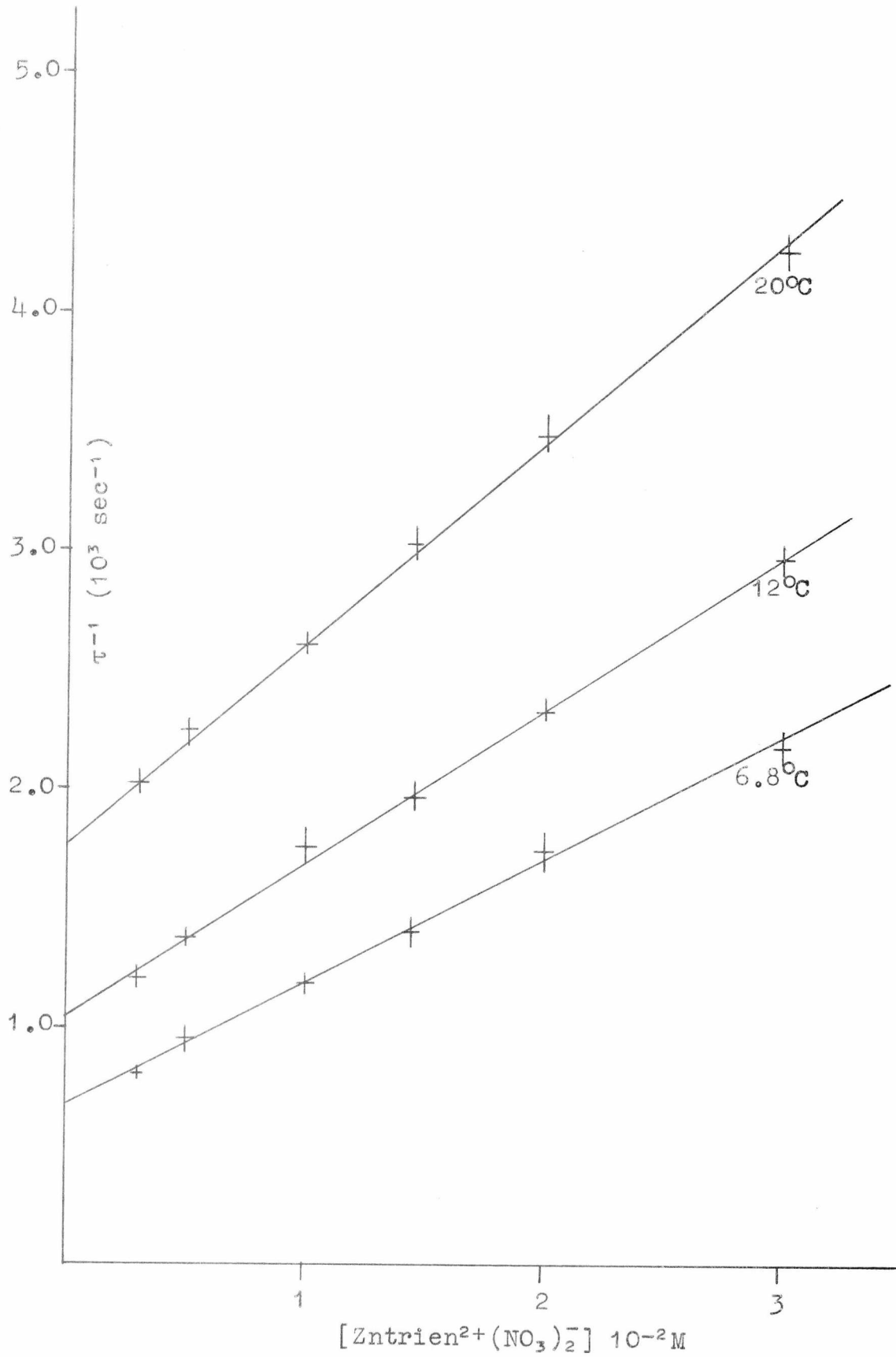


Fig. 4.3.3.7. $\log_{10} k_f, k_b$ and K vs. $1/T$ for Zn^{2+} (NO_3^-)₂ + PADA.

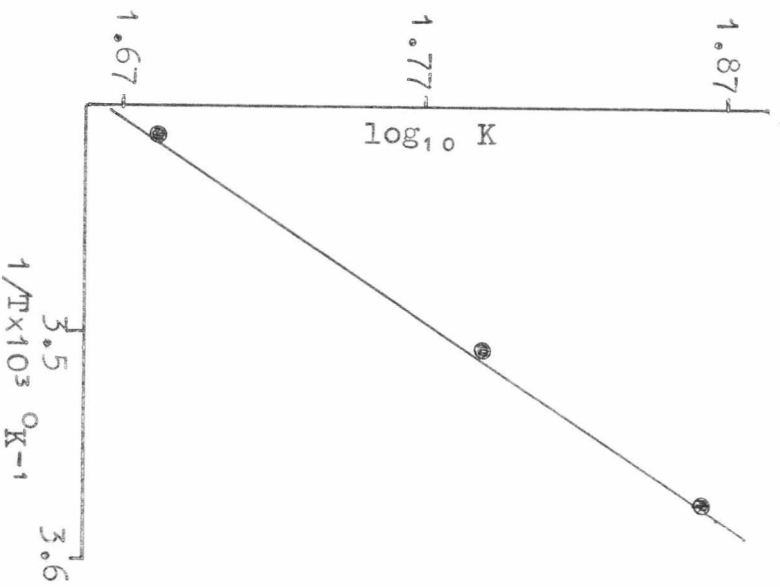
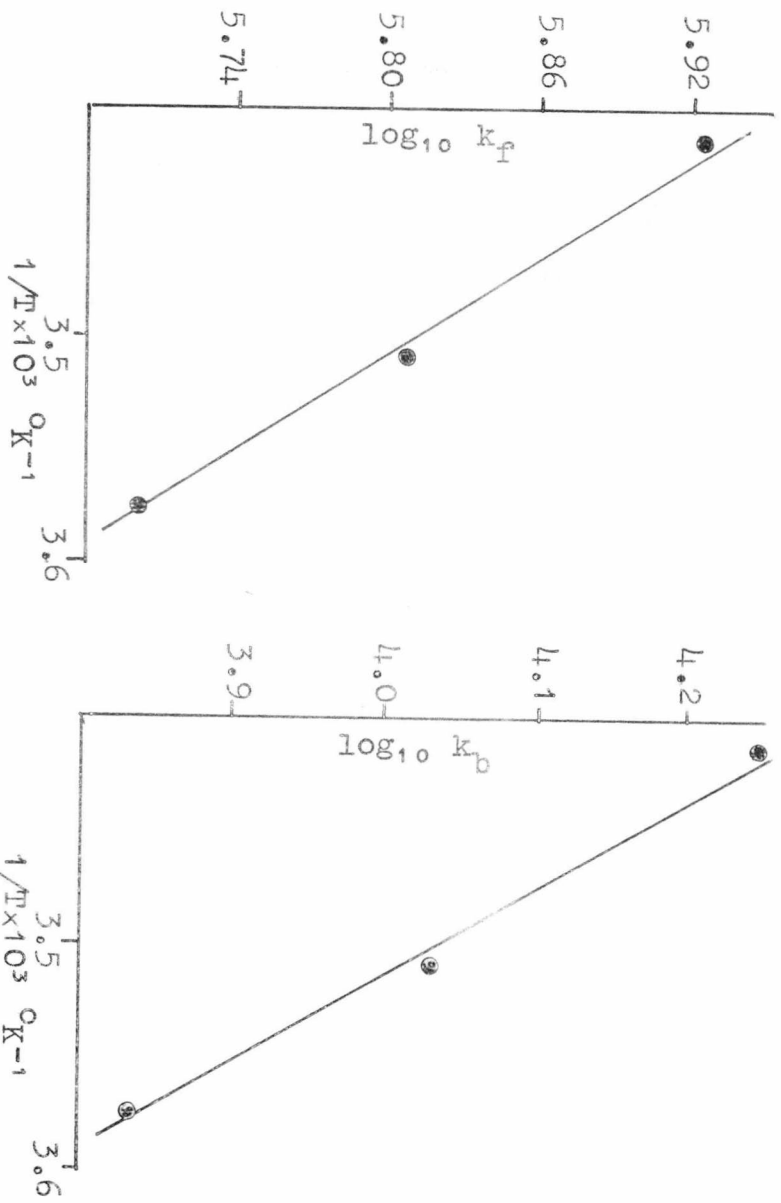


Fig. 4.3.3.8. τ^{-1} vs. $[\text{ZnIDA}^{\circ}]$ for $\text{ZnIDA}^{\circ} + \text{PADA}$.

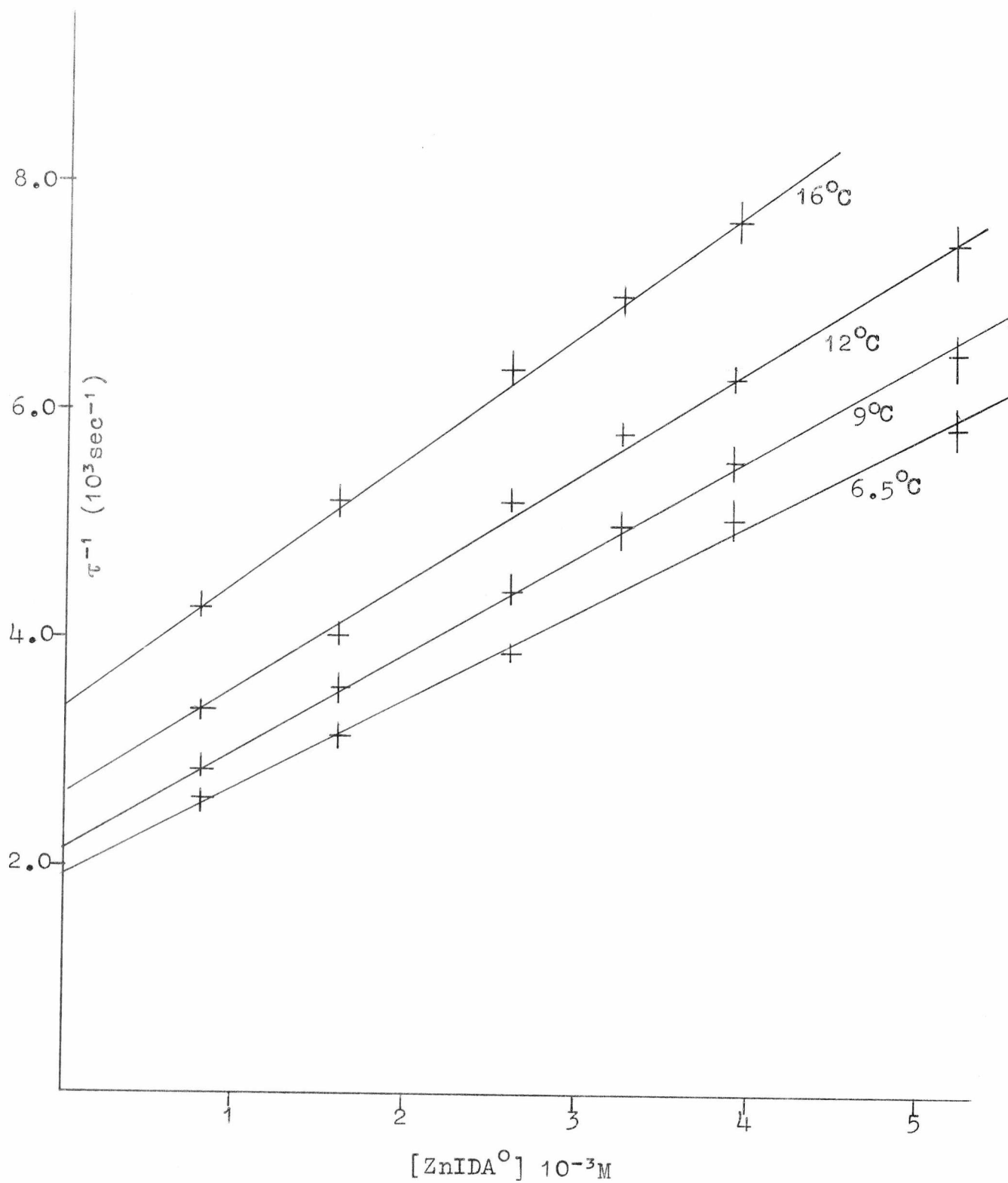
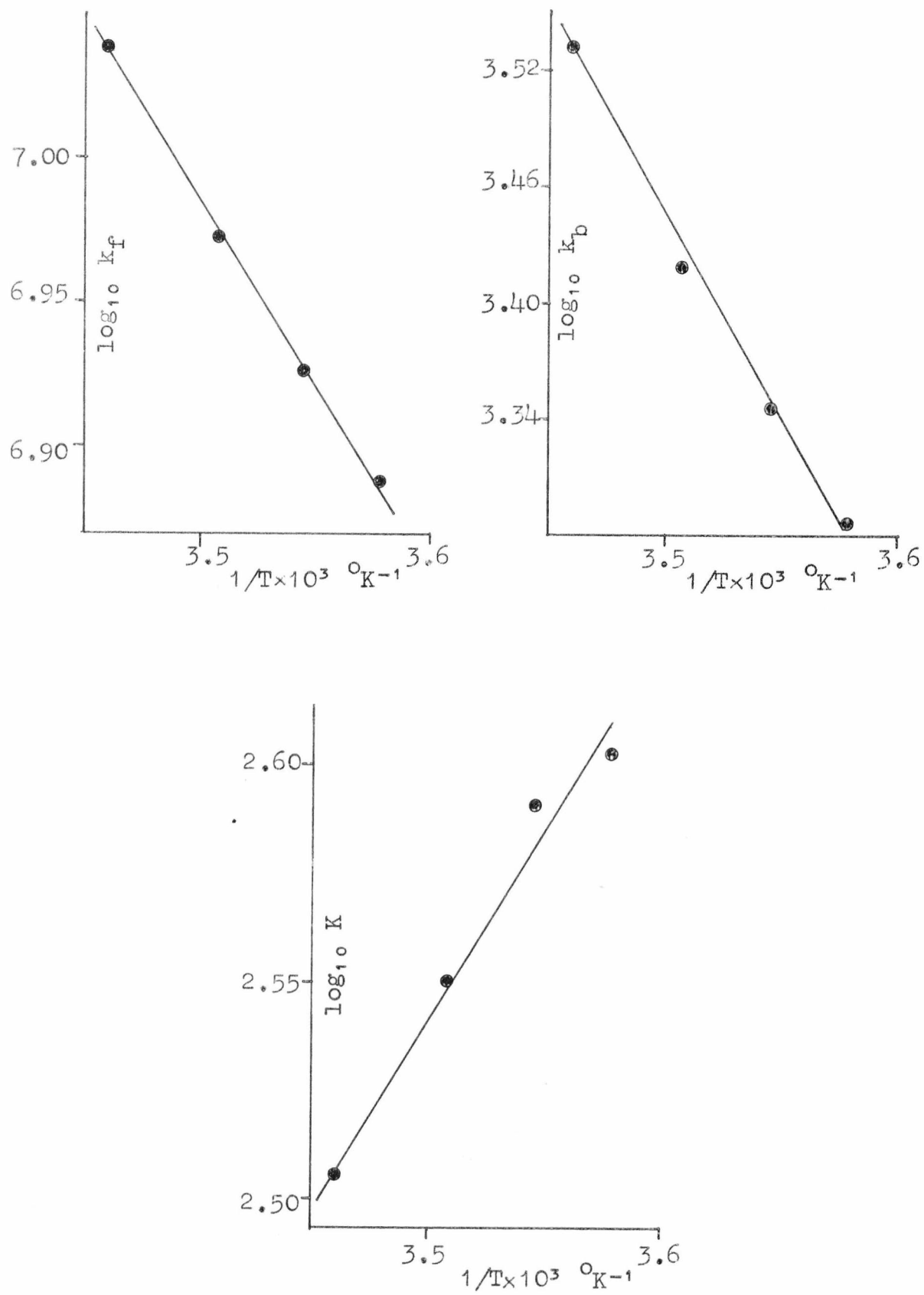


Fig. 4.3.3.9. $\log_{10} k_f, k_b$ and K vs. $1/T$ for $\text{ZnIDA}^\ominus + \text{PADA}$.



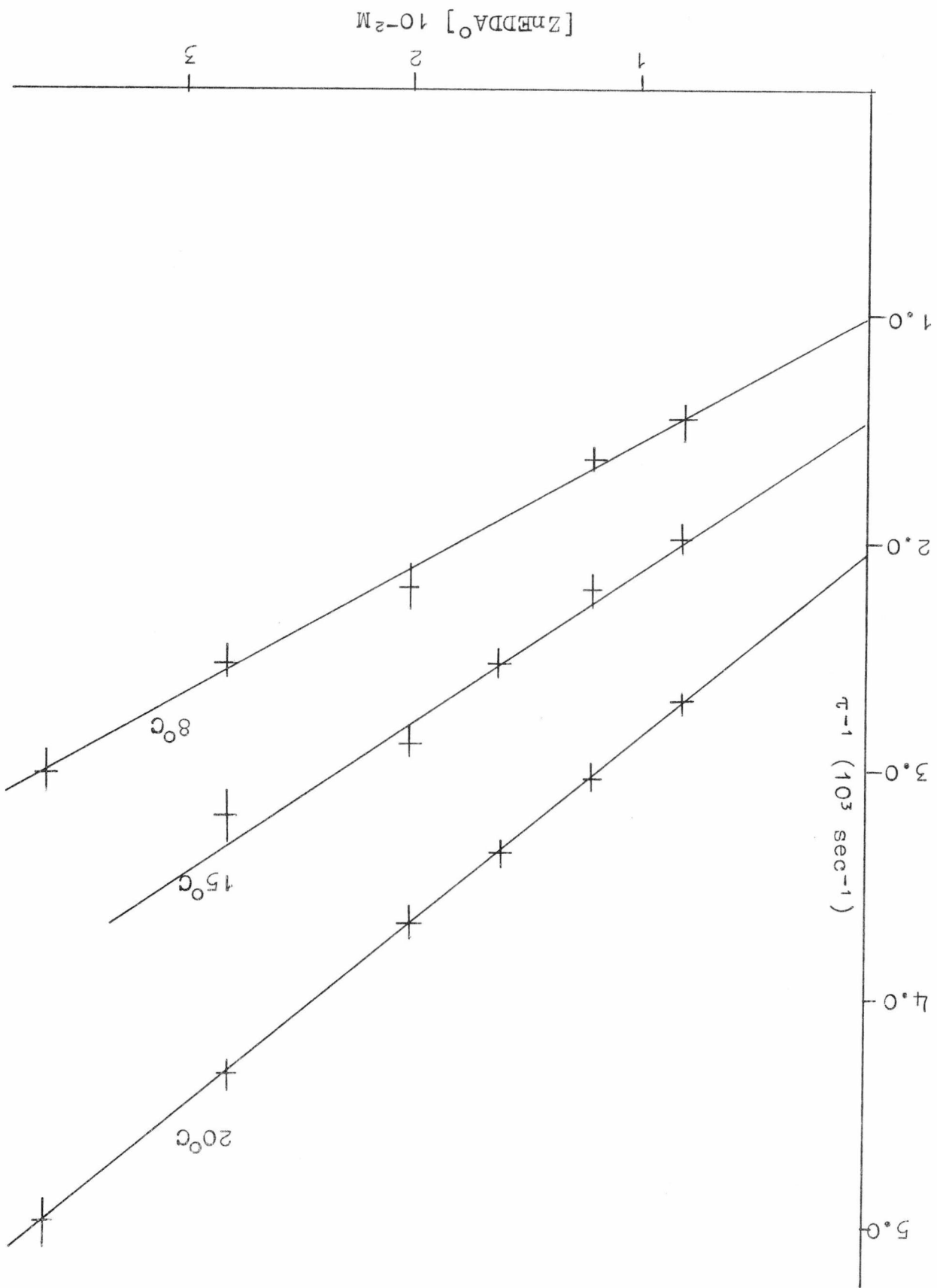


Fig. 4.3.5.10. τ^{-1} vs. [ZnEDDA] for ZnEDDA + PADA.

Fig. 4.3.3.11. $\log_{10} k_f, k_b$ and K vs. $1/T$ for ZnEDDA°
+ PADA.

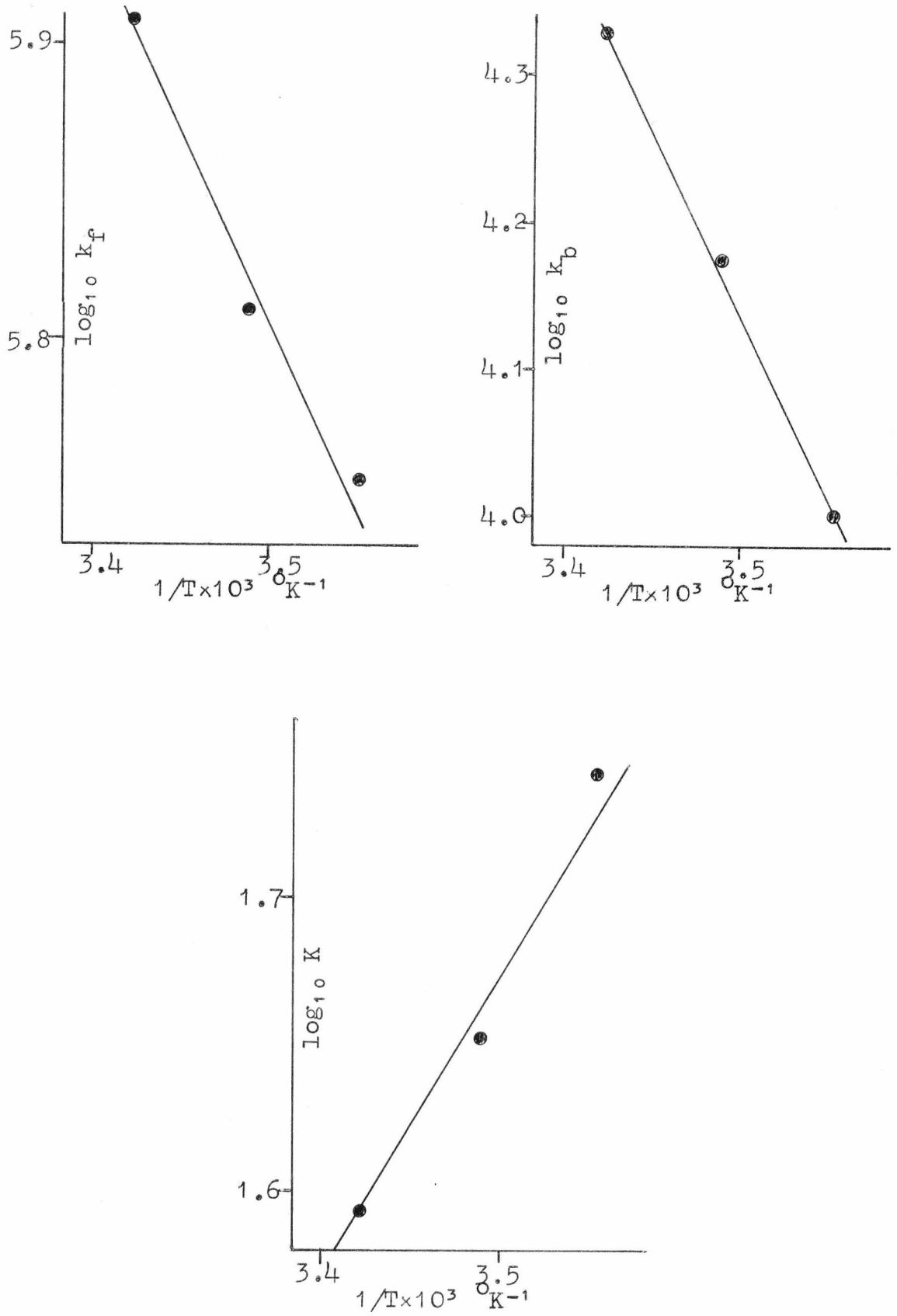


Fig. 4.3.3.12. τ^{-1} vs. $[\text{Zncyst}^{\circ}]$ for $\text{Zncyst}^{\circ} + \text{PADA}$.

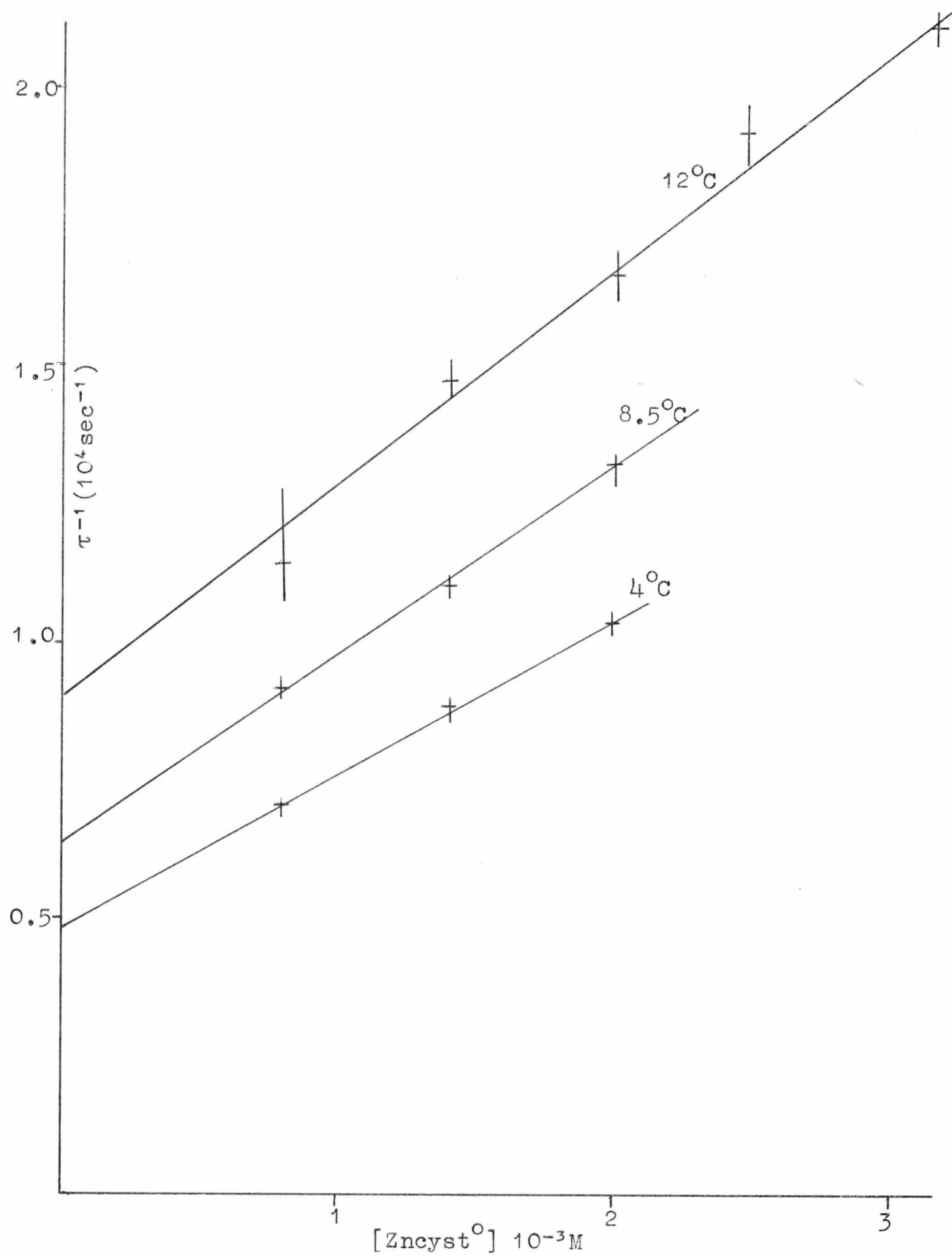


Fig. 4.3.3.13. $\log_{10} k_f, k_b$ and K vs. $1/T$ for $\text{Zncyst}^{\circ} + \text{PADA}$.

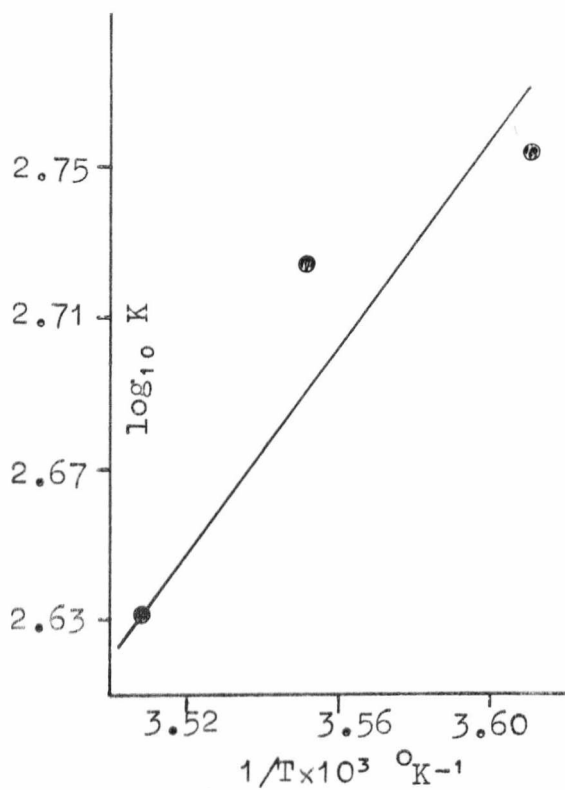
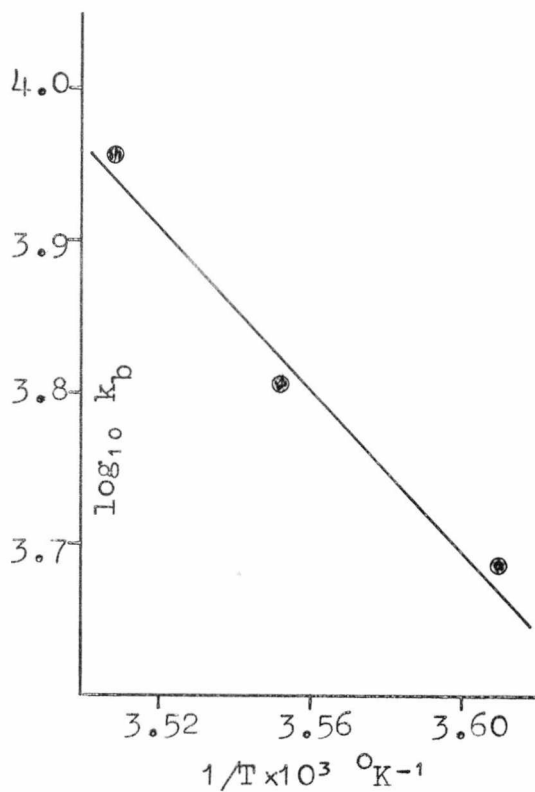
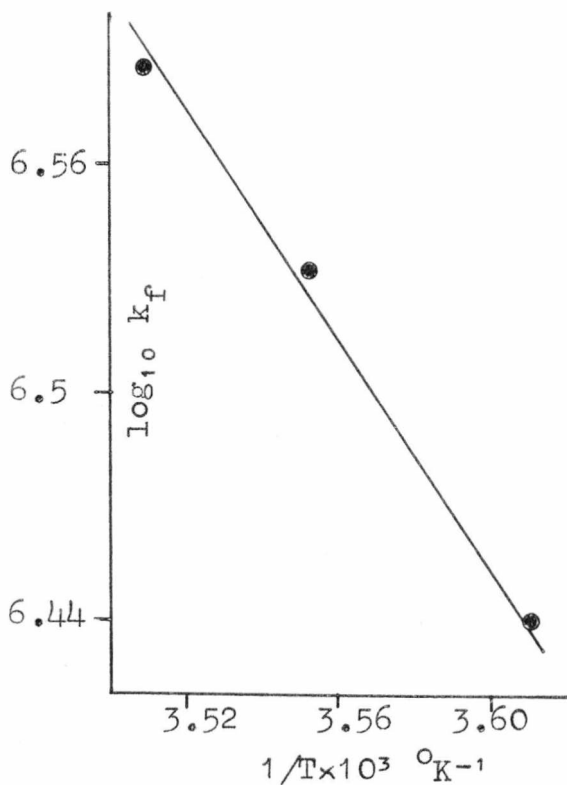


Fig. 4.3.3.14. τ^{-1} vs. $[\text{ZnTP}^{3-}]$ for $\text{ZnTP}^{3-} + \text{PADA}$.

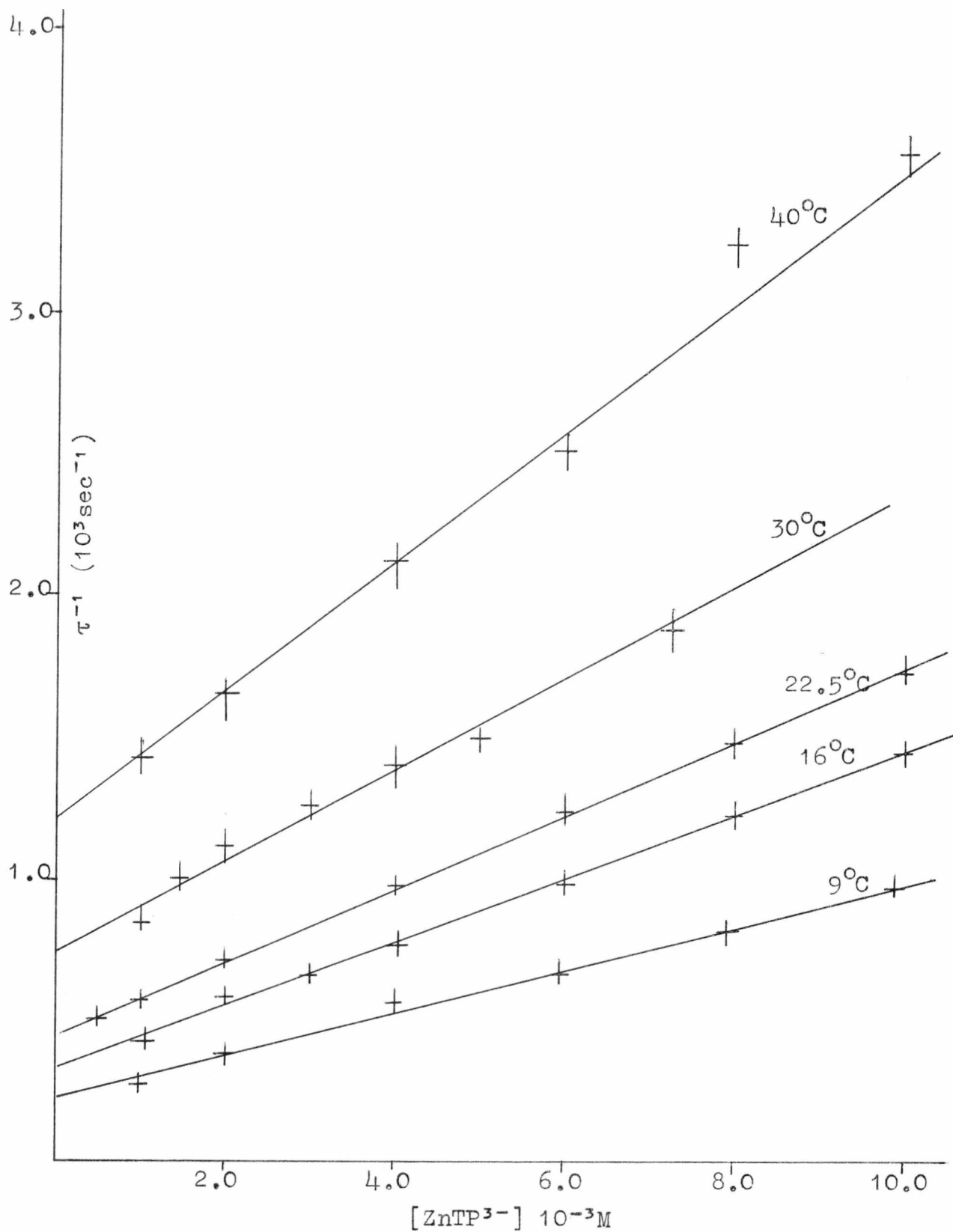


Fig. 4.3.3.15. $\log_{10} k_f$, k_p and K vs. $1/T$ for $ZnTPP^3-$ + PADA.

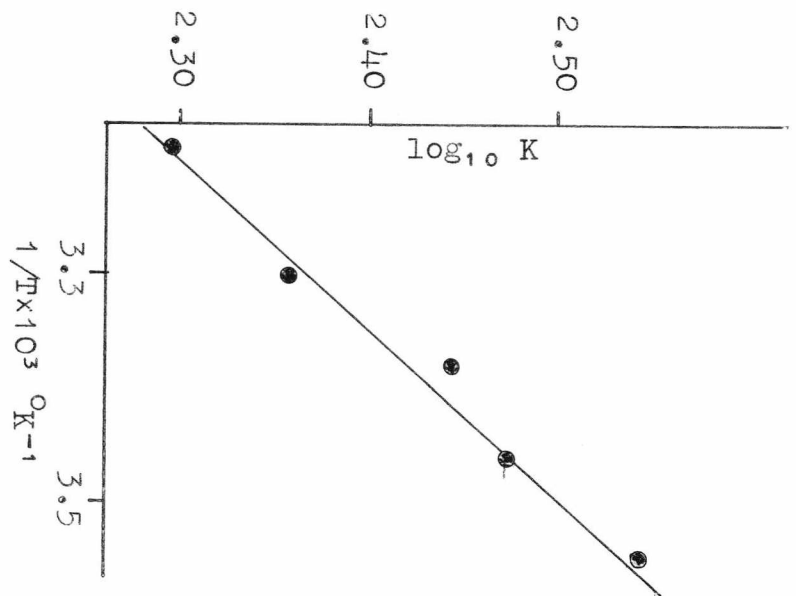
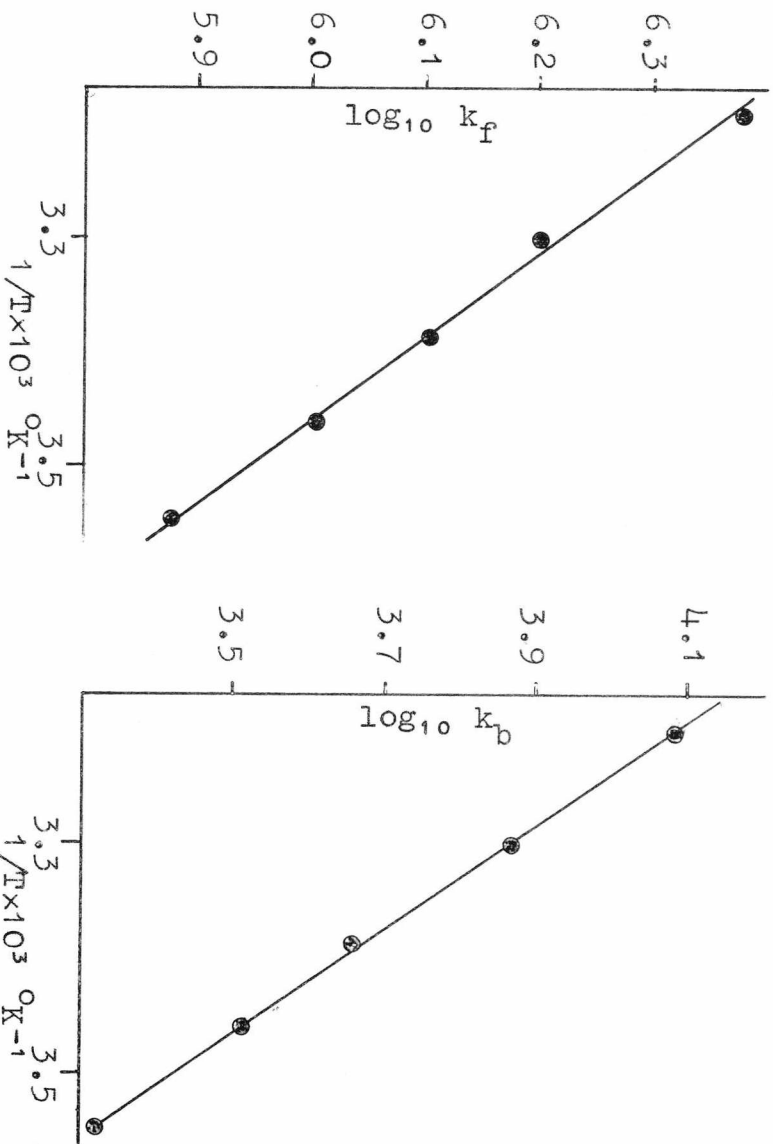


TABLE 4.3.4.1.

Experimental rate constants for ZnL + PADA systems

<u>System</u>	<u>Temp.</u> <u>°C</u>	$\frac{k_f \times 10^{-5}}{1. \text{mol}^{-1} \text{sec}^{-1}}$	$\frac{k_b \times 10^{-3}}{\text{sec}^{-1}}$	$\frac{K}{1. \text{mol}^{-1}}$
Zn(H ₂ O) ₆ ⁺²	4.0	20.8(1)	5.29(1)	393
	9.0	28.8(.3)	8.10(1)	355
	14.5	36.5(3)	11.1(1)	318
	17.0	42.8(7)	14.2(2)	301
	22.0	58.6(7)	21.6(2)	271
Zntrien(NO ₃) ₂ ⁺¹	6.8	5.03(.1)	6.8(.3)	74
	12.0	6.43(.07)	10.8(.3)	61.8
	20.0	8.36(.1)	17.6(.5)	48
Zntrien(ClO ₄) ₂ ⁺²	12.0	13.5(.6)	7.73(.7)	175
	20.0	16.2(.9)	15.5(1)	105
	24.0	18.8(1.3)	21(1.4)	90
Zncyst ⁰	4.0	27.5(7)	4.85(1.4)	567
	8.5	34.0(8)	6.40(0.9)	531
	12.0	38.5(8)	9.0(1.0)	428

TABLE 4.3.4.2.

Experimental rate constants for ZnL + PADA systems

<u>System</u>	<u>Temp.</u> <u>°C</u>	$\frac{k_f \times 10^{-5}}{1. \text{mol}^{-1} \text{sec}^{-1}}$	$\frac{k_b \times 10^{-3}}{\text{sec}^{-1}}$	$\frac{K}{1. \text{mol}^{-1}}$
ZnIDA ⁰	6.5	77.2(0.2)	19.3(0.4)	400
	9.1	84.4(0.3)	21.6(0.4)	390
	12.0	93.6(0.2)	26.2(0.5)	357
	16.0	109(0.3)	34.1(0.6)	320
ZnEDDA ⁰	8.0	5.53(0.5)	10.0(0.2)	55.3
	15.0	6.60(0.6)	14.7(0.3)	44.9
	20.0	8.10(0.4)	20.6(0.2)	39.3
ZnTP ³⁻	9.0	7.56(0.3)	2.15(0.2)	352
	16.0	11.0(0.2)	3.25(0.2)	296
	22.5	12.7(0.2)	4.58(0.4)	279
	30.0	16.1(0.3)	7.32(0.5)	227
	40.0	23.8(0.3)	12.10(0.5)	197
Zndien ⁺²	4.0	137	43	300

TABLE 4.3.4.3.

Final rate constants and activation parameters at 298°K and
0.3 ionic strength for some ZnL + PADA systems

	$\text{Zn}^{2+}(\text{H}_2\text{O})_6$	$\text{Zn}^{2+}\text{trien}(\text{NO}_3)_2$	$\text{Zn}^{2+}\text{trien}(\text{ClO}_4)_{(98)}_2$	ZnIDA^0
$k_f \text{ M}^{-1}\text{sec}^{-1}$	6.8×10^6	1.1×10^6	1.9×10^6	1.5×10^7
$k_b \text{ M}^{-1}\text{sec}^{-1}$	2.7×10^4	2.9×10^4	2.3×10^4	5.2×10^4
$\Delta H_f^\ddagger \text{ kcal mol}^{-1}$	8.8(0.8)	6.2(2.0)	4.0(0.4)	4.2(1.3)
$\Delta H_b^\ddagger \text{ kcal mol}^{-1}$	12.5(0.6)	12.5(1.7)	13.4(1.7)	8.5(1.0)
$\Delta S_f^\ddagger \text{ e.u.}$	+2(3)	-10(6)	-16(3)	-8(3)
$\Delta S_b^\ddagger \text{ e.u.}$	+4(2)	4(5)	6(5)	-8(3)
$\log_{10} K_{\text{kin}} \text{ M}^{-1}$	2.4(0.07)	1.57(0.1)		2.45(0.11)
$\log_{10} K_{\text{spec}} \text{ M}^{-1}$	2.31(0.06)	1.94(0.04)		2.39(0.04)

TABLE 4.3.4.4.

Final rate constants and activation parameters at 298°K and
0.3 ionic strength for some ZnL + PADA systems

	<u>ZnEDDA</u> ⁰	<u>Zncyst</u> ⁰	<u>ZnTP</u> ³⁻
k_f M ⁻¹ sec ⁻¹	9.1(0.6)x10 ⁵	5.4(2.1)x10 ⁶	1.4(0.1)x10 ⁶
k_b sec ⁻¹	2.6(0.2)x10 ⁴	2.3(0.5)x10 ⁴	5.6(0.2)x10 ³
ΔH_f^\ddagger kcal mol ⁻¹	4.2(1.3)	4.9(3.1)	6.2(0.9)
ΔH_b^\ddagger kcal mol ⁻¹	8.8(1.6)	11.2(1.6)	9.2(1.4)
ΔS_f^\ddagger e.u.	-17(4)	-11(9)	-10(3)
ΔS_b^\ddagger e.u.	-9(5)	-1(4)	-10(4)
$\log_{10}K_{kin}$ M ⁻¹	1.54(0.07)	2.37(0.25)	2.40(0.04)
$\log_{10}K_{spec}$ M ⁻¹	1.57(0.05)	2.76(0.03)	2.46(0.03)

4.4 Discussion

The scarcity of kinetic data for complex formation reactions of Zn^{2+} makes a detailed discussion of these results difficult. A comparison of the rate constants at $15^{\circ}C$ ($\log k_f = 6.58$; $\log k_b = 4.09$) and those obtained by Wilkins⁽⁹⁷⁾ ($\log k_f = 6.59$; $\log k_b = 4.00$) show surprising agreement, considering that Wilkins obtained his values from a relaxation observed at one metal concentration and a spectrophotometric stability constant. A comparison of the forward rate constants for the aquo species with a variety of neutral ligands at $25^{\circ}C$, NH_3 ($\log k_f$ 6.5 at $11^{\circ}C$)^(30a), 2,2',2''-terpyridyl (6.1)⁽³¹⁾, o-phenanthroline (6.3)⁽⁹⁹⁾ and bipyridyl (6.0)⁽⁹⁹⁾, shows that the PADA result is similar and so it is unlikely that ring closure has become rate limiting. Even fewer activation parameters have been measured, but the value of ΔH_f^{\ddagger} of $8.8 \text{ kcal mol}^{-1}$ is similar to those of 8 kcal mol^{-1} and 6 kcal mol^{-1} for 2,2',2''-terpyridyl and 2,2'-bipyridyl, respectively.⁽⁹⁹⁾

It has not been possible to measure the water exchange rate constant, k_{ex} , for aquo zinc directly using n.m.r. techniques, but a value has been obtained, of $3 \times 10^7 \text{ sec}^{-1}$, from the ultrasonic relaxation of zinc sulphate in water-glycol mixtures⁽¹⁰⁰⁾. Using this value of k_{ex} it is possible to calculate a value of K_{OS} , 0.23 M^{-1} , which is in good agreement with the value of 0.15 M^{-1} calculated from the Fuoss equation by Rorabacher^(30a), 0.1 M^{-1} by Wilkins⁽⁹⁷⁾ and 0.3 M^{-1} by Hammes⁽¹⁰¹⁾.

The presence of bound ligands on the zinc ion has little effect on the rate of complex formation with PADA in comparison with the Ni^{2+} system⁽⁸⁵⁾. (The difference in k_f from ligand to ligand would have been even smaller if it had been possible to

apply statistical corrections to account for the different numbers of water molecules available for substitution, but because in some cases, e.g. Zndien^{2+} , nitrate is bound to the metal, while in others, e.g. Zntrien^{2+} , there are no bound water molecules, such a treatment has not been undertaken.) Thus, there is only a factor of 5 difference (2.5 if the statistical effect is taken into account) in the rates of complex formation for $\text{Zn}(\text{H}_2\text{O})_6^{2+}$ and ZnTP^{3-} with PADA while the charge on the metal species changes from +2 to -3.

In the Zntrien^{2+} systems there is the possibility that ZnHtrien^{3+} could also be reactive. Using the published stability constants⁽³⁸⁾

$$K_1 = \frac{[\text{Zntrien}]}{[\text{Zn}][\text{trien}]} = 10^{12.1}$$

$$K_2 = \frac{[\text{ZnHtrien}]}{[\text{Zn}][\text{Htrien}]} = 10^{7.3}$$

$$K_3 = \frac{[\text{Htrien}]}{[\text{H}][\text{trien}]} = 10^{9.92}$$

and omitting charges for clarity, it can be shown that

$$\frac{[\text{Zntrien}]}{[\text{ZnHtrien}]} = \frac{K_1[\text{Zn}][\text{trien}]}{K_2K_3[\text{Zn}][\text{H}][\text{trien}]}$$

Thus at the lowest pH used, 6.5, $[\text{Zntrien}]/[\text{ZnHtrien}]$ is 25. If the reactive species is the protonated form then the relaxation time should be sensitive to pH and the kinetic data would be expected to resemble those for Zndien^{2+} . However, the reaction is independent of pH and there is a marked difference in the dissociation rate constants for Zndien^{2+} and Zntrien^{2+} , so it is concluded that Zntrien^{2+} is the reactive species.

As the geometry at Zn^{2+} is flexible and depends on the nature of the coordinated ligand, the free energies of the tetrahedral, 5-coordinate and octahedral species must be comparable. Since it is likely that there is an entropic difference between the different coordination states, there must be a large degree of compensation between ΔH° and ΔS° for the interconversion process. The fact that the rates of formation of PADA with (tetrahedral) $Zn^{2+}(\text{trien}(\text{ClO}_4)_2)$, (5-coordinate) $Zn^{2+}(\text{trien}(\text{NO}_3)_2)$, and octahedral $Zn^{2+}(\text{H}_2\text{O})_6$ are similar implies that the interconversion between the coordination states must be at least as rapid as the substitution process. (No evidence was found for the transition previously reported in the microsecond time range⁽¹⁰¹⁾ and attempts to repeat this work were unsuccessful.) The failure of Zn^{2+} to form a complex with PADA can probably be explained by the particular requirements of the ligand (see section 3.5.1.) making the expansion of the coordination shell to six impossible, while the "normal" rates and activation parameters for $ZnEDDA^\circ$ imply that the formation of a tetrahedral complex of this species with PADA is unlikely although it has been suggested that the ternary complex formed by the reaction of ethylenediamine with $ZnEDDA^\circ$ ^{is tetrahedral.} The marked similarity in the dissociation rates of the ternary complexes⁽⁹⁰⁾ indicates once more the small effect of the bound ligand: the zinc ion behaving as a symmetrical sphere of positive charge and any covalent contributions⁽⁶⁾ arising from the binding of the ligands to the zinc ion do not affect the rates of substitution.

CHAPTER 5

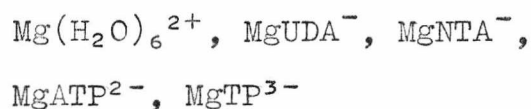
Complex formation and dissociation involving Mg(II) and
5-nitrosalicylic acid

5.1 Introduction

5-nitrosalicylic acid (NSA) has been shown to bind to metal ions⁽¹⁰³⁾ to give complexes which have characteristic absorption bands in the visible region of the spectrum, around 380 nm. The binding of metals to NSA is pH dependent and the nature of this dependence indicates complex formation between the dianion and the metal ions and, from the stability of the metal-NSA complexes, it can be deduced that NSA acts as a bidentate ligand.

The spectra of each of the NSA species (fig. 5.1.1) are such that it is possible to investigate the relevant equilibria involving NSA by spectrophotometric techniques.

The kinetics of complexation between NSA and the following magnesium species have been studied:

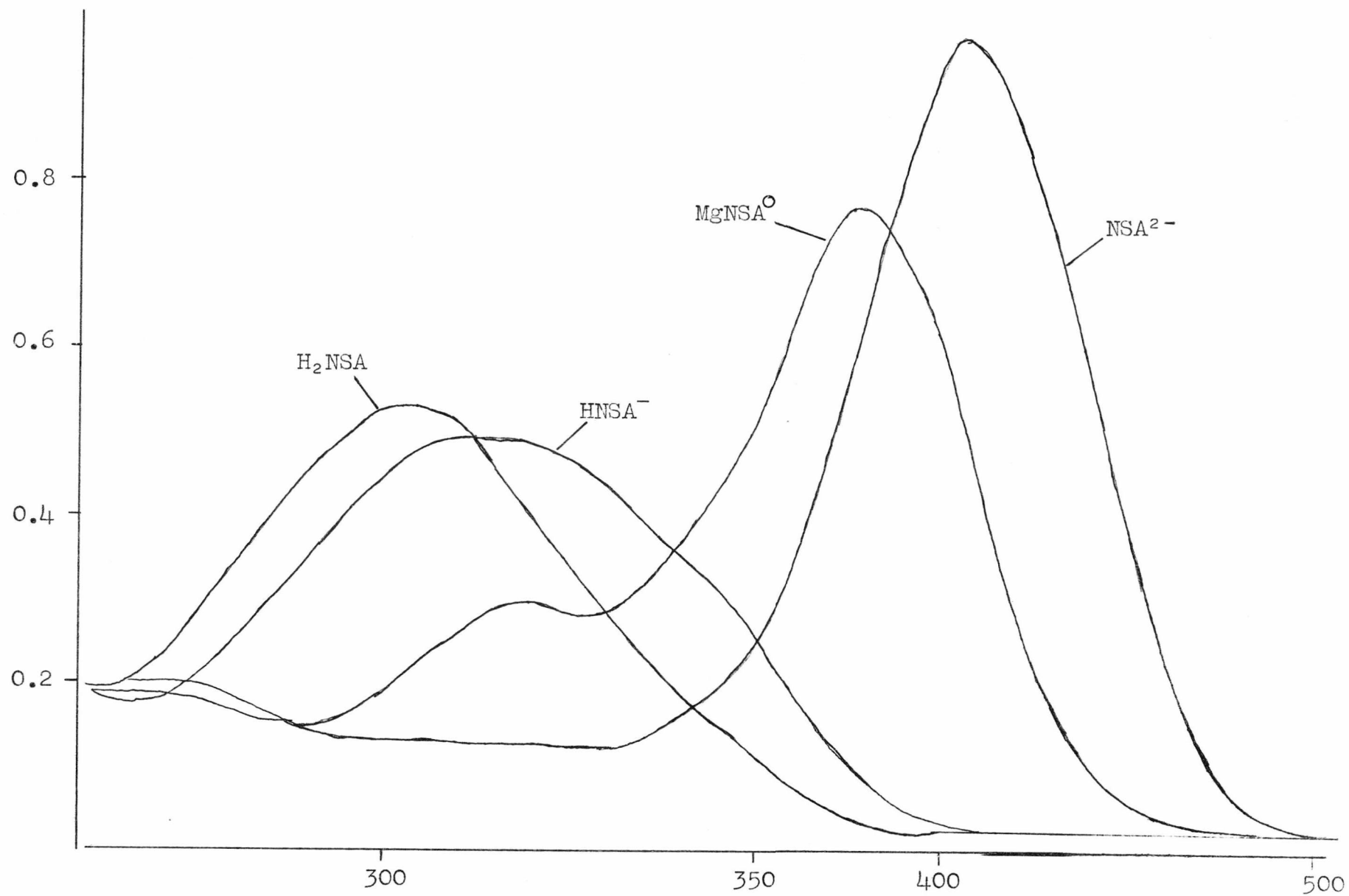


together with those of the reaction between $\text{Mg}(\text{H}_2\text{O})_6^{2+}$ and 8-hydroxyquinoline-5-sulphonic acid at 25°C.

The temperature-jump method was used to study the kinetics of each system at five temperatures over the range 6-38°C.

The first protonation of NSA has also been studied spectroscopically over a range of temperatures from 13-36°C and the second protonation at 25°C. The stability constants for the ternary complexes of all the magnesium complexes have been determined spectroscopically at 25°C.

Fig. 5.1.1. Absorption spectra of NSA species.



5.2 Determination of K_1

Above pH 6 only the mono and dianions are present in significant amounts so that

$$d = \epsilon_{HA}[HA] + \epsilon_A[A] \quad \dots (5.2.1)$$

where ϵ_{HA} , ϵ_A are the extinction coefficients of $HNSA^-$ and NSA^{2-} respectively and d is the optical density of the solution.

If the total concentration of NSA is C , the stability constant

$$K_1 = \frac{[HA]}{[H][A]}$$

and the effective extinction coefficient of the test solution is ϵ , then equation (5.2.1) becomes

$$C\epsilon = \epsilon_{HA}[HA] + \epsilon_A[A]$$

and, substituting for $[HA]$ and rearranging,

$$\epsilon(K_1[H][A]) + \epsilon[A] - \epsilon_{HA}(K_1[H][A]) - \epsilon_A[A] = 0$$

$$\text{or} \quad (\epsilon - \epsilon_{HA})(K_1[H][A]) + (\epsilon - \epsilon_A)[A] = 0$$

Multiplying by C/A gives

$$\begin{aligned} C(\epsilon - \epsilon_{HA})K_1[H] + C(\epsilon - \epsilon_A) &= 0 \\ &= (d - C\epsilon_{HA})K_1[H] + d - C\epsilon_A = 0 \end{aligned}$$

$$\text{or} \quad -d = (d - C\epsilon_{HA})K_1[H] - C\epsilon_A$$

Thus a plot of d vs. $(d - C\epsilon_{HA})[H]$ gives a straight line of slope $-K$ and intercept $C\epsilon_A$.

Experimental conditions

For each determination the NSA concentration was kept constant at $5 \times 10^{-5}M$ and the optical density of a series of solutions was measured as a function of pH using $10^{-2}M$ borax buffer (fig. 5.2.1) and a constant ionic strength (of 0.3 using sodium nitrate). The extinction coefficient of $HNSA^-$ was measured using the same NSA concentration at pH 6.8 with $10^{-2}M$ phosphate buffer.

The plots of d vs. $(d - C\epsilon_{HA})[H]$ for a series of temperatures are shown in figs. 5.2.2 - 5.2.3. The values of K_1 obtained are shown in table 5.2.1.

TABLE 5.2.1 Results for K_1

<u>Temp.</u> <u>°C</u>	<u>K_1</u>	<u>pK_1</u>
13	$11.1(.05) \times 10^9$	10.04(.02)
20	8.60×10^9	9.93(.04)
28	6.60×10^9	9.82(.01)
36	$5.04(0.10) \times 10^9$	9.70(.01)

A graph of $\log K_1$ against $1/T^\circ K$ is shown in fig. 5.2.4. From the slope and intercept of this graph values of

$$\begin{aligned} \Delta H^\circ &= -6.2(0.1) \text{ kcal mol}^{-1} \\ \Delta S^\circ &= +24.3(0.4) \text{ e.u.} \\ \Delta G^\circ &= -13.4(0.2) \text{ kcal mol}^{-1} \end{aligned}$$

were obtained.

These results are in good agreement with those of Agren⁽¹⁰⁶⁾ taken from Ashcroft and Mortimer⁽¹⁰⁷⁾ for the reaction $HL^- \rightleftharpoons H^+ + L^{2-}$ shown in table 5.2.2.

Fig. 5.2.1. pK₁ determination of NSA at 20°C.

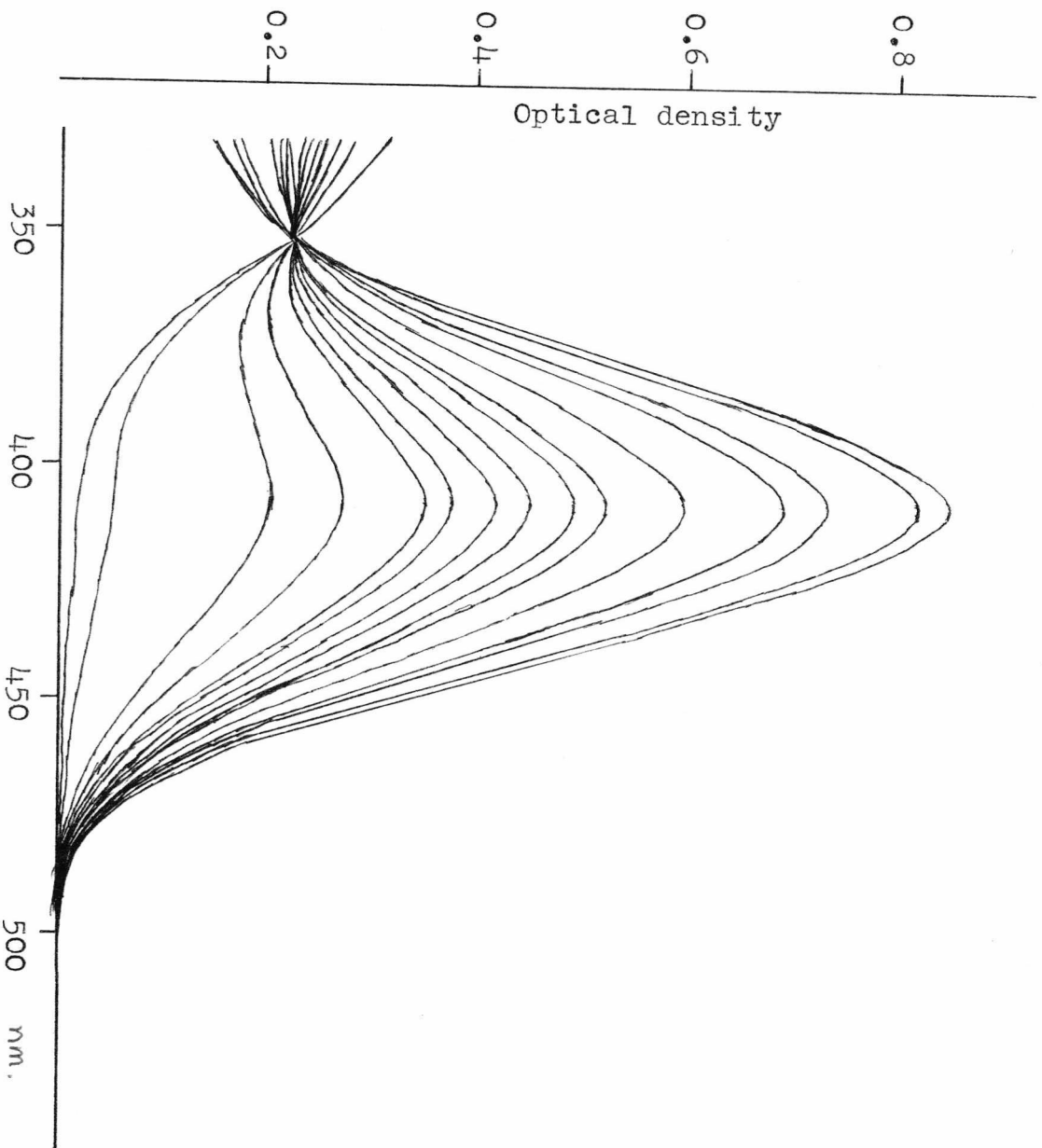


Fig. 5.2.2. pK_1 determination of NSA.

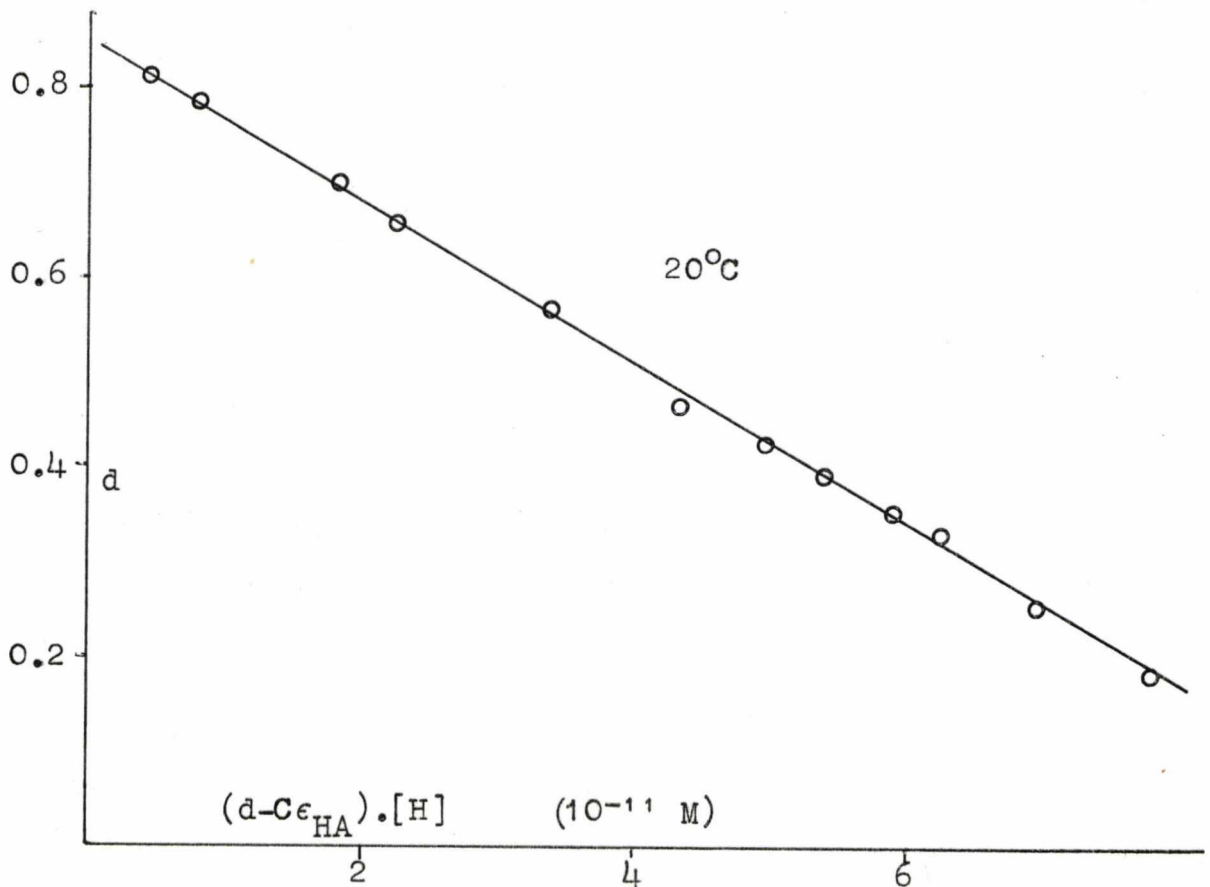
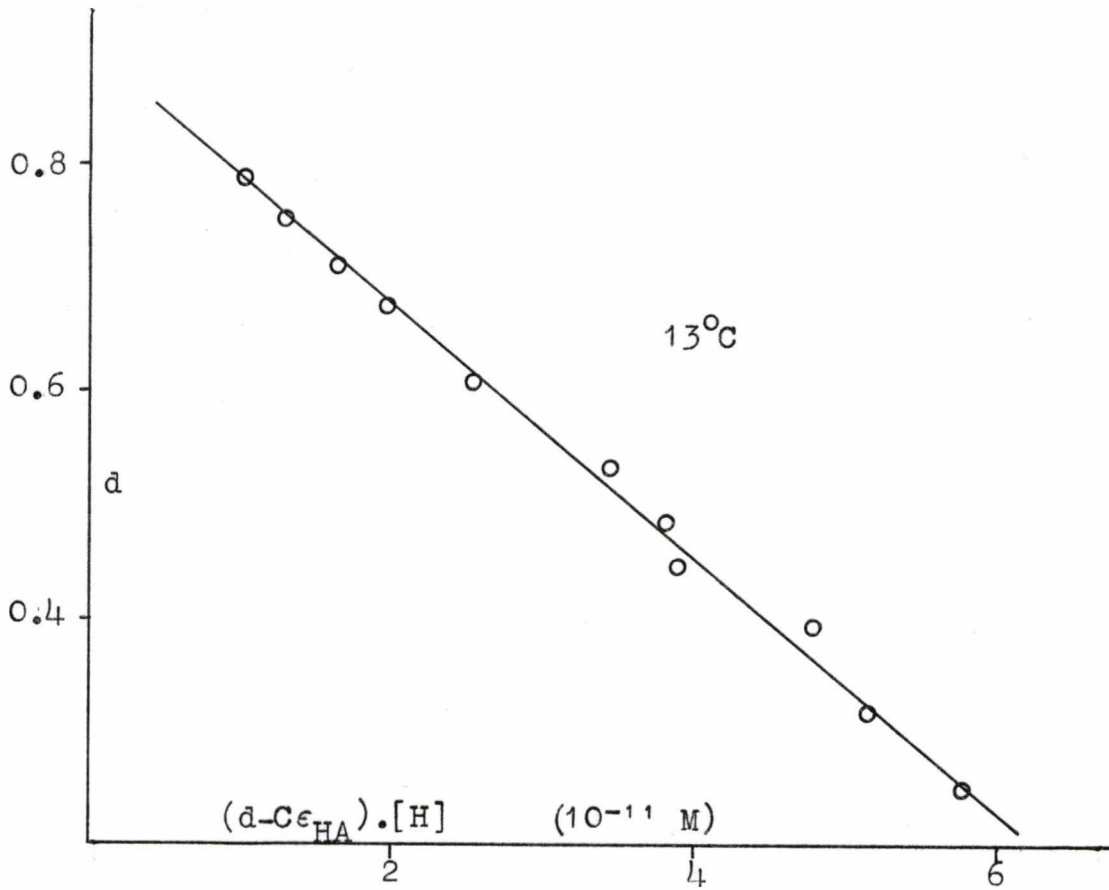


Fig. 5.2.3. pK_1 determination of NSA.

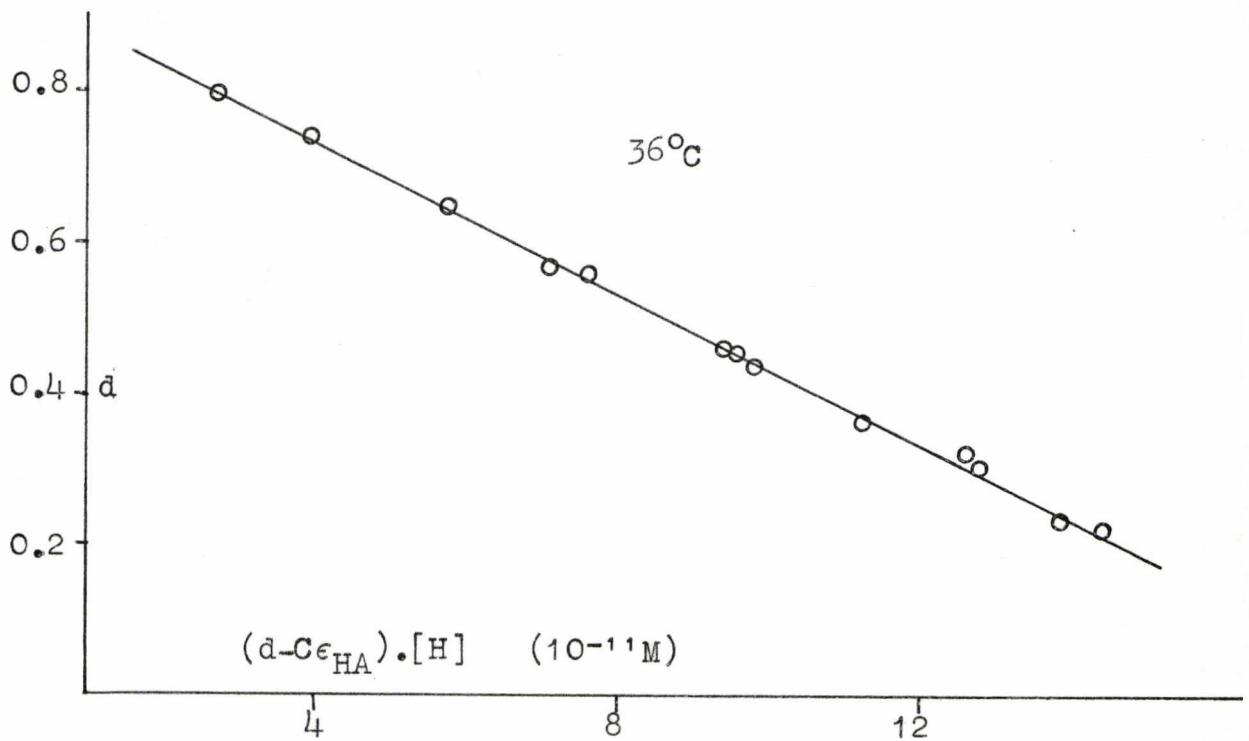
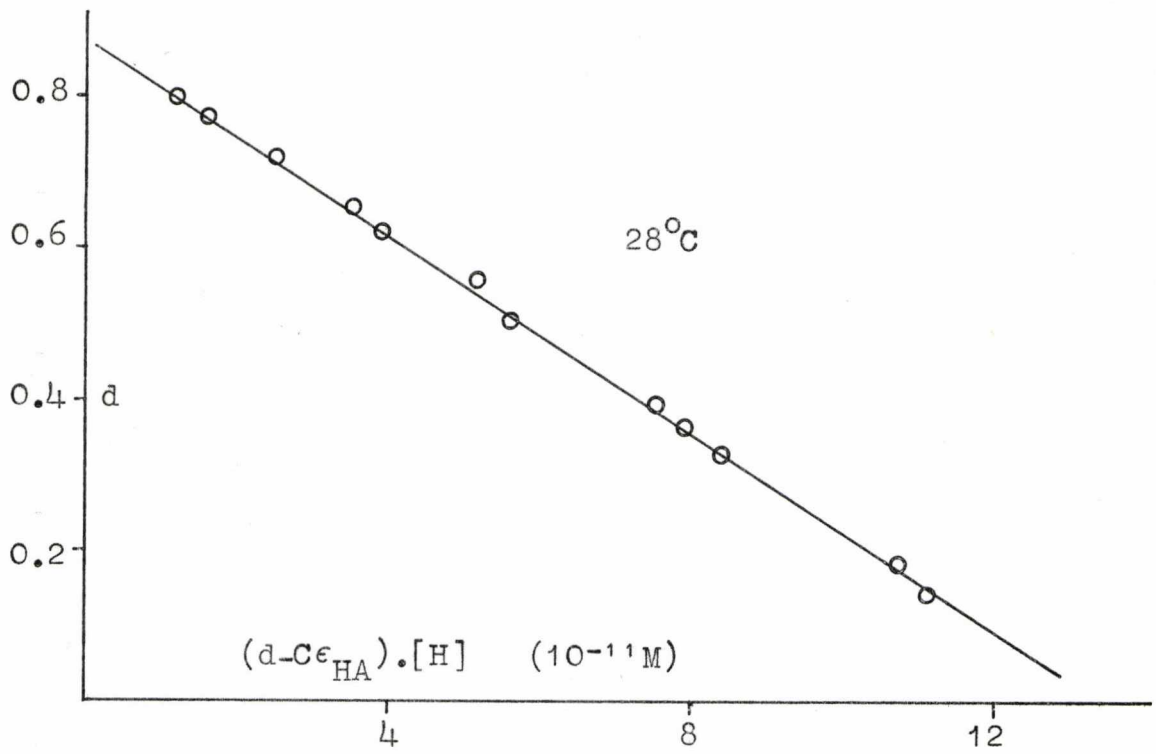


Fig. 5.2.4. $\log K_1$ vs. $1/T^{\circ}\text{K}$ for NSA^{2-} .

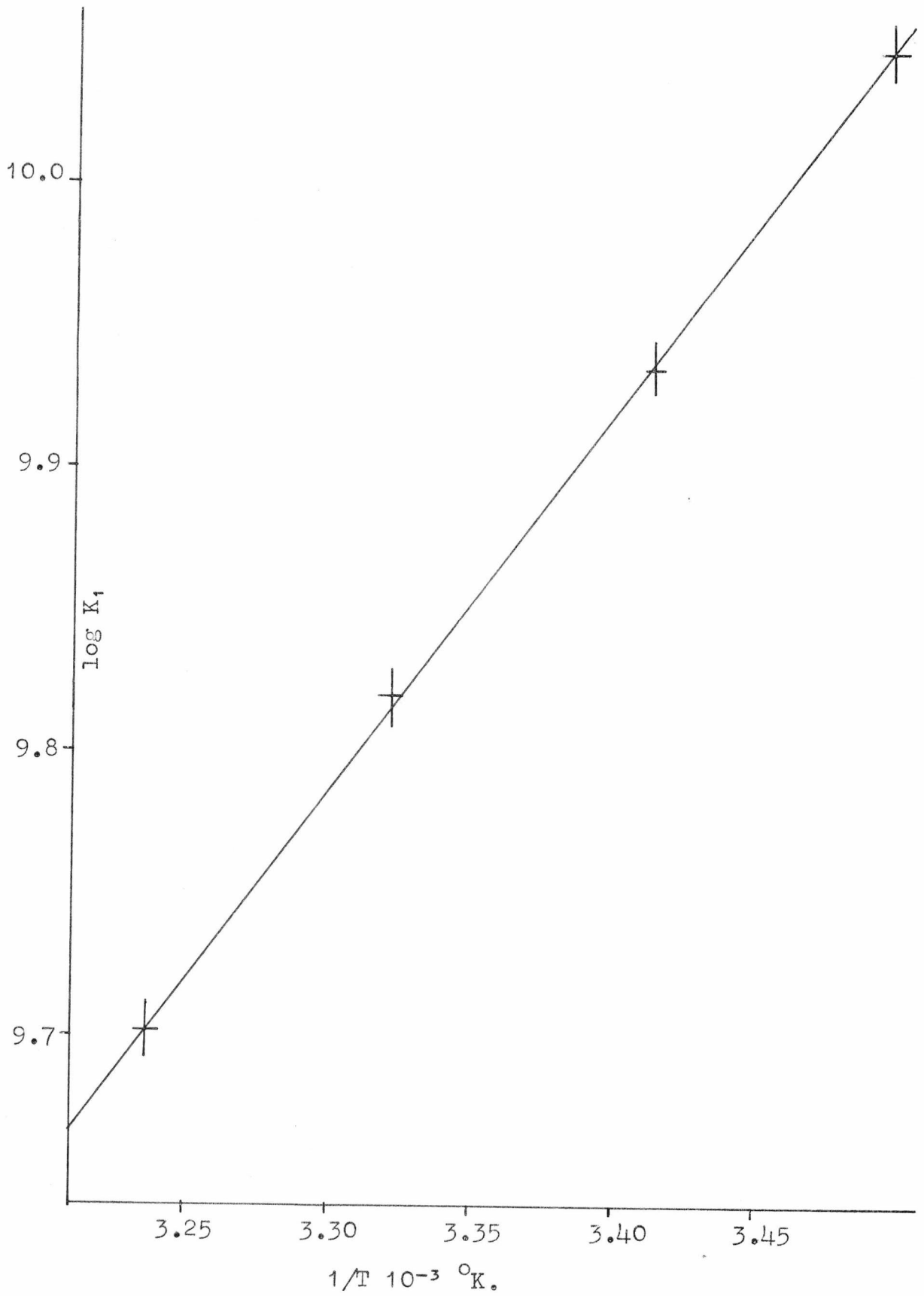


TABLE 5.2.2. Thermodynamic data for the dissociation of the phenolic hydrogen from a series of salicyl compounds.

<u>Ligand</u>	<u>ΔH kcal mol⁻¹</u>	<u>ΔG kcal mol⁻¹</u>	<u>ΔS e.u.</u>
salicylaldehyde	6.3	12.1	-20
salicylic acid	8.6	18.0	-32
sulphosalicylic acid	7.1	16.1	-30
p-aminosalicylic acid	11.0	18.9	-27
p-aminosalicylamide	5.1	12.5	-25
methylsalicylic acid	7.5	14.0	-22
salicylamide	6.7	12.2	-18

5.3 Determination of K_2

$$K_2 = \frac{[H_2NSA]}{[H^+][HNSA^-]}$$

Below pH 6 the concentration of the dianion is negligible so that the absorbance of any test solution is due entirely to the neutral molecule and the mono anion. Using a similar treatment to that in section 5.2.1, it can be shown that

$$d = (d - C\epsilon_{H_2A})K_1[H] - C\epsilon_{HA}$$

where d is the optical density of the solution and ϵ_{HA} and ϵ_{H_2A} are the extinction coefficients of $HNSA^-$ and H_2NSA , respectively. Thus a plot of d vs. $(C\epsilon_{HA} - d)/[H]$ gives a straight line of slope $1/K$ and intercept $C\epsilon_{H_2A}$.

Experimental conditions

The total NSA concentration was kept constant at $4 \times 10^{-5}M$ and the optical density of a series of solutions was measured as a function of pH using $4 \times 10^{-2}M$ oxalic acid as a buffer and keeping the ionic strength at 0.3 by the addition of varying

amounts of sodium perchlorate. The extinction coefficient of HNSA^- was measured at pH 6.8 using 10^{-2}M phosphate as a buffer.

Result

At 25°C , the plot of d vs. $(C\epsilon_{\text{HA}} - d)/[\text{H}]$ (fig. 5.3.1) gave a straight line of slope 4.4×10^1 and intercept 0.251 O.D. units. The intercept was checked by taking a solution of exactly the same NSA concentration and measuring the optical density of the solution in $3 \times 10^{-1}\text{M}$ perchloric acid (under which conditions all the NSA should be present as H_2NSA). The measured O.D. was 0.25 O.D. units, in excellent agreement with the graphical value.

Values at 25°C :

$$K_2 = 4.4(\pm 2) \text{ M}^{-1}$$

$$\text{p}K_2 = 1.64(.02)$$

These two $\text{p}K$'s are in reasonable agreement with those reported in the literature^(104,105) at infinite dilution, there being a constant difference of .48 in the $\text{p}K$'s.

5.4 Stability constants of magnesium-NSA complexes

5.4.1 Determination of K_3 at 25°C

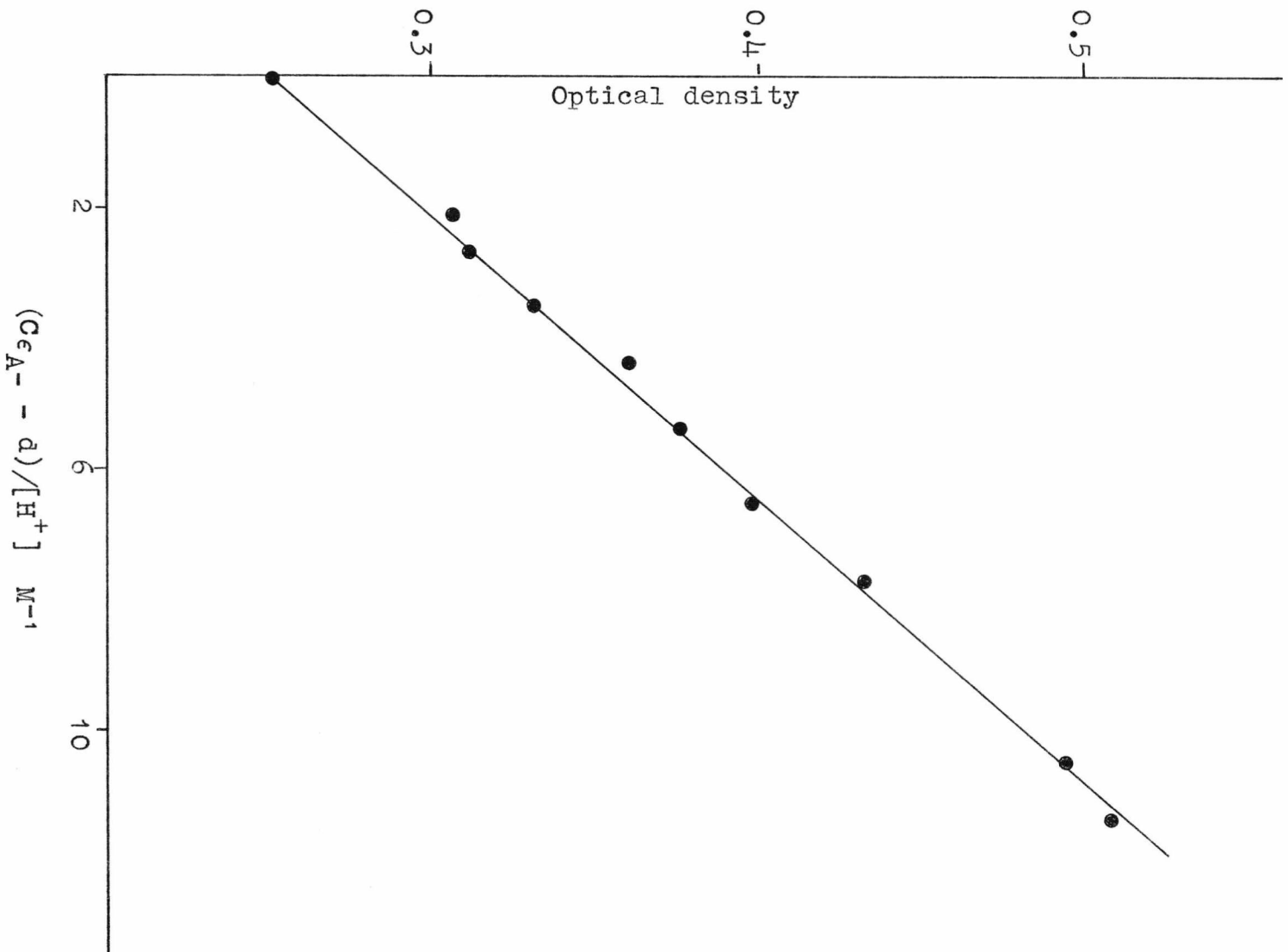
By a method analogous to that used for deriving the $\text{p}K$'s of NSA, it can be shown that a plot of

$$\text{od vs. } \frac{(\text{od} - C\epsilon_{\text{A}^-}) + (\text{OD} - C\epsilon_{\text{HA}})K_1[\text{H}]}{[\text{M}]}$$

gives a straight line of slope $-1/K_3$ and intercept $C\epsilon_{\text{MA}}$, where $C\epsilon_{\text{MA}}$ is the extinction coefficient of the metal NSA complex and all other symbols are as in sections 5.2.1 and 5.2.2.

(Appendix 4).

Fig. 5.3.1. pK_2 of NSA at 25°C.



5.4.2. Conditions used

For all these determinations the optical density of a set of solutions was measured as a function of pH. If it was not possible to get a large variation in optical density by this method, the metal concentration was also varied. (The metal:ligand ratios and total metal concentrations used are shown in table 5.4.1.1.) The total concentration of NSA was always $5 \times 10^{-5}M$. In all cases $4 \times 10^{-2}M$ ammonium nitrate was used as a buffer (changing the buffer concentration was found to have no effect on the stability constant) and the ionic strength was kept constant at 0.3 by the addition of varying amounts of sodium nitrate.

TABLE 5.4.1.1. Conditions used in spectrophotometric determinations

<u>System</u>	<u>M:L</u>	<u>[ML]</u>	<u>pH range used</u>
MgNTA ⁻	1:1.1	$3.2 \times 10^{-2}M$	7.8 - 9.3
MgUDA ⁻	1:1.1	$3.2 \times 10^{-2}M$	8.3 - 9.3
MgATP ²⁻	1:2	$1.6-4.0 \times 10^{-2}M$	8.6 - 9.6
MgTP ³⁻	1:2	$1.2 \times 10^{-2}M$	8.2 - 10.2
Mg(H ₂ O) ₆ ²⁺		$5 \times 10^{-3}M$	7.5 - 10.3

5.4.3. Results

The results for K_3 are shown in table 5.4.3.1 and the plots of

$$\text{od vs. } \frac{(\text{od}-C\epsilon_{A^-}) + (\text{od}-C\epsilon_{HA})K_1[H]}{[M]}$$

are shown in figs. 5.4.3.1 - 5.4.3.3.

Fig. 5.4.3.1. Stability constant for $Mg(H_2O)_6^{2+}$ + NSA at 25°C.

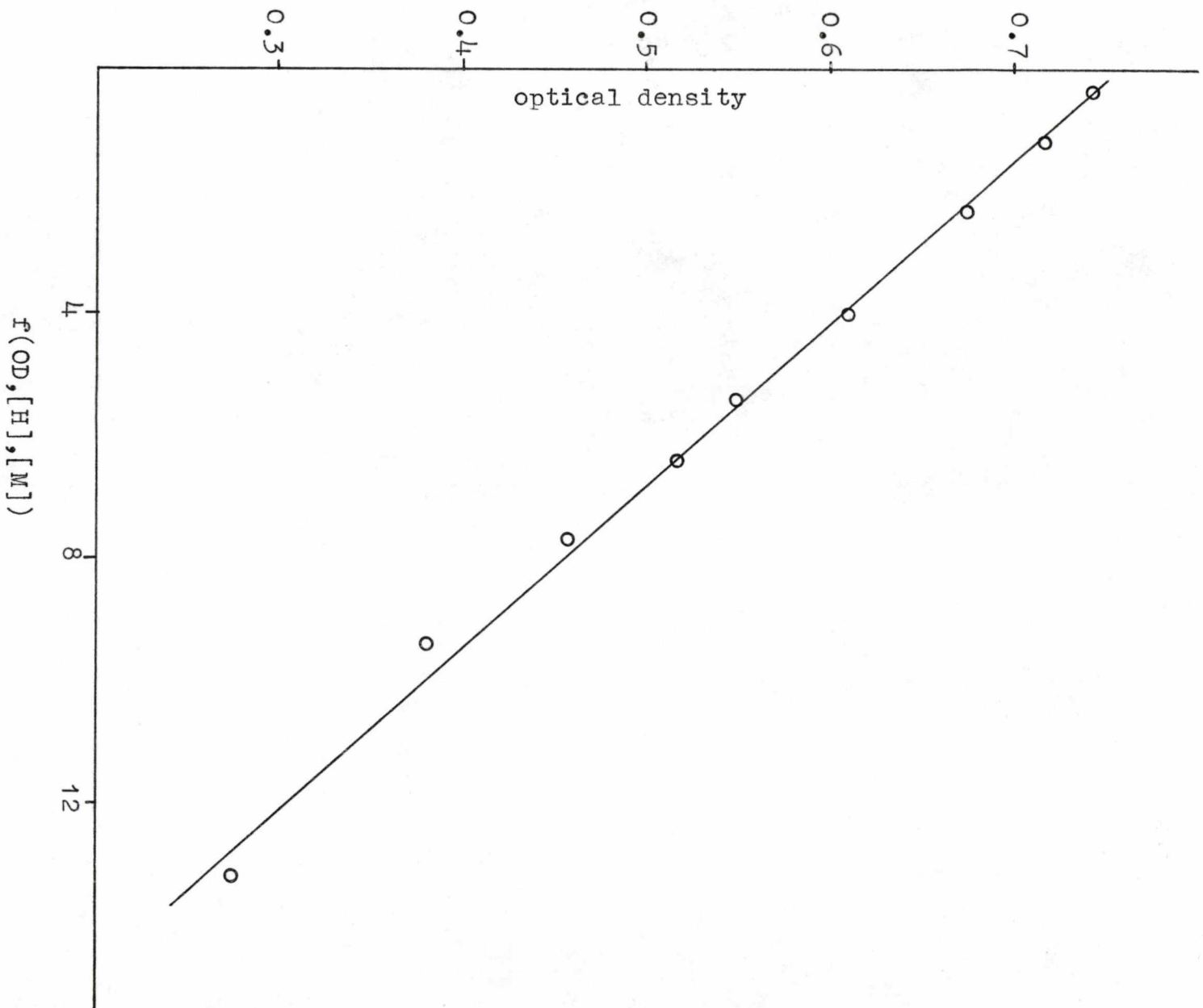


Fig. 5.4.3.2. Stability constants for MGATP²⁻ and MGUDA⁻ with NSA at 25°C.

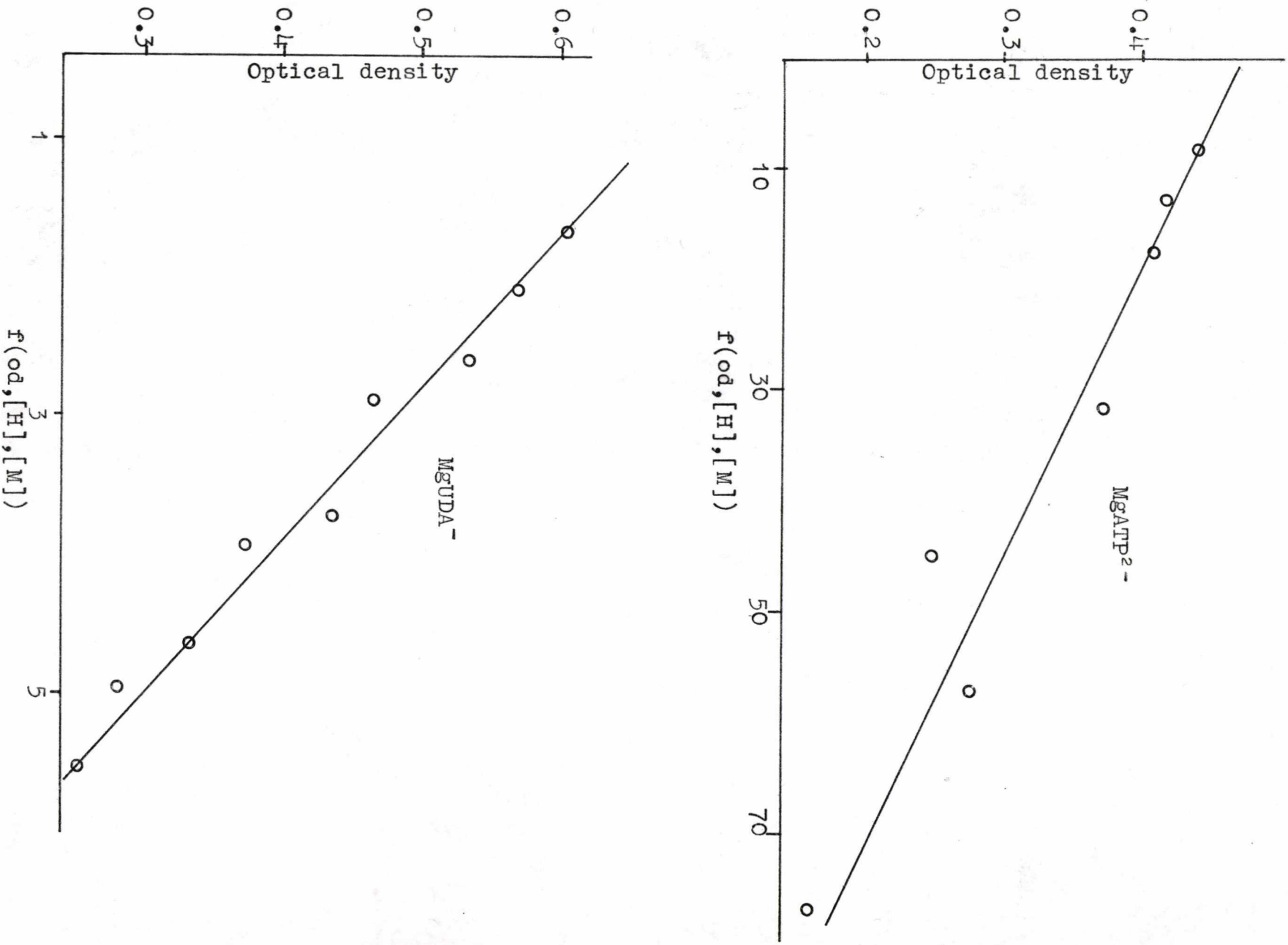


Fig. 5.4.3.3. Stability constants for MgTP^{3-} and MgNTA^- with NSA^{2-} at 25°C .

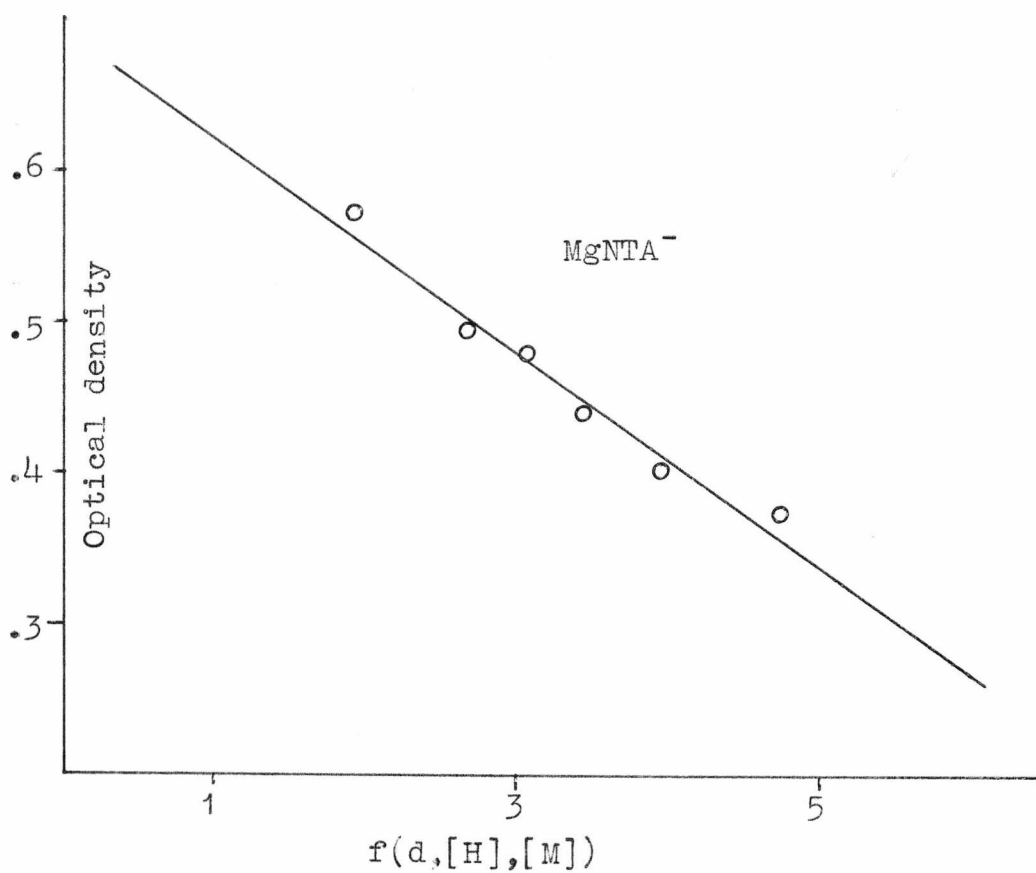
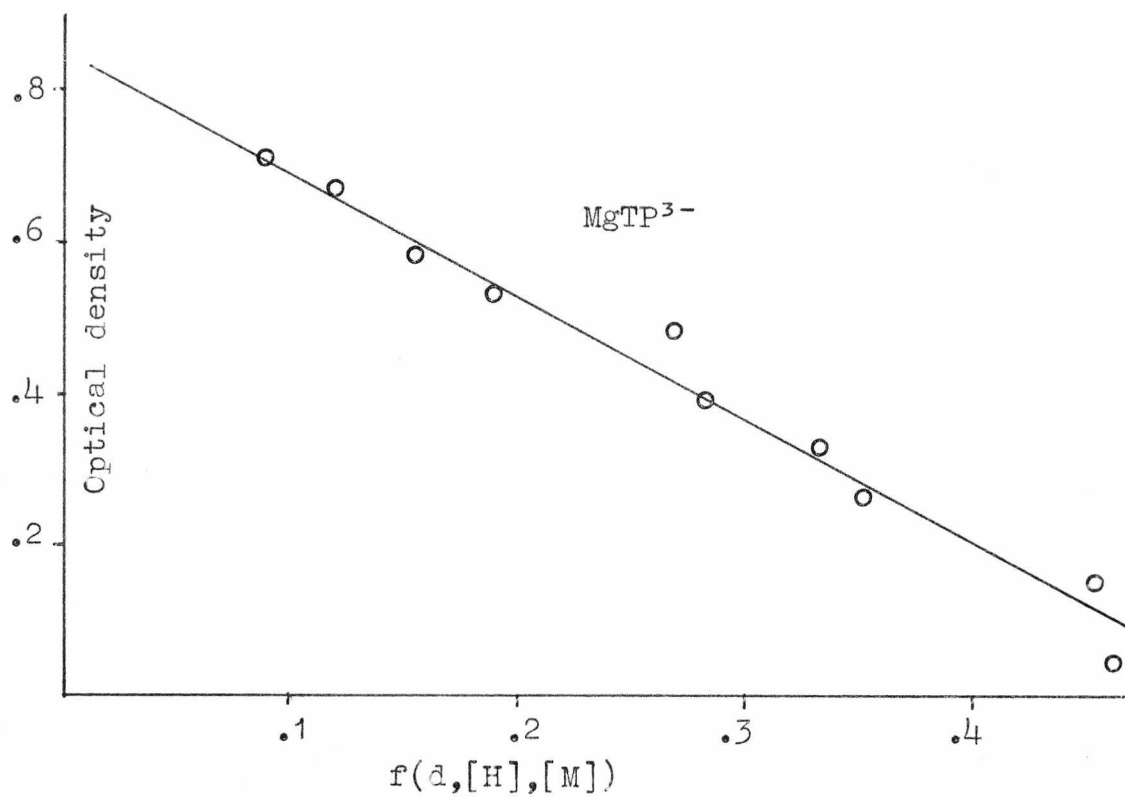


TABLE 5.4.3.1. Results for K_3 at 25°C.

<u>System</u>	<u>log K_3</u>
Mg(H ₂ O) ²⁺	4.03(0.05)
MgUDA ⁻	2.53(0.03)
MgNTA ⁻	2.67(0.06)
MgATP ²⁻	2.41(0.06)
MgTP ³⁻	1.71(0.02)

5.5 Choice of conditions for the kinetics

5.5.1 Ligand:metal ratio

The low stability constants for magnesium with TP and ATP necessitates the use of a ligand:metal ratio of 2:1. There is no evidence for the formation of complexes other than the 1:1 complex for either ligand⁽¹⁰⁸⁾, although evidence for Mn(ATP)₂ does exist⁽¹⁰⁹⁾. For both NTA and UDA the use of 1:1 metal to ligand ratios give rise to relaxations which can be attributed to free magnesium, whilst large excess of both these ligands give rise to bis complex formation with an accompanying second relaxation effect (see fig. 2.9.1). Thus ligand to metal ratios of 1.1:1 were used since under these conditions both additional relaxation effects are absent.

5.5.2 Choice of buffer

The choice of buffer is extremely critical in the study of magnesium systems because of the small value of ΔH° associated with these reactions and to get an easily observable spectral change it is necessary to rely on a pH jump. This can be achieved by using buffers with large d pH/dT, provided that the change in pH occurs rapidly, so that the pH can be assumed to be constant for the duration

of the metallation step. It was found that different buffers were suitable for different systems and the buffers used are shown in table 5.5.2.1.

TABLE 5.5.2.1. Buffers for the study of Mg-NSA systems.

<u>System</u>	<u>Buffer</u>
Mg(OH ₂) ₆ ²⁺	Triethanolamine; Ammonia
MgNTA ⁻	Triethylamine
MgUDA ⁻	Ammonia
MgATP ²⁻	Ammonia
MgTP ³⁻	Tris

The two buffers were used for the aquo magnesium system to obtain the best signal to noise ratio throughout the entire pH range. The pH ranges for which the two buffers were used overlapped and as both sets of points fit the same pH profile there can be no special effects due to the buffers. In all systems the buffer concentration was varied without affecting the relaxation time of the system.

5.5.3 Choice of metal concentrations and pH range

The metal concentrations and pH ranges were chosen to give as large a variation in relaxation time as possible without the formation of hydroxy-metal species. The conditions used are shown in table 5.5.3.1.

TABLE 5.5.3.1. Experimental conditions for Mg-NSA systems

<u>System</u>	<u>[M]</u>	<u>pH range</u>
Mg(OH ₂) ₆ ²⁺	8x10 ⁻⁴ - 4x10 ⁻² M	5.8 - 9.5
MgNTA ⁻	1.6 - 4.8x10 ⁻² M	8.7 - 9.6
MgUDA ⁻	1 x 10 ⁻² M	8.9 - 10.2
MgATP ²⁻	8x10 ⁻³ - 2x10 ⁻² M	9.0 - 10.0
MgTP ³⁻	6x10 ⁻³ - 3.6x10 ⁻² M	9.0 - 10.3

5.6 Experimental Data

It was only possible to obtain a complete pH profile for the magnesium aquo system for which a typical plot of τ^{-1} v. pH is shown in fig. 5.6.1. Twenty points were usually obtained for each of these profiles, spread over the widest possible pH range. For the other systems studied it was only possible to obtain the high pH sections of the profile; in these cases, the experimental data are presented as plots of τ^{-1} v. $[ML]/(1 + K_1[H])$. These plots are shown, along with the corresponding activation plots, in figs. 5.6.2 - 5.6.13 (see table 5.6.1).

TABLE 5.6.1. Index to plots.

<u>System</u>	<u>Figure number</u>	
	<u>τ^{-1} v. $[M]/1+K_1[H]$</u>	<u>log K v. $1/T^{\circ}K$</u>
Mg(H ₂ O) ₆ ²⁺	5.6.2	5.6.3
MgNTA ⁻	5.6.4	5.6.5
MgUDA ⁻	5.6.6	5.6.7
MgATP ²⁻	5.6.8	5.6.9
MgTP ³⁻	5.6.10	5.6.11
	τ^{-1} v. C_H	
Mg(H ₂ O) ₆ ²⁺ + HNSA	5.6.12	5.6.13

As the pH of the solution approached pK, a very fast relaxation, attributable to the protonation of NSA, was sometimes observed but this was always too fast to measure.

5.7 Interpretation of Data

5.7.1 Proposed mechanism

The symmetrical pH profile obtained for the magnesium aquo system is similar to those obtained^(110,111) for the reaction of magnesium and manganese with oxine and it

Fig. 5.6.1. pH profile for $\text{Mg}(\text{H}_2\text{O})_6^{2+}$ + NSA at 20°C .

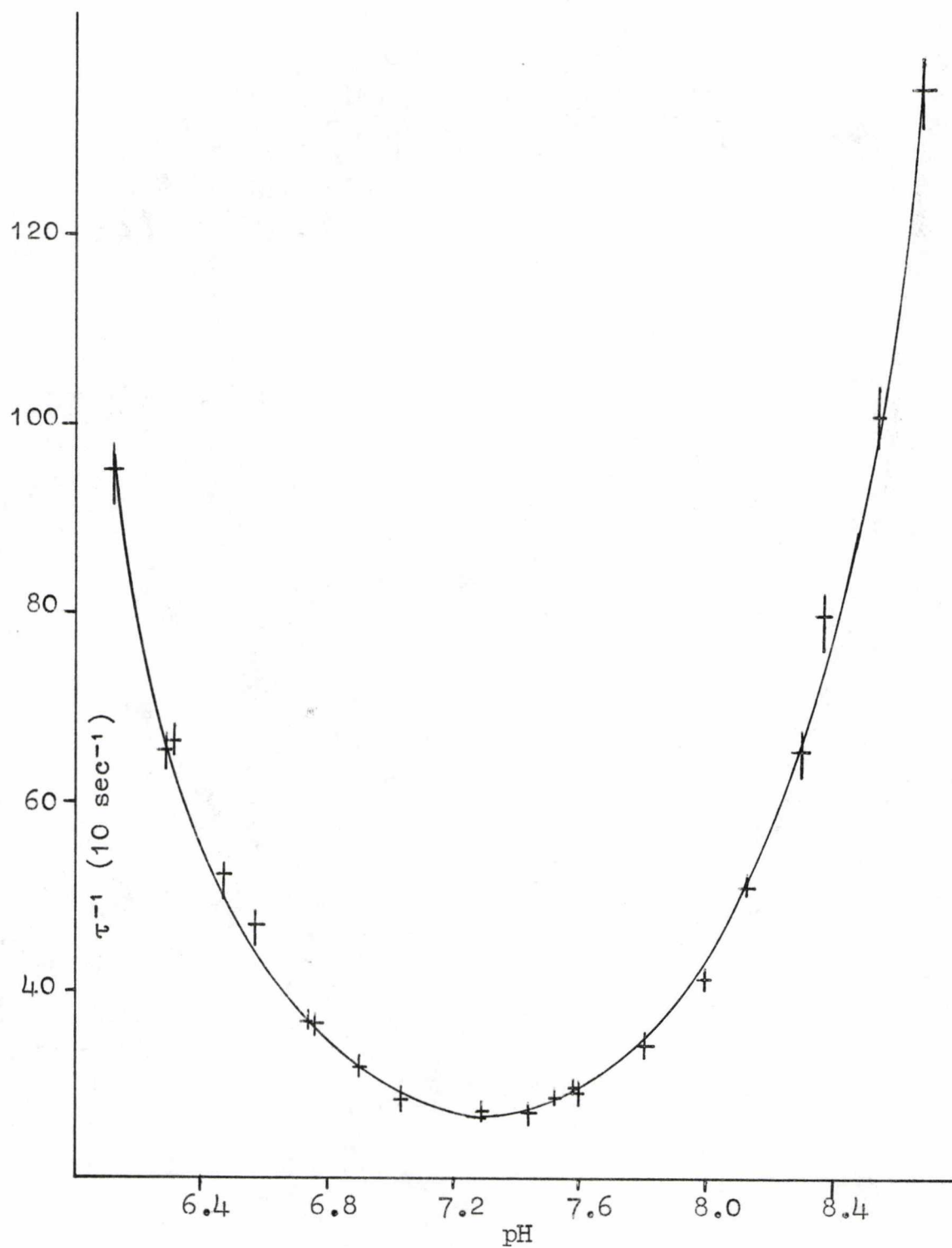


Fig. 5.6.2. τ^{-1} vs. $[M]/(1 + K_1[H])$ for $Mg(H_2O)_6^{2+} + NSA^{2-}$.

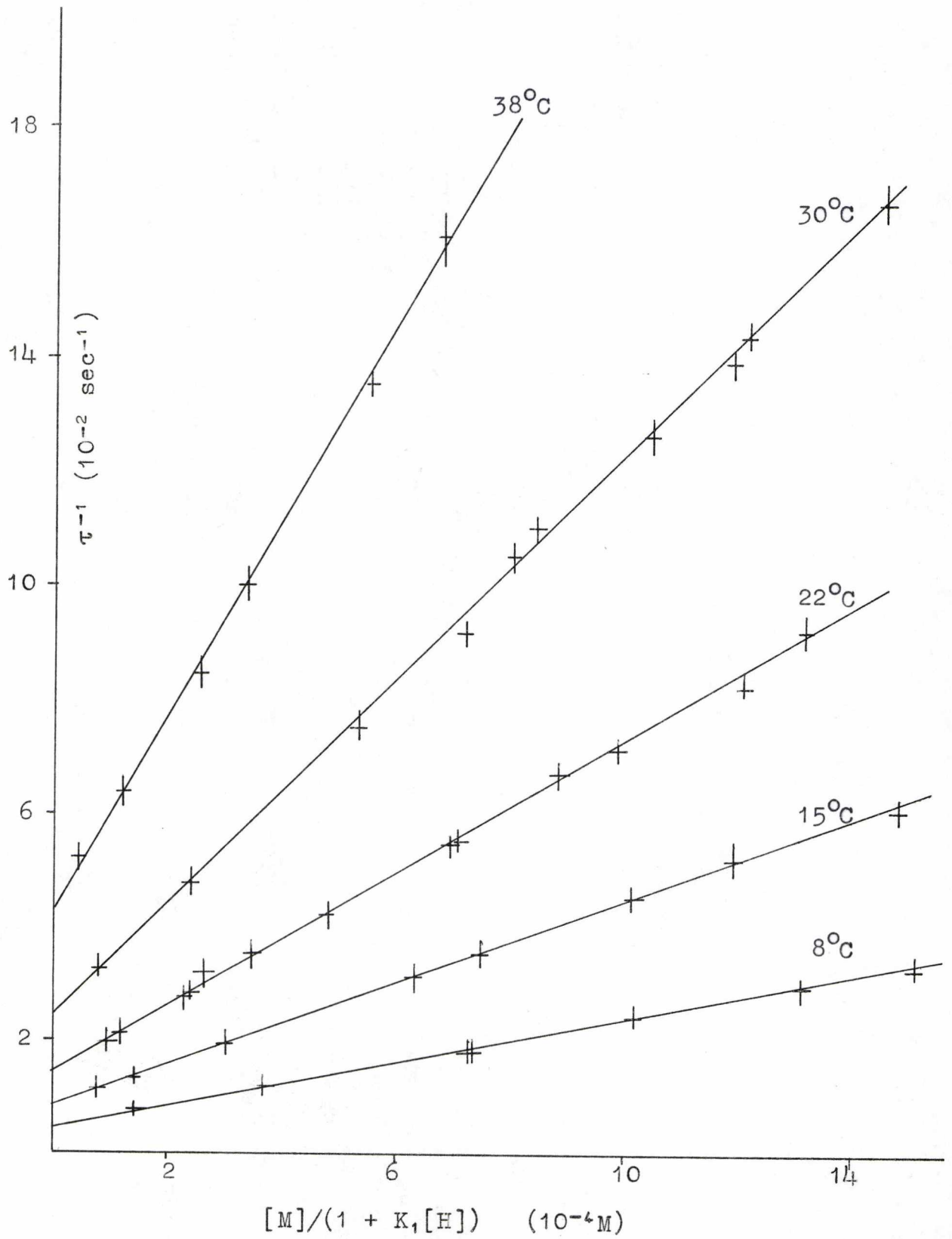


Fig. 5.6.3. $\log_{10} k$ vs. $1/T$ for $\text{Mg}(\text{H}_2\text{O})_6^{2+} + \text{NSA}^{2-}$.

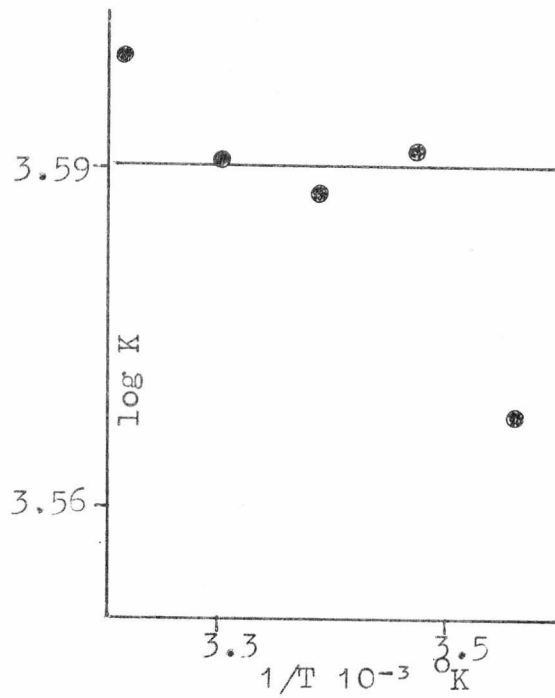
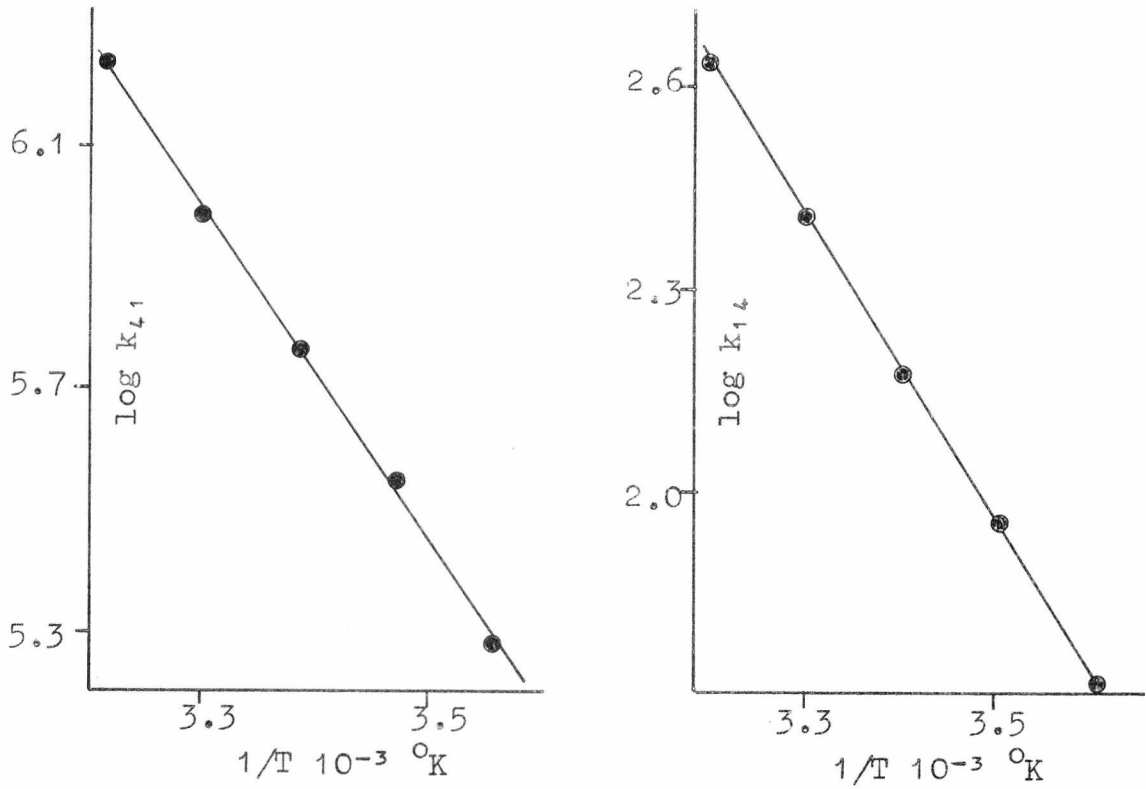


Fig. 5.6.4. τ^{-1} vs. $[M]/(1 + K_1[H])$ for $\text{MgNTA}^- + \text{NSA}^{2-}$.

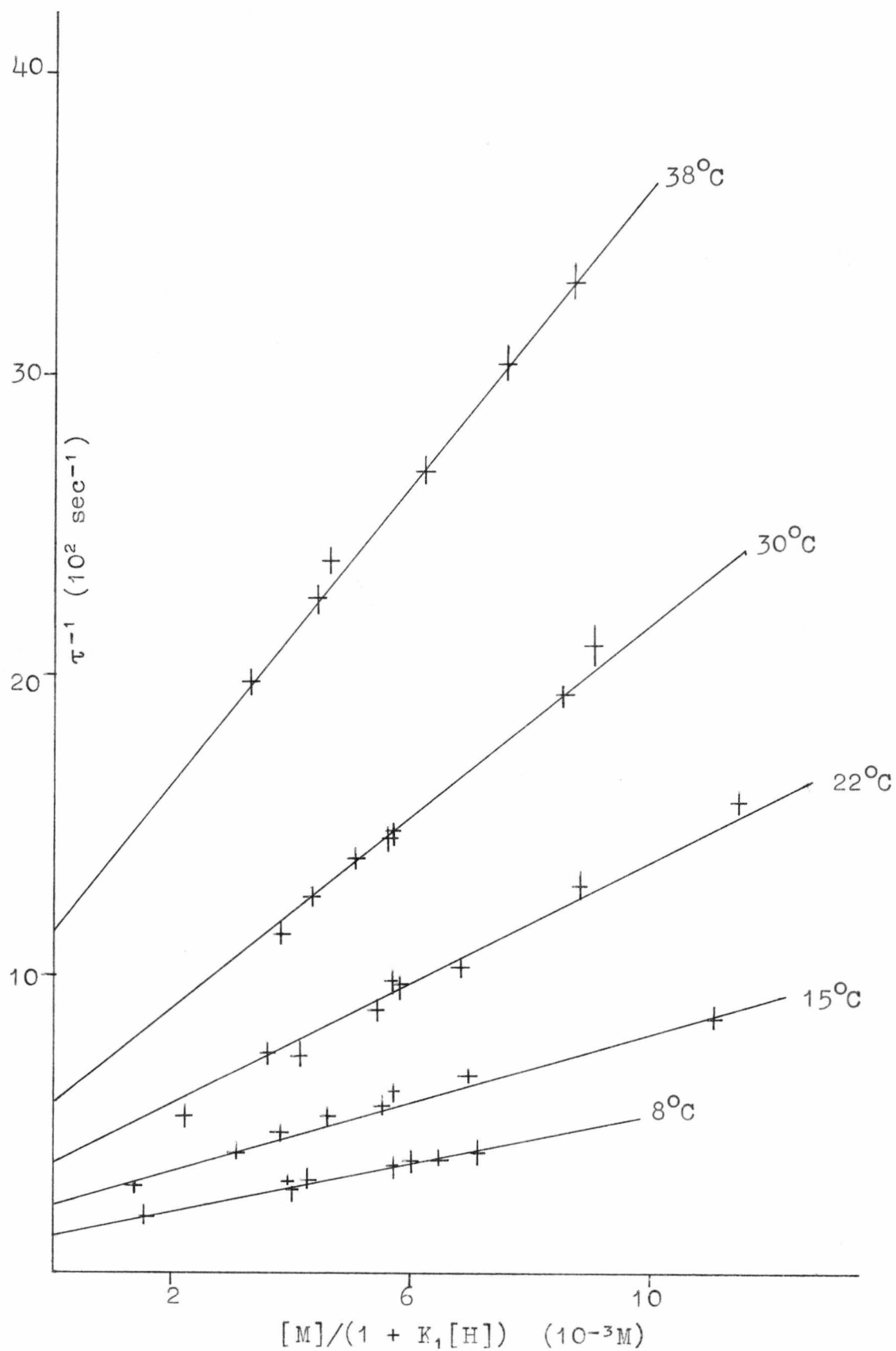


Fig. 5.6.5. $\log_{10} k$ vs. $1/T$ for $\text{MgNTA}^- + \text{NSA}^{2-}$.

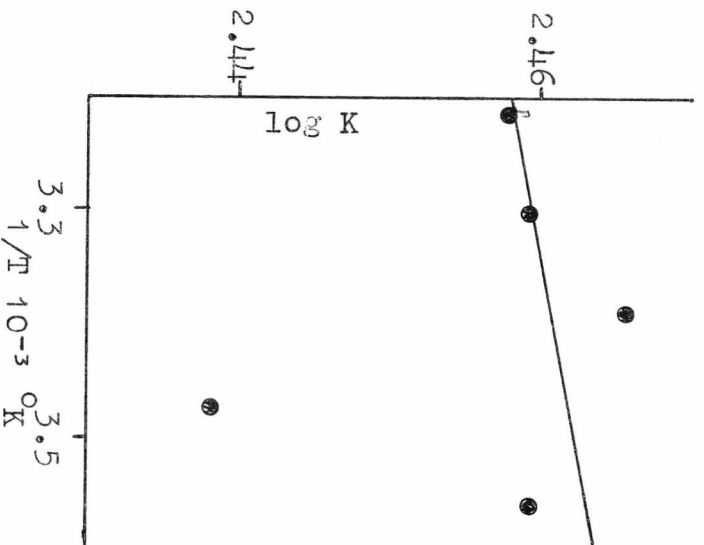
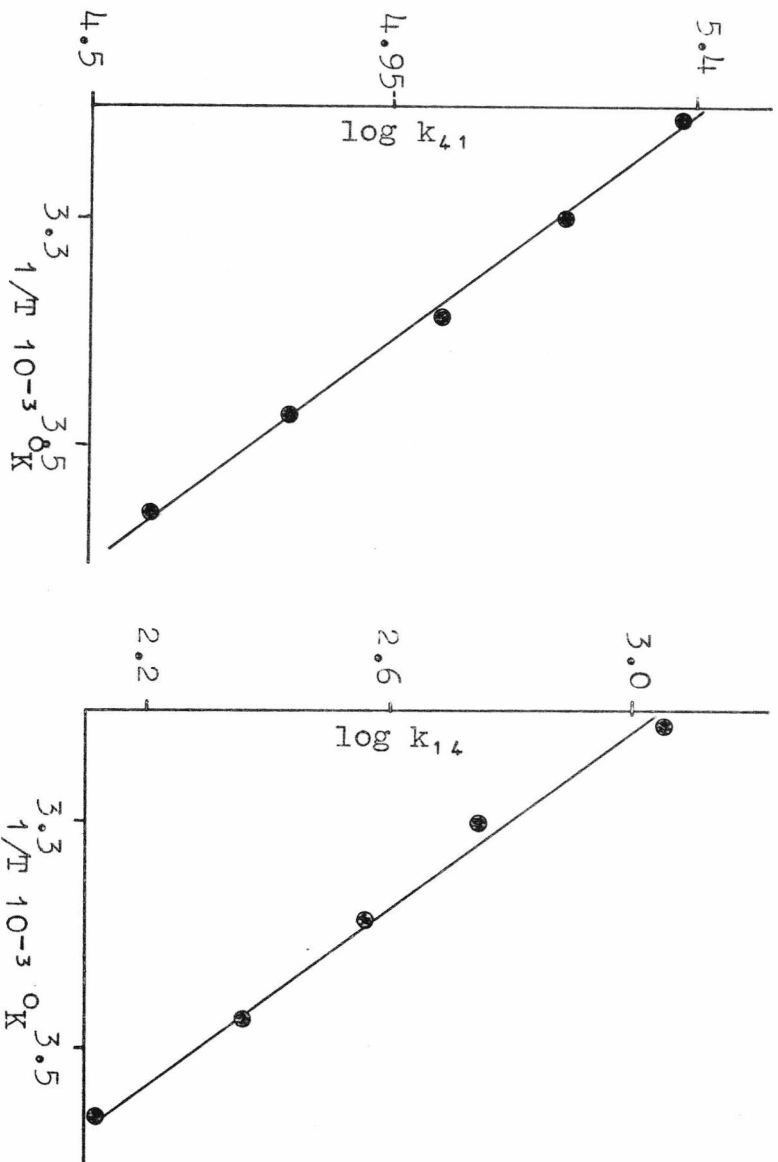


Fig. 5.6.6. τ^{-1} vs. $[M]/(1 + K_1[H])$ for $MgUDA^- + NSA^{2-}$.

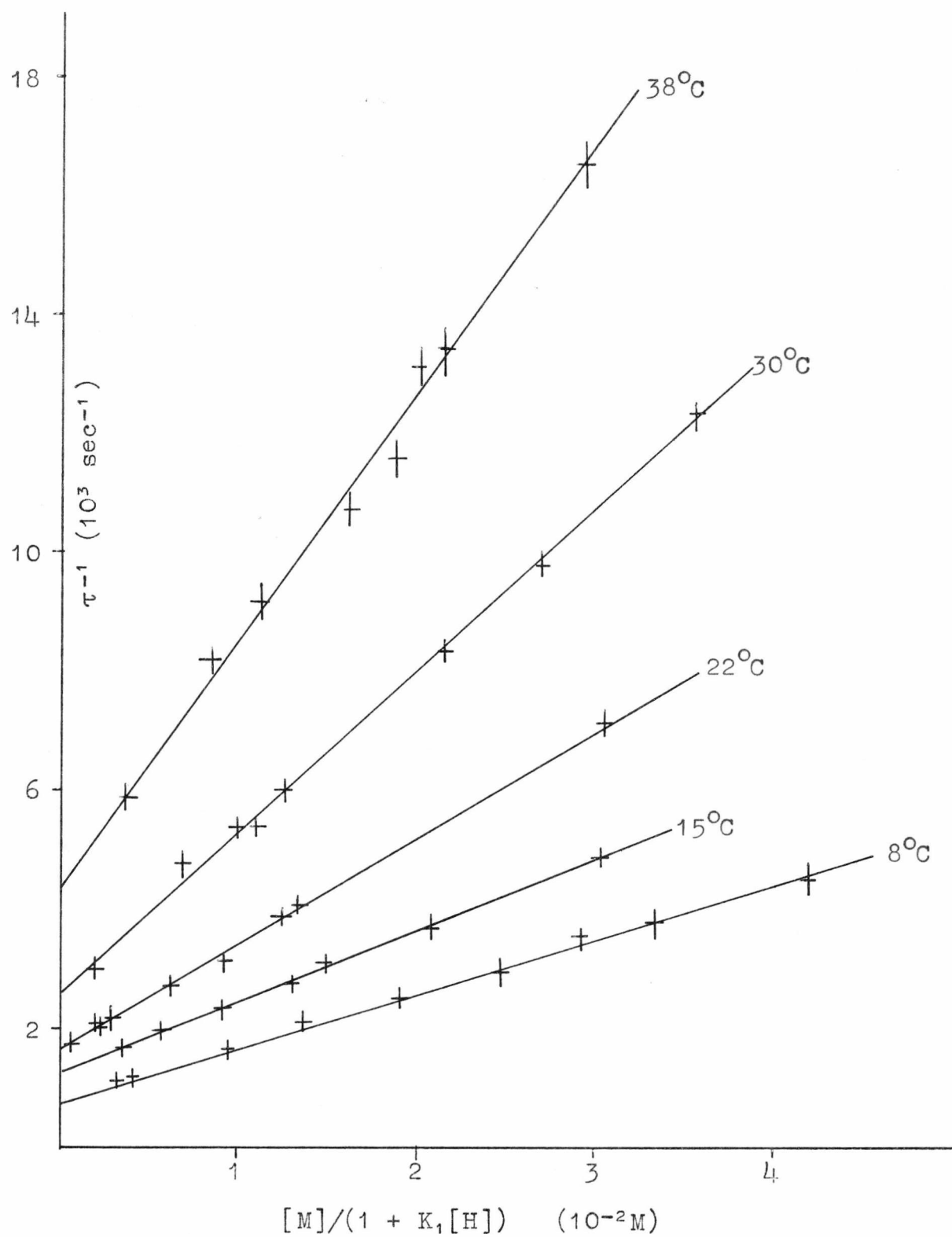


Fig. 5.6.7. $\log_{10}k$ vs. $1/T$ for $\text{MgUDA}^- + \text{NSA}^{2-}$.

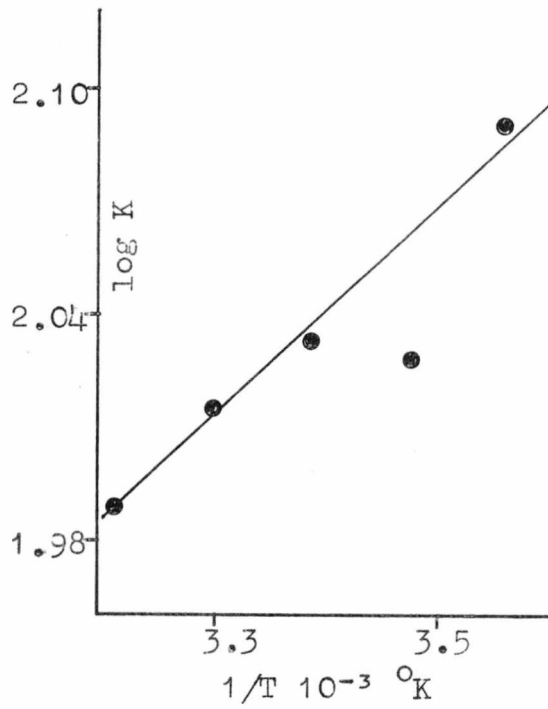
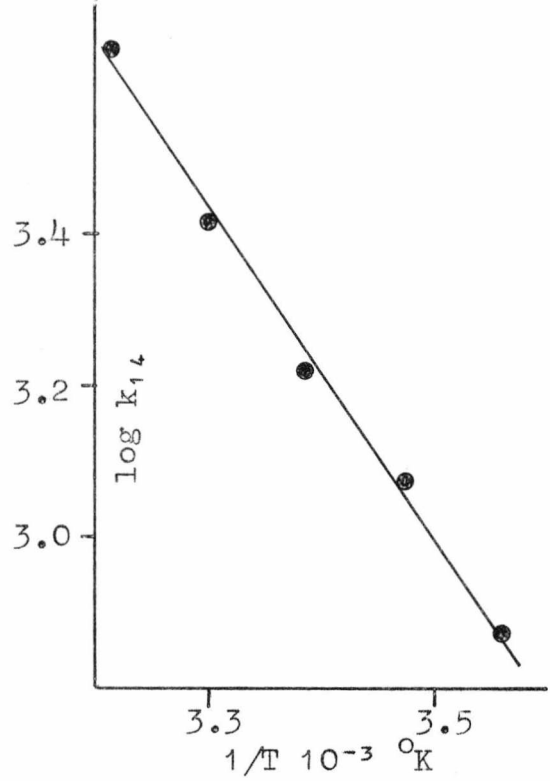
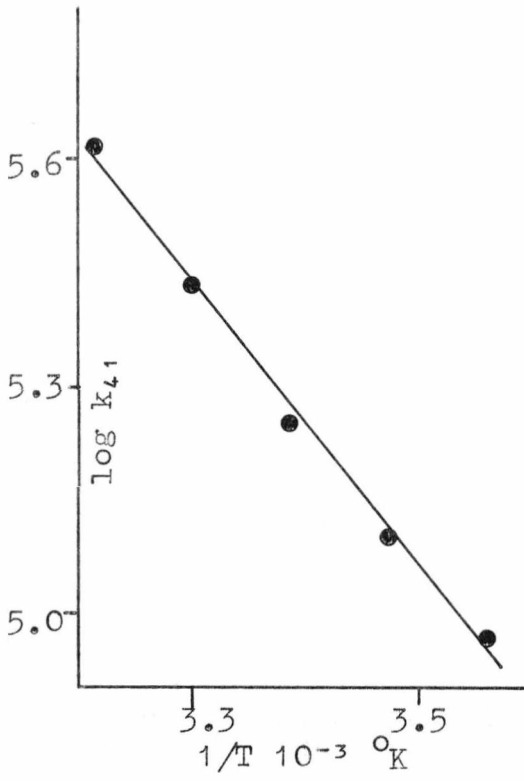


Fig. 5.6.8. τ^{-1} vs. $[M]/(1 + K_1[H])$ for $\text{MgATP}^{2-} + \text{NSA}^{2-}$.

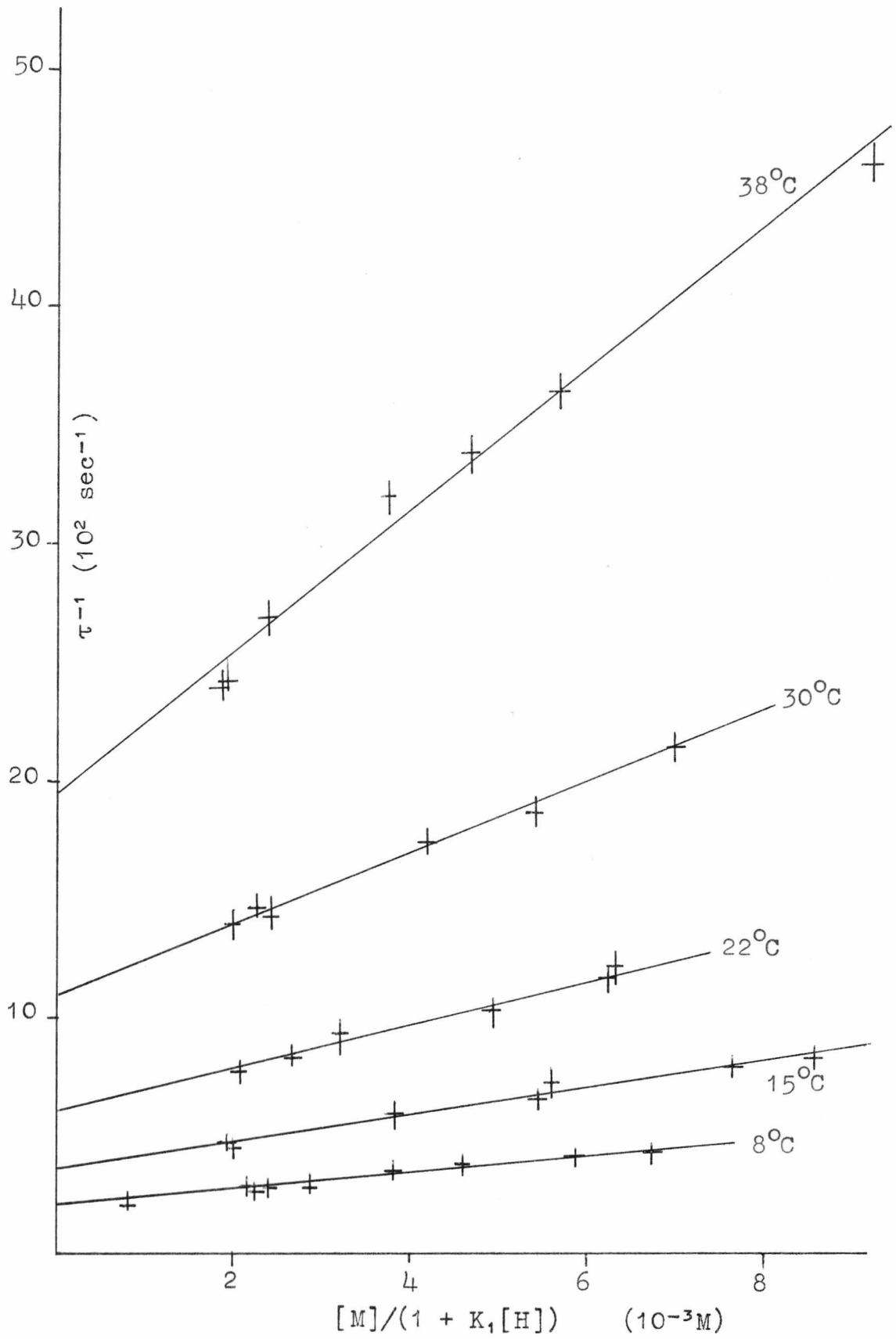


Fig. 5.6.9. $\log_{10} k$ vs. $1/T$ for MGATP²⁻ + NSA²⁻.

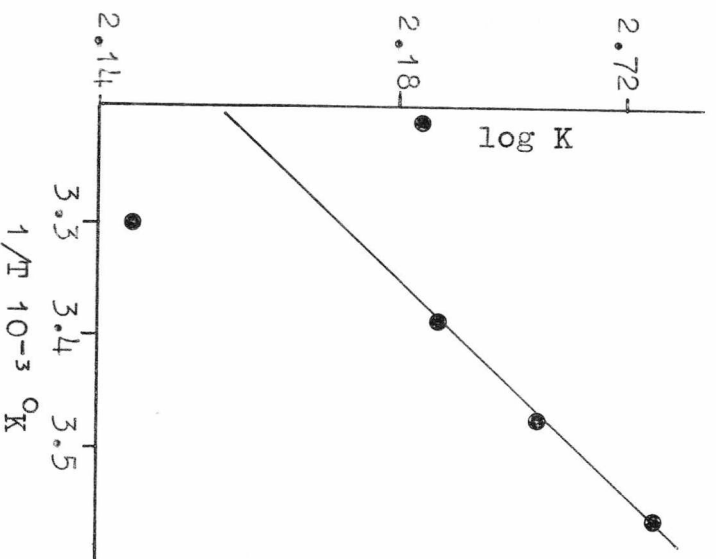
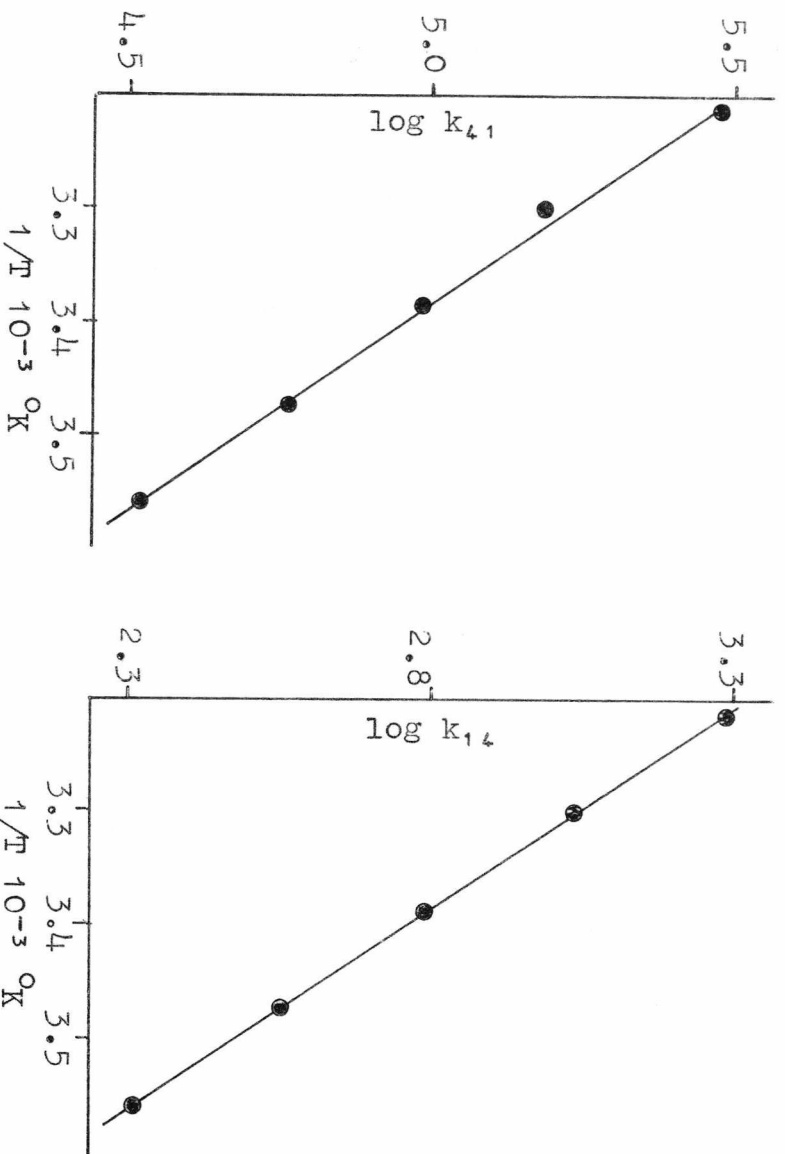


Fig. 5.6.10. τ^{-1} vs. $[M]/(1 + K_1[H])$ for $MgTP^{3-} + NSA^{2-}$.

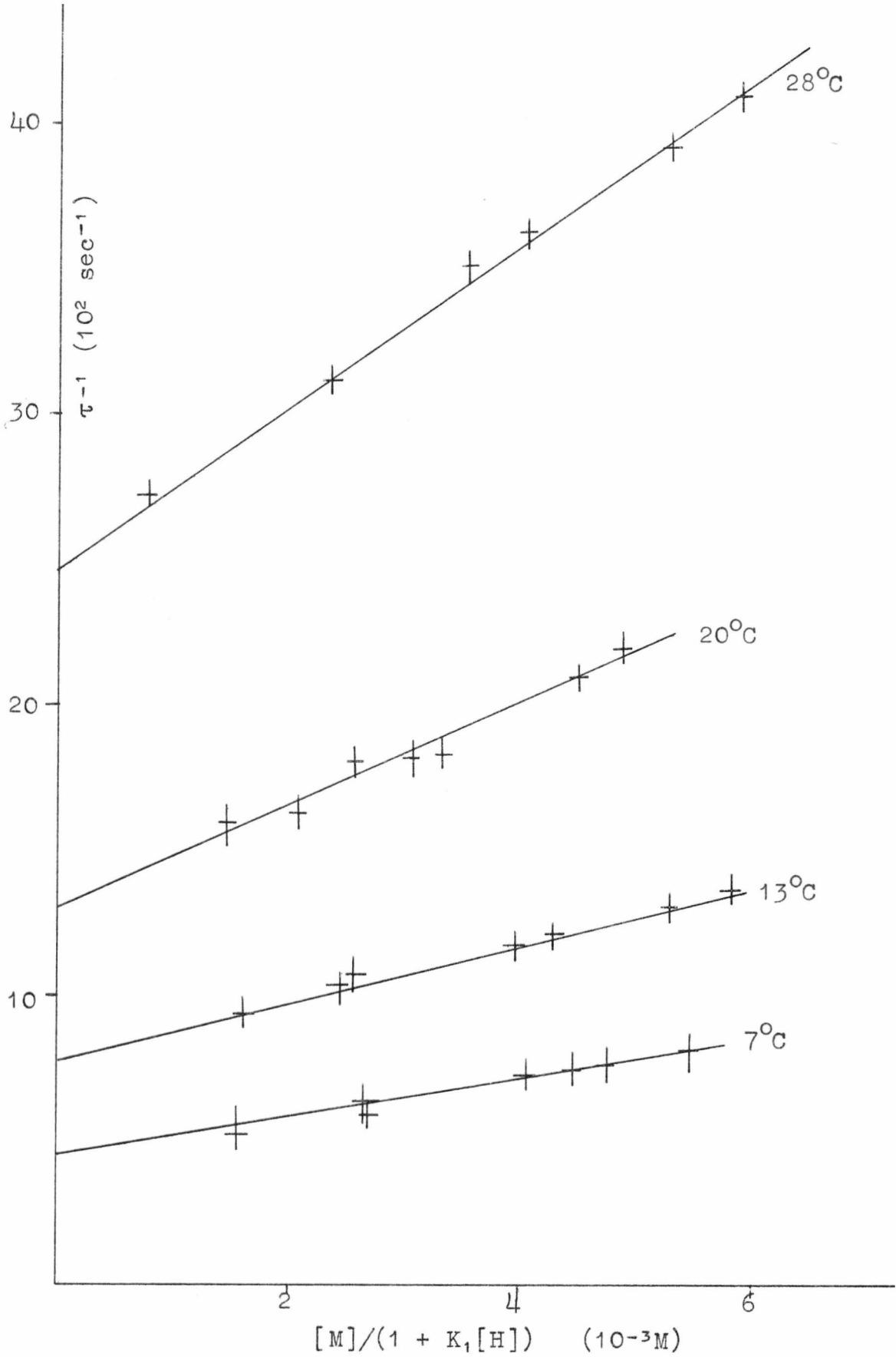


Fig. 5.6.11. $\log_{10} k$ vs. $1/T$ for $MSTP^3-$ + NSA^2- .

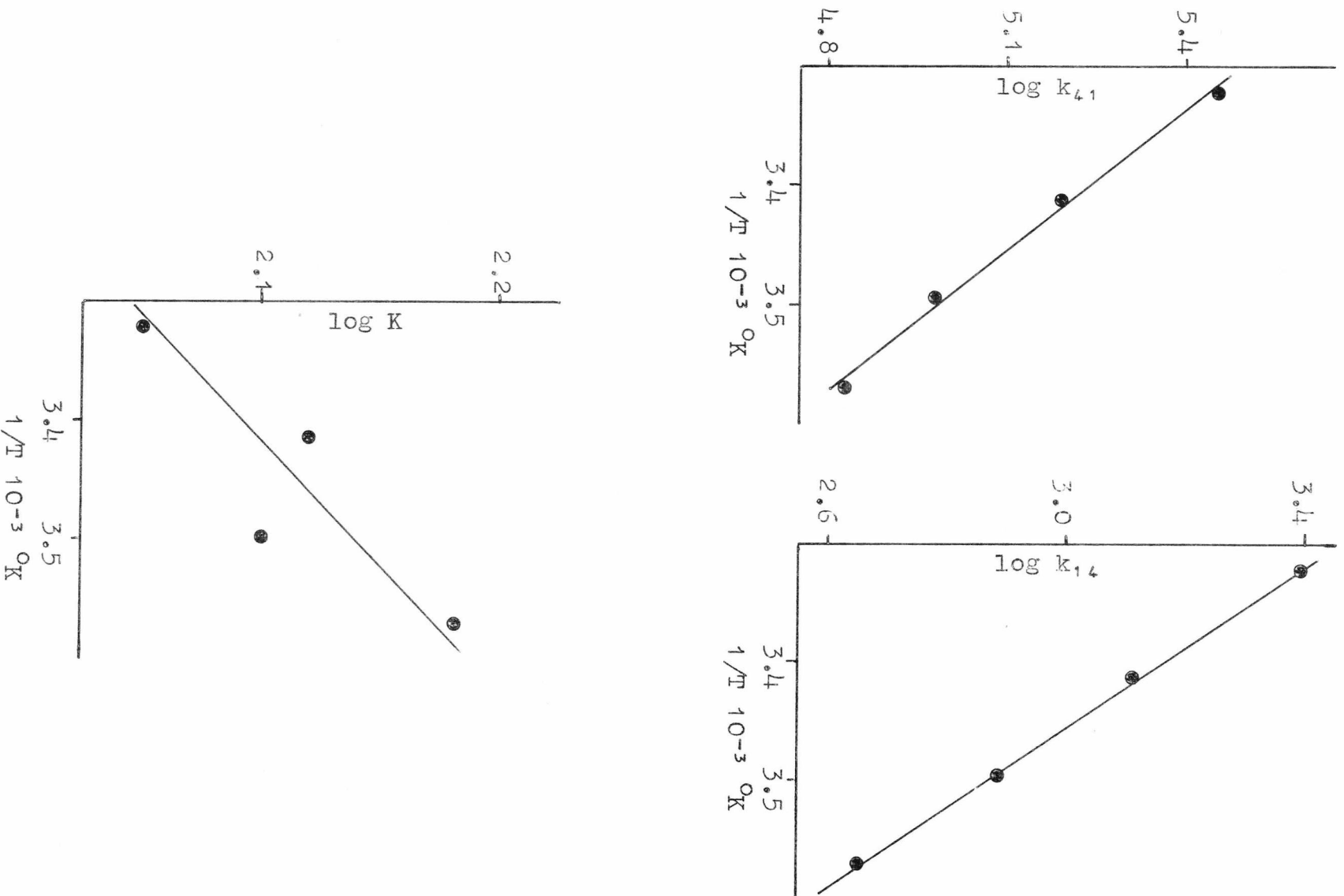


Fig. 5.6.12. τ^{-1} vs. $[H^+]$ for $Mg(H_2O)_6^{2+} + HNSA^-$.

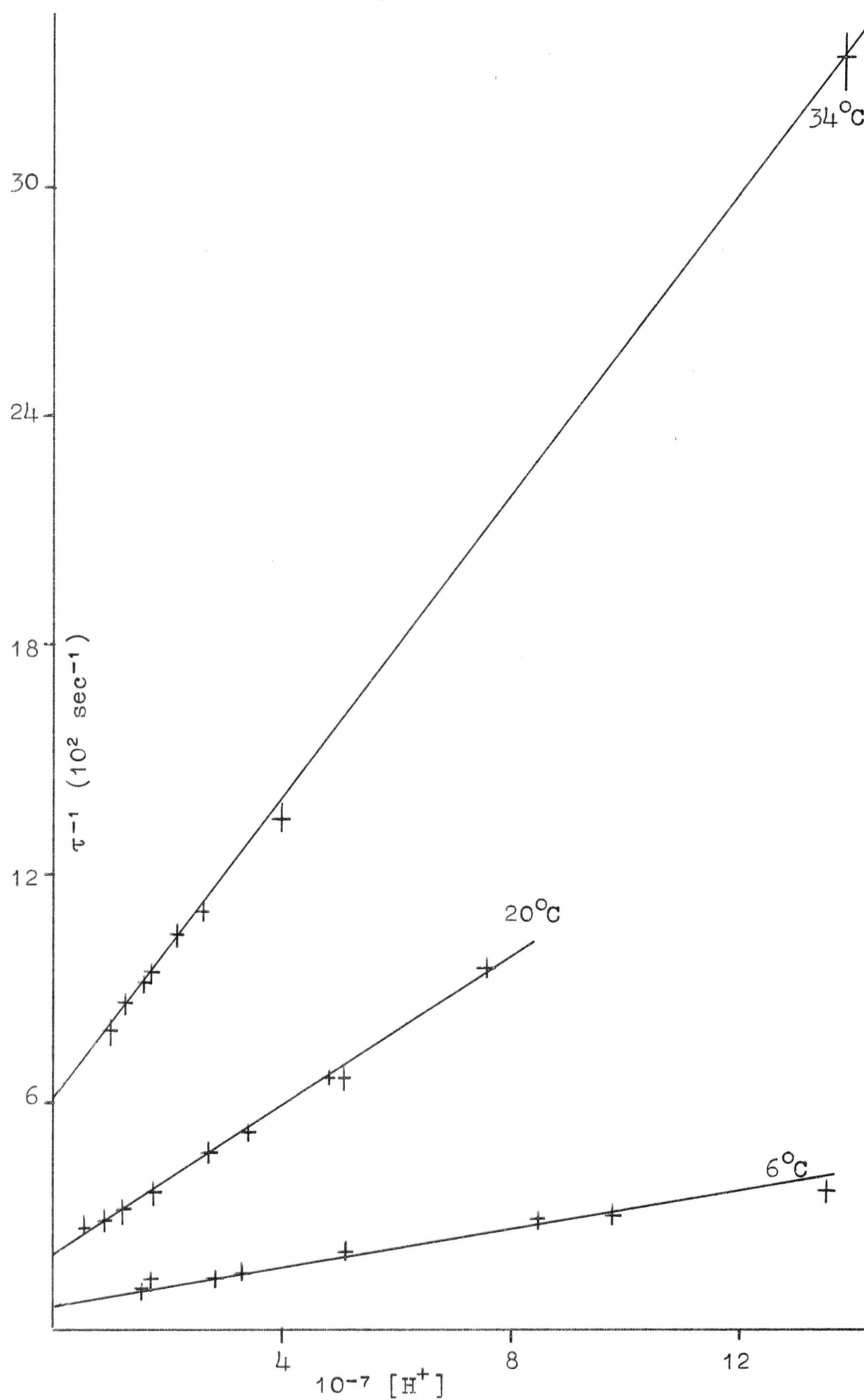
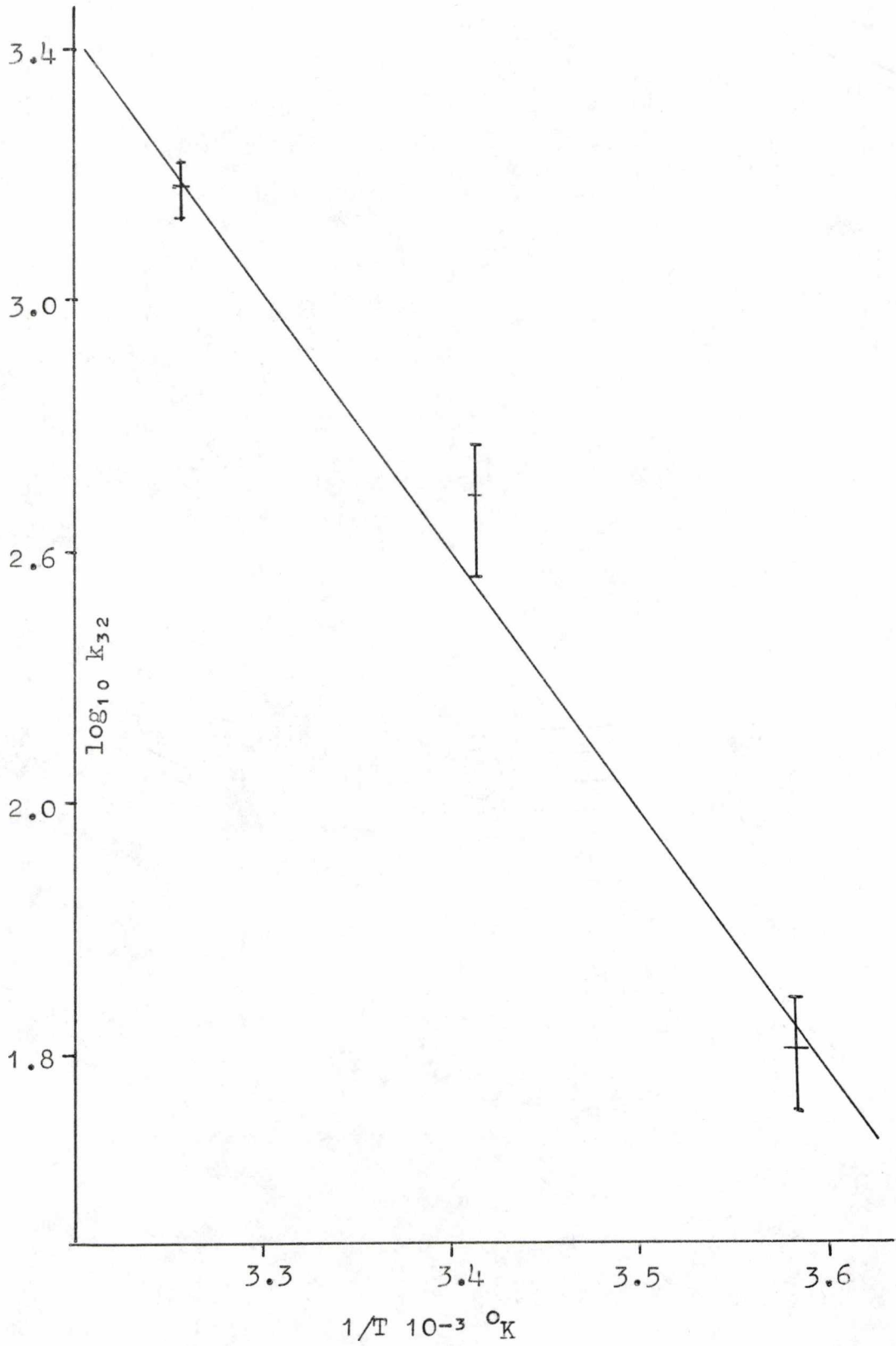
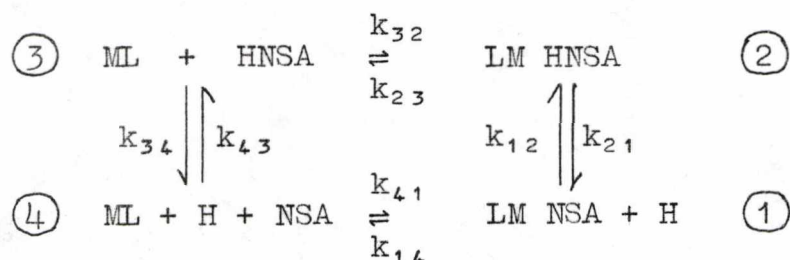


Fig. 5.6.13. $\log_{10} k_{32}$ vs. $1/T$ for $\text{Mg}(\text{H}_2\text{O})_6^{2+} + \text{HNSA}^-$.



is possible to interpret all the experimental data using the mechanism originally proposed in reference (110), i.e.



Charges have been omitted for the sake of clarity.

5.7.2 Derivation of the relaxation expression for the proposed mechanism

A completely general treatment of the above mechanism would lead to a complicated expression for each of three relaxation times⁽¹¹²⁾ but it is possible to make several simplifications. Since steps $\textcircled{3} \rightleftharpoons \textcircled{4}$ and $\textcircled{1} \rightleftharpoons \textcircled{2}$ involve protonation reactions, these may be treated as fast pre-equilibria to the metalation steps $\textcircled{3} \rightleftharpoons \textcircled{2}$ and $\textcircled{4} \rightleftharpoons \textcircled{1}$. In addition, it is possible to buffer $[\text{H}^+]$ and $[\text{ML}]$ by the use of a pH buffer and pseudo first order conditions, respectively, so that $\Delta\text{H} = 0$ and $\Delta\text{ML} = 0$. The relaxation expression may then be derived as follows:

Let $\Delta[\text{X}]$ terms represent the concentration displacement of species X from the final equilibrium at time t and $[\text{X}]$ be the final equilibrium concentration.

Then
$$\frac{d(\text{LM NSA})}{dt} = k_{41}[\text{ML}][\text{NSA}] - k_{14}[\text{LMNSA}]$$

and
$$\frac{d(\text{LMHNSA})}{dt} = k_{32}[\text{ML}][\text{HNSA}] - k_{23}[\text{LMHNSA}]$$

At time t , with $[ML]$ and $[H]$ buffered and small displacements,

$$\begin{aligned} & \frac{d([LMNSA] + \Delta[LMNSA])}{dt} + \frac{d([LMHNSA] + \Delta[LMHNSA])}{dt} \\ &= k_{41}[ML]\Delta[NSA] - k_{14}\Delta[LMNSA] + k_{32}[ML]\Delta[HNSA] - k_{23}\Delta[LMHNSA]. \end{aligned}$$

But at equilibrium

$$k_{41}[ML][NSA] = k_{14}[LMNSA]$$

and

$$k_{32}[ML][HNSA] = k_{23}[LMHNSA]$$

$$\begin{aligned} \therefore \frac{d(\Delta[LMNSA])}{dt} + \frac{d(\Delta[LMHNSA])}{dt} &= k_{41}[ML]\Delta[NSA] - k_{14}\Delta[LMNSA] \\ &+ k_{32}[ML]\Delta[HNSA] - k_{23}\Delta[LMHNSA] \quad \dots (5.7.1) \end{aligned}$$

If

$$K_9 = \frac{[LMHNSA]}{[LMNSA][H]} = \frac{k_{12}}{k_{21}}$$

$$\Delta[LMHNSA] = K_9\Delta[LMNSA][H] \quad \dots (5.7.2)$$

Similarly, if

$$K_1 = \frac{[HNSA]}{[H][NSA]} = \frac{k_{43}}{k_{34}}$$

$$\Delta[NSA] = \frac{\Delta[HNSA]}{K_1[H]} \quad \dots (5.7.3)$$

From the stoichiometry

$$\Delta[NSA] + \Delta[HNSA] + \Delta[LMNSA] + \Delta[LMHNSA] = 0 \quad \dots (5.7.4)$$

Substituting (5.7.3) and (5.7.4) in (5.7.5) gives

$$\Delta[HNSA] = - \frac{\Delta[LMNSA](1 + K_9[H])}{(1 + K_1[H])} \quad \dots (5.7.5)$$

and substituting (5.7.2) and (5.7.3) and (5.7.6) in (5.7.5) gives

$$\begin{aligned} - \frac{d(\Delta[LMNSA])}{dt} &= \Delta[LMNSA] \left(\frac{k_{41}[ML]}{1+K_1[H]} + \frac{k_{14}}{1+K_9[H]} + \frac{k_{32}[ML]K_1[H]}{(1+K_1[H])} \right. \\ &\quad \left. + \frac{k_{23}K_9[H]}{1+K_9[H]} \right) \end{aligned}$$

Integration of this expression gives the reciprocal relaxation time

$$\tau^{-1} = \frac{k_{41}[\text{ML}]}{1+K_1[\text{H}]} + \frac{k_{14}}{1+K_9[\text{H}]} + \frac{k_{32}[\text{ML}]K_1[\text{H}]}{1+K_1[\text{H}]} + \frac{k_{23}K_9[\text{H}]}{1+K_9[\text{H}]} \dots (5.7.7)$$

5.7.3 Calculation of rate constants

Under the conditions used, several simplifications can be made to the relaxation expression:

(a) For all the systems investigated $K_9[\text{H}^+] \ll 1$ so, at low pH, a plot of τ^{-1} against $[\text{H}^+]$ gives a straight line of slope $k_{23}K_9$ and intercept $k_{32}[\text{ML}] + k_{14}$.

(b) At high pH's and low $[\text{ML}]$

$\frac{k_{41}[\text{ML}]}{1+K_1[\text{H}^+]} \gg k_{32}[\text{ML}]$ and $k_{23}K_9[\text{H}]$ is very small, so the relaxation expression simplifies to

$$\tau^{-1} = \frac{k_{41}[\text{ML}]}{1+K_1[\text{H}^+]} + k_{14}.$$

(This is the expression that would be obtained if the protonated form of NSA did not react). If this simplification cannot be made the plot of τ^{-1} vs. $[\text{ML}]/1+K_1[\text{H}^+]$ becomes curved at low values of $[\text{ML}]/1+K_1[\text{H}^+]$ due to the additional term involving k_{32} .

The pH profile for the aquo magnesium system can be analysed because at high pH $k_{23}K_9[\text{H}]$ is insignificant and as $K_1[\text{H}^+] \gg 1$ a plot of τ^{-1} vs. $1/[\text{H}^+]$ gives a straight line of slope $\frac{k_{41}[\text{ML}]}{K_1}$ and intercept $k_{14} + k_{32}[\text{ML}]$. Similarly, for the low pH side of the profile a plot of τ^{-1} vs. $[\text{H}^+]$ gives a straight line of slope $k_{23}K_9$ and intercept $k_{14} + k_{32}[\text{ML}]$. k_{14} can be obtained from the intercept of the high pH plot at low metal concentrations as described in 5.7.3(b) and so it is possible to calculate the value of k_{32} . k_{32} can be calculated either by subtracting the value of k_{14} from the intercept

$k_{32}[\text{ML}] + k_{14}$ or, more accurately, by using the following procedure:

From thermodynamic principles,

$$\frac{k_{32}}{k_{23}} \cdot \frac{k_{21}}{k_{12}} = \frac{k_{34}}{k_{43}} \cdot \frac{k_{41}}{k_{14}}$$

From the low metal plot it is possible to get a value of $K_3 = \frac{k_{41}}{k_{14}}$, and $K_1 = \frac{k_{43}}{k_{34}}$ (the protonation constant for NSA) has been measured spectrophotometrically, so

$$k_{32} = \frac{k_{23}K_9}{K_1} \cdot K_3$$

But, $k_{23}K_9$ is the slope of the low pH plot and thus a value can be calculated for k_{32} .

5.8 Results

The results for k_{41} , k_{14} and k_{32} and $\log K_3$ are given in tables 5.8.1 and 5.8.2, and the activation parameters obtained from these results are shown in table 5.8.3.

TABLE 5.8.1. Results for the $\text{Mg}(\text{OH}_2)^{2+}$ + NSA system.

<u>Temp. °C</u>	<u>$k_{41} \text{ M}^{-1} \text{ sec}^{-1}$</u>	<u>$k_{14} \text{ sec}^{-1}$</u>	<u>$\log K_3$</u>
8	1.88×10^5	51	3.57
15	3.55×10^5	90	3.60
22	5.80×10^5	150	3.59
30	9.75×10^5	250	3.59
38	1.71×10^6	430	3.60

<u>Temp. °C</u>	<u>$k_{32} \text{ M}^{-1} \text{ sec}^{-1}$</u>
6	65
20	420
34	1460

In order to compare complexes which have different numbers of water molecules (n) available for substitution a statistical correction was made and the $k_{41}^{(s)}$ values were calculated using

$$k_{41}^{(s)} = k_{41} \times 6/n .$$

It is assumed in all cases that the magnesium complex is octahedral⁽¹¹³⁾. The values of n have been obtained on the assumption that:

- (1) UDA³⁻ and NTA³⁻ both act as quadridentate ligands^(114,115).
- (2) TP⁵⁻ is tridentate.
- (3) ATP⁴⁻ is tridentate.

The complex of ATP with magnesium has received a great deal of attention in the past but agreement has still not been reached over the number of binding positions occupied by the ATP. Most workers agree that both the β and γ phosphate groups are bound to the metal^(116,117) but some have suggested that the N-7 of the adenine ring also binds weakly to the metal ion, as has been shown for the corresponding complexes of manganese and zinc^(118,119). An investigation of the reaction between MgATP²⁻ and NSA showed some interesting effects at low metal concentrations (fig. 5.8.1). Under the conditions used, the plot of τ^{-1} vs. $M/1+K_1[H]$ would be expected to give a straight line of slope k_{41} , and intercept k_{14} , but there was marked curvature at low metal concentrations. This suggests that there is a large change in the value of k_{14} at these concentrations and this can possibly be explained by the dissociation of one of the ligand "arms" from the complex (cf. Chapter 3). On the assumption that ATP acts as a bidentate ligand, if one of the phosphate groups dissociates, the resulting complex would have a low stability constant and so there should be a large amount of free magnesium in the test solutions and therefore there should be two observable relaxations. Perhaps a more likely explanation is that under certain metal concentrations and pH

Fig. 5.8.1. To show the effect of low MgL concentrations.

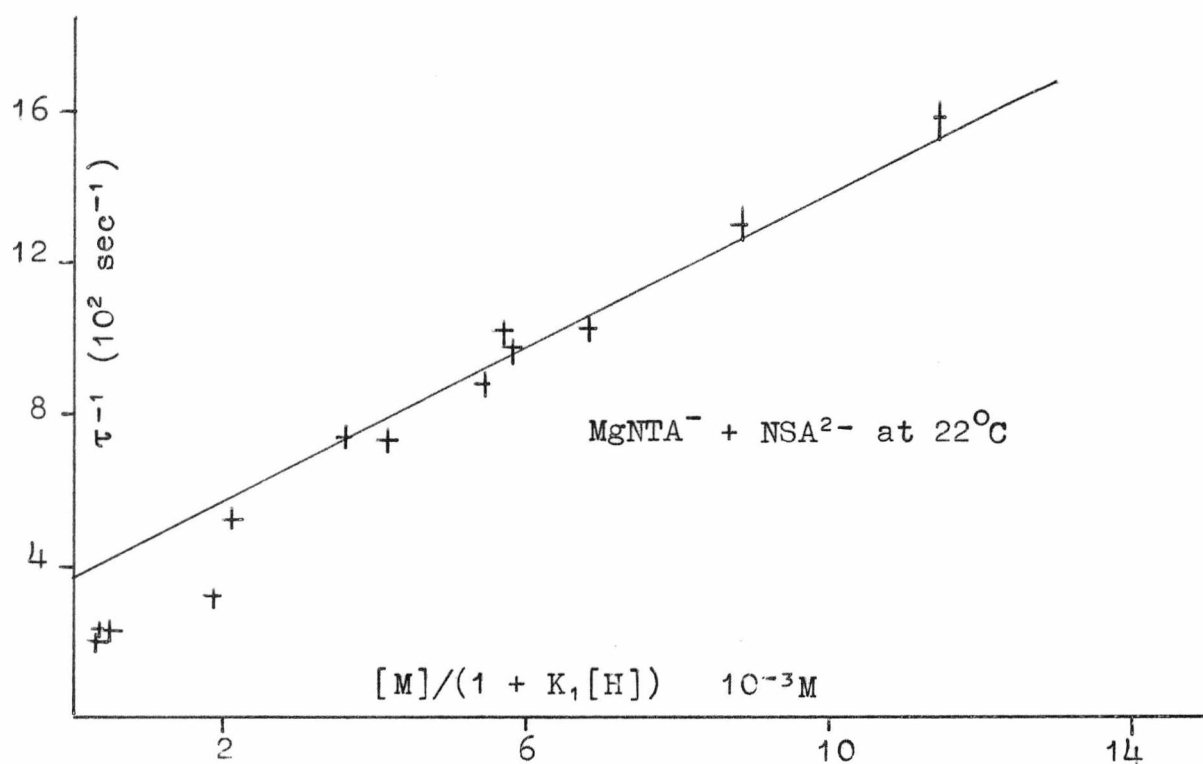
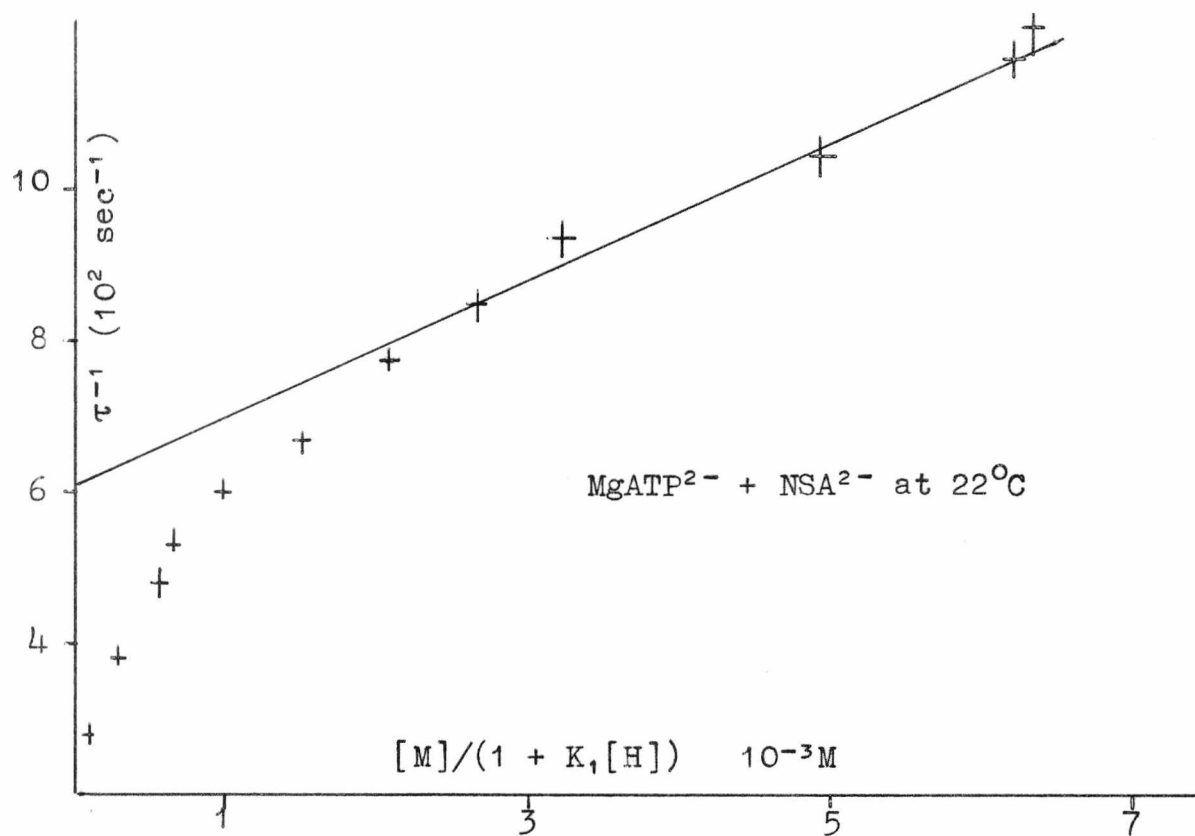


TABLE 5.8.2. Results for MgL + NSA systems.

<u>System</u>	<u>Temp.</u> <u>°C</u>	<u>$\frac{k_{14}}{M^{-1} \text{sec}^{-1}}$</u>	<u>$\frac{k_{14}}{\text{sec}^{-1}}$</u>	<u>logK_s</u>
MgNTA ⁻	8	3.92 x 10 ⁴	1.36 x 10 ²	2.46
	15	6.3 x 10 ⁴	2.3 x 10 ²	2.44
	22	1.06 x 10 ⁵	3.65 x 10 ²	2.47
	30	1.61 x 10 ⁵	5.6 x 10 ²	2.46
	38	2.5 x 10 ⁵	1.14 x 10 ³	2.46
MgUDA ⁻	8	9.25 x 10 ⁴	7.5 x 10 ²	2.09
	15	1.26 x 10 ⁵	1.18 x 10 ³	2.03
	22	1.78 x 10 ⁵	1.65 x 10 ³	2.03
	30	2.70 x 10 ⁵	2.60 x 10 ³	2.02
	38	4.15 x 10 ⁵	4.40 x 10 ³	1.98
MgATP ²⁻	8	3.4 x 10 ⁴	2.00 x 10 ²	2.23
	15	5.8 x 10 ⁴	3.6 x 10 ²	2.21
	22	9.54 x 10 ⁴	6.1 x 10 ²	2.19
	30	1.52 x 10 ⁵	1.09 x 10 ³	2.15
	38	3.0 x 10 ⁵	1.94 x 10 ³	2.19
MgTP ³⁻	7	6.8 x 10 ⁴	4.48 x 10 ²	2.18
	13	9.6 x 10 ⁴	7.8 x 10 ²	2.10
	20	1.55 x 10 ⁵	1.3 x 10 ³	2.12
	28	2.8 x 10 ⁵	2.45 x 10 ³	2.05

TABLE 5.8.3. Activation parameters for magnesium-NSA systems

	<u>Mg(H₂O)₆²⁺</u>	<u>MgNTA⁻</u>	<u>MgUDA⁻</u>	<u>MgATP²⁻</u>	<u>MgTP³⁻</u>
k_f (M ⁻¹ s ⁻¹)	7.1x10 ⁵	1.17x10 ⁵	2.09x10 ⁵	1.18x10 ⁵	2.3x10 ⁵
log k_f (s)	5.851	5.56	5.80	5.37 (5.25)	5.66
ΔH_f^\ddagger kcal/mole	11.6(1.6)	10.6(1.6)	7.6 [*] (1.8)	11.5(1.3)	10.7(3.3)
ΔS_f^\ddagger (s) e.u.	+7.2(5)	+3.0(5)	-7.8(7)	+4.7(4)	+3.4(11)
k_b sec ⁻¹	1.82x10 ²	4.56x10 ²	2.08x10 ³	7.68x10 ²	2.02x10 ³
log k_b	2.26	2.66	3.31	2.88	3.31
ΔH_b^\ddagger kcal/mole	11.76(1.6)	11.2(2)	9.5 [*] (1.7)	12.5(1.9)	12.3(2.8)
ΔS_b^\ddagger e.u.	-8.6(5)	-10.6(8.6)	-11.3(6)	-3.3(6)	-2.1(9)
log ₁₀ K _{kin}	3.59	2.45	2.03	2.18	2.07
log ₁₀ K _{spec}	4.03	2.67	2.53	2.41	1.71

the adenine ring is bound to the metal ion and that this shows up in the kinetic study and in some of the spectral studies.

5.9 Preliminary investigation of the reaction between the aquo magnesium ion and 8-hydroxyquinoline-5-sulphonic acid (OXS).

5.9.1 pK₁ of OXS at 25°C

To provide a comparison with the oxine^(110,111) and NSA results for magnesium the reaction between OXS and aquo magnesium was investigated at 25°C and ionic strength 0.3. The relevant pK of OXS was measured using a similar method to the one described in section 5.2 (see Appendix 5) ([OXS] 2.5 x 10⁻⁴M, buffer borax 2 x 10⁻³M). The optical densities and the pK's obtained for several wavelengths are shown in table 5.9.1.1.

TABLE 5.9.1.1. Optical density data for the pK₁ for OXS at 25°C.
μ = 0.3; pH₁ = 8.478; pH₂ = 9.505.

	335	340	343	364	λnm
C _ε OXS-	.776	.851	.901	.988	
OD ₁	.621	.644	.682	.754	OD
OD ₂	.750	.816	.864	.942	units
K ₁	2.97x10 ⁸	2.97x10 ⁸	3.00x10 ⁸	2.96x10 ⁸	nil
pK ₁	8.47(2)	8.47(2)	8.47(7)	8.47(1)	

Mean pK₁ = 8.47(3)

5.9.2 Kinetics at 25°C

The reaction between OXS and magnesium was followed spectrophotometrically at 365 nm. For this system a U-shaped pH profile can be obtained at a constant metal concentration and the data obtained fits the oxine mechanism⁽¹¹⁰⁾. From the

relaxation expression for this mechanism (equation 5.7.7) it can be seen that, if the high pH side of the profile is obtainable, a plot of τ^{-1} vs. $1/1+K_1[H]$ for two different metal concentrations should give two straight lines of slope $k_{4,1}[M]$ and intercept $k_{1,4} + k_{3,2}[M]$. Thus, from the differences in the intercepts, it is possible to evaluate $k_{1,4}$ and $k_{3,2}$. In this work the metal concentrations used were $3.2 \times 10^{-3}M$ and $8 \times 10^{-3}M$. The plots of τ^{-1} vs. $1/1+K_1[H]$ are shown in fig. 5.9.2.1 and the rate constants at $25^\circ C$ in table 5.9.2.1.

TABLE 5.9.2.1. Rate constants for $Mg(OH_2)_6^{2+} + OXS$ at $25^\circ C$.

$k_{4,1}$	$3.8(\pm 0.1) \times 10^5 M^{-1}sec^{-1}$
$k_{3,2}$	$1.2(\pm 0.2) \times 10^4 M^{-1}sec^{-1}$
$k_{1,4}$	$4.9(\pm 1.1) \times 10^1 sec^{-1}$

5.10 Discussion

In studies with magnesium oxine⁽¹¹¹⁾ Hague and Zetter have suggested that the bound ligand has little effect other than reducing the solid angle of the metal ion over which effective substitution may occur. This is confirmed by the formation rate constants at $25^\circ C$ and the activation enthalpies for the magnesium NSA systems (except for MgUDA which will be discussed in Chapter 7) which are approximately the same and close to the rate and enthalpy for the water exchange reaction ($k_{ex} = 5.3 \times 10^5 sec^{-1}$, $\Delta H_{ex}^\ddagger = 10.2 kcal.mol^{-1}$ ⁽¹²⁰⁾) using $K_{OS} = 3M^{-1}$.

The similarity between the results for the ^{reaction of} oxine and NSA with aquo magnesium (fig. 5.10.1) seems at first very surprising as the calculated values of K_{OS} for the two ligands with magnesium are considerably different and this should lead to much larger

Fig. 5.9.2.1. τ^{-1} vs. $1/(1+K_1[H])$ for $\text{Mg}(\text{H}_2\text{O})_6^{2+} + \text{OXS}^-$ at 25°C .

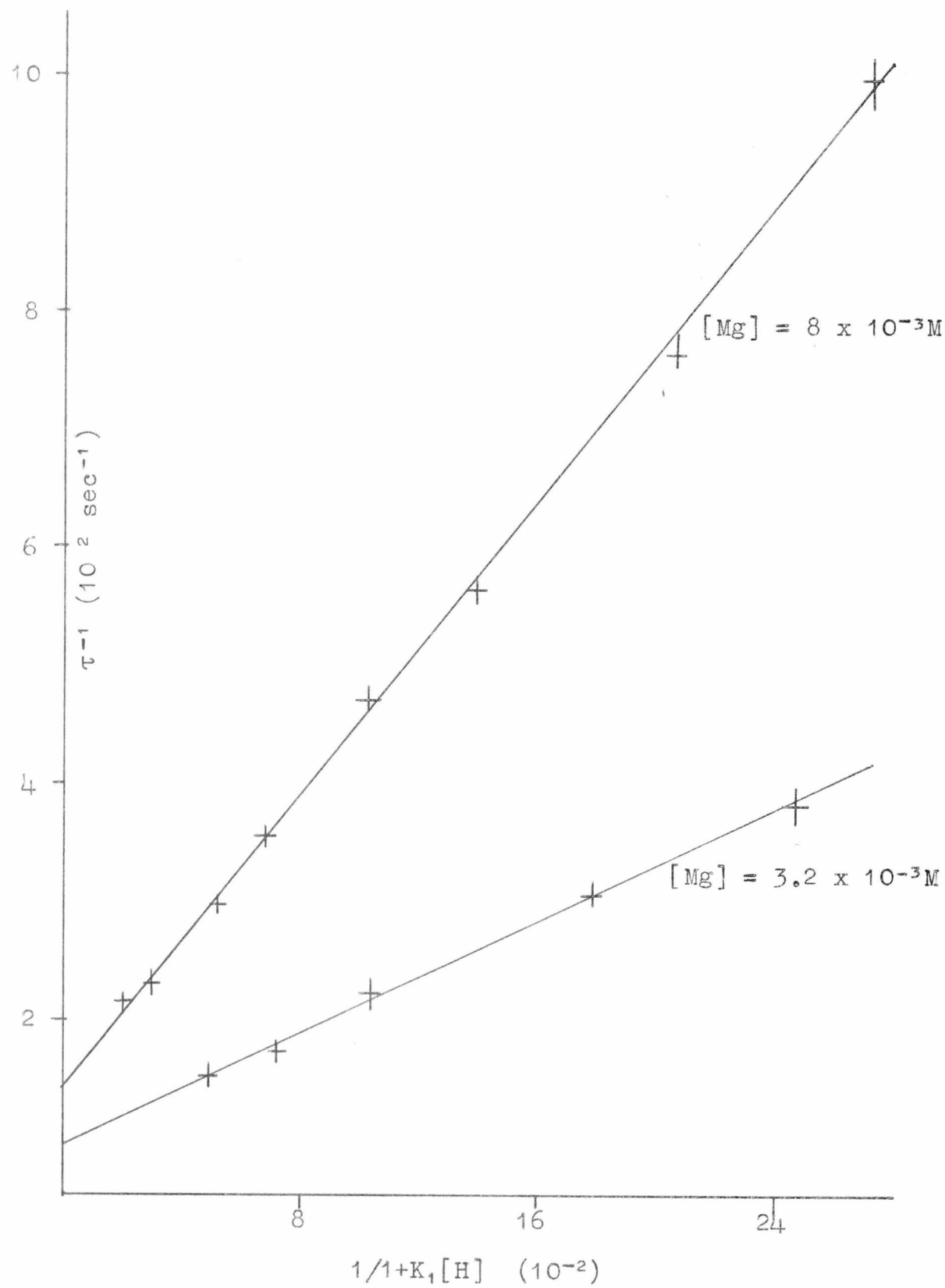
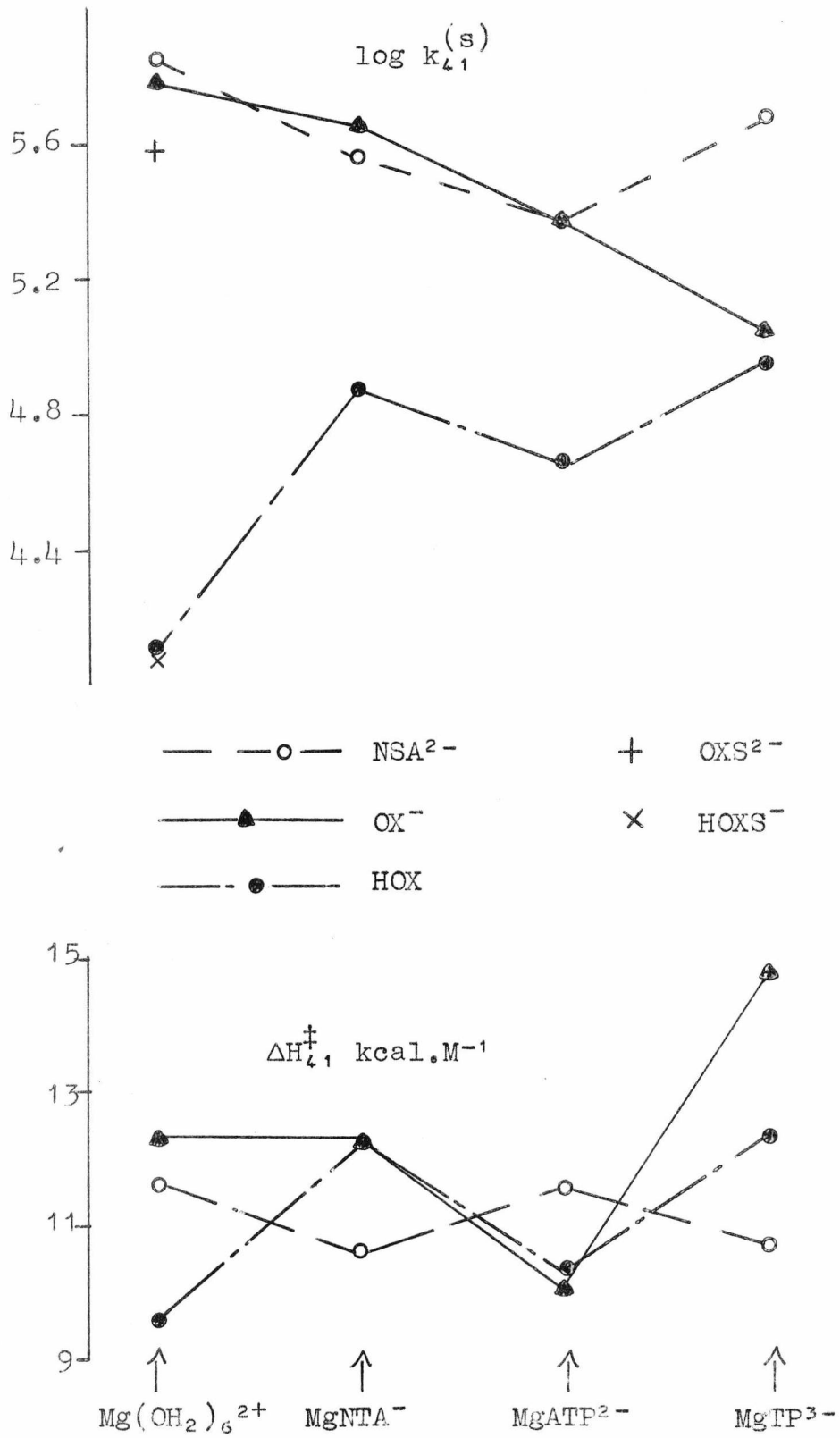


Fig. 5.10.1.



values of $K_{OS}k_{ex}$ for the NSA system. (Too much weight must not be placed on the k_{41} values for MgTP with oxine since this value was obtained by extrapolation from low pH and this method can give rise to unexpectedly large errors). However, it can be shown by a Hückel treatment⁽¹²¹⁾ on these ligands that there is a considerable amount of charge delocalisation and that the electron density at the phenolic oxygen, the point of highest electron density and thus presumably the group that forms the first bond with the metal, is almost identical for the two ligands. Any increase in K_{OS} that would be expected from the neighbouring carboxylate group is offset by a decrease effect due to the formation of non-reactive outer sphere complexes between the similarly charged oxygens of the nitro group and the metal. Although a Hückel treatment on the OXS molecule and anion have not yet been performed, it seems reasonable to expect the presence of the sulphonate group to lower the electron density on the phenolic oxygen as compared to that on the same atom in the oxine anion. This would lead to a decrease in K_{OS} and hence to the lowered value of k_{41} .

The rates of formation of the ternary complexes with oxine and oxine sulphonic acid are approximately ten times lower than for the corresponding anions. For these reactions the phenolic oxygen atom of the oxines are protonated leaving the nitrogen atom as the centre of highest electron density (and hence the attacking "arm" of the ligand) and the difference in rates between the oxine molecule and anion with aquo magnesium is attributable to the change in K_{OS} for a neutral ligand and a -1 ligand. Thus, as there is only a small difference between the electron densities on the nitrogen atoms in the oxine and oxine sulphonic acid molecules, the forward rate constants for the reaction of these species with aquo magnesium (k_{32}) are very similar.

The accuracy of the values for $k_{1,4}$ does not permit such a detailed discussion of the results, but it can be seen for the NSA systems that there is a general increase in the dissociation rate constants as the effective charge on the metal becomes more negative. This is probably due to an increased electrostatic repulsion between the bound groups and the NSA dianion. The larger $k_{1,4}$ for the NSA systems compared to the oxine systems indicates the greater stability of a five-membered as compared to a six-membered ring.⁽¹²²⁾

CHAPTER 6

Complex formation and dissociation involving Zn(II) species
and 5-nitrosalicylic acid

6.1 Introduction

A comparison of the stability constant of zinc NSA, $\log K = 6.7$,⁽¹⁰³⁾ with those for zinc with benzoic acid, $\log K = 0.9$,⁽¹²³⁾ and 2,4 dinitrophenol, $\log \beta_2 = 2.29$,⁽¹²⁴⁾ shows that NSA must act as a bidentate ligand towards zinc.

The kinetics of complexation between NSA and some zinc complexes have been studied over a range of temperatures using the temperature-jump method.

The systems investigated were:-

$Zn(H_2O)_6^{2+}$, $Zndien^{2+}$, $Zntrien^{2+}$, $Zntet^{2+}$,
 $Zntren^{2+}$, $ZnIDA^0$, $ZnEDDA^0$, $ZnUDA^-$, $ZnNTA^-$,
 $ZnTP^{3-}$.

For the $Zndien^{2+}$, $Zntet^{2+}$ and $ZnEDDA^0$ systems the effect of the anion on the kinetics was investigated using ClO_4^- and Cl^- as well as NO_3^- . The stability constants for the complexes listed above with NSA were investigated spectrophotometrically at 25°C using the method described in section 5.4.

6.2 Stability constants of Zinc NSA complexes

6.2.1 Determination of K_3 at 25°C

For all cases except the $Zntet^{2+}$ and $Zn(OH_2)_6^{2+}$ systems the data have been analysed using the equation derived in Appendix 4.

$$OD = \frac{(OD-C_{\epsilon A^-}) + (OD-C_{\epsilon HA})K_1[H]}{[M]} \cdot \frac{1}{K_3} + C_{\epsilon MA}$$

In the $Zntet^{2+}$ system under the conditions used the reactive metal species is believed to be $[Zntet(OH)]^+$; analysis thus required the modified optical density expression derived in Appendix .

The aquo zinc system was investigated using the method described in ref. 110.

6.2.2 Conditions used

Zinc complex concentrations and pH were chosen to give the largest possible variation in optical density while keeping the pH at least one pH unit below the pK's of the zinc complexes. The ionic strength was kept at 0.3 by the addition of varying amounts of $NaNO_3$, $NaClO_4$ or $NaCl$ as required and the pH was kept constant by buffering with $2 \times 10^{-2}M E_3N$. In all cases the total NSA concentration was $5 \times 10^{-5}M$. The metal concentrations and pH ranges used are shown in table 6.2.2.1.

TABLE 6.2.2.1. Conditions used in the spectrophotometric determinations

<u>System</u>	<u>[ML]</u>	<u>pH range</u>
$Zndien^{2+}$	$1.2 \times 10^{-3} - 1.2 \times 10^{-2}M$	< 8.0
$Zntrien^{2+}$ nitrate	$2.4 \times 10^{-2}M$	8.2 - 10
$Zntrien^{2+}$ perchlorate	$2 \times 10^{-2}M$	8.4 - 9.8
$Zntet^{2+}$ perchlorate	$8 \times 10^{-4} - 8 \times 10^{-3}M$	9.2 - 10.5
$ZnEDDA^{\circ}$	$4 \times 10^{-2}M$	7.7 - 9.2
$ZnUDA^{-}$	$5 \times 10^{-3}M$	8.3 - 10.1
$ZnNTA^{-}$	$3 \times 10^{-2}M$	7.9 - 9.3
$ZnTP^{3-}$	$2 \times 10^{-2}M$	8.0 - 9.3
$Zn(OH_2)_6^{2+}$	$8 \times 10^{-3}M$	7.075 and 7.297

6.2.3 Results

The plots of d against $f(d[H])M$ (see section 5.4.1) are shown in figs. 6.2.3.1 - 6.2.3.10 and the optical density data for the aquo zinc system are shown in table 6.2.3.2. The final values of $\log K_3$ are shown in table 6.2.3.3.

TABLE 6.2.3.1. Index to plots

<u>System</u>	<u>Figure No.</u>
ZnTP ³⁻ nitrate	6.2.3.1
ZnEDDA ⁰ nitrate	6.2.3.2
ZnUDA ⁻ nitrate	6.2.3.3
ZnNTA ⁻ nitrate	6.2.3.4
Zntrien ²⁺ nitrate	6.2.3.5
Zntrien ²⁺ perchlorate	6.2.3.6
Zntet ²⁺ perchlorate	6.2.3.7
Zndien ²⁺ perchlorate	6.2.3.8
Zndien ²⁺ chloride	6.2.3.9
Zndien ²⁺ nitrate	6.2.3.10

6.3 Kinetics of the Zn(II) species with NSA

6.3.1 Choice of conditions

The choice of conditions for the zinc systems is considerably more difficult than for magnesium.

(i) To be able to use the simplified relaxation expression derived in section 5.7.3, it is necessary to work at low metal concentrations and low pH so that the term in $k_{32}CM$ can be neglected.

(ii) To get accurate values of k_{41} and k_{14} it is necessary to get a large change in τ^{-1} either by varying $[ML]$ or $[H]$.

Figure 6.2.3.1. Stability constant for $ZnTP3^-$ with NSA^{2-} at $25^\circ C$.

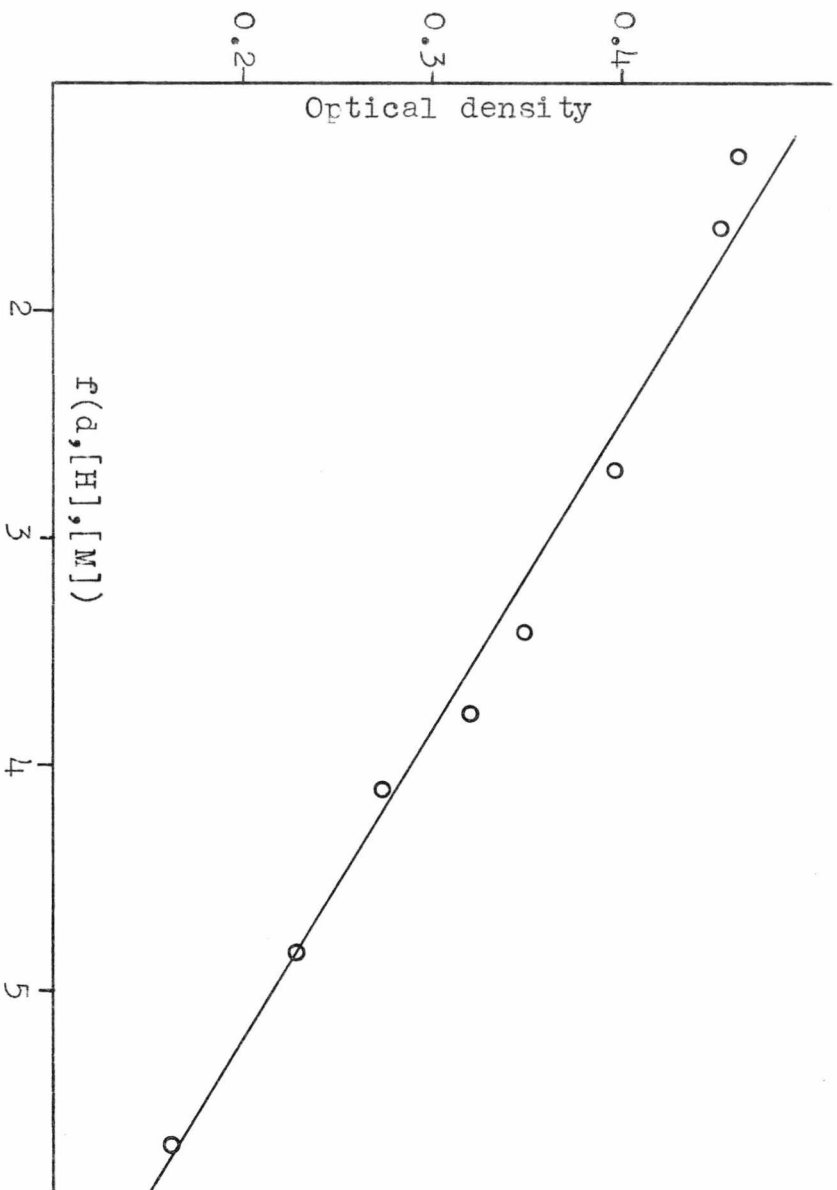


Figure 6.2.3.2. Stability constant for $ZnEDDA^0$ with NSA^{2-} at $25^\circ C$.

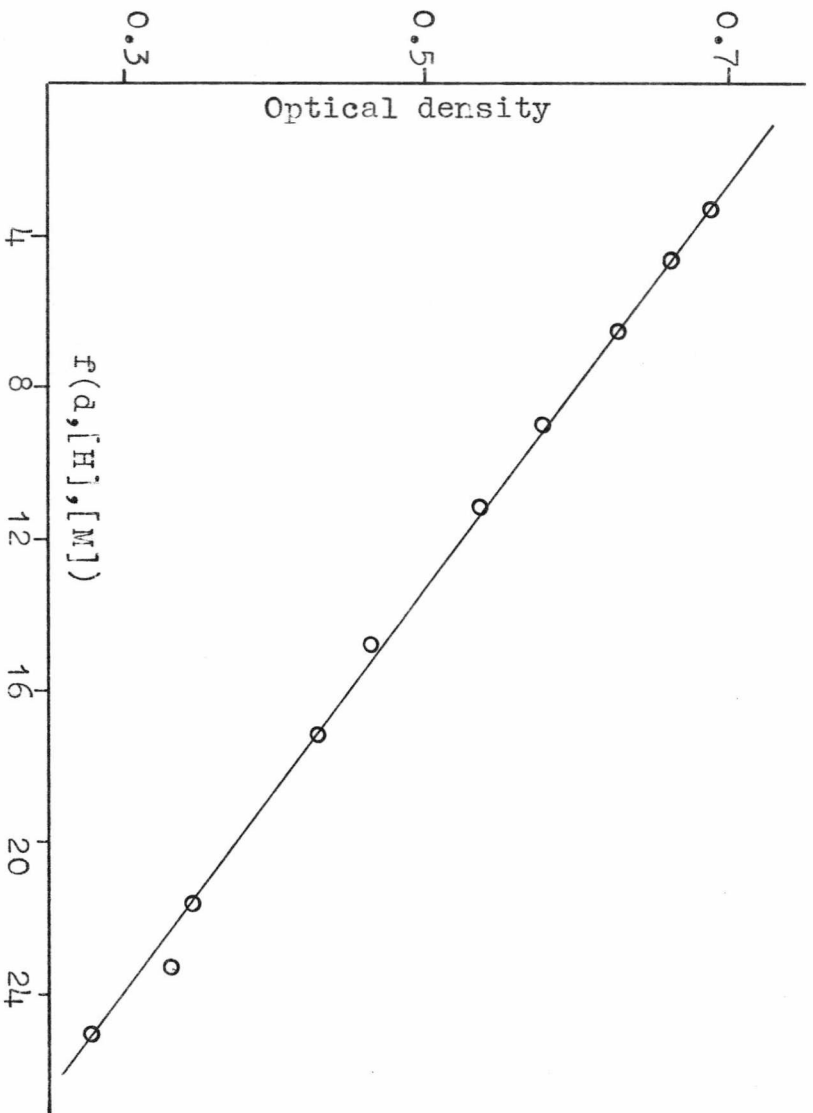


Figure 6.2.3.3. Stability constant for ZnUDA^- with NSA^{2-} at 25°C .

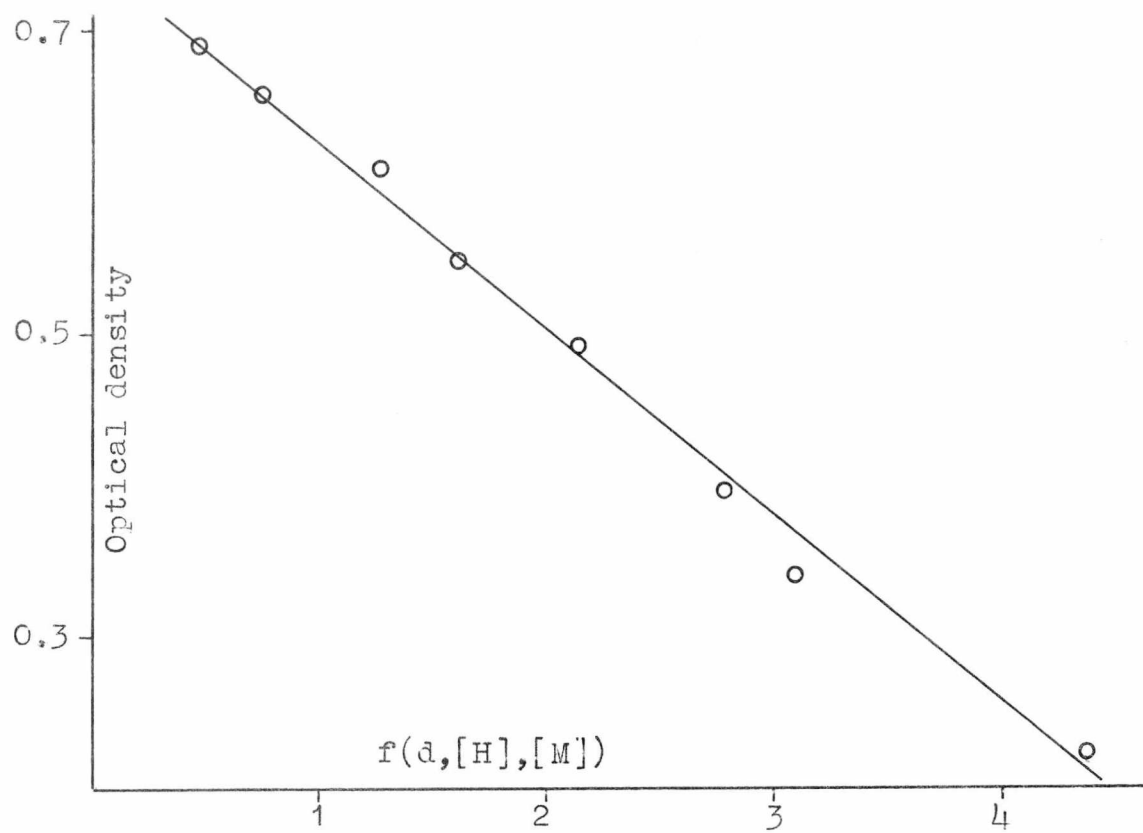


Figure 6.2.3.4. Stability constant for ZnNTA^- with NSA^{2-} at 25°C .

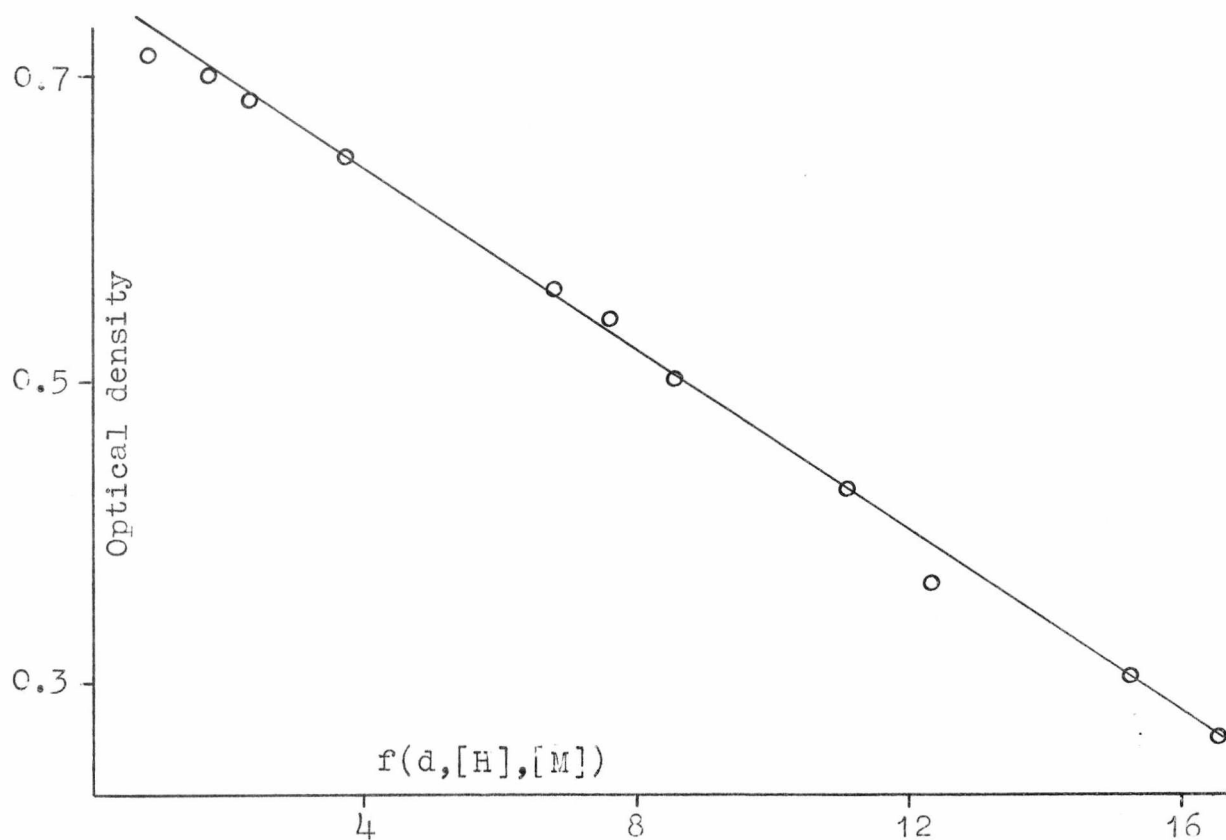


Figure 6.2.3.5. Stability constant for $Zntrien^{2+}$ with NSA^{2-} in $0.3M NaNO_3$ at $25^{\circ}C.$

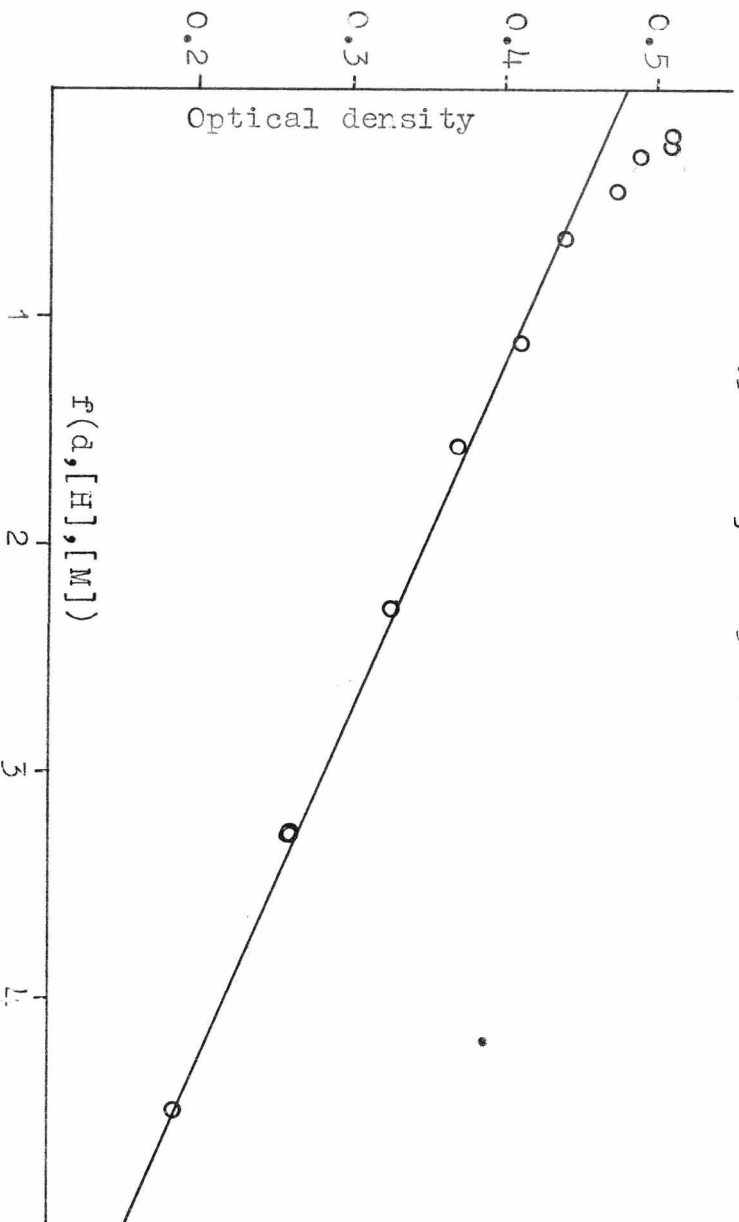


Figure 6.2.3.6. Stability constant for $Zntrien^{2+}$ with NSA^{2-} in $0.3M NaClO_4$ at $25^{\circ}C.$

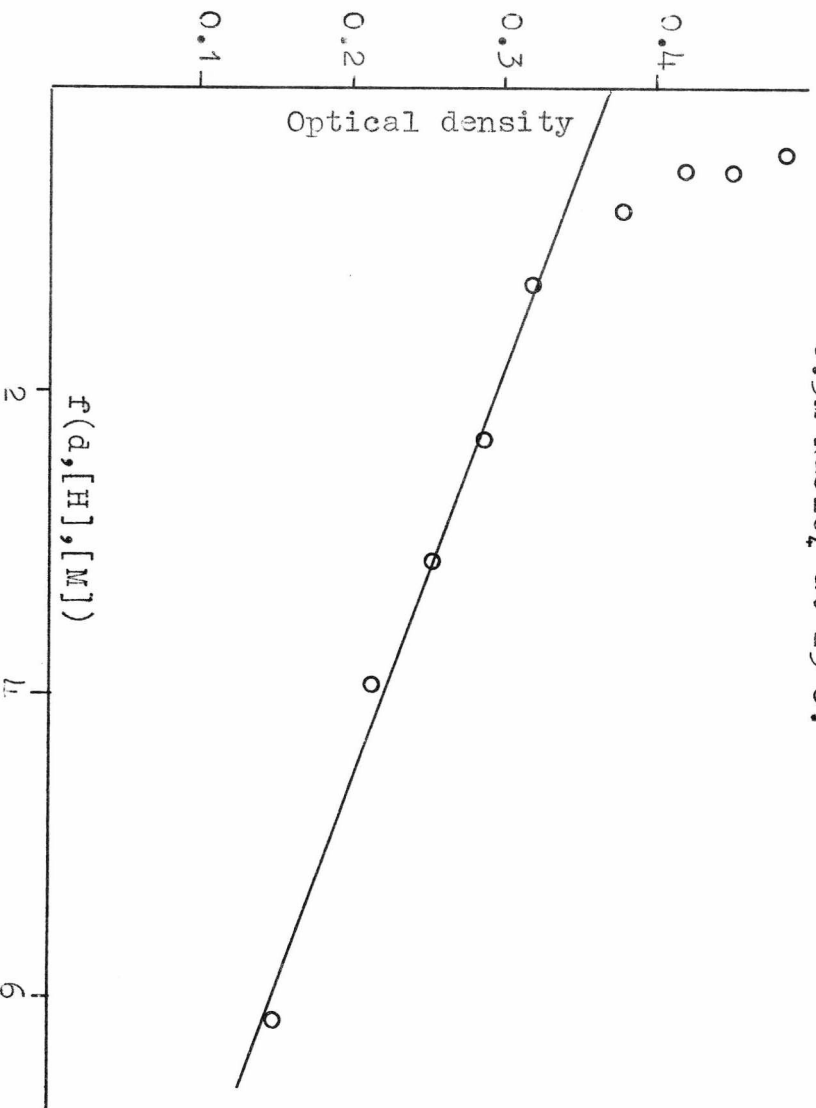


Figure 6.2.3.7. Spectrophotometric determination of the stability constant of $Zntet^{2+}$ with NSA^{2-} at $25^{\circ}C$.

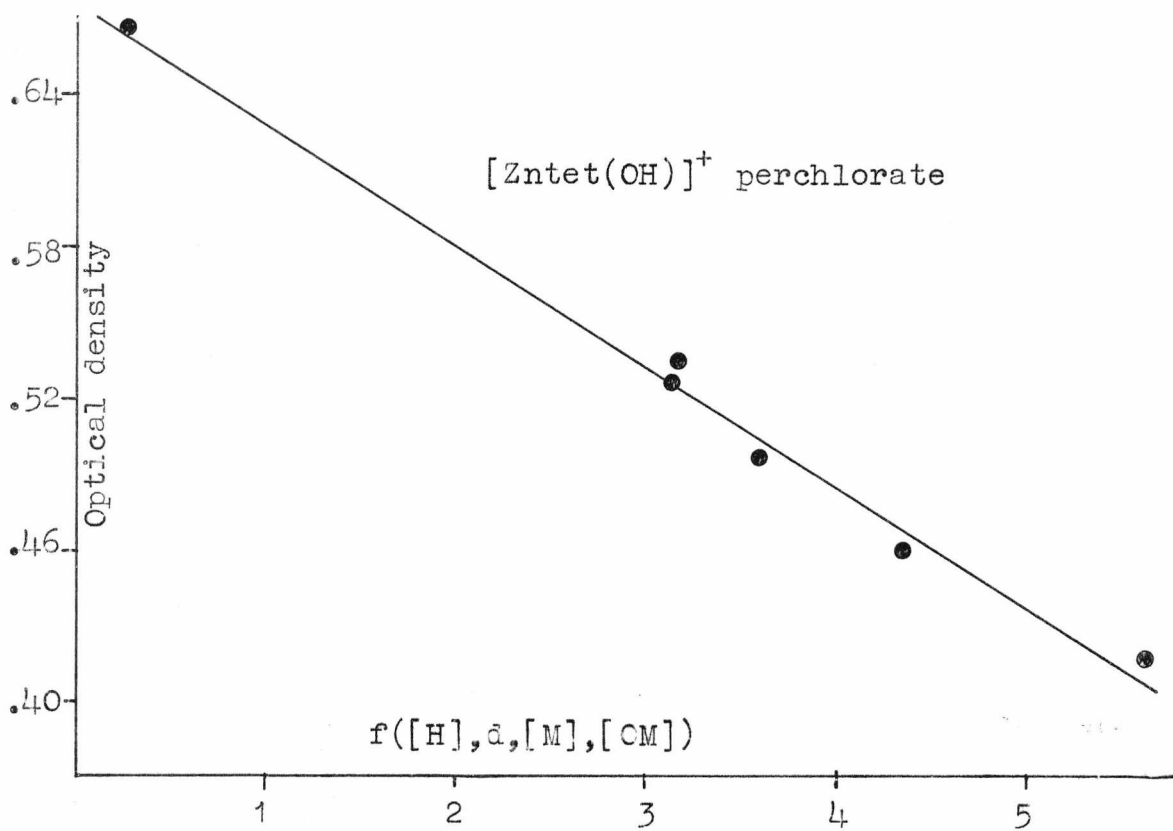
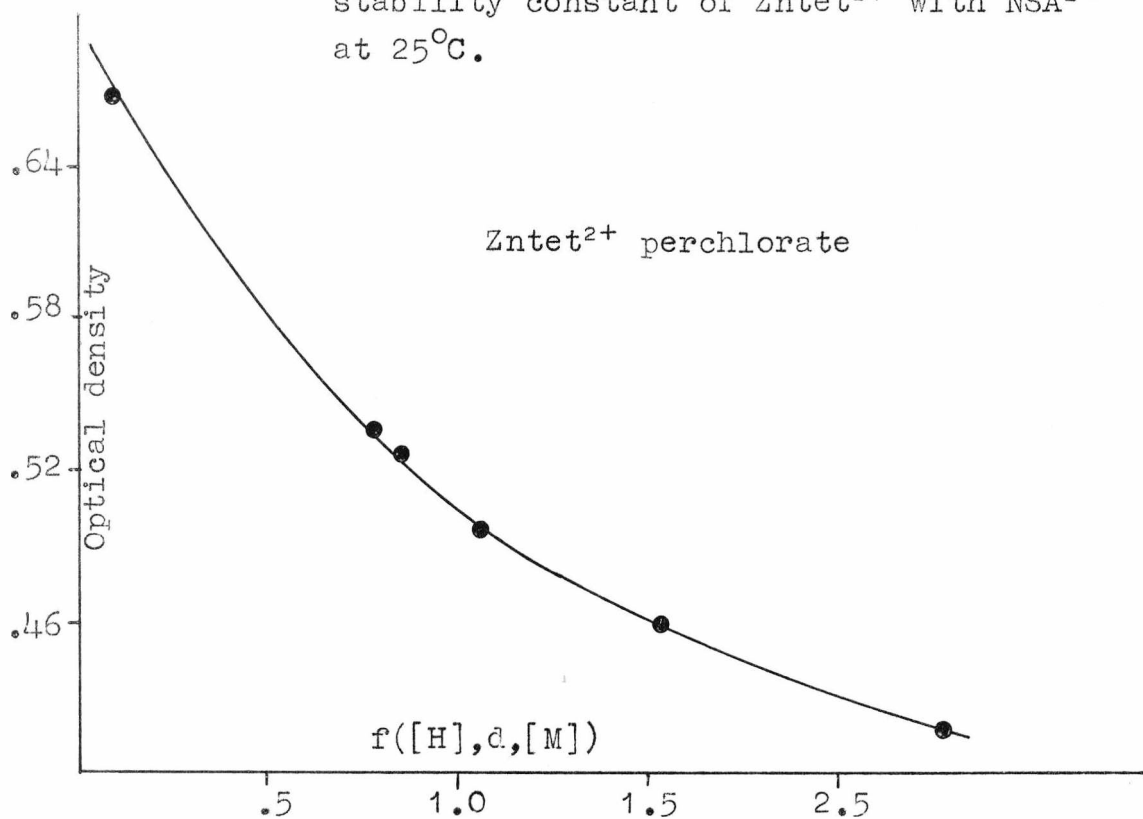


Figure 6.2.3.8. Stability constant for $Zndien^{2+}$ with NSA^{2-} in $0.3M NaClO_4$ at $25^{\circ}C$.

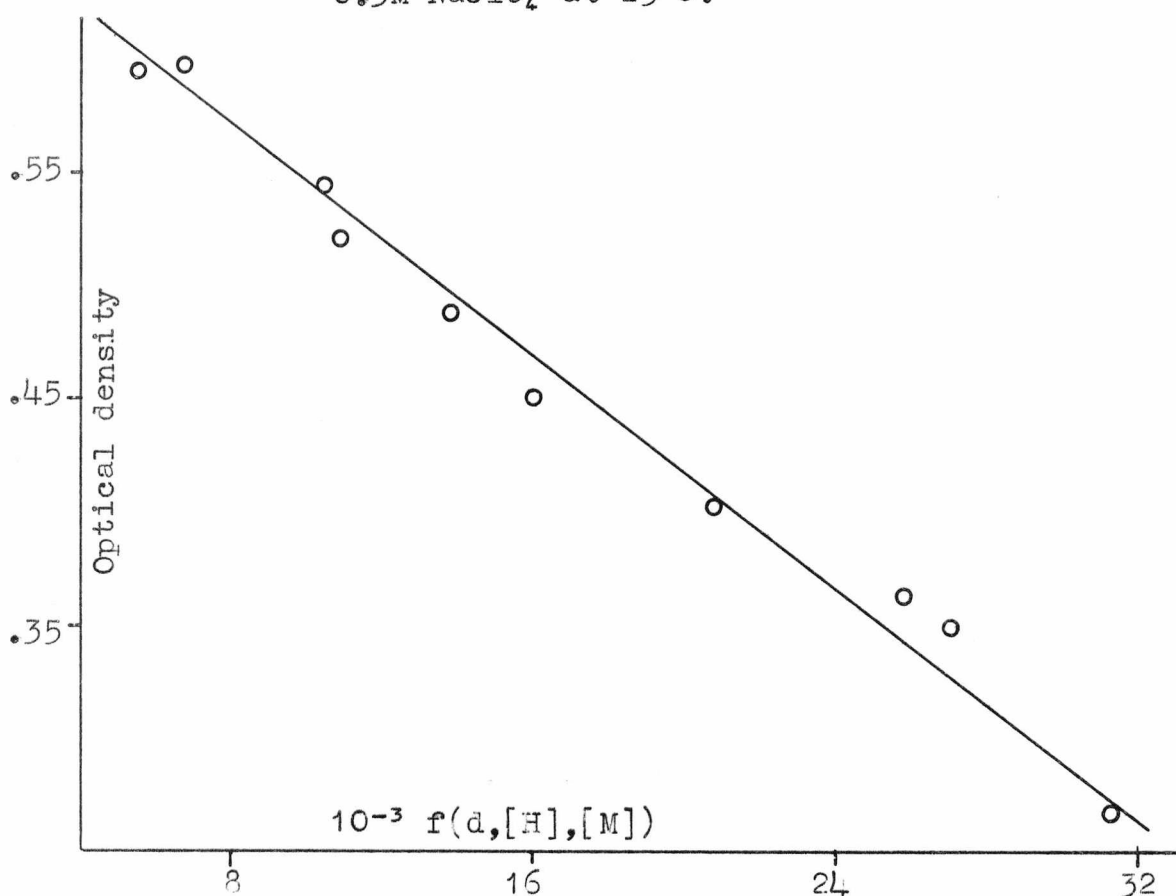


Figure 6.2.3.9. Stability constant for $Zndien^{2+}$ with NSA^{2-} in $0.3M NaCl$ at $25^{\circ}C$.

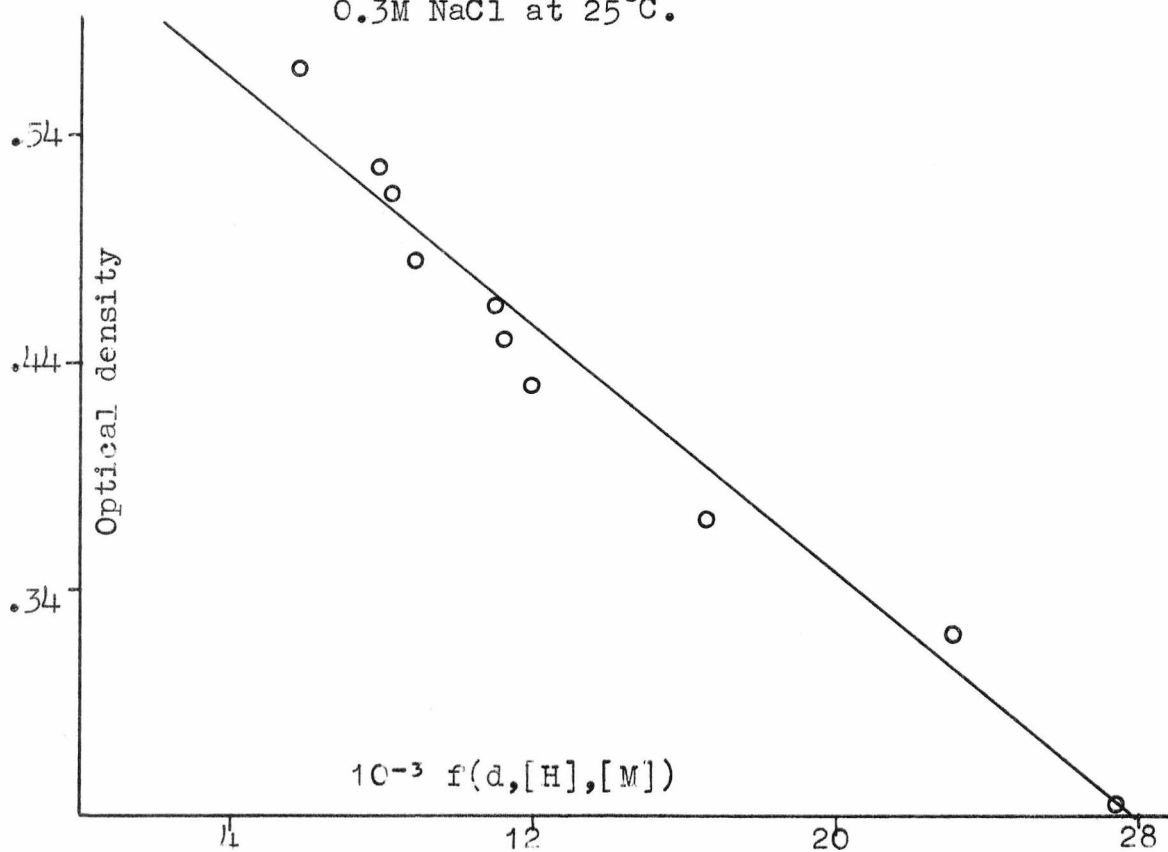


TABLE 6.2.3.2. Optical density data for the aquo zinc NSA²⁻ system at 25°C.

$\lambda = 380 \text{ nm.}$

pH ₁	8.611	OD ₁	0.104
pH ₂	9.308	OD ₂	0.182
pH ₃	7.297	OD ₃	0.441
pH ₄	7.075	OD ₄	0.391

Figure 6.2.3.10. Stability constant for $Zndien^{2+} + NSA^{2-}$ in 0.3M $NaNO_3$ at 25°C.

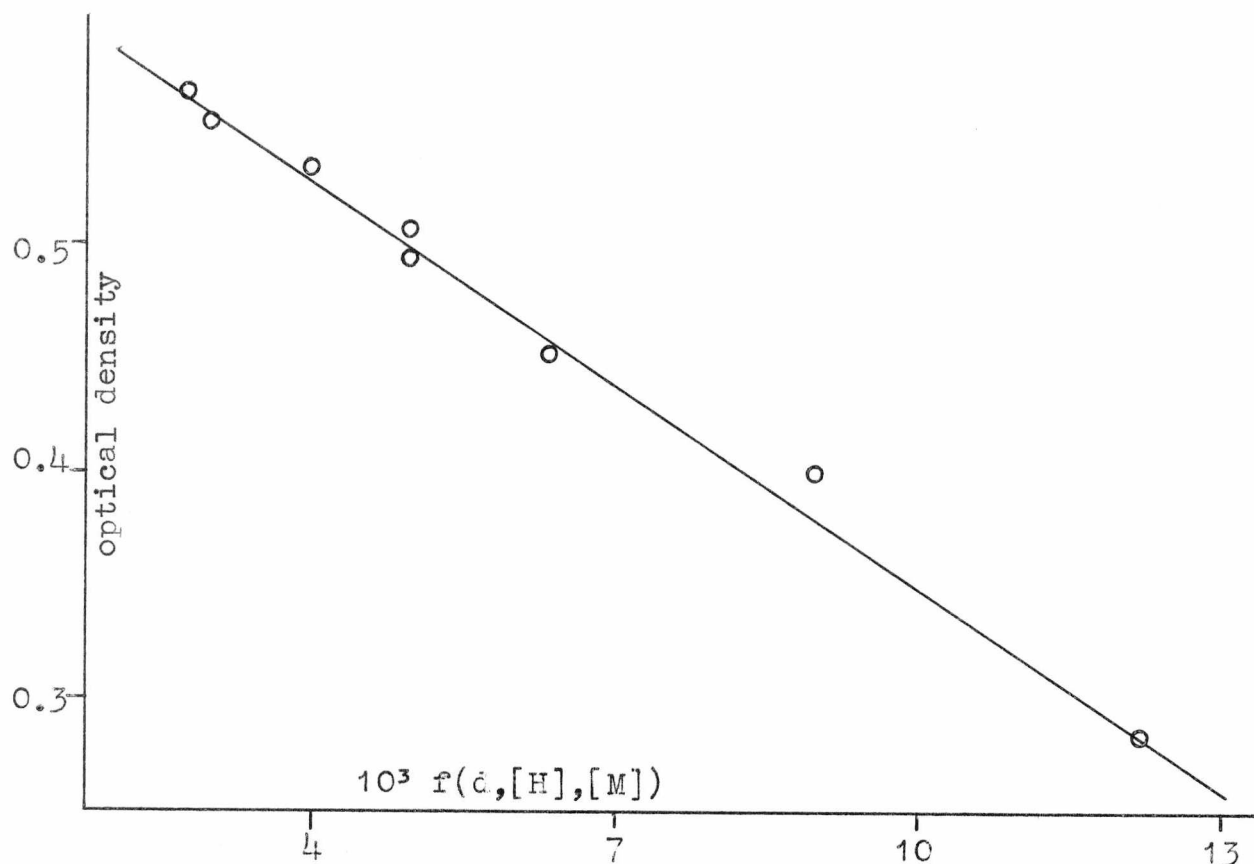


TABLE 6.2.3.3. Results for K_3 at 25°C, $\mu = 0.3$.

<u>System</u>	<u>log K_3</u>
$Zn(OH_2)^{2+}$	5.18(\pm 0.08)
$Zndien^{2+}$ chloride	4.85(\pm 0.08)
nitrate	4.52(\pm 0.08)
perchlorate	4.91(\pm 0.07)
$Zntrien^{2+}$ perchlorate	3.45(\pm 0.02)
$Zntrien^{2+}$ nitrate	2.83(\pm 0.02)
$ZnEDDA^0$	3.12(\pm .04)
$ZnNTA^-$	3.05(\pm .04)
$ZnUDA^-$	3.22(\pm .04)
$ZnTP^{3-}$	2.82(\pm .06)
$Zntet(ClO_4)_2$	<2.84

(iii) At high pH zinc complexes tend to form hydroxy species which affect the kinetics either by giving a second reactive metal species or simply by reducing the concentration of ML.

(iv) The relaxation effects are often extremely sensitive to an excess of L which often produces a second relaxation which can be ascribed to the formation of the ML_2 complex.

(v) For the $ZnIDA^0$ system above pH 9 a small amount of zinc hydroxide precipitates from solution which makes the concentration of $ZnIDA^0$ inaccurate because of shifts in the complex formation equilibria.

The metal : ligand ratios, concentrations and pH ranges are shown in table 6.3.1.1.

TABLE 6.3.1.1. Experimental conditions for Zn(II) NSA systems.

<u>System</u>	<u>M:L</u>	<u>[ML]</u>	<u>pH range</u>
$Zn(OH_2)_6^{2+}$		$0.8-8 \times 10^{-2} M$	6.2 - 7.2
$Zndien^{2+}$	1:1.02	$0.8-8 \times 10^{-3} M$	7.5 - 8.0
$Zntet^{2+}$ nitrate	1:1.02	$0.8-8 \times 10^{-3} M$	9.2 - 9.5
$Zntet^{2+}$ perchlorate	1:1.02	$0.8-8 \times 10^{-3} M$	9.2 - 9.5
$ZnIDA^0$	1:1.03	$1.6 \times 10^{-3} M$	7.8 - 9.0
$ZnEDDA^0$	1:1.1	$0.8-4 \times 10^{-2} M$	8.6 - 9.2
$ZnNTA^-$	1:1.02	$0.8-4 \times 10^{-2} M$	8.6 - 9.4
$ZnUDA^-$	1:1.01	$10^{-2} M$	7.5 - 9.8
$ZnTP^{3-}$	1:1.1	$0.8-3.2 \times 10^{-2} M$	8.5 - 9.5

6.3.2. Choice of buffer

The conditions outlined above make it necessary to carry out kinetic experiments in the pH range 7 - 10 where unfortunately it is difficult to find a buffer which will not complex with zinc. In this pH range the usual buffering groups are amines, phenols and phosphates but all these groups are known to form complexes with zinc. In enzyme studies in this pH range it is usual to use one of three buffers, namely:-

- (1) Tris
- (2) phosphate
- (3) diethyl barbituric acid

These three buffers do, however, show marked effects on the complexes of zinc.

It is difficult to tell if a colourless buffer forms a complex with zinc but it has been found that buffers can have large effects on the relaxation times of zinc containing solutions under control conditions. In this work the "innocence" of the buffer was checked by taking fixed concentrations of ZnL and NSA and fixed pH and varying the buffer concentration. If the relaxation time observed was independent of the buffer concentration the buffer was assumed not to interfere in the reaction.

It has been shown⁽¹²⁵⁻⁷⁾ that tris buffer readily forms complexes with Cu(II) and Ni(II) and so it is reasonable to suggest that it also forms complexes with zinc. It can be shown that the addition of tris to a zinc solution suppresses the precipitation of zinc hydroxide and at low zinc and tris concentrations a relaxation is observable using phenol red as an indicator probably due to the formation of a complex between zinc and tris. The interference of tris in the

complexation kinetics of several zinc complexes with NSA is shown in figs. 6.3.2.1 - 6.3.2.3. As this effect could possibly be attributed to a specific interaction between tris and NSA a similar experiment was conducted using Zndien^{2+} and 2-hydroxy-5-nitrobenzyl phosphonic acid as the incoming ligand. A plot of τ^{-1} against tris buffer concentration for this system is shown in fig. 6.3.2.4 and this shows that the most likely explanation of the effect of tris on these zinc systems is an interaction between tris buffer and the zinc complex.

The solubility product of $\text{Zn}_3(\text{PO}_4)_2$ is so small, 10^{-32}M^{-5} (128) that a precipitate of zinc phosphate always forms under the conditions necessary for the temperature-jump experiments and so phosphate cannot be used as a buffer. Veronal buffer, like tris and several other buffers including 3,5 dichlorophenol, imidazole and triethenolamine, had a marked effect on the zinc-NSA relaxation time; of the buffers tried, only triethylamine had no effect. Yoke (129) found no evidence for the formation of zinc-triethylamine complexes.

Choice of counterion

For convenience, nitrate was commonly used as the counterion since this anion presents no problems in pH measurements. The use of perchlorate requires either a lithium chloride or sodium chloride salt bridge for the reference electrode as the potassium chloride in a calomel electrode leads to the formation of insoluble potassium perchlorate at the surface of the calomel electrode and hence to unreliable pH values. The effect of the counterion on the zinc-dien and -tet systems has been investigated; in addition, some preliminary work has been done on zincEDDA and zincUDA.

Fig. 6.3.2.1. The effect of tris on the reaction between ZnIDA° and NSA^{2-} .

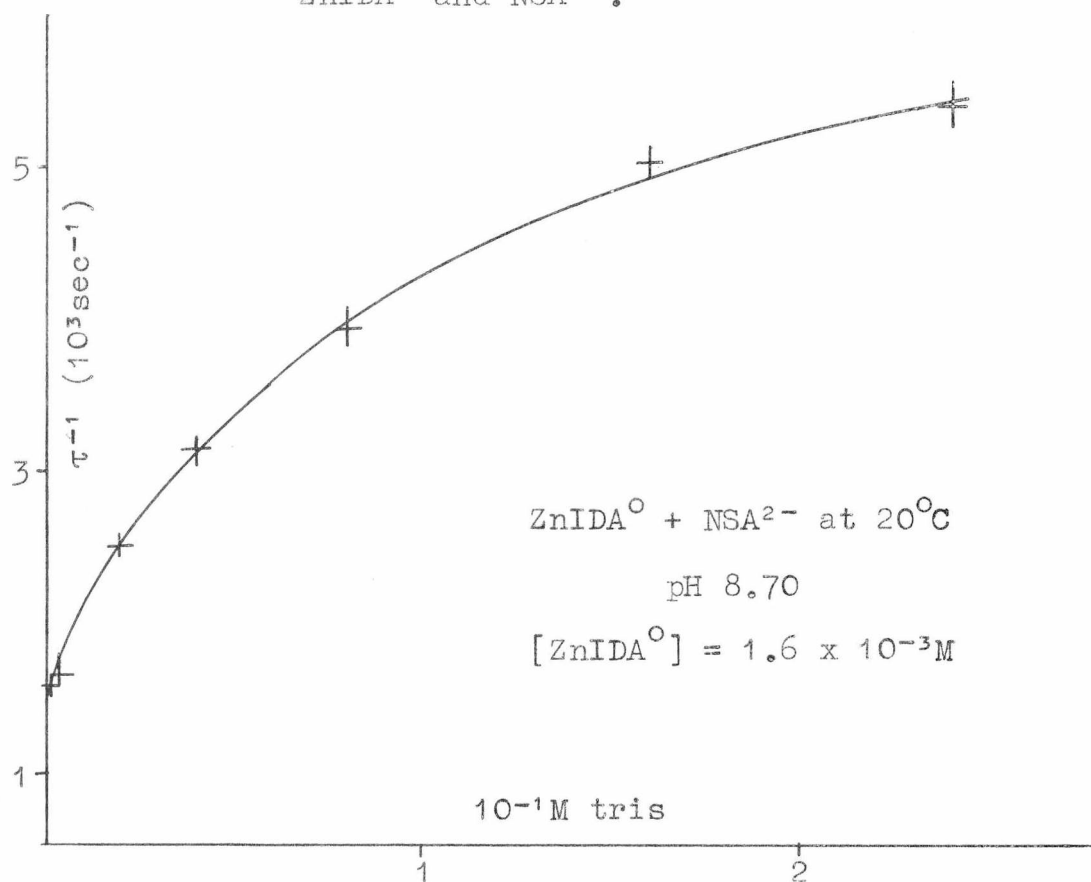


Fig. 6.3.2.2. The effect of tris on the reaction between ZnNTA^{-} and NSA^{2-} .

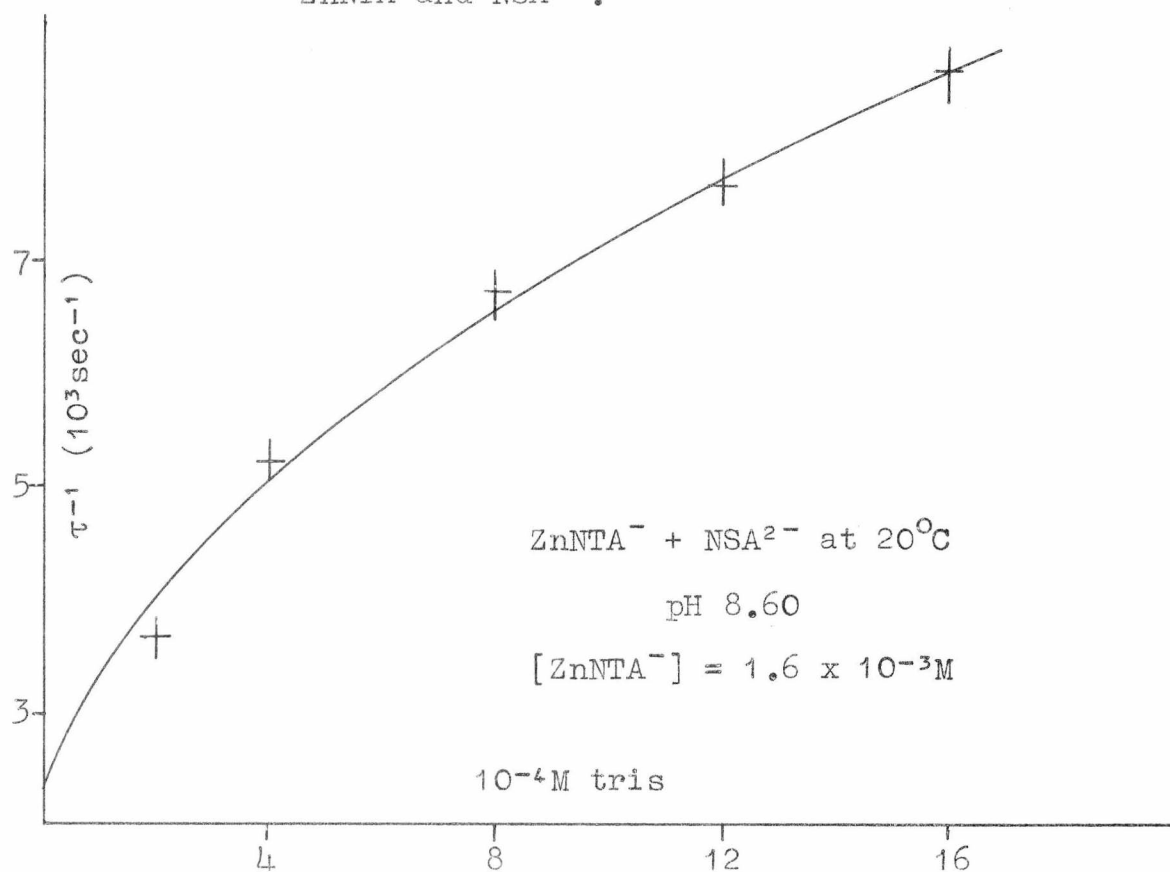


Fig. 6.3.2.3. The effect of tris on the reaction between $Zndien^{2+}$ and NSA^{2-} .

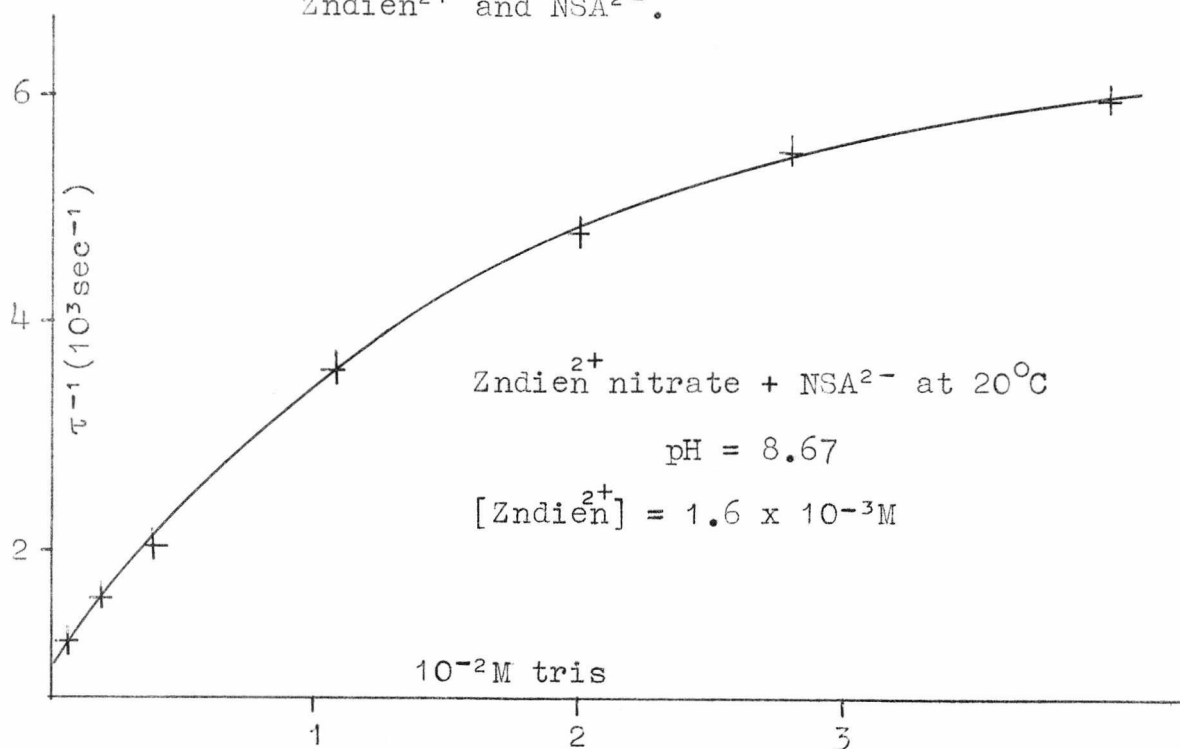
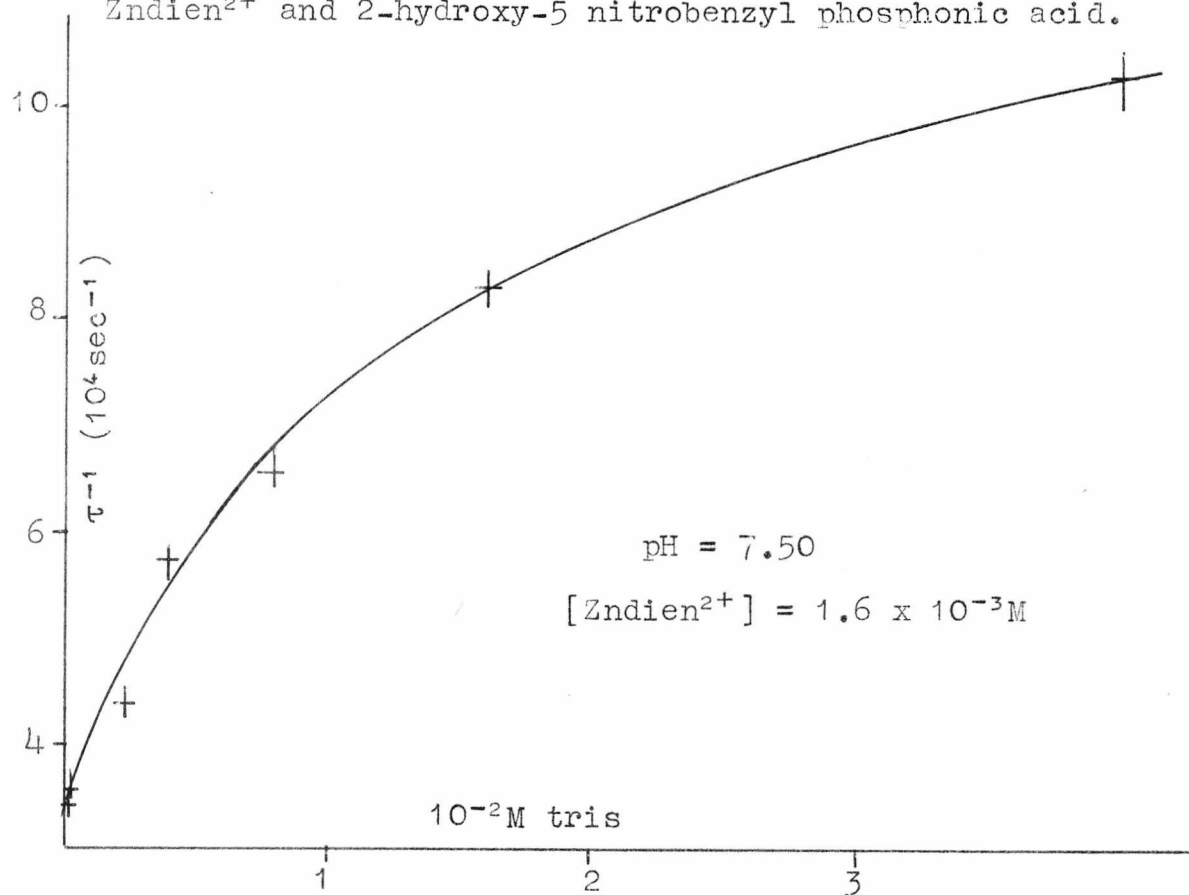


Fig. 6.3.2.4. The effect of tris on the reaction between $Zndien^{2+}$ and 2-hydroxy-5 nitrobenzyl phosphonic acid.



6.4 Kinetic Data

It is not possible to obtain complete pH profiles for most of the zinc systems and so only the high pH side of the profile was fully investigated. A typical plot of τ^{-1} vs. pH for the ZnUDA^- system is shown in fig. 6.4.1 showing the pH range for which measurable relaxation effects are observed. For all the systems investigated except $\text{Zn}(\text{OH}_2)_6^{2+}$ the metal concentrations are low so that the relaxation expression may be simplified as for the magnesium systems and plots of τ^{-1} vs. $[\text{M}]/1 + K_1[\text{H}]$ give straight lines of slope $k_{4,1}$ and intercept $k_{1,4}$. These plots and the related activation plots are shown in figs. 6.4.2 - 6.4.20.

For the $\text{Zn}(\text{H}_2\text{O})_6^{2+}$ system the relaxation time was found to be independent of pH but dependent on the concentration of zinc. This can only be the case if the terms $k_{4,1}[\text{M}]/1 + K_1[\text{H}]$ and $k_{2,3}K_9[\text{H}]$ are small compared to $k_{1,4} + k_{3,2}[\text{M}]$ so a plot of τ^{-1} against $[\text{M}]$ should give a straight line of slope $k_{3,2}$ and intercept $k_{1,4}$. The plot of τ^{-1} vs. $[\text{M}]$ and the associated activation plots are shown in figs. 6.4.21 and 6.4.22.

An index to the plots of τ^{-1} against $[\text{M}]/1 + K_1[\text{H}]$ is given in table 6.4.1.

6.5 Results

The results for $k_{4,1}$, $k_{1,4}$ and $\log K_3$ are given in table 6.5.1 and the activation parameters obtained from these results are shown in table 6.5.2.

Fig. 6.4.1. pH profile for the reaction between ZnUDA^- and NSA^{2-} at 28°C .

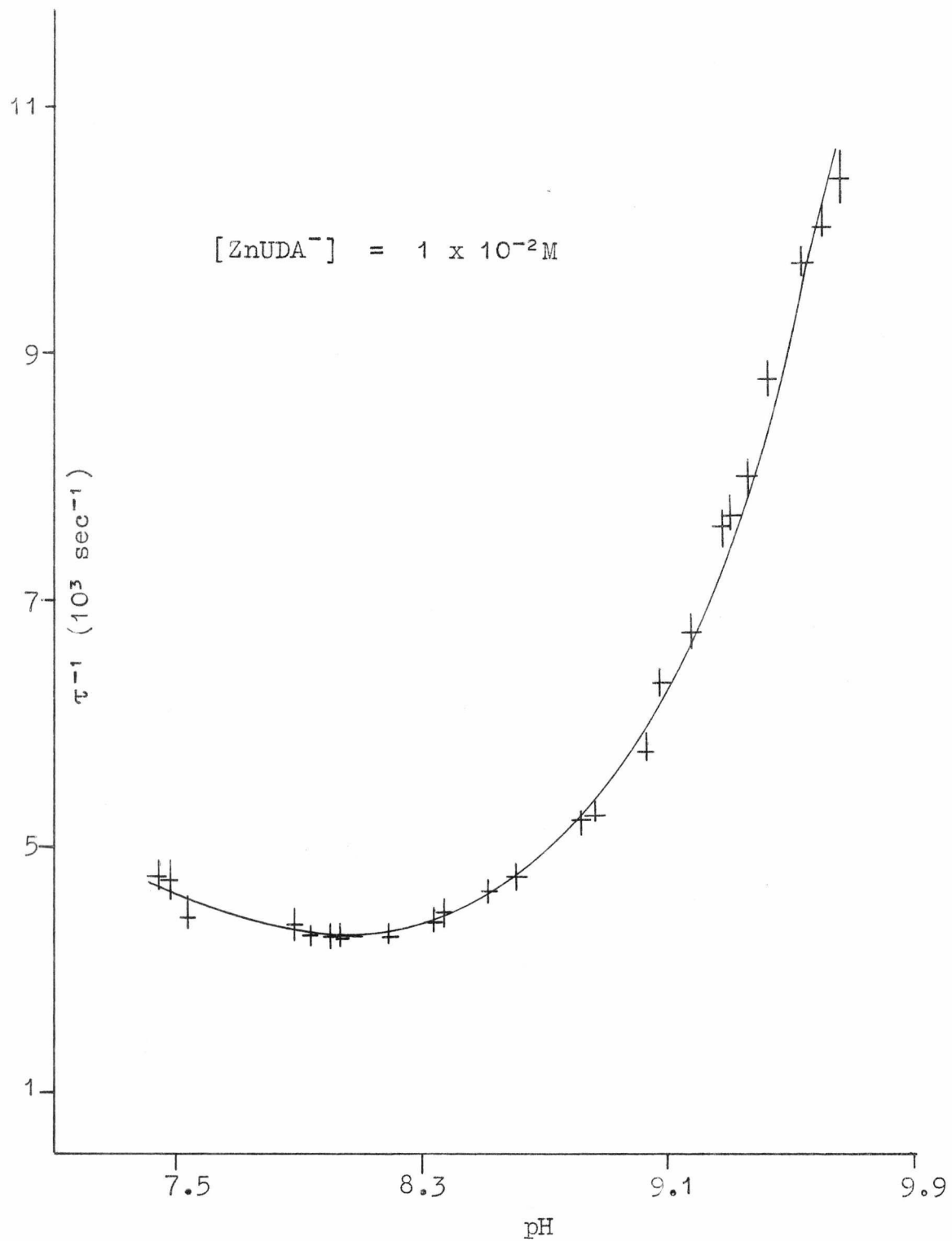


TABLE 6.4.1. Index to kinetic plots.

<u>System</u>	<u>Figure number</u>	
	<u>τ^{-1} vs. $[M]/1+K_1[H]$</u>	<u>logK vs. $1/T$</u>
Zndien ²⁺ perchlorate	6.4.2	6.4.3
Zndien ²⁺ nitrate	6.4.4	6.4.5
Zndien ²⁺ chloride	6.4.6	6.4.7
Zntet ²⁺ perchlorate	6.4.8	6.4.9
Zntet ²⁺ nitrate	6.4.10	6.4.9
ZnIDA ⁰	6.4.11	6.4.12
ZnEDDA ⁰	6.4.13	6.4.14
ZnNTA ⁻	6.4.15	6.4.16
ZnUDA ⁻	6.4.17	6.4.18
ZnTP ³⁻	6.4.19	6.4.20
	<u>τ^{-1} vs. $[M]$</u>	<u>logK vs. $1/T$</u>
Zn(OH ₂) ₆ ²⁺	6.4.21	6.4.22

Unless otherwise stated the counter ion used was nitrate.

Fig. 6.4.2. Plot of τ^{-1} vs. $[M]/(1 + K_1[H])$ for $Zndien^{2+}$ perchlorate + NSA^{2-} .

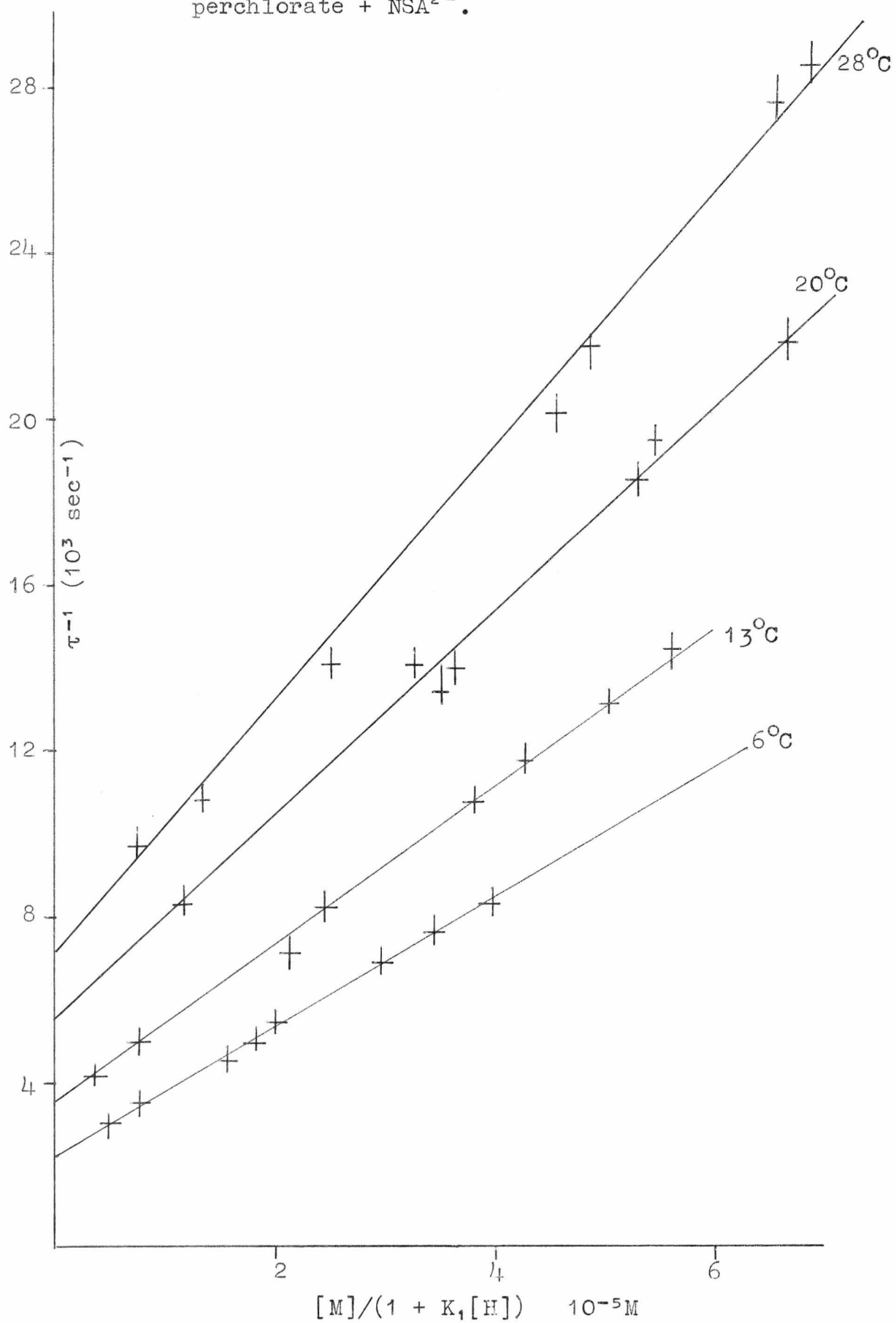


Fig. 6.4.3. Plots of $\log_{10}K$ vs. $1/T$ for Zn^{2+} perchlorate + NSA^{2-} .

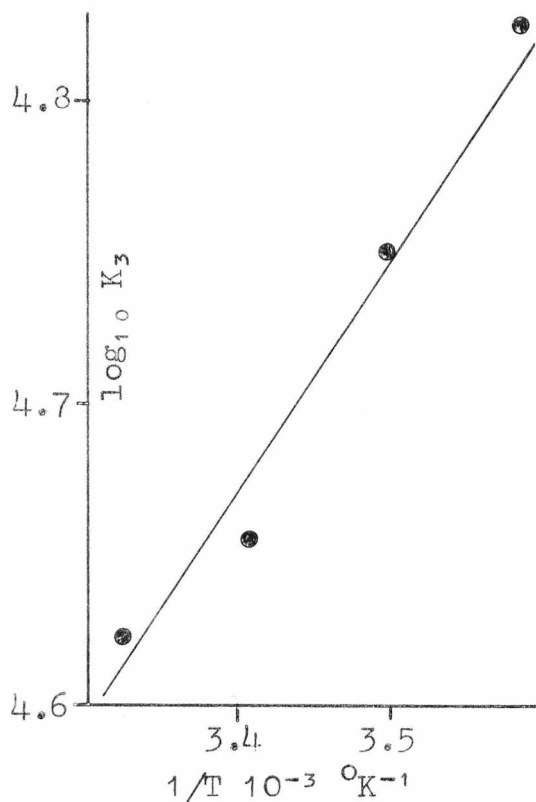
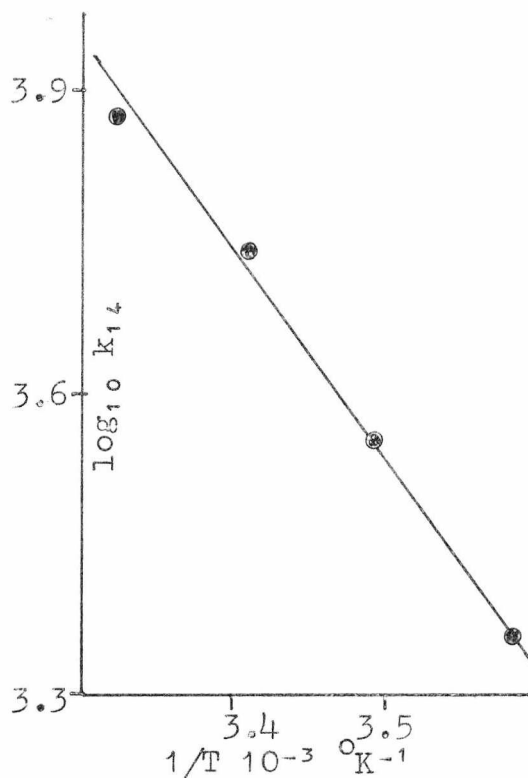
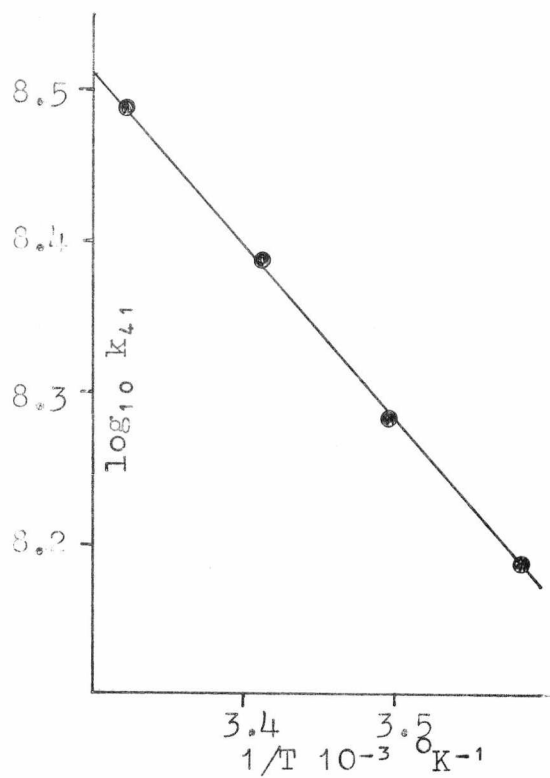


Fig. 6.4.4. Plot of τ^{-1} vs. $[M]/(1 + K_1[H])$ for $Zn dien^{2+}$ nitrate + NSA^{2-} .

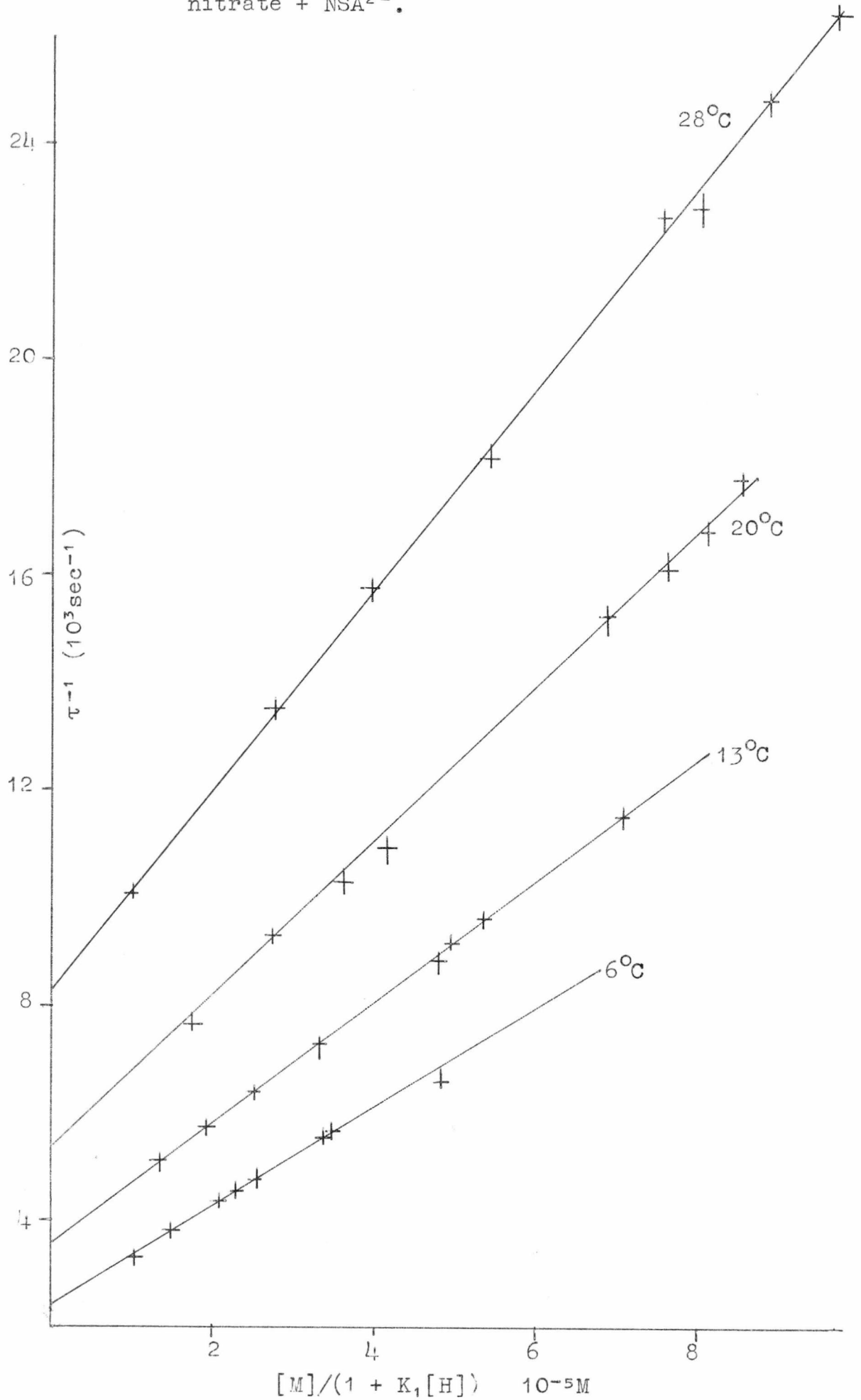


Fig. 6.4.5. Plots of $\log_{10} k$ vs. $1/T$ for Zn^{2+} nitrate + NSA^{2-} .

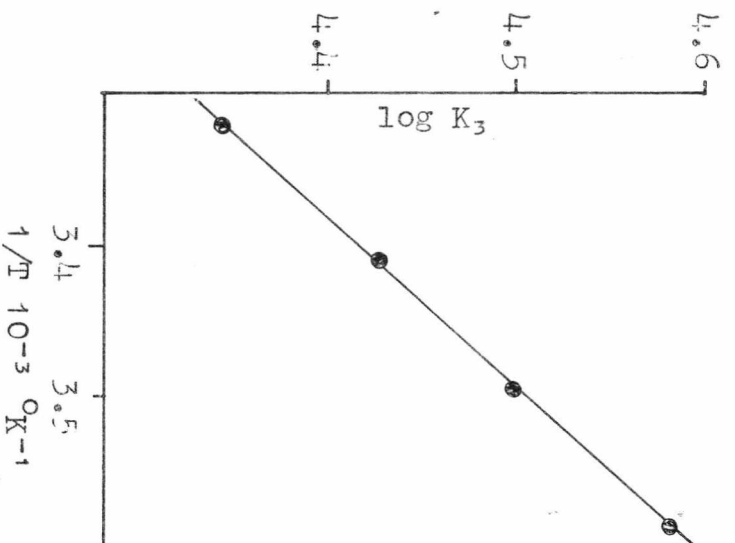
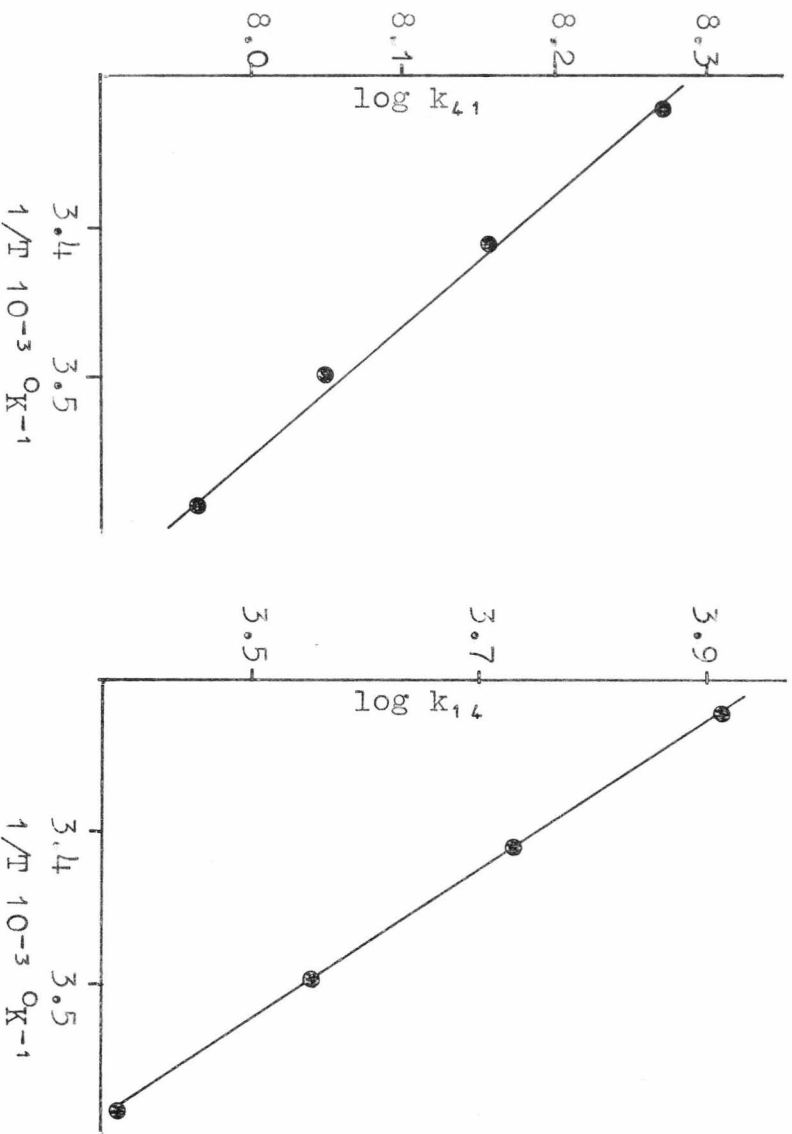


Fig. 6.4.6. Plot of τ^{-1} vs. $[M]/(1 + K_1[H])$ for $Zndien^{2+}$ chloride + NSA^{2-} .

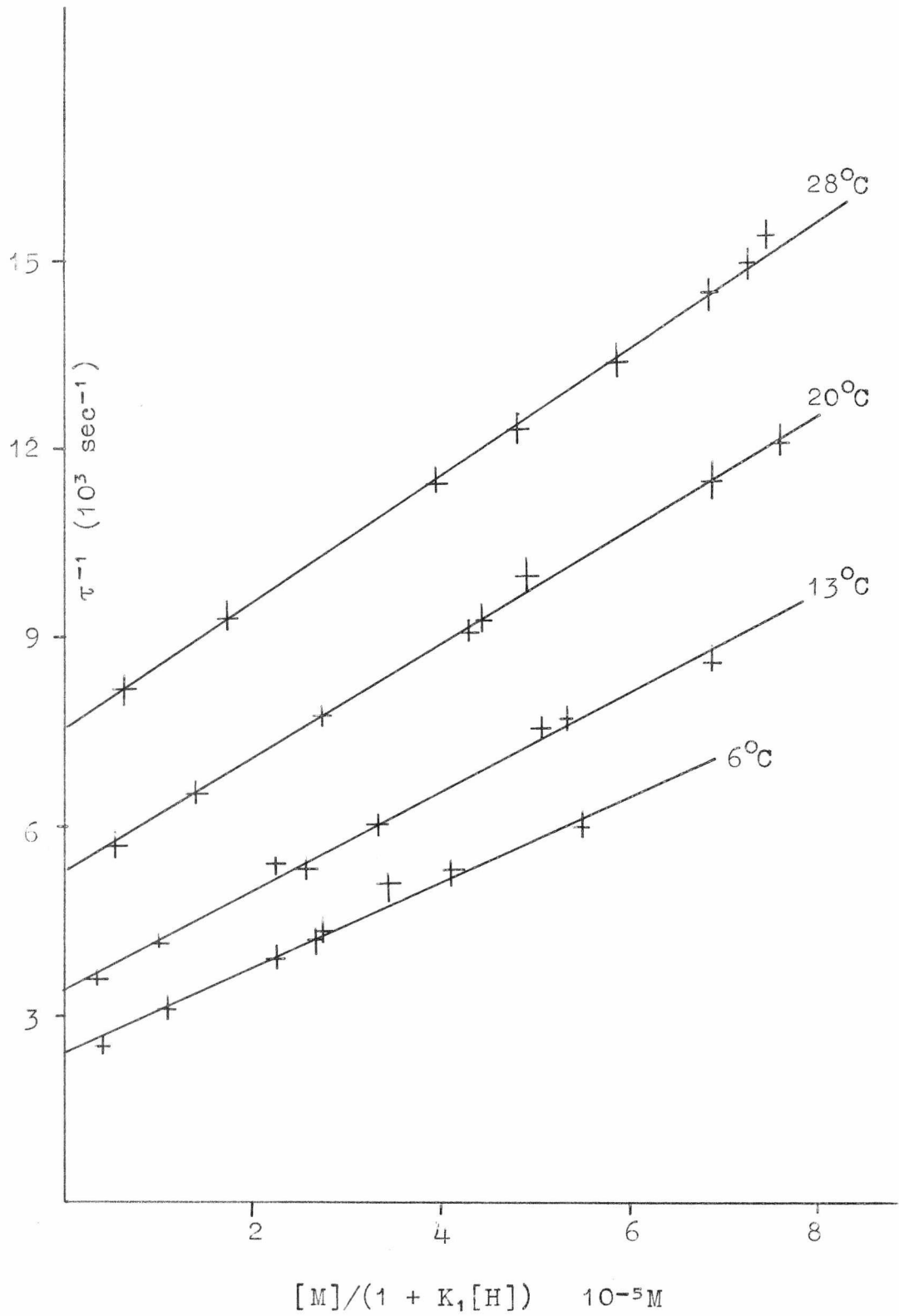


Fig. 6.4.7. Plots of $\log_{10}K$ vs. $1/T$ for $Zndien^{2+}$ chloride + NSA^{2-} .

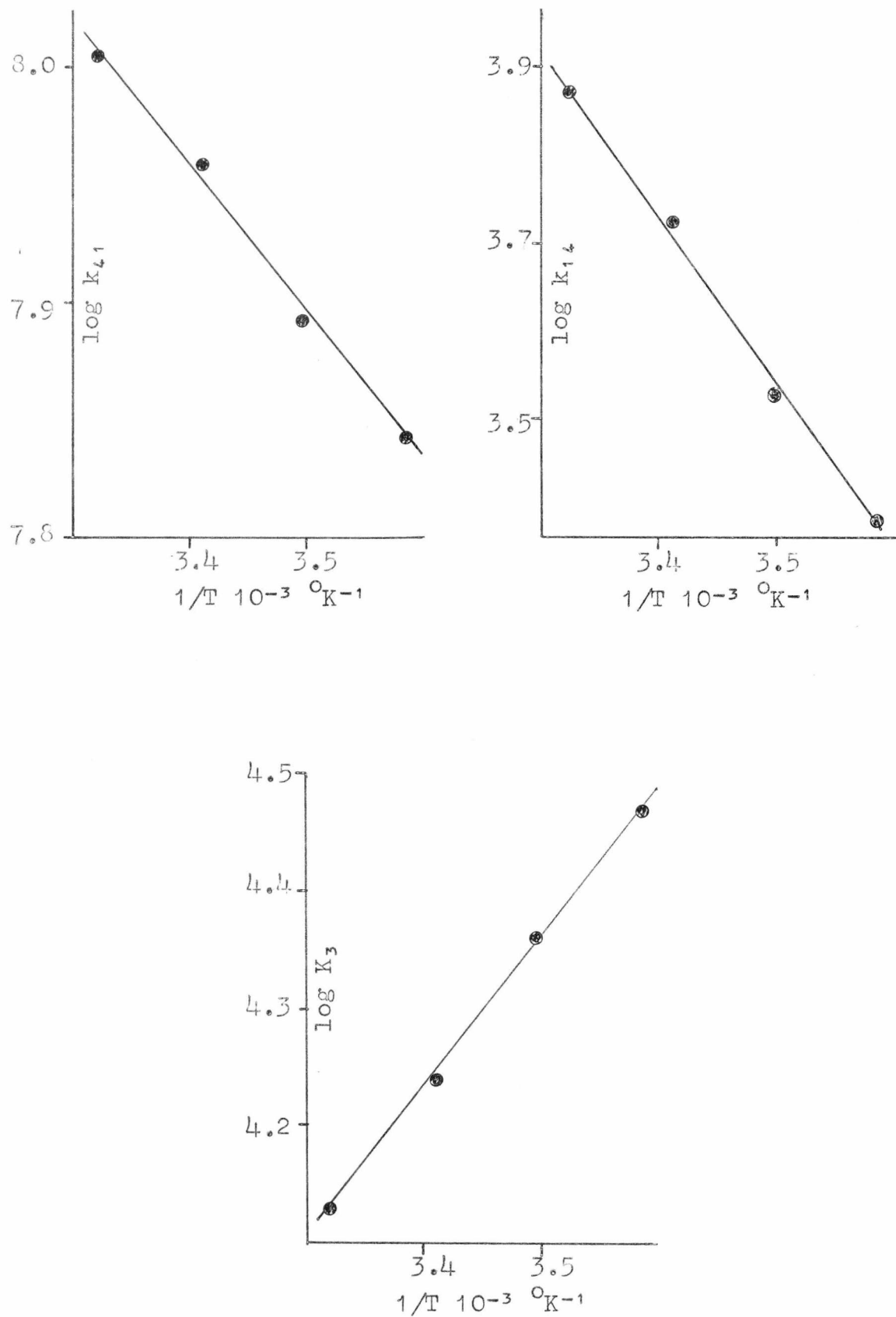


Fig. 6.4.8. Plot of τ^{-1} vs. $[M]/(1 + K_1[H])$ for $Zn tet^{2+}$ perchlorate + NSA^{2-} .

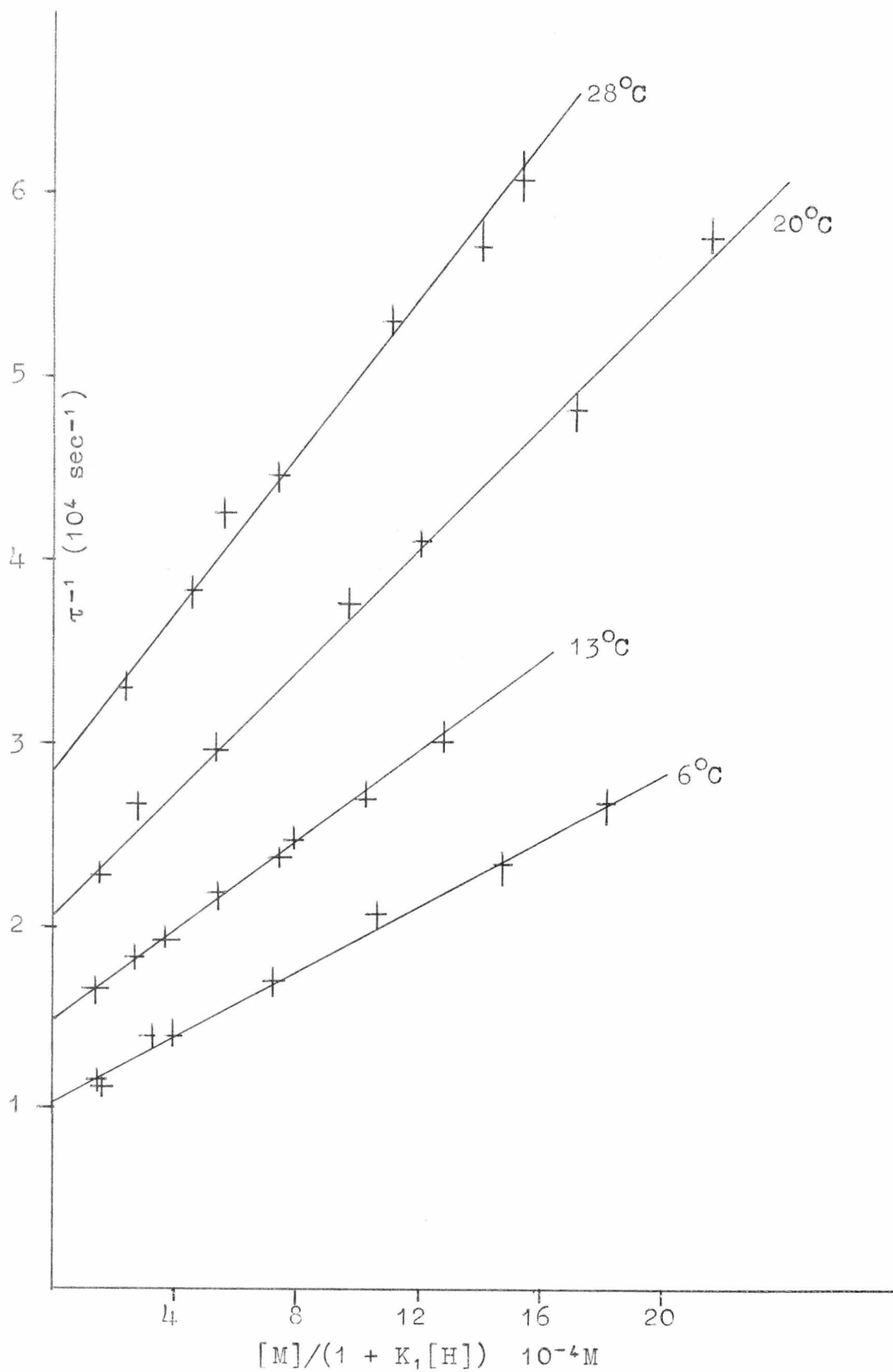


Fig. 6.4.9. Plots of $\log_{10} k_{41}$ for $\text{Zntet}^{2+} + \text{NSA}^{2-}$.

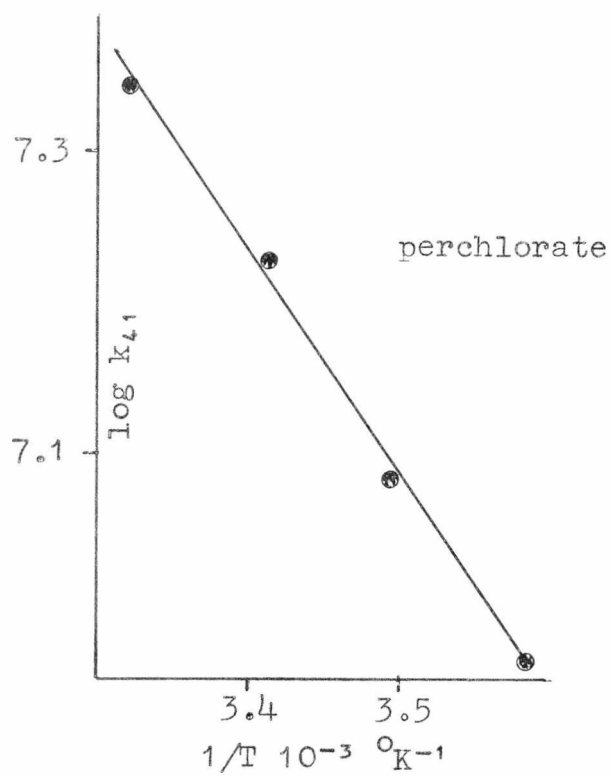
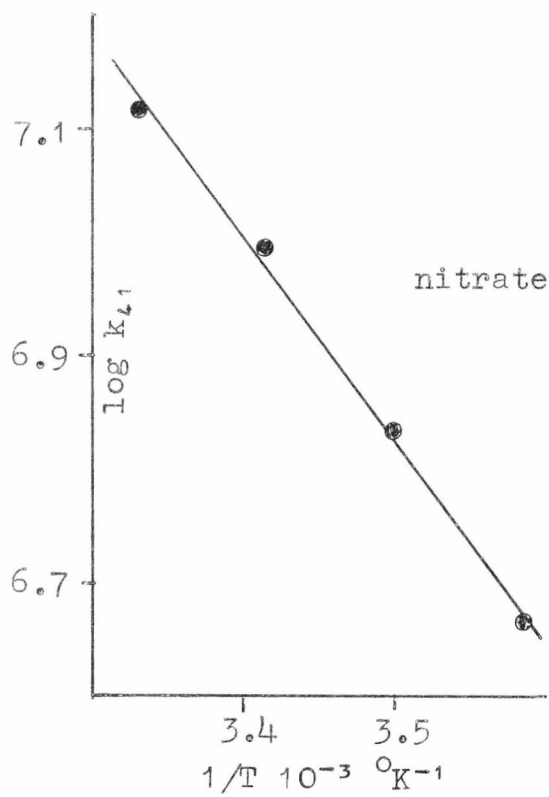


Fig. 6.4.10. Plot of τ^{-1} vs. $[M]/(1 + K_1[H])$ for Zn_{tet}^{2+} nitrate + NSA^{2-} .

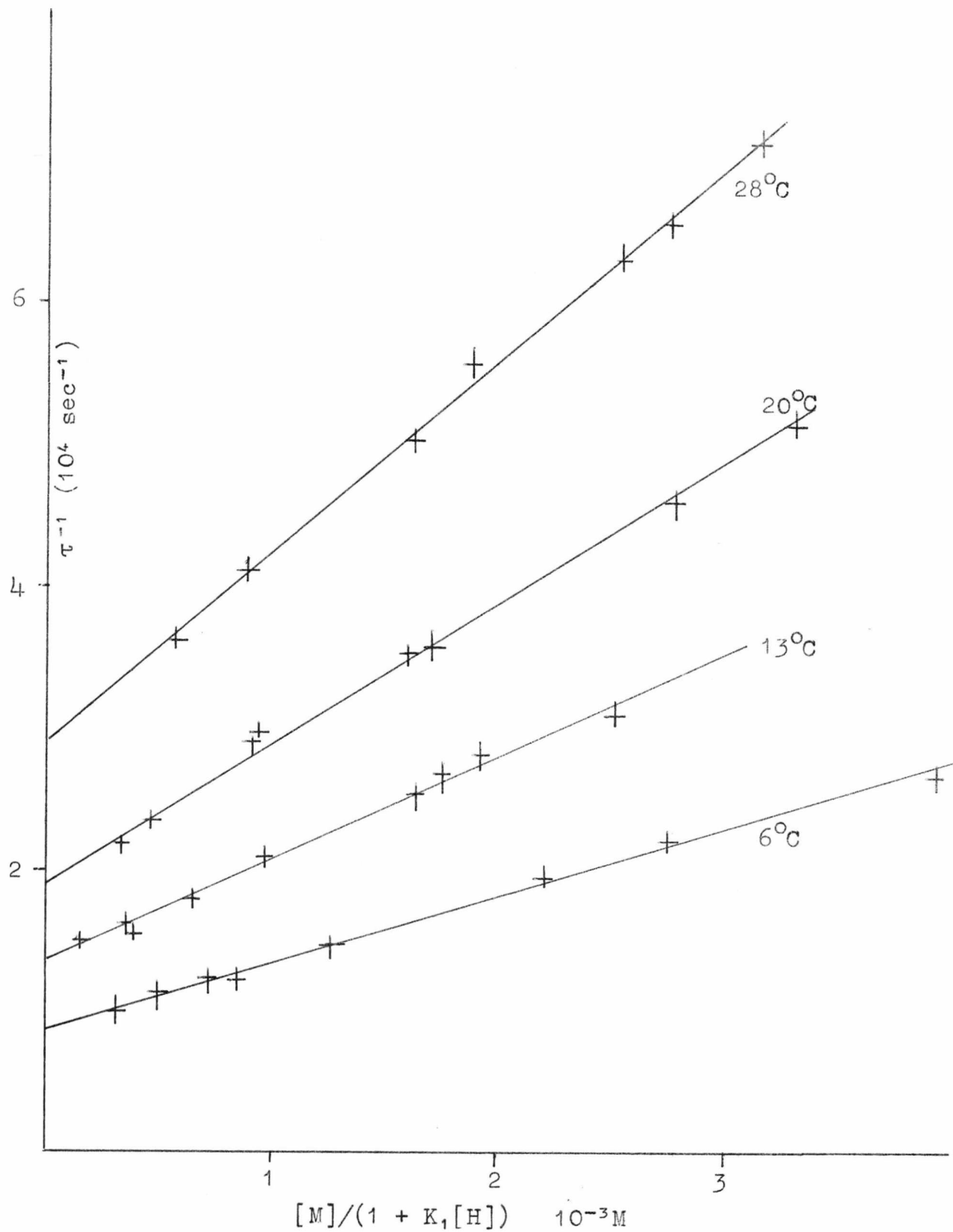


Fig. 6.4.11. Plot of τ^{-1} vs. $[M]/(1 + K_1[H])$ for $\text{ZnIDA}^\circ + \text{NSA}^{2-}$.

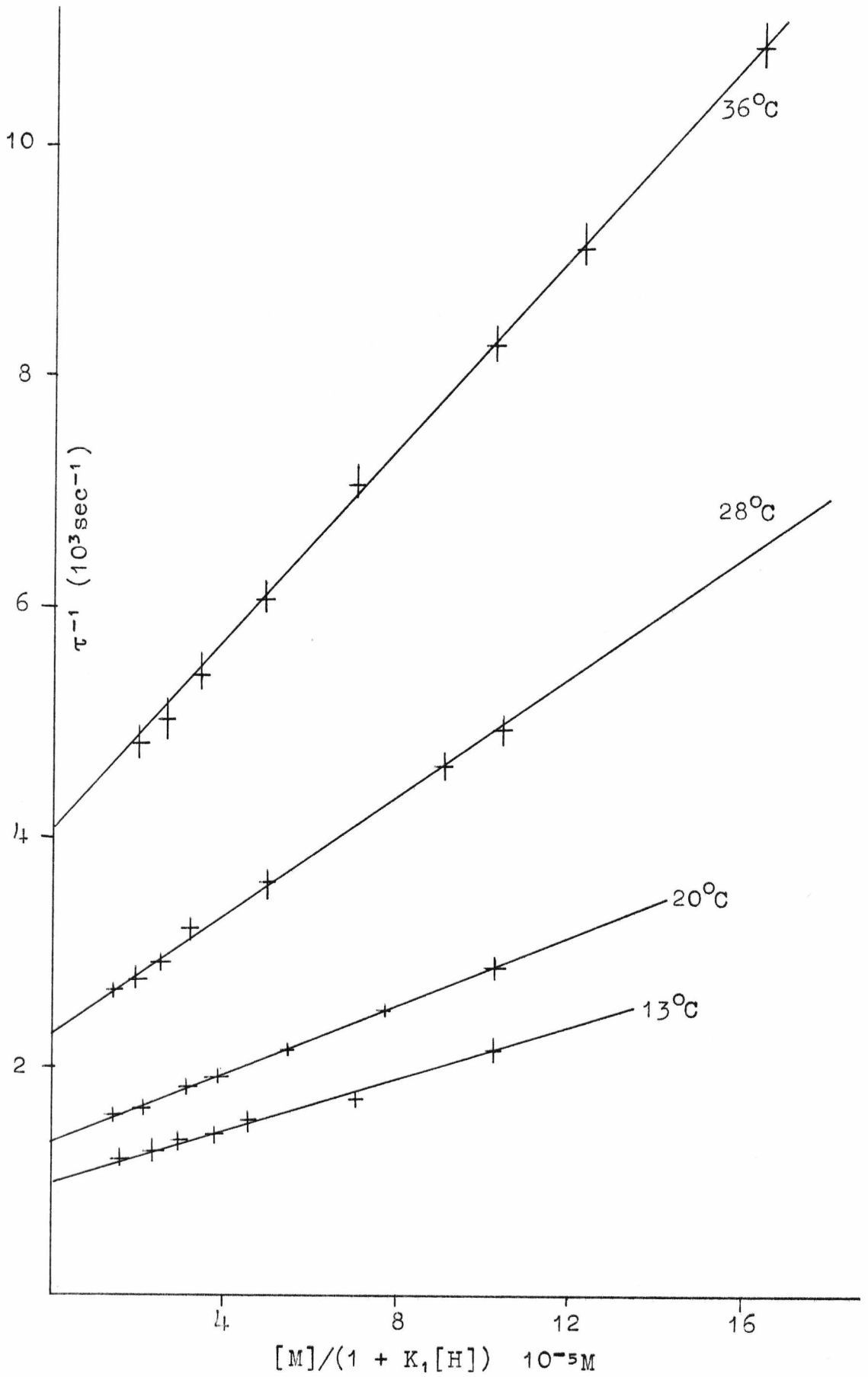


Fig. 6.4.12. Plots of $\log_{10}K$ vs. $1/T$ for $\text{ZnIDA}^{\circ} + \text{NSA}^{2-}$.

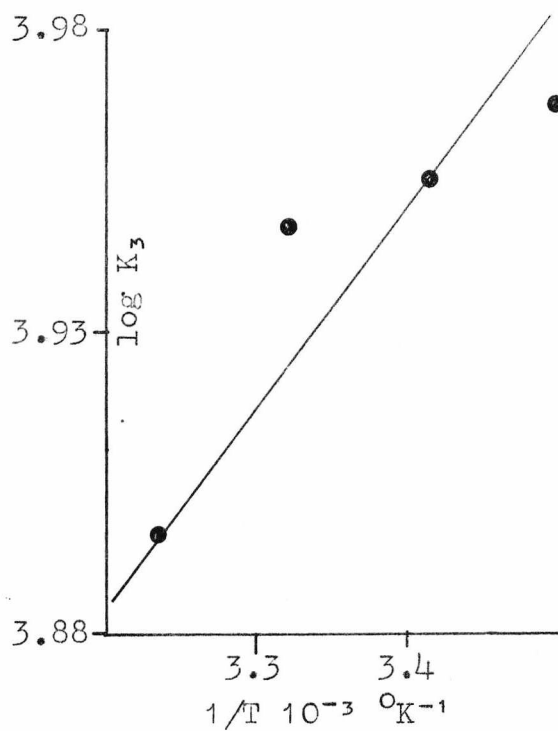
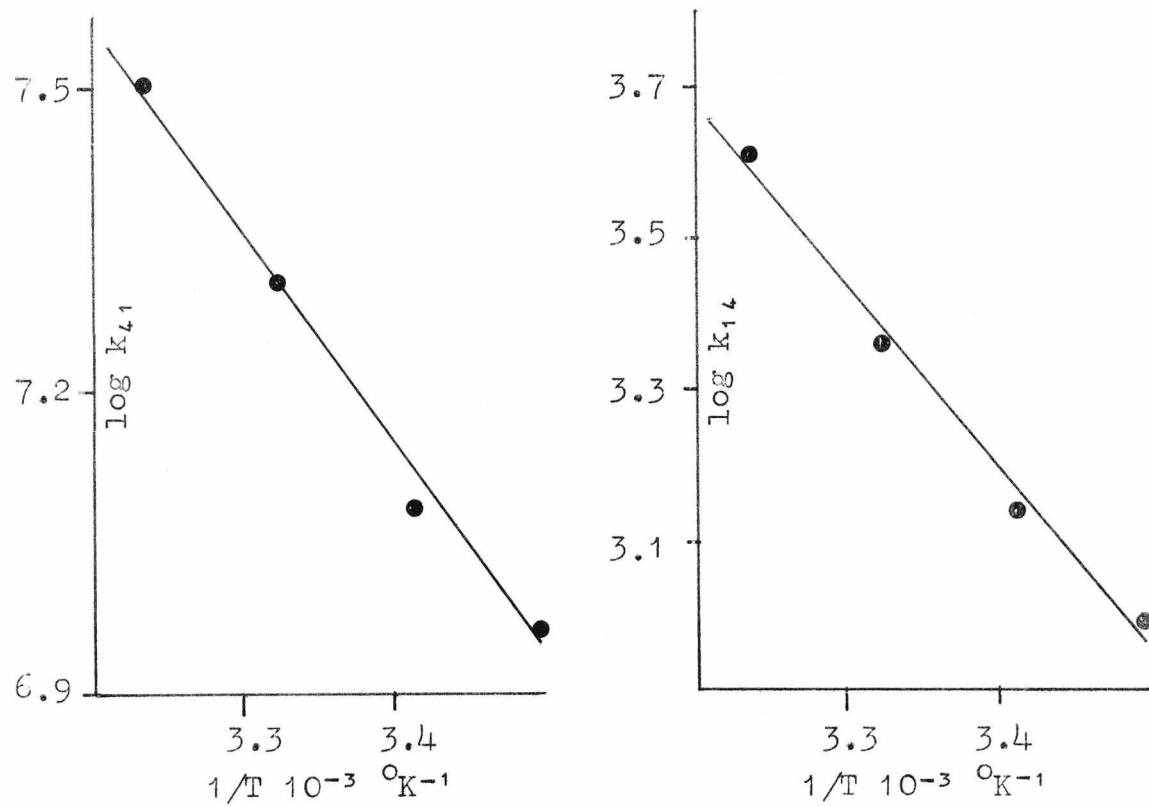


Fig. 6.4.13. Plot of τ^{-1} vs. $[M]/(1 + K_1[H])$ for $ZnEDDA^0 + NSA^{2-}$.

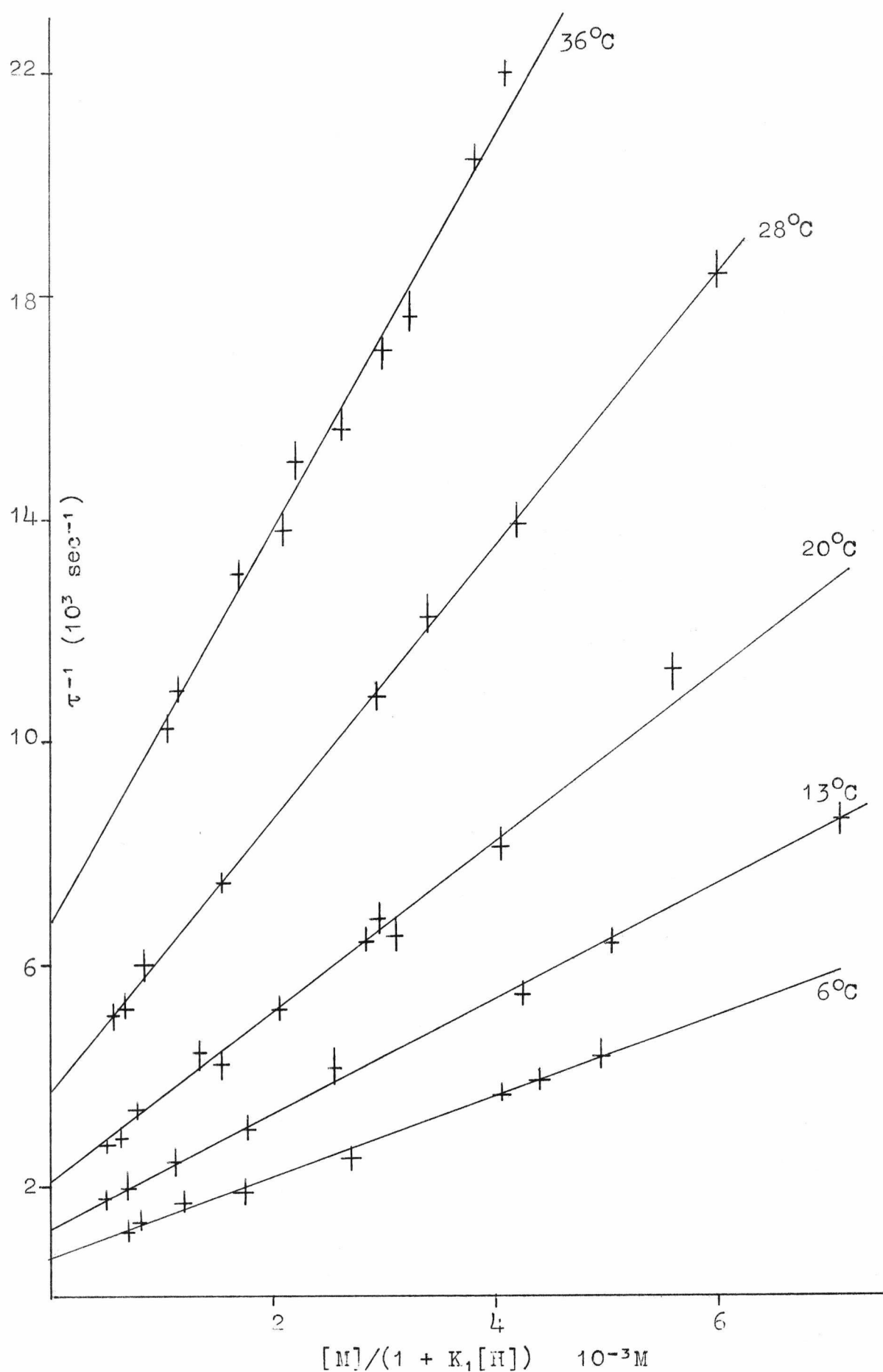


Fig. 6.4.14. Plots of $\log_{10}K$ vs. $1/T$ for $\text{ZnEDDA}^{\circ} + \text{NSA}^{2-}$.

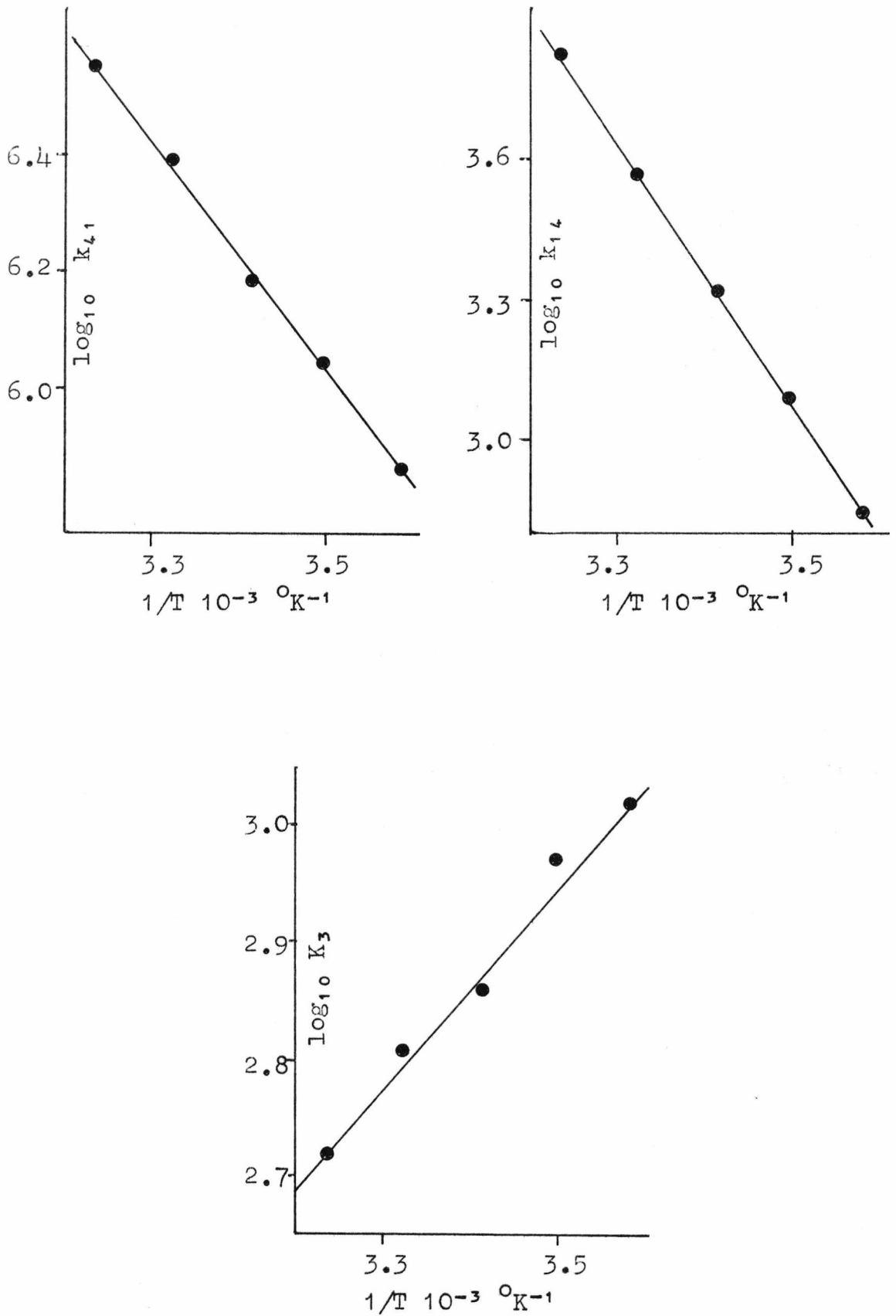


Fig. 6.4.15. Plot of τ^{-1} vs. $[M]/(1 + K_1[H])$ for $ZnNTA^- + NSA^{2-}$.

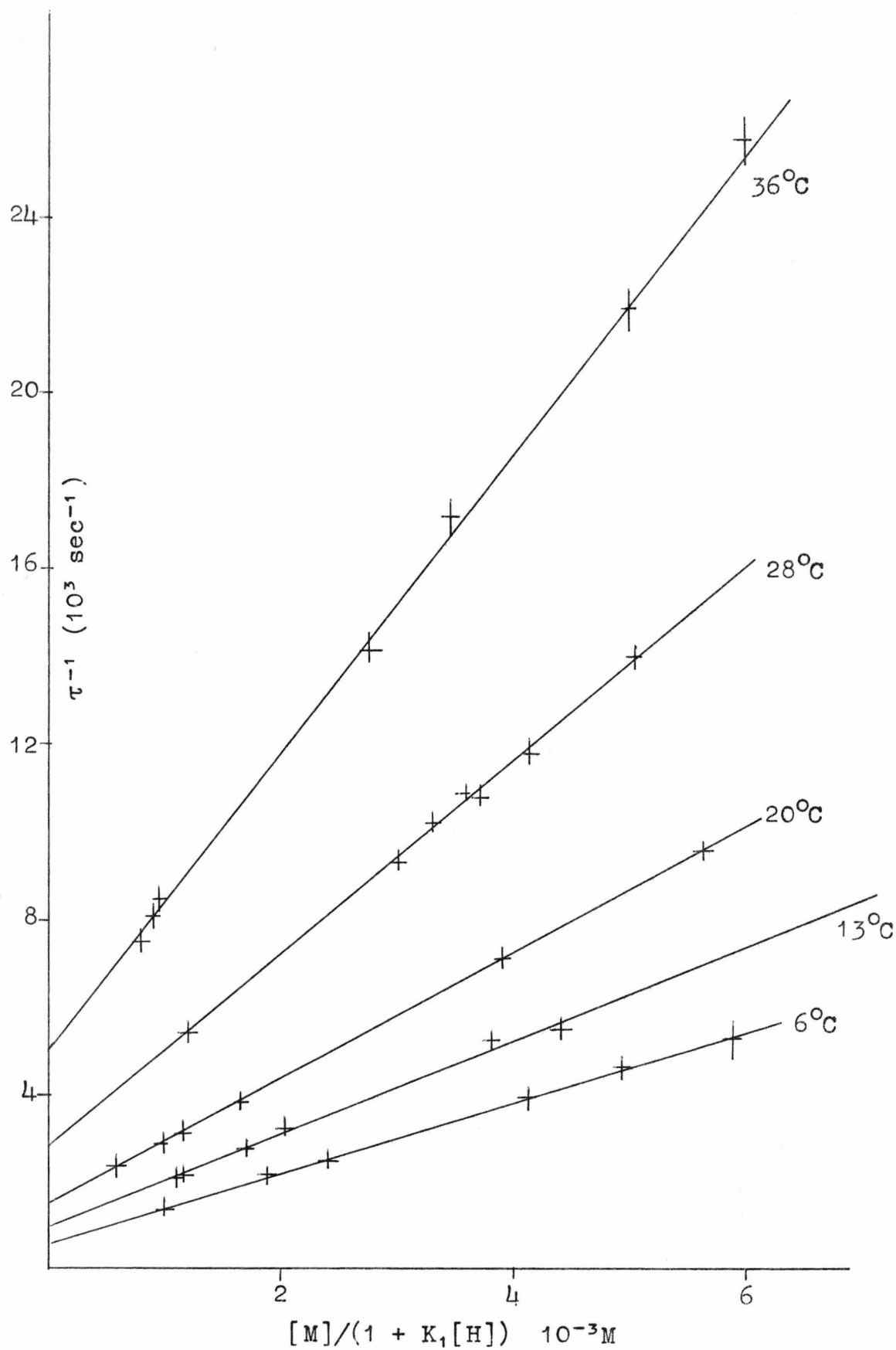


Fig. 6.4.16. Plots of $\log_{10} K$ vs. $1/T$ for $\text{ZnNTA}^- + \text{NSA}^{2-}$.

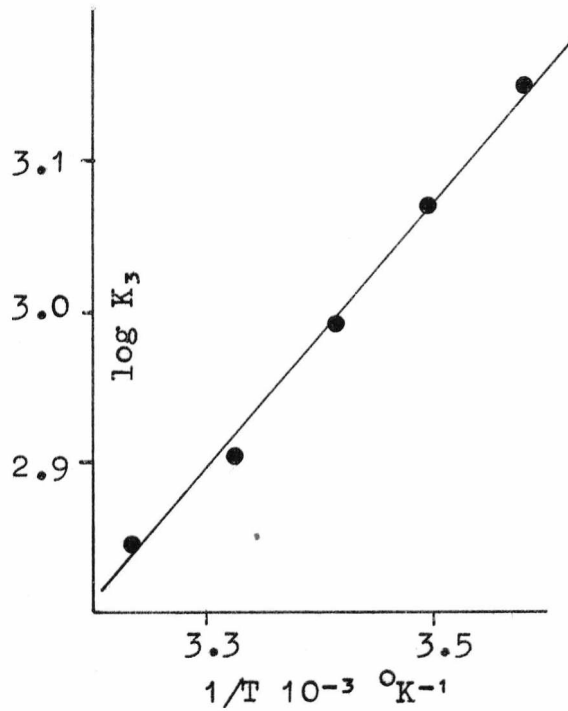
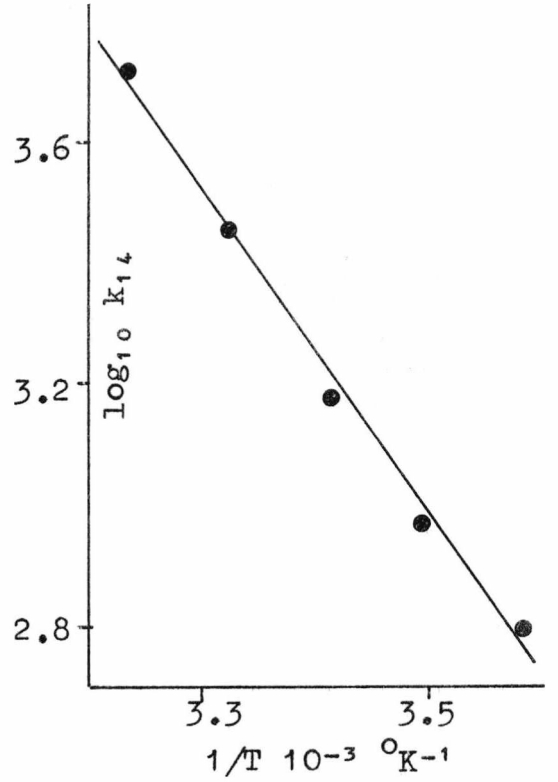
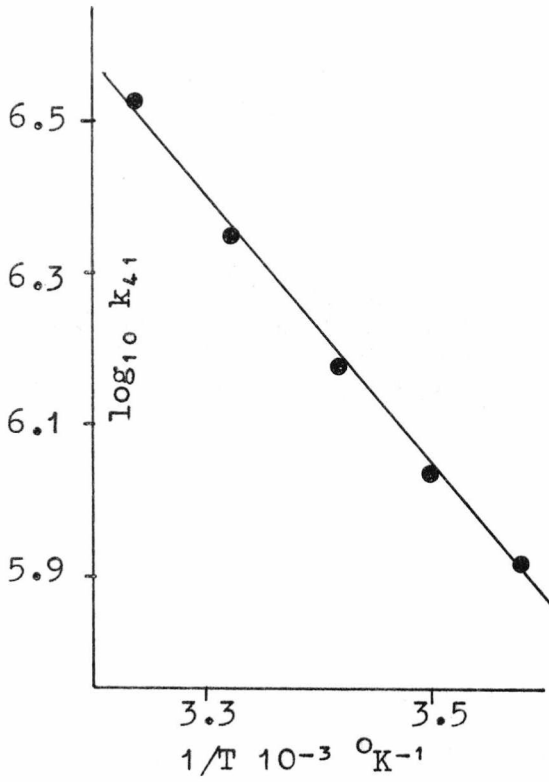


Fig. 6.4.17. Plot of τ^{-1} vs. $[M]/(1 + K_1[H])$ for ZnUDA^- + NSA^{2-} .

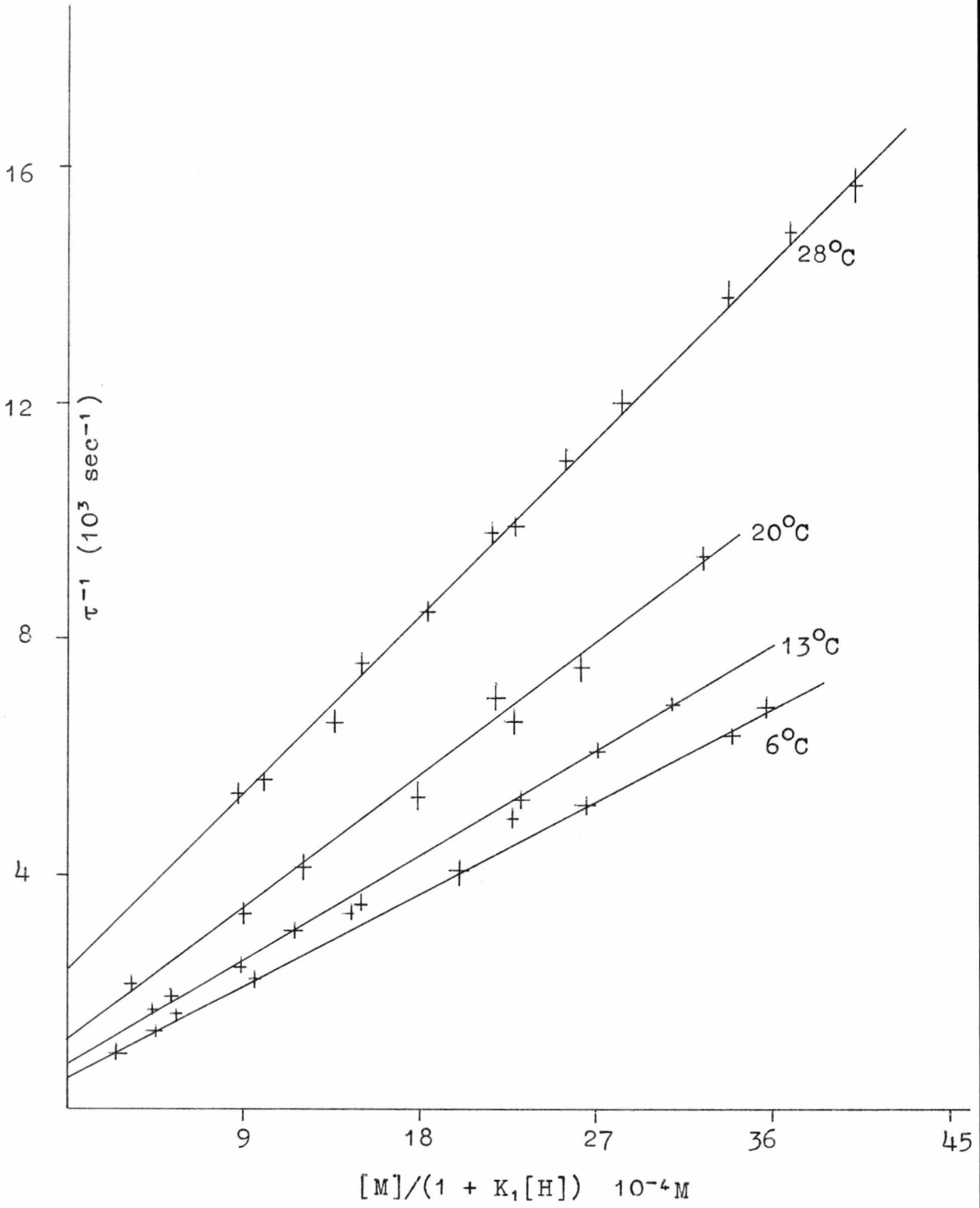


Fig. 6.4.18. Plots of $\log_{10} K$ vs. $1/T$ for $\text{ZnUDA}^- + \text{NSA}^{2-}$.

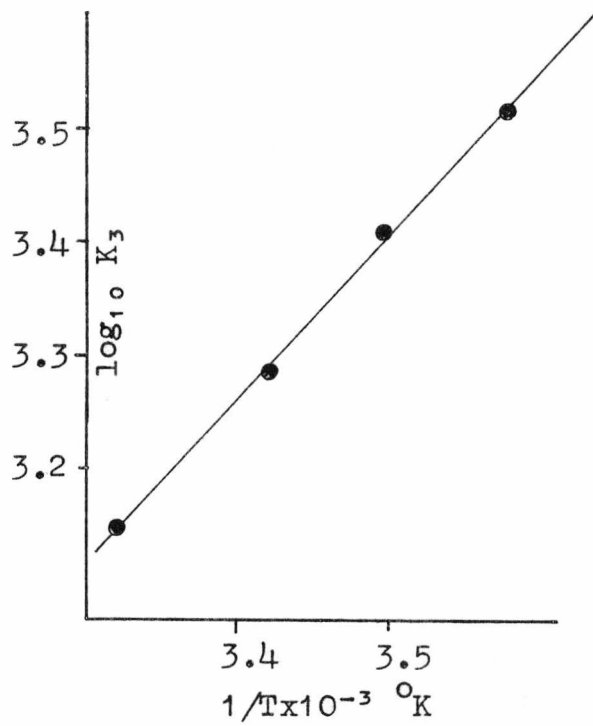
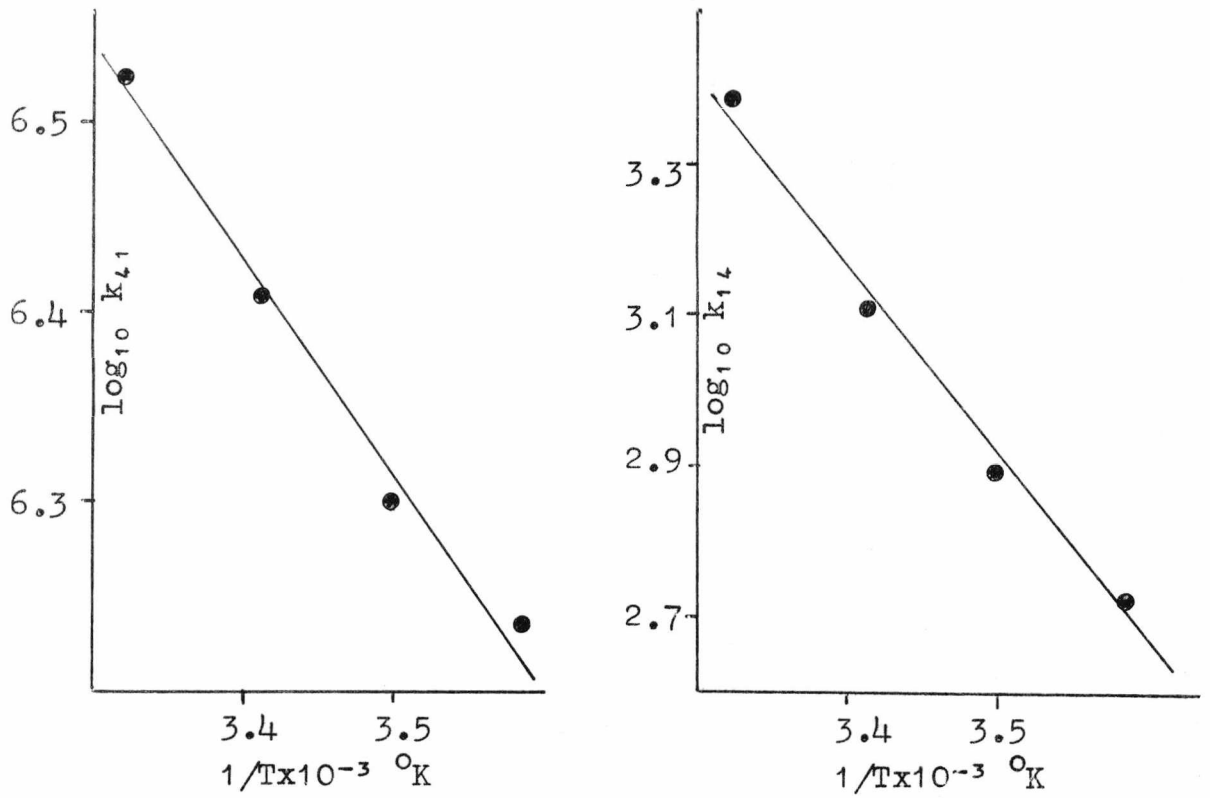


Fig. 6.4.19. Plot of τ^{-1} vs. $[M]/(1+K_1[H])$ for $ZnTP^{3-} + NSA^{2-}$.

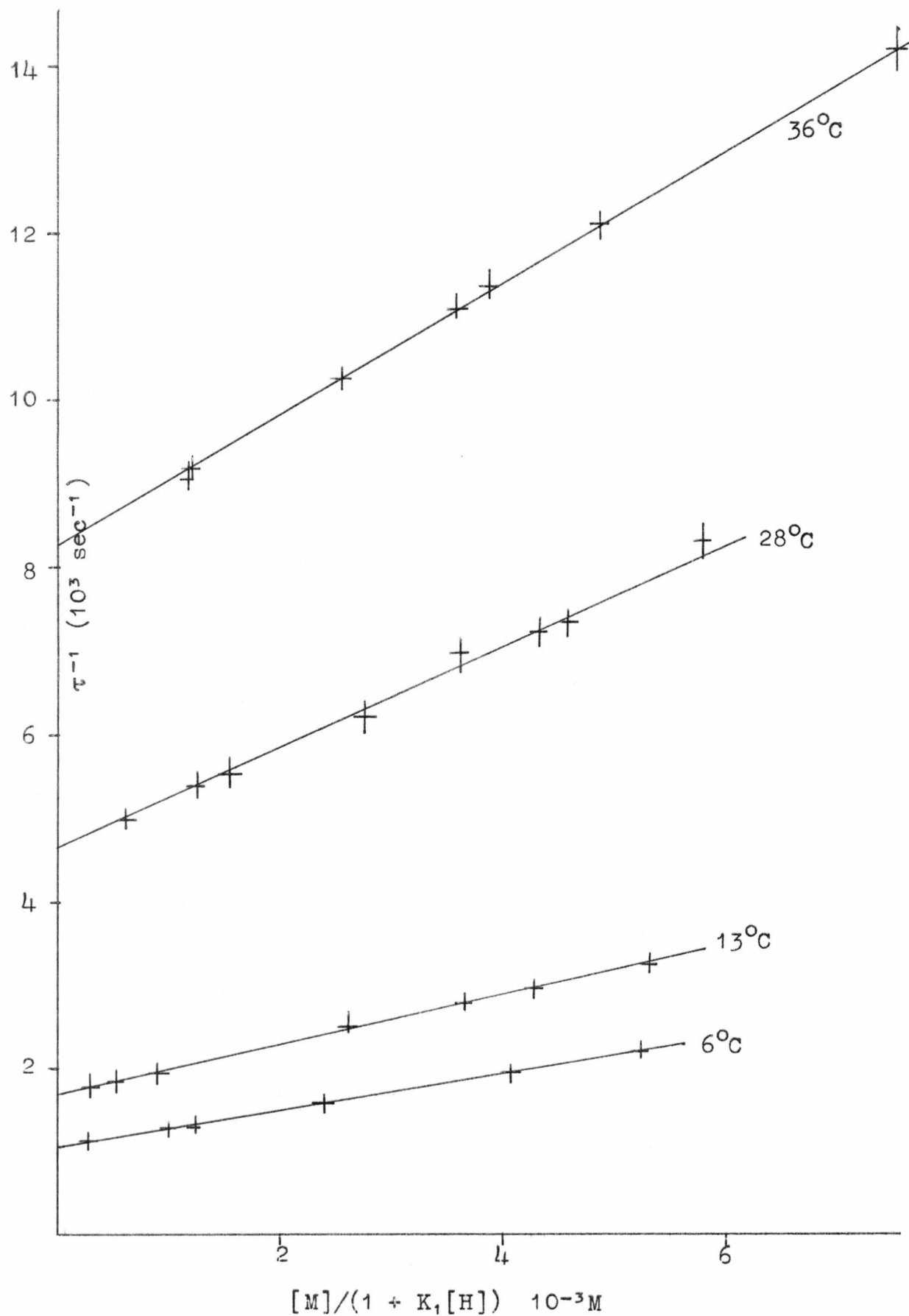


Fig. 6.4.20. Plots of $\log_{10} K$ vs. $1/T$ for $\text{ZnTP}^{3-} + \text{NSA}^{2-}$.

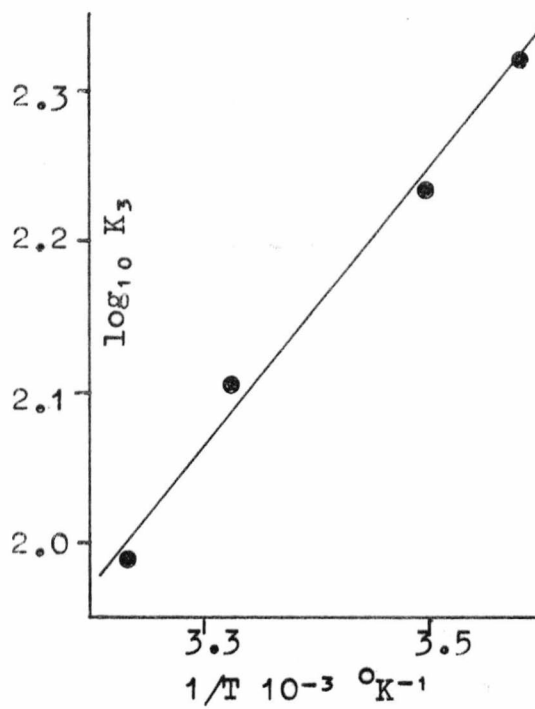
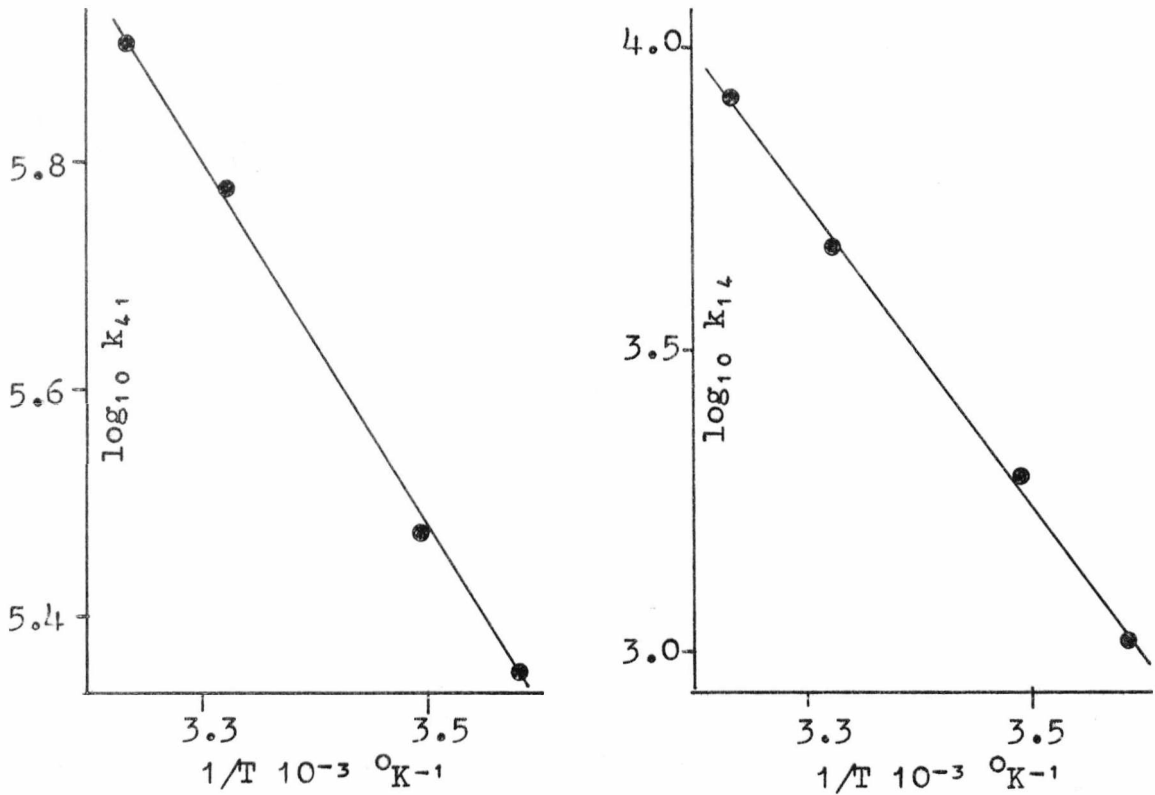


Fig. 6.4.21. Plot of τ^{-1} vs. $[M]$ for $Zn(H_2O)_6^{2+} + NSA^{2-}$.

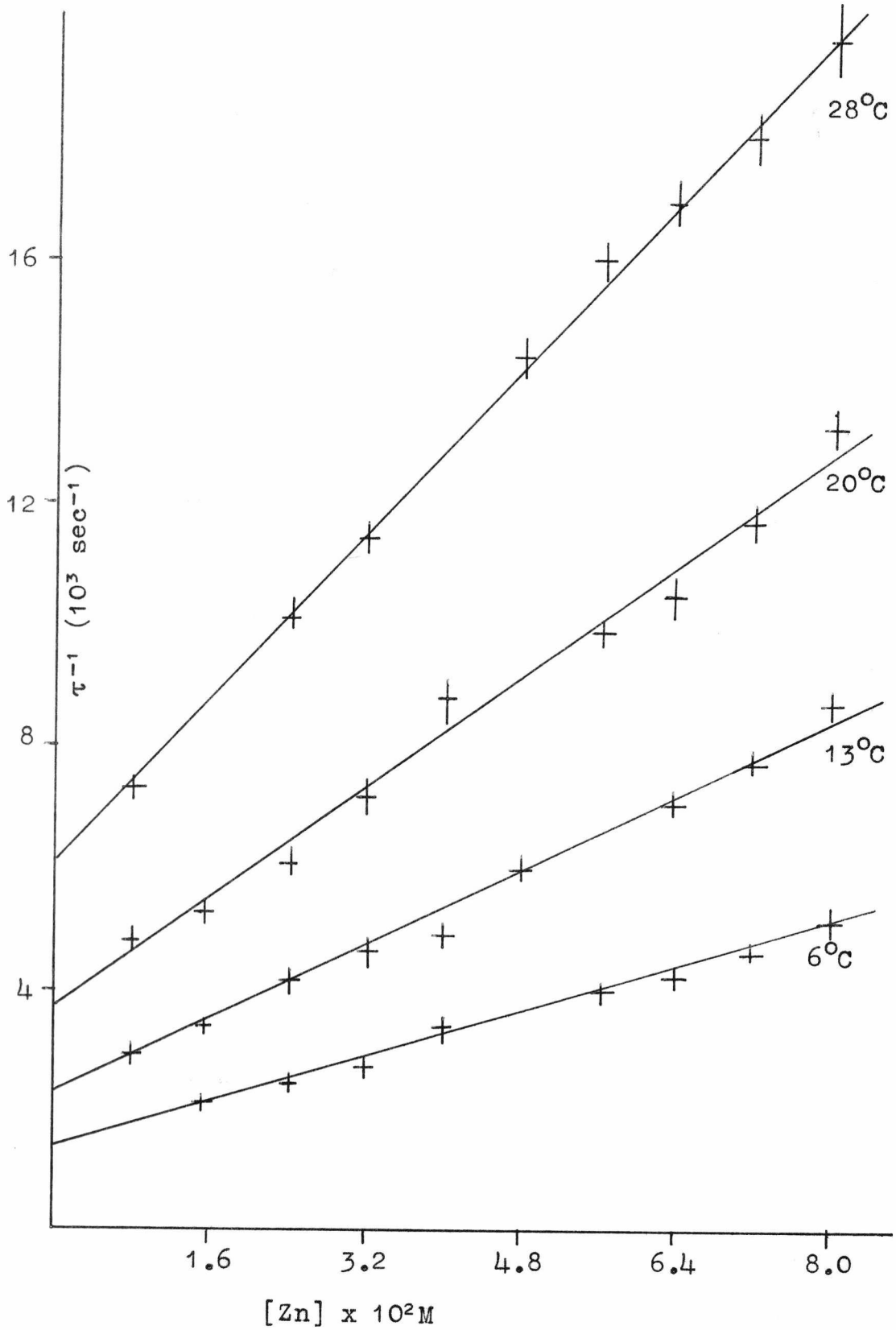


FIG. 6.4.22. $\log_{10} K$ vs. $1/T$ for $\text{Zn}(\text{H}_2\text{O})_6^{2+} + \text{NSA}^{2-}$.

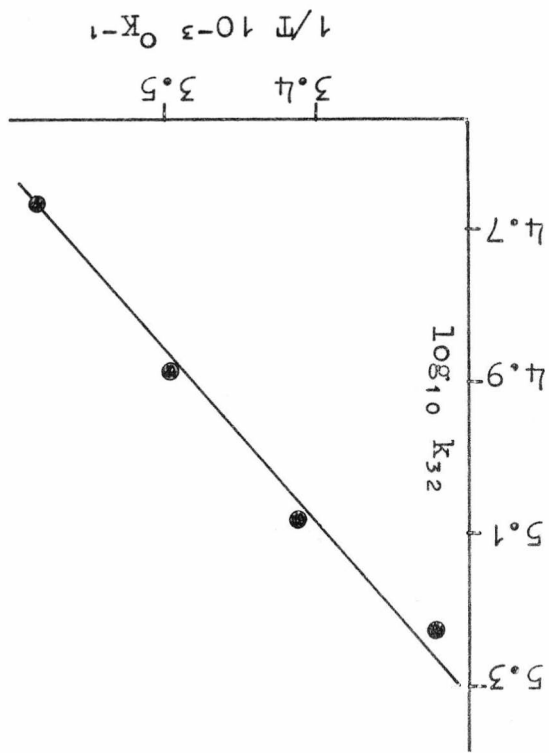
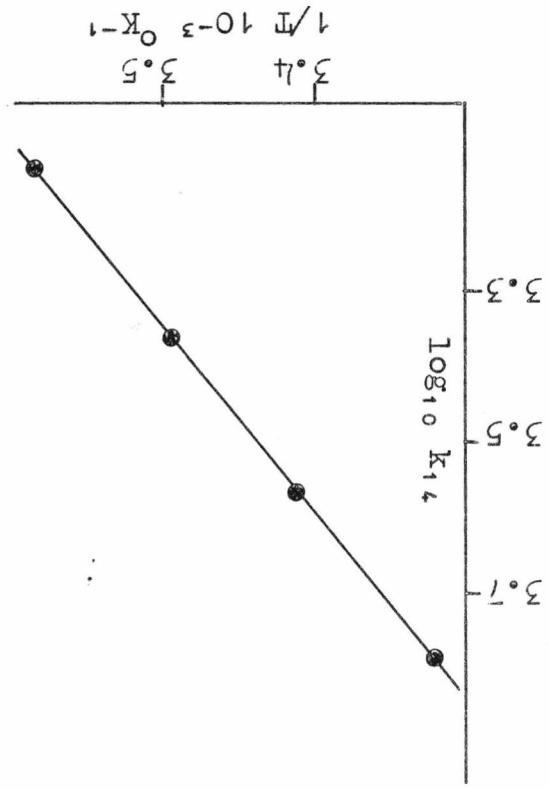


TABLE 6.5.1. Rate constants for Zn(II) + NSA systems.

<u>System</u>	<u>Temp.</u> <u>°C</u>	<u>k₁₁</u> <u>10⁶M⁻¹sec⁻¹</u>	<u>k₁₂</u> <u>10³sec⁻¹</u>	<u>K</u> <u>10³M⁻¹</u>
Zndien ²⁺ perchlorate	6	150(15)	2.3(.2)	66.5
	13	190(20)	3.5(.2)	54.9
	20	240(20)	5.5(.4)	44.4
	28	290(20)	7.5(.7)	28.9
Zndien ²⁺ nitrate	6	92(4)	2.4(.1)	38.3
	13	112(4)	3.6(.15)	31.1
	20	143(6)	5.3(.2)	27.0
	28	187(8)	8.3(.3)	22.5
Zndien ²⁺ chloride	6	70(3)	2.4(.2)	29.1
	13	78(3)	3.4(.1)	22.9
	20	91(3)	5.3(.2)	17.2
	28	101(4)	7.5(.1)	13.5
ZnIDA ⁰ nitrate	13	9.2(0.4)	.98(0.04)	9.39
	20	12.0(0.5)	1.36(0.03)	8.82
	28	19.7(1.1)	2.3(0.15)	8.56
	36	31.7(2.3)	4.1(0.13)	7.73
ZnEDDA ⁰ nitrate	6	.73(0.03)	.7(0.1)	1.04
	13	1.1(0.12)	1.24(0.11)	0.89
	20	1.5(0.08)	2.1(0.2)	0.71
	28	2.4(0.04)	3.2(0.2)	0.65
	36	3.5(0.1)	6.7(0.4)	0.52
ZnNTA ⁻ nitrate	6	.82(0.04)	.58(0.1)	1.41
	13	1.1(0.1)	.93(0.13)	1.18
	20	1.5(0.13)	1.5(0.15)	1.00
	28	2.2(0.18)	2.8(0.2)	0.79
	36	3.4(0.17)	5.2(0.25)	0.65
ZnUDA ⁻ nitrate	6	1.7(0.1)	.53(0.05)	3.21
	13	2.0(0.16)	.78(0.07)	2.56
	20	2.6(0.17)	1.28(0.15)	2.03
	28	3.4(0.1)	2.40(0.2)	1.42

continued

TABLE 6.5.1 (continued)

<u>System</u>	<u>Temp.</u> <u>°C</u>	$\frac{k_{41}}{10^6 \text{M}^{-1} \text{sec}^{-1}}$	$\frac{k_{14}}{10^3 \text{sec}^{-1}}$	$\frac{K}{10^3 \text{M}^{-1}}$
ZnTP ³⁻ nitrate	6	.22(0.01)	1.05(0.03)	0.21
	13	.30(0.02)	1.7(0.03)	0.17
	28	.60(0.5)	4.65(0.1)	0.13
	36	.80(0.2)	8.3(0.15)	0.09
Zntet ²⁺ perchlorate	6	8.9(0.8)		
	13	12.1(1.1)		
	20	18.0(1.4)		
	28	22.5(1.5)		
Zntet ²⁺ nitrate	6	4.75(0.3)		
	13	7.20(0.7)		
	20	9.6(0.9)		
	28	13.0(1.3)		
<u>System</u>	<u>Temp.</u> <u>°C</u>	$\frac{k_{32}}{10^4 \text{M}^{-1} \text{sec}^{-1}}$	$\frac{k_{14}}{\text{sec}^{-1}}$	
Zn(OH ₂) ₆ ²⁺ nitrate	6	4.6(0.3)	1.37(0.13)	
	13	7.6(0.6)	2.3(0.15)	
	20	11.4(1.1)	3.7(0.4)	
	28	18.0(0.8)	6.1(0.6)	

TABLE 6.5.2. Activation parameters and final rate constants
at 298°K

	<u>ZnEDDA</u> ⁰	<u>ZnNTA</u> ⁻	<u>ZnUDA</u> ⁻	<u>ZnTP</u> ³⁻
k_{k1} M ⁻¹ sec ⁻¹	2.1x10 ⁶	2.0x10 ⁶	3.0x10 ⁶	5.2x10 ⁵
k_{1k} sec ⁻¹	3.07x10 ³	2.3x10 ³	2.3x10 ³	4.0x10 ³
ΔH_{k1}^{\ddagger} kcal.M ⁻¹	8.3(.5)	7.4(.5)	4.3(±.7)	6.7(.5)
ΔH_{1k}^{\ddagger} kcal.M ⁻¹	12.2(±1.3)	11.7(.7)	10.9(±1.2)	11.3(.5)
ΔS_{k1}^{\ddagger} e.u.	-2(2)	-5(1)	-14(3)	-10(2)
ΔS_{1k}^{\ddagger} e.u.	-2(4)	-4(2)	-7(6)	-4(2)
K_{3kin} M ⁻¹	7x10 ²	8.7x10 ²	1.3x10 ³	1.3x10 ²
K_{3spec} M ⁻¹	1.3x10 ³	1.1x10 ³	1.66x10 ³	6.6x10 ²
	<u>Zndien</u> ²⁺ perchlorate	<u>Zndien</u> ²⁺ nitrate	<u>Zndien</u> ²⁺ chloride	<u>ZnIDA</u> ⁰
k_{k1} M ⁻¹ sec ⁻¹	2.82x10 ⁸	1.7x10 ⁸	9.72x10 ⁷	1.8x10 ⁷
k_{1k} sec ⁻¹	6.8x10 ³	7.0x10 ³	6.5x10 ³	2.1x10 ³
ΔH_{k1}^{\ddagger} kcal.M ⁻¹	4.9(.5)	4.7(.5)	2.2(.4)	8.6(1.1)
ΔH_{1k}^{\ddagger} kcal.M ⁻¹	9.2(1.8)	8.3(1.6)	7.0(1.2)	10.7(.4)
ΔS_{k1}^{\ddagger} e.u.	-4(2)	-5(2)	-15(3)	+3.6(4)
ΔS_{1k}^{\ddagger} e.u.	-10(4)	-12(2)	-14(2)	-7(2)
K_{3kin} M ⁻¹	4.1x10 ⁴	2.4x10 ⁴	1.5x10 ⁴	8.6x10 ³
K_{3spec} M ⁻¹	8.1x10 ⁴	3.3x10 ⁴	7x10 ⁴	

Table 6.5.2. (continued)

	<u>Zntet²⁺</u> perchlorate	<u>[ZtetOH]⁺</u> perchlorate	<u>[ZtetOH]⁺</u> nitrate	<u>Zntrien²⁺</u> NO ₃	<u>Zn(OH₂)₆²⁺</u>
k _{4,1} M ⁻¹ sec ⁻¹	(a) <2.8x10 ⁶	2.0x10 ⁷	1.2x10 ⁷	(a) 2x10 ⁶	(a) 2.1x10 ⁸
k _{1,4} sec ⁻¹	4x10 ³			3x10 ³	4.8x10 ³
ΔH _{4,1} [‡] kcal.M ⁻¹		2.9(0.4)	3.0(0.6)		
ΔH _{1,4} [‡] kcal.M ⁻¹					10.1(0.9)
ΔH _{3,2} [‡] kcal.M ⁻¹					8.1(0.6)
ΔS _{4,1} [‡] e.u.		-15(2)	-16(2)		
ΔS _{1,4} [‡] e.u.					-8(3)
ΔS _{3,2} [‡] e.u.					-8(2)
K _{3,spec} M ⁻¹	<6.9x10 ²			6.8x10 ²	1.5x10 ⁵

(a) Estimated from K_{3,spec} and k_{1,4}.

For the zinc dien²⁺ and zinc tet²⁺ systems the plots of τ⁻¹ vs. M/1 + K₁[H] or τ⁻¹ vs. 1/1 + K₁[H] at constant metal concentration do not give straight lines over the whole pH range used (figs. 6.5.1 - 6.5.4). The zinc dien system was studied by working below pH 8 and changing the [Zdien]²⁺. An attempt was made to study the zinc tet²⁺ system in the same way but, at the low pH necessary, a change in Ztet²⁺ concentration did not change the relaxation time, indicating that the value of k_{4,1} must be considerably lower than that for Zdien²⁺. For the tet systems it was found that the plot of τ⁻¹ against [M]/1 + K₁[H] was linear above pH 9.3 and the reaction was investigated above this pH using the relaxation expression derived in Appendix 8 .

Unfortunately it is not possible to measure $k_{4,1}$ for the reaction of $\text{Zn}(\text{OH}_2)_6^{2+}$ with NSA^{2-} . It has been shown already (section 6.4) that the reaction of $\text{Zn}(\text{OH}_2)_6^{2+}$ with HNSA^- can be investigated but attempts to raise the pH of the solutions used for these measurements leads to the precipitation of zinc hydroxide (solubility product $10^{-15.5}$ ⁽¹³⁰⁾). To prevent this precipitation the metal concentration has to be reduced to such an extent that the experimental conditions can no longer be assumed to be pseudo-first order. Then, in order to get a change in the relaxation time with pH, it becomes necessary to work through the pK of $\text{Zn}(\text{OH}_2)_6^{2+}$ ($\text{pK}_a = 8.7$ ⁽¹⁵⁾) so that at least two reactive species are present. This system was not investigated further. A relaxation expression is derived in Appendix 8. An approximate value of $k_{4,1}$ can be obtained from the spectrophotometrically determined stability constant, K_3 , and the value of $k_{1,4}$.

An attempt was made to study the $\text{Zntr}^{\text{en}2+}$ system but even at high concentrations of $\text{Zntr}^{\text{en}2+}$ (10^{-2}M) and NSA ($1 \times 10^{-4}\text{M}$) no relaxation effect was observed and no spectral evidence was obtained for complex formation. For the Zntrien^{2+} system a relaxation effect was observed below pH 8 at a Zntrien^{2+} concentration of $1.6 \times 10^{-3}\text{M}$. Attempts to obtain a value for $k_{4,1}$ were not successful because at higher pH a second relaxation effect was observed, probably due to the formation of a hydroxy species, while a change in metal concentration at pH 8 gives an unknown contribution to the relaxation time from $k_{3,2}[\text{M}]$ as well as from $k_{4,1}[\text{M}]/1 + K_1[\text{H}]$. An approximate value of $k_{4,1}$ has been obtained using a value for $k_{1,4}$ and the spectrophotometric stability constant determined at low pH.

Fig. 6.5.1.

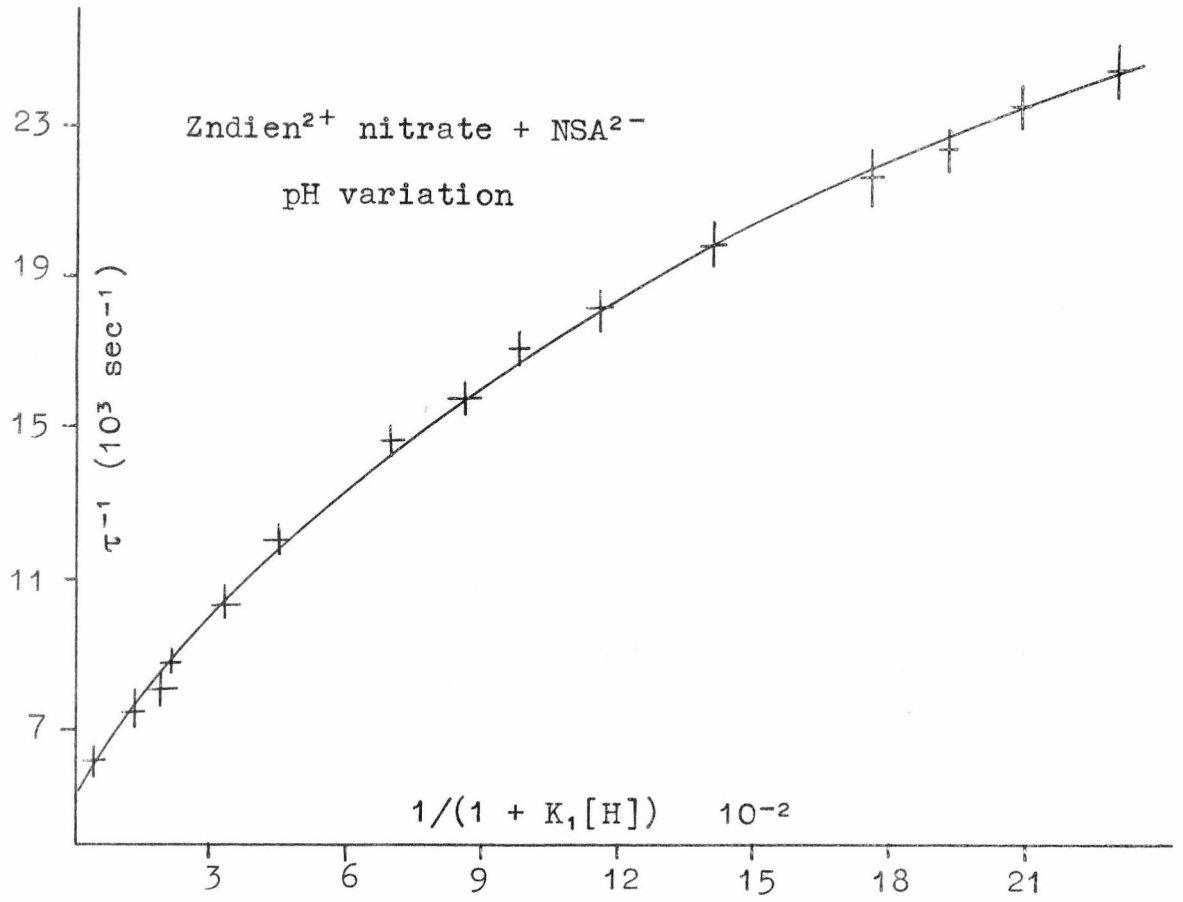


Fig. 6.5.2.

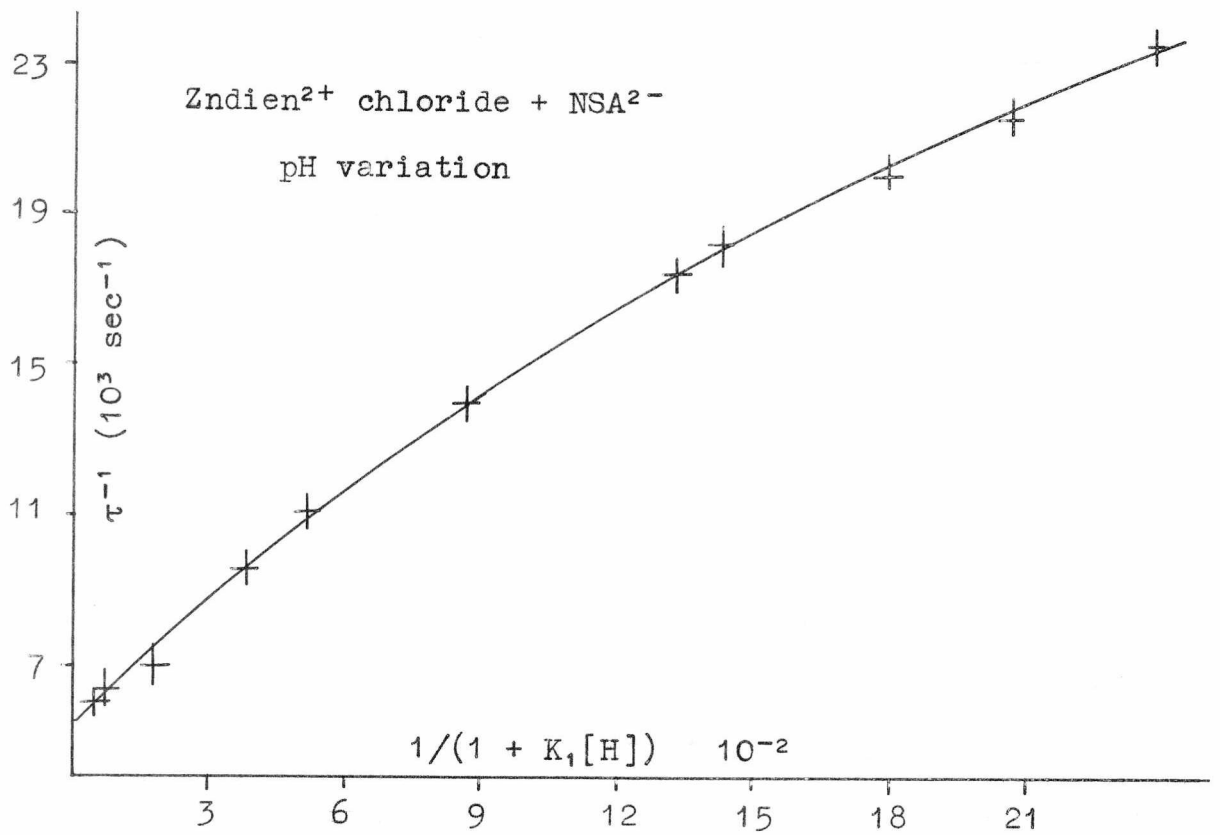


Fig. 6.5.3.

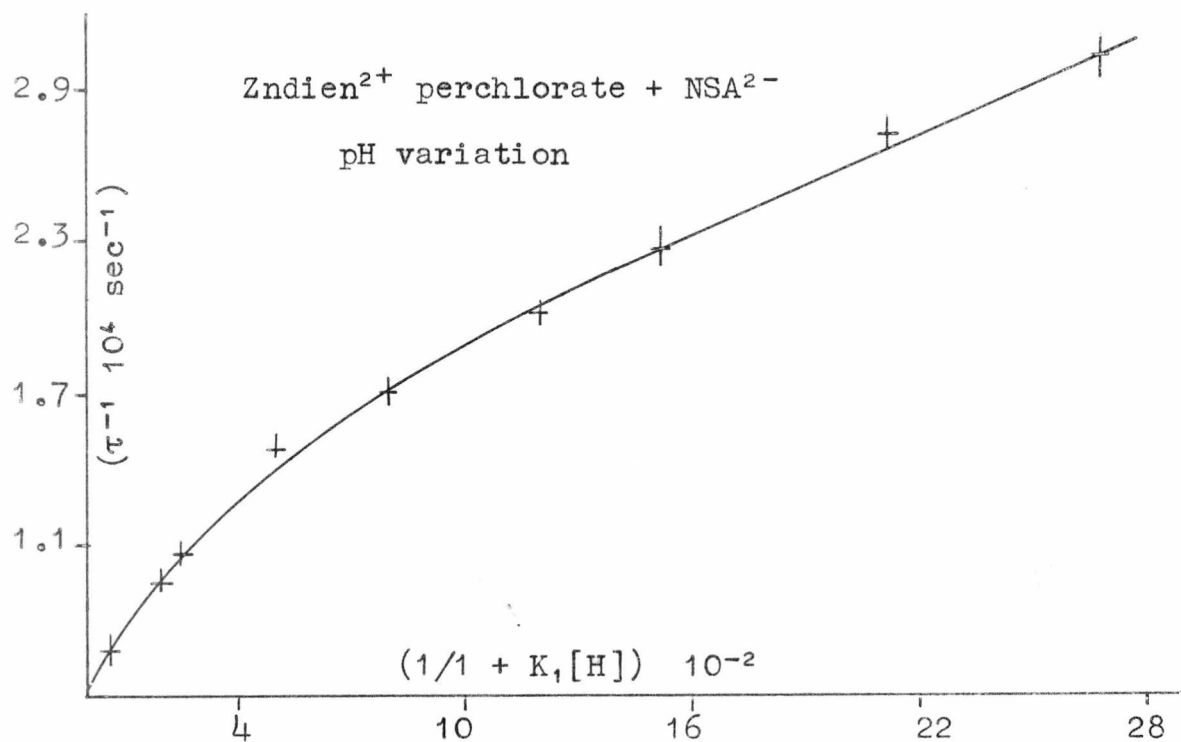
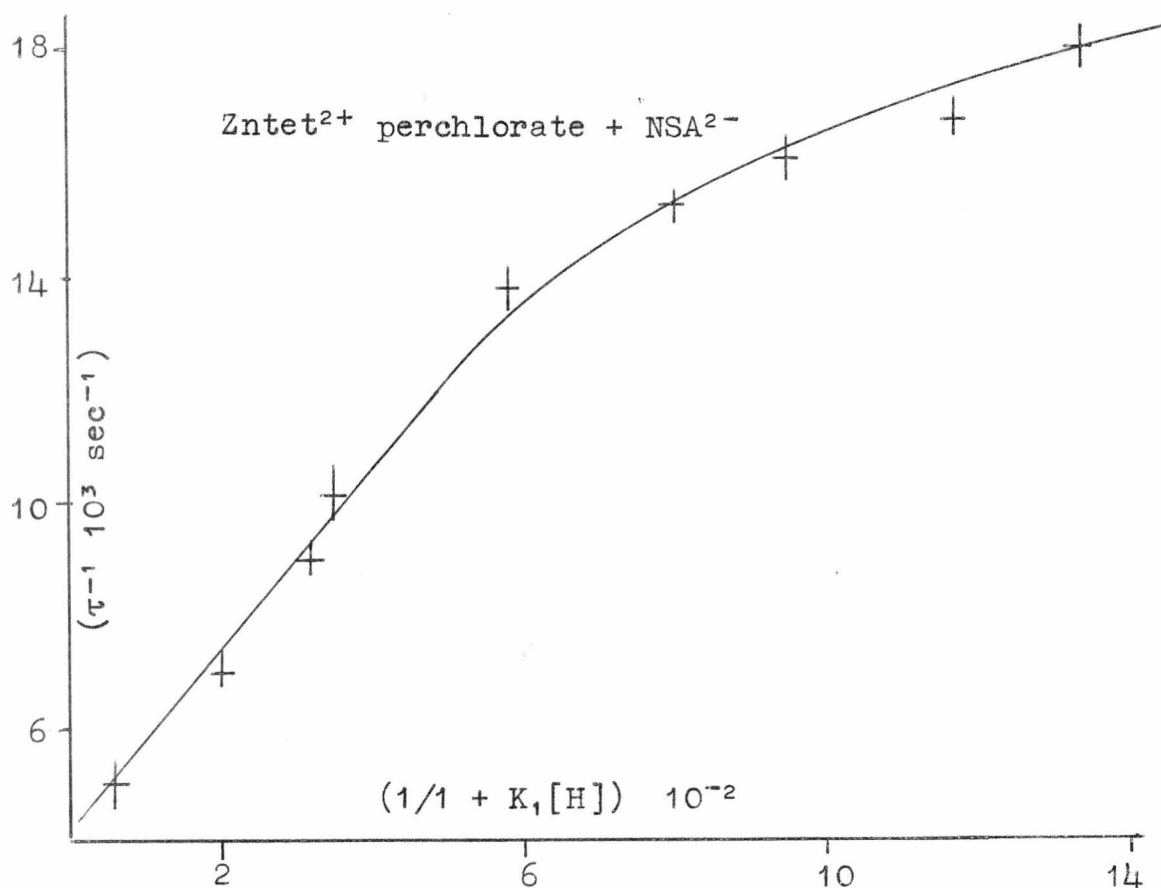


Fig. 6.5.4.



6.6 Discussion

None of the rate constants discussed in this section have been corrected statistically for the number of water molecules available for substitution because it is not known how to treat species of differing coordination number. The value of $k_{4,1}$ for the reaction of aquo zinc with NSA^{2-} gives a value for K_{OS} within the range predicted from the Fuoss equation, but the value of $k_{3,2}$ gives a value for K_{OS} which is rather small, although similar to the values obtained for the reaction of the oxine molecule with aquo manganese(II)⁽¹¹¹⁾.

Examination of the formation rate constants (table 6.5.2) for the reaction of ZnL with NSA^{2-} shows that the presence of the bound ligand L has a considerable effect on the reaction with NSA^{2-} . It appears that the forward rate constant is dependent on the negative charge on the bound ligand, L , and for ligands of the same charge type the forward rate constant is dependent on the nature of the donor atoms and the geometry that the bound ligand forces on the metal ion.

The decrease in $k_{4,1}$ as the negative charge on the bound ligand increases can perhaps be explained in terms of an electrostatic repulsion between the bound and incoming ligands. Thus there is a 500-fold decrease in $k_{4,1}$ as the initial complex is changed from $\text{Zn}(\text{H}_2\text{O})_6^{2+}$ to ZnTP^{3-} .

As for the reactions with $\text{PADA}^{(95)}$, the activation enthalpies are approximately constant for ZnIDA° , ZnEDDA° and ZnTP^{3-} , the actual value of the activation enthalpy depending on the charge type of the incoming ligand. Thus, the variation in the forward rate constants from complex to complex is determined largely by the entropy of activation. At a first glance the difference in the formation rates for ZnIDA° and ZnEDDA° seem to contradict this, since both complexes have

the same formal charge. However, for the ZnIDA^{\ominus} complex it is possible for the incoming ligand to approach the metal from the opposite side to the bound ligand, thus reducing the interaction between the two ligands, but for the tetradentate EDDA ligand this is impossible. Consequently, the ligand-ligand interaction is larger for EDDA than for IDA, resulting in a lowering of the formation rate constant as compared to ZnIDA^{\ominus} .

The donor effect of the bound groups on the formation rate constant is clearly illustrated by the large differences between $\text{Zndien}(\text{ClO}_4)_2^{2+}$ and $\text{Zntrien}(\text{ClO}_4)_2^{2+}$ and $\text{Zntet}(\text{ClO}_4)_2^{2+}$. All of these amine complexes contain tetrahedral zinc⁽⁵⁸⁾ but in the dien complex the fourth coordination position is occupied by a water molecule instead of a nitrogen. The large difference in the forward rate constants for these complexes probably indicates the particular stability associated with four coordinated nitrogen groups. It is unlikely that this difference in rate constant reflects the ease with which zinc can change its coordination number because the forward rate constants for the reaction of NSA with the nitrate and perchlorate complexes of zinc dien²⁺, which have different coordination numbers, are very similar. Where nitrate is used instead of perchlorate as the counter ion there are two possible outcomes: the nitrate ion can replace one of the remaining coordinated water molecules (as seems to be the case for ZnEDDA^{\ominus}) or the nitrate ion can change the coordination number of the metal (as in Zntrien^{2+}). In both of these cases the changes in the rate constants and the activation parameters are very small. For ZnEDDA^{\ominus} there is just a statistical change in the formation rate constant related to the number of replaceable water molecules and this does not lead to a change in the activation enthalpy for the process

and the dissociation rate constant is not changed. However, the change in rate constants for the zinc amine systems with change in anion is more complicated.

The low activation enthalpies for the formation of the NSA complexes of ZndienCl_2^{2+} and ZnUDA^- suggest the existence of one or more pre-equilibrium steps but the large entropic compensation means that the rate constants are similar to those for the other Zndien^{2+} and Zncarboxylate species, respectively. The activation parameters for the reaction of ZnUDA^- with NSA will be discussed further in Chapter 7.

The dissociation rate parameters are not as reliable as those for the forward reaction but there is a marked similarity between the constants and activation parameters for all the reactions of ZnL with NSA^{2-} .

For the amine systems it is found that there are two reactive metal species which can be attributed to the formation of hydroxy complexes. For Zndien^{2+} the formation of a hydroxy complex has been reported by Prue and Schwarzenbach⁽³⁹⁾ but the stability constant for its formation has not been measured. Although no evidence has been obtained for the other zinc amines, hydroxy complexes have been reported for the corresponding copper complexes⁽¹³¹⁾. The hydroxide stability constants for the zinc and copper complexes of 3,3' diamino-propylamine have been shown to be similar⁽¹³²⁾ and so it is likely that the pK's of the zinc amines are similar to the copper values.

The hydroxy complexes were not investigated thoroughly because the dependence of both the NSA^{2-} reaction and the hydroxy complex concentration on pH could lead to a very complicated relaxation expression. The ideal method to

investigate the reactivity of these complexes would be to use an incoming ligand which is unaffected by pH, such as bipyridyl. For the reaction of $Zntet^{2+}$ with NSA^{2-} above pH 9.3, the analysis of the relaxation data indicated that only the hydroxy species of important and this is in agreement with the spectrophotometric data. Fig. 6.3.10 shows the spectrophotometric data obtained on the assumption that either $Zntet^{2+}$ or $(ZntetOH)^+$ is the reactive species. As both plots should give straight lines the reactive species at high pH must be $(ZntetOH)^+$. The spectrophotometric observations for the $Znrien^{2+}$ systems, shown in fig. 6.3.4.5, are similar to those of $Zntet^{2+}$ and it is assumed that here, too, the formation of a hydroxy complex is important at high pH. This would explain the appearance of a second relaxation effect in the reaction with NSA^{2-} . The high pH at which the second relaxation effect becomes important indicates that the low pH form of $Zntet^{2+}$ is not one in which the $Zntet^{2+}$ is protonated. Also, if this were the case, the protonated complex would be expected to react with NSA^{2-} at a faster rate than the high pH form (comparable to $Zndien^{2+}$) but this is not so. For both the $Znrien^{2+}$ and $Zntet^{2+}$ complexes it seems likely from the Raman work that the hydroxide complex is formed by the attack of OH^- on the low pH form of the complex rather than the hydrolysis of a coordinated water molecule. For the dien complex, however, the concentrations necessary to prevent the precipitation of the hydroxy complex are too low to obtain reliable spectra using the Coderg spectrometer and it is not possible to determine the coordination number of the complex from the kinetic results.

CHAPTER 7General Discussion7.1 Outer-sphere complex formation

In the derivation of relaxation expressions for metal complexation it is usual to assume that outer-sphere complex formation can be treated as a fast pre-equilibrium. However, for very labile metals it is necessary to take into account the coupling between the outer-sphere complex formation and the metalation steps. This usually results in a multiplication by $1/1 + K_{OS}(\bar{C}_M + \bar{C}_L)$ to the k_f term of the relaxation expression so that, for the simple case $M + L \rightleftharpoons ML$, the relaxation expression becomes

$$\tau^{-1} = \frac{K_{OS}k_f(\bar{C}_M + \bar{C}_L)}{1 + K_{OS}(\bar{C}_M + \bar{C}_L)} + k_b .$$

Thus, a plot of τ^{-1} against $(\bar{C}_M + \bar{C}_L)$ should show curvature when $K_{OS}(\bar{C}_M + \bar{C}_L)$ becomes 0.1. Using the deviation from linearity, it should be possible to calculate a value of K_{OS} .

This coupling should be particularly noticeable for the complexation of highly charged ligands since the K_{OS} values predicted by the Fuoss equation⁽²⁷⁾ are comparatively large. For the reaction of aquo magnesium with NSA the Fuoss equation predicts that K_{OS} should be about 5 M^{-1} and so at magnesium concentrations of about 0.1M it should be possible to detect the coupling. However, no deviation from linearity is detectable⁽¹³³⁾.

Ternary complex formation involving metal UDA complexes often gives rise to unusual activation parameters. For zinc-, magnesium- and nickel UDA⁻⁽¹³⁴⁾, ΔH_f^\ddagger is about 4 kcal mol⁻¹ lower than the typical activation enthalpy for the reaction

of NSA with a metal carboxylate complex. In each case, the activation entropy is more unfavourable than for the other carboxylate complexes, resulting in rate constants which appear to be normal for the reactions of a metal carboxylate with NSA. A similar result has been observed for the reaction of MgUDA^- with the oxine molecule⁽¹¹¹⁾. In this case it has been suggested that the unusual activation parameters can be explained by a small increase in the value of K_{OS} (with a correspondingly more favourable ΔH_{OS} but unfavourable ΔS_{OS}) due to hydrogen bonding between the oxine molecule and the bound UDA. However, with NSA^{2-} the possibility of forming a double hydrogen bond does not exist but there could conceivably be a π -bonding interaction between the delocalised electron systems of UDA and the incoming ligand.

Probably the easiest way to test this hypothesis is to investigate the reaction of NiUDA^- with ammonia using a pH indicator to follow the reaction. If the explanation of the low activation parameters is a π -interaction, then the activation parameters for the reaction of NiUDA^- with ammonia should be similar to those for the reaction of other nickel carboxylates with ammonia ($\Delta H_{\text{f}}^{\ddagger} \approx 13 \text{ kcal mole}^{-1}$ based on the values in ref. 85).

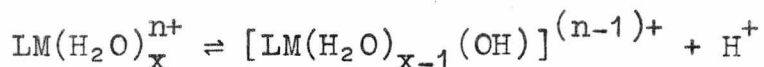
7.2 Hydroxy complexes of zinc

The tendency of zinc to form hydroxy complexes is well known^(15,131) but so far there has been no systematic study to determine the factors affecting the stability of hydroxy complexes. Often the first row transition metals (e.g. Co and Cu) form polymeric hydroxy complexes, but this tendency is less common in the case of zinc which tends to form discrete complexes. The presence of bound groups on the zinc

ion can have a marked effect on the pK of the remaining water molecules (see table 7.2.1).

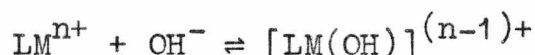
The formation of a hydroxy complex can be envisaged as occurring in two distinct ways:

(i) Where the complex has one or more bound water molecules the reaction can be considered as a hydrolysis



In this case, the more covalent the metal-OH₂ bonds, the more acidic are the water protons.

(ii) Where the complex has a low coordination number and all the coordination positions are occupied by the bound ligand, hydroxide ions can react with the complex to give a new complex of increased coordination number



The stability of a metal complex is usually determined by pH titrations but this method does not allow for any distinction in the type of hydroxy complex formed.

Using the simple picture of coordination as envisaged by Pauling in his "postulate of the essential neutrality of atoms"⁽¹⁴⁴⁾ electron donation from a ligand to a metal ion must bring about the reduction of the formal charge of the metal ion. The relative stability of metal complexes can then be explained in terms of the magnitude of the electrostatic and covalent interactions between the metal and the ligand and the geometry of the metal. One would naively expect the pK of a bound water molecule to be greater the greater the donating ability of the other donors. Thus the pK of Zn N,N-EDDA is greater than that of Zinc thiomalate because of the extra donating ability of two amine groups compared to

TABLE 7.2.1. pK values of some zinc complexes.

<u>Complex</u>	<u>pK</u>	<u>Binding groups</u>	<u>Ref.</u>
Carbonic anhydrase	~7		135
trien	8.0	2 x O ⁻	136
thiomalic acid	8.36	S, 2 x COO ⁻	137
ATP	8.50	 (PO ₃) ₂	138
ADP	8.51	 (PO ₃) ₂	139
aquo	8.70	(H ₂ O) ₆	15
3,3'Diaminodipropylamine	8.8	3 x N	131
Diethylenetriamine	>9	3 x N	(a)
N-2 hydroxyethylida	9.44	N, 2 x COO ⁻ , O ⁻	140
N-2 methoxyethylida	9.65	N, 2 x COO ⁻ , CH ₃ O	140
N-(2-methylthioethyl)ida	9.68	N, 2 x COO ⁻ , CH ₃ S	140
N,N EDDA	10.13	2 x N, 2 x COO ⁻	140
NTA	10.45	N, 3 x COO ⁻	86
cis cyclohexane 1,2 diamine	10.6	2 x N	141
trans cyclohexane 1,2 diamine	10.9	2 x N	141
α-β dimercaptosuccinic acid	12.28	2 x COO ⁻ , 2 x S ⁻	142
EDTA	~ 12	2 x N, 3 x COO ⁻	143

(a) This work.

one sulphide group. The slight difference in pK for the zinc complexes of cis- and trans-cyclohexane 1,2 diamine can possibly be attributed to the greater strain in the cis complex which gives rise to the lower stability of this complex and thus to a need for a greater electron donation from the remaining water molecules. Similarly, the lower pK of Zinc 3,3' diamino-dipropylamine as compared to zinc dien reflects the greater donating ability of 5-membered rings as shown by the stability constants of the two aquo complexes.

The existence of a zinc complex with a pK lower than that of hexaquo zinc might be rationalised in the following terms. When there is a reduction of the coordination number of zinc on complex formation the electron donation per donor atom has to be greater than when there were six donor atoms. Thus, when the bound ligand provides only two or three of the donor atoms in a tetrahedral complex the electron donation from these atoms may not be enough to satisfy the neutrality of the metal ion and so the strength of the remaining M-OH₂ bonds is enhanced, making the water protons more acidic. In the examples in table 7.2.1, where the pK of the zinc complex is considerably lower than the pK of aquo zinc, it has been suggested that the zinc atom has a coordination number of less than six; Zinc trien has two water molecules⁽¹³⁶⁾ and Zinc thiomalate has one water molecule⁽¹³⁷⁾ completing the tetrahedral coordination sphere. Pauling's postulate⁽¹⁴⁴⁾ of electroneutrality obviously needs modifying to explain the high stability of zinc-ammine complexes which on the simple basis of electronegativities should form less stable complexes than the corresponding carboxylate complexes, but in reality the reverse is true. This additional affinity of zinc for amine donors manifests

itself in the pK of zinc dien which, although the complex is tetrahedral with one bound water molecule, has a pK greater than that of aquo zinc.

Most of the zinc complexes which have been investigated kinetically in this work are known to form hydroxy species although, under the conditions used (except for Zn 2,3,2 tet) the hydroxy species were not important. Since the hydroxy species of the zinc complexes studied in this work can be used to illustrate the two pathways for hydroxy complex formation, described earlier in this section, it would be interesting to investigate the kinetic behaviour of these complexes and to compare them with the corresponding aquo complexes (particularly as models for carbonic anhydrase).

7.3 Comparison of the kinetic data for zinc and magnesium

A comparison of the kinetic data for zinc (d^10) and magnesium (d^0) should be interesting in that the kinetics of neither metal is complicated by the presence of partially filled d-orbitals but, while magnesium invariably has a coordination number of six, zinc forms complexes in which the coordination number ranges from four to six.

A comparison of the kinetic data (tables 5.8.3, 6.5.2) shows that there is a considerable difference in the effect of the bound ligands on the reactivity of these two metals with NSA^{2-} . For the magnesium systems, the bound ligand reduces the number of water molecules available for substitution and when a statistical correction is made to the formation rate constants at $25^\circ C$ (see section 5.8) the resulting values are approximately constant. The value of K_{OS} calculated by dividing this rate constant by the rate constant for water exchange at aquo magnesium ($5.3 \times 10^5 \text{ sec}^{-1}$) ⁽¹²⁰⁾

is in good agreement with the value of 3 M^{-1} calculated from the Fuoss equation. The activation parameters for the formation reaction can be represented by

$$\Delta H_f^\ddagger = \Delta H_{os} + \Delta H_{ex}^\ddagger$$

and

$$\Delta S_f^\ddagger = \Delta S_{os} + \Delta S_{ex}^\ddagger$$

For all the LMgNSA systems (except $L = \text{UDA}^{3-}$) the values of ΔH_f^\ddagger and ΔS_f^\ddagger are slightly larger than the values for activation parameters for water exchange ($\Delta H_{ex}^\ddagger = 10.2 \text{ kcal.M}^{-1}$ and $\Delta S_{ex}^\ddagger = 2 \text{ eu}^{(120)}$) giving values of ΔH_{os} and ΔS_{os} with the range of the "reasonable values" quoted in reference 25.

The interpretation of the experimental rate constants and activation parameters for the reaction of zinc complexes with NSA^{2-} is more difficult than for the magnesium systems. The large variation in the formation rate constants cannot be explained solely by a statistical reduction of the number of replaceable water molecules and so the bound ligand must have some other effect.

Since the complexes of zinc with trien and 2-3-2 tet in perchlorate media are both tetrahedral, with all the coordination positions taken up by nitrogen atoms, the rate-determining step must involve an increase in the coordination sphere and thus be dependent to a certain extent on the incoming ligand. It is also possible that the reaction of Zndien^{2+} with NSA^{2-} in perchlorate media proceeds by an S_N2 type mechanism as it has already been suggested (section 3.5.3) that the presence of high concentrations of chloride ions causes the coordination number of zinc in Zinc dien complex to increase to five rather than to substitute a chloride ion for the bound water molecule. This suggests that the replacement of the bound water molecule is an energetically

unfavourable process, and yet the reaction of zinc dien with NSA^{2-} has a lower activation energy than most of the other systems studied.

For the reaction of NSA^{2-} with complexes of zinc containing oxygen ligands the charge of the bound ligand appears to have a considerable effect on the formation rate constant while in the magnesium systems the charge of the bound ligands apparently only influences the rates of ternary complex dissociation. It is therefore necessary to suggest a different rate-determining step for zinc complex formation as compared to magnesium. It is possible to suggest two mechanisms for the zinc reactions in which either the formation of the first or second bond from NSA to the zinc ion is rate-determining. In both of these situations the rate-determining step would be dependent on the incoming ligand and it is not possible to distinguish between them using the available data.

7.4 Comparison of Zinc(II) with the divalent metal ions of the first transition metal series

A considerable amount of kinetic work has been done on the reactions of Ni(II) because the half-times generally fall conveniently into the stopped-flow range. For most of the systems the rate determining step is the loss of a water molecule from the inner-sphere of the metal ion, although in some cases (particularly when the bound ligand is a polyamine, where the dissociation rate of the intermediate where one of the "arms" of the bidentate ligand is bound to the ~~aque~~ (k_{21}) metal becomes comparable to the rate of ring closure (k_{23}) because the first band formed is weak, see scheme 1.1) there is a contribution from ring-closure. For ternary complex formation at nickel centres it has been found that the

presence of bound ligands has a considerable effect on the rate of substitution of the remaining water molecules^(145,146). Contrary to an early suggestion by Hammes and Steinfeld⁽¹⁰¹⁾, several workers have found that it is not so much the charge of bound groups but the number of coordinated aliphatic nitrogens that increases the substitution rate^(145,146). Thus, there is only a five-fold increase in k_{12}^S on going from $Ni(H_2O)_6^{2+}$ to $NiNTA^-$ but an increase of a factor 10^3 on going to $Nitren^{2+}$ for the reaction with ammonia⁽¹⁴⁶⁾. This is almost entirely due to an increase in k_{ex} (as determined by n.m.r.).

In a study of the nickel complexes of some substituted phenanthrolines, Steinhaus and Margerum have found⁽¹⁴⁷⁾ that ternary complex formation with NTA^- and $Hdien^+$ correlates fairly well with the Hammett parameters obtained using the pK_a values of the phenanthrolines. This, together with the negative ρ values, supports the assignment of water loss as the rate-determining step and also suggests that the changes in formation rate constant reflect the electron donating or withdrawing properties of the substituents.

Kinetic studies of ternary complex formation involving Co(II) species and PADA⁽⁸⁷⁾ show that the bound ligand has a large effect on the rates of complexation. For the complexes of Co(II) with oxygen-containing ligands the reaction with PADA has been interpreted in terms of the Eigen mechanism with the variation in the formation rate constant reflecting the "loosening" of the remaining coordinated water molecules. However, with the Co(II) tren complex there must be a change in the rate-determining step as this complex is five coordinate⁽⁷⁵⁾.

In view of the ability of Co(II) to replace zinc in many metallo-enzymes, the similarity in the patterns found for the

formation rate constants for Co(II) with PADA and Zn(II) with PADA and NSA²⁻ is particularly interesting (fig. 7.4.1).

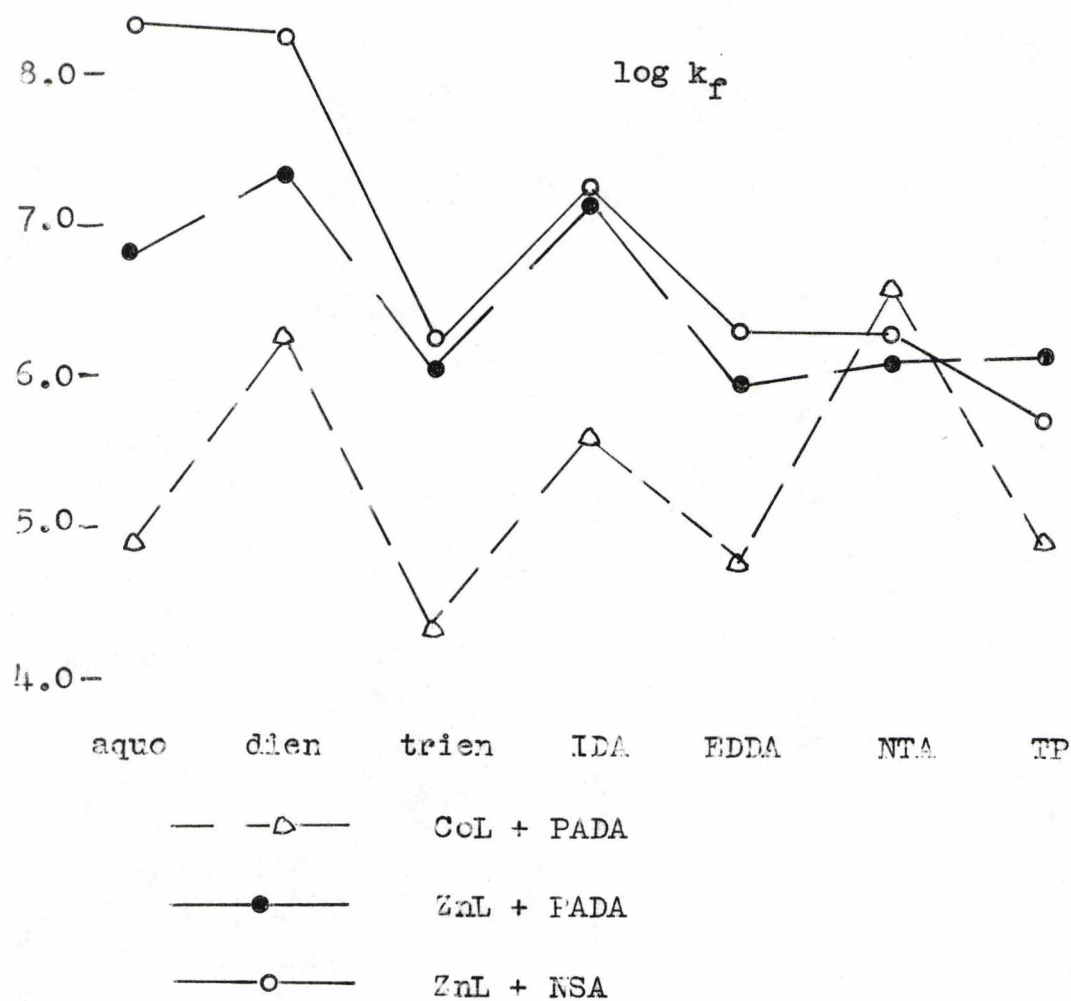


Fig. 7.4.1.

APPENDIX 1

PROGRAM GRC1 - Equilibrium concentrations for ZnL systems.

The program is shown overleaf (in the title, M is represented by ZN). The identifiers used in the data and printout are as follows:

K1 and K2 are the ligand-proton stability constants;
K3 and K4 are the metal-ligand stability constants;
C and M are the total ligand and metal concentrations, respectively;

PH1, PH2 and HP are the limits of the pH range and the pH step required in the printout, respectively;

ZN, ZNL, ZNL2 are the equilibrium concentrations of M, ML and ML_2 , respectively;

HL and H2L are the equilibrium concentrations of HL and H_2L , respectively;

ION is the ionic strength.

The remainder of the identifiers are required to solve the cubic equation.

The data required, in the order in which it is entered, is:

C, M, K1, K2, K3, K4, ION, PH1, PH2, HP.

The printout gives:

PH (from PH1 to PH2), ML, L, M, ML_2 , HL and H_2L .

The contributions to the total metal and ligand concentrations from all the species are added together and printed under TOTAL M and TOTAL L, respectively. As an internal check on the program, the ratio ML/ML_2 is also printed out.

PROGRAM GRC1

```
EQUILIBRIUM CONCENTRATIONS FOR ZNL SYSTEMS;
"BEGIN" "REAL" K1, K2, K3, K4, C, M, ION, PH, H, PH1, PH2, HP, K, AA, BB, CC,
P, Q, ZN, ZNL, ZNL2, L, HL, H2L, TL, TM, LANDA, TF, F1, F2, F3, UUU, U, ML1, ML2, ML3;
SPECIAL (5);
"READ" C, M, K1, K2, K3, K4, ION, PH1, PH2, HP;
"PRINT" "SYSTEM IS", 'L1';
"PRINT" "METAL CONC.=", SAMELINE, SCALED(4), M, 'L1';
"PRINT" "LIGAND CONC.=", SAMELINE, SCALED(4), C, 'L1';
"PRINT" "PK1=", SAMELINE, FREEPOINT(4), -LN(K1)/2.3026, 'L1';
"PRINT" "PK2=", SAMELINE, FREEPOINT(4), -LN(K2)/2.3026, 'L1';
"PRINT" "LOG K3=", SAMELINE, FREEPOINT(4), LN(K3)/2.3026, 'L1';
"PRINT" "LOG K4=", SAMELINE, FREEPOINT(4), LN(K4)/2.3026, 'L1';
"PRINT" "IONIC STRENGTH=", SAMELINE, ALIGNED(0,2), ION, 'L3';
"PRINT" "S'PH'S6'ZNL'S8'L'S8'ZN'S7'ZNL2'S7'HL'S7'H2L'S6'',
SAMELINE, 'TOTAL L'S3'TOTAL M'S9'ZNL/ZNL2';
"FOR" PH:=PH1 "STEP" HP "UNTIL" PH2 "DO"
"BEGIN" H:=EXP(-PH*2.3026);
BB:=(2*K3*K4*M+4*K4+4*K1*K4*M+4*K1*K2*K4*M+2-K1*K3*M-K1*K2*K3*M+2-K3)/
(4*K4+2-K3*K4);
CC:=(K3*M+K1*K3*M*M+K1*K2*K3*M*M+2-2*K3*K4*C*M+1+2*K1*M+2*K1*K2*M+2+
K1+2*M+2+2*K1+2*K2*M+3+K1+2*K2+2*M+4+K3*C+K1*K3*C*M+K1*K2*K3*M+2*C+
K4*C+2*K3)/(4*K4+2-K3*K4);
AA:=-K3*C*M*(1+K1*K2*M+2+K1*M)/(4*K4+2-K3*K4);
P:=CC-(BB+2)/3;
Q:=AA-BB*CC/3+2*(BB+3)/27;
"IF" 4*(P+3)+27*(Q+2) > 0 "THEN" "BEGIN"
UUU:=((-27*Q)-SQRT((27*Q)+2+108*(P+3)))/54;
U:=SIGN(UUU)*(ABS(UUU)+(1/3));

ZNL:=(U-P/(3*U))-BB/3;
"END" "ELSE" "BEGIN" LANDA:=SQRT(-4*P/3);
TF:=ARCCOS(-4*Q/(LANDA+3));
F1:=TF/3;
F2:=(6.283184+TF)/3;
F3:=(6.283184-TF)/3;
ML1:=(LANDA*COS(F1))-BB/3;
ML2:=(LANDA*COS(F2))-BB/3;
ML3:=(LANDA*COS(F3))-BB/3;
"IF" ML1>0 "AND" ML1<C "AND" ML1<M "THEN" ZNL:=ML1;
"IF" ML2>0 "AND" ML2<C "AND" ML2<M "THEN" ZNL:=ML2;
"IF" ML3>0 "AND" ML3<C "AND" ML3<M "THEN" ZNL:=ML3;
"END";
L:=(C-ZNL)/(1+K1*M+K1*K2*M+2+2*K4*ZNL);
ZN:=ZNL/(K3*L);
ZNL2:=K4*ZNL*L;
HL:=K1*M*L;
H2L:=K2*HL*M;
TL:=L+HL+H2L+ZNL+2*ZNL2;
TM:=ZN+ZNL+ZNL2;
"PRINT" FREEPOINT(3), PH, PREFIX('S'), SCALED(3), ZNL, L, ZN, ZNL2, HL, H2L,
TL, TM, ZNL/ZNL2;
"END";
"END";
```

APPENDIX 2

PROGRAM GRC 4 - Iterative calculation of K from spectrophotometric data.

This program, due to M.S. Zetter and M.A. Cobb, is shown overleaf.

The identifiers used in the data and printout are as follows:

OD[C], AT[C] and BT[C] are the optical density and the corresponding total concentrations of M and D respectively for the Cth solution;

N is the total number of solutions;

OB is the optical density of the free dye, ODD;

W is the wavelength of the measurement;

K1 and P are the first approximation for the stability constant and the maximum percentage difference between the last two values for K, respectively;

G and I are multiplication factors for AT and BT, respectively, to simplify the input data;

RK, INT, ERRRK and ERRINT are the slope and intercept of the plot and the standard deviations in same, respectively.

This program can be used to compute the stability constants for systems of the type



where M does not absorb at the wavelength of the measurement.

The program operates by using the value of K, to compute the equilibrium concentrations of M and L and then to "plot" OD vs. $(OD-ODd)/([M] + [L])$ (see section 4.2) using a least

squares procedure to give a new approximation for K. The process is repeated until the $(n+1)^{\text{th}}$ approximation for K is within P% (usually 0.5%) of the n^{th} approximation. The final print out shows the equilibrium concentrations and the final value for K.

PROGRAM GRCL4

```
ITERATIVE CALCULATION OF K FROM SPECTROPHOTOMETRIC DATA;
"BEGIN" "REAL" W,OB,K1,P,K,SX,SY,S2X,SXY,S2D,AA,BB,CC,AB,A,B,
DENOM,RK,ERRRK,INT,ERRINT,EAB,G,I;
"INTEGER" N,R,C;
"ARRAY" OD,AT,BT,Y,X[1:99];
SPECIAL(5);
"READ" N,W,OB,K1,P,G,I;
"FOR" C:=1 "STEP" 1 "UNTIL" N "DO"
"BEGIN" "READ" OD[C],AT[C],BT[C];
      AT[C]:=AT[C]*G;
      BT[C]:=BT[C]*I;
"END";
"PRINT" 'SYSTEM IS 'L2'';
"PRINT" 'WAVELENGTH=',SAMELINE,SCALED(3),W,' 'S1'NM'L2'';
K:=K1*100;
"FOR" R:=1, R+1 "WHILE" ABS(K-K1) > P*K1/100 "DO"
"BEGIN" SX:=SY:=S2X:=SXY:=S2D:=0;
"PRINT" 'L1'VALUE OF K=',SAMELINE,SCALED(4),K1,' 'L2'';
      "PRINT" 'S1'TOTAL A'S3'TOTAL B'S6'[A]'S7'[B]'S6'[AB]',SAMELINE,
      'S6'OD'S6'(OD-OB)/[A]';
      K:=K1;
"FOR" C:=1 "STEP" 1 "UNTIL" N "DO"
"BEGIN" AA:=K;
      BB:=- (1+K*AT[C]+K*BT[C]);
      CC:=K*AT[C]*BT[C];
      AB:=(-BB-SQRT(BB^2-4*AA*CC))/(2*AA);
      B:=BT[C]-AB;
      A:=AT[C]-AB;

      Y[C]:=OD[C];
      X[C]:=(OD[C]-OB)/A;
      SX:=SX+X[C];
      SY:=SY+Y[C];
      S2X:=S2X+X[C]^2;
      SXY:=SXY+X[C]*Y[C];
      "PRINT" SCALED(3),AT[C],PREFIX('S1'), SCALED(3),
      BT[C],A,B,AB,OD[C],X[C];
"END";
DENOM:=N*S2X-SX^2;
RK:=(N*SXY-SX*SY)/DENOM;
INT:=(SY*S2X-SXY*SX)/DENOM;
"FOR" C:=1 "STEP" 1 "UNTIL" N "DO"
      S2D:=S2D+(Y[C]-RK*X[C]-INT)^2;
      ERRRK:=SQRT((N*S2D)/((N-2)*DENOM));
      ERRINT:=SQRT((S2X*S2D)/((N-2)*DENOM));
      K1:=-1/RK;
      EAB:=INT/BT[1];
      "PRINT" 'L3'SLOPE=',SAMELINE,SCALED(4),RK,
      'S5'STD. DEV. IN SLOPE =',
      SCALED(4),ERRRK,'L1'INTERCEPT =',SCALED(4),INT,SAMELINE,
      'S5'STD. DEV. IN INTERCEPT =',SCALED(4),ERRINT,
      'L1'EXTINCTION COEFF. OF COMPLEX =',SCALED(4),EAB,
      'L2S2'NEW APPROX. FOR K=', SCALED(4),K1,' 'L5'';
"END";
"END";
```

APPENDIX 3

PROGRAM GRC2 - Least squares for kinetic data.

This program is shown overleaf.

The identifiers used in the data and printout are as follows:

Y[C] and V[C] are the reciprocal relaxation time
and the total metal concentration for the Cth
solution;

N is the total number of sets of data;

F and G are multiplication factors for Y and V
respectively;

KF, KB, ERRKF, ERRKB are k_f , k_b and the standard
deviations in same, respectively.

The program "plots" τ^{-1} vs. [M] and prints out values for
 k_f and k_b and their respective standard deviations using a
least squares procedure.

PROGRAM GRC2

```
LEAST SQUARES FOR KINETIC DATA;
"BEGIN" "REAL" SX,SY,SXY,S2X,S2D,DENOM,KF,KB ,ERRKF,ERRKB,K2,F,G;
"INTEGER" C,N,R;
"ARRAY" X,Y,V[1:100];
"READ" N,F,G;
SPECIAL(5);
"FOR" C:=1 "STEP" 1 "UNTIL" N "DO"
"READ" V[C],Y[C];
  "PRINT" 'SYSTEM IS'L2'';
  SX:=SY:=SXY:=S2X:=S2D:=0;
  "BEGIN" X[C]:=V[C]*G;
  SX:=SY:=SXY:=S2X:=S2D:=0;
  "FOR" C:=1 "STEP" 1 "UNTIL" N "DO"
    Y[C]:=Y[C]*F;
    SX:=SX+X[C];
    SY:=SY+Y[C];
    S2X:=S2X+X[C]*2;
    SXY:=SXY+X[C]*Y[C];
    "PRINT" SCALED(4),Y[C],SAMELINE,'S4'',SCALED(4),X[C];
  "END";
  DENOM:=N*S2X-SX*2;
  KF:=(N*SXY-SX*SY)/DENOM;
  KB:=(SY*S2X-SXY*SX)/DENOM;
  "FOR" C:=1 "STEP" 1 "UNTIL" N "DO"
    S2D:=S2D+(Y[C]-KF*X[C]-KB)*2;
    ERRKF:=SQRT((N*S2D)/((N-2)*DENOM));
    ERRKB:=SQRT((S2X*S2D)/((N-2)*DENOM));
  "PRINT" 'L3'SLOPE    =',SAMELINE,SCALED(4),KF,SAMELINE,

'S3'STD. DEV. IN SLOPE    =',SCALED(4),ERRKF,'L1'',
SAMELINE,'INTERCEPT=',SCALED(4),KB,
'S3'STD. DEV. IN INTERCEPT=',SCALED(4),ERRKB;
"END";
```

APPENDIX 4

Determination of K_3 for M-NSA systems

Above pH 6 the only significant species absorbing at the wavelength of the measurements are NSA^{2-} , HNSA^- and MNSA , so that

$$\text{od} = \epsilon_{\text{MA}}[\text{MA}] + \epsilon_{\text{A}}[\text{A}] + \epsilon_{\text{HA}}[\text{HA}] \quad \dots \text{(A.2.1)}$$

where ϵ_{MA} , ϵ_{A} and ϵ_{HA} are the extinction coefficients of MNSA , NSA^{2-} and HNSA^- , respectively, and od is the optical density of the solution.

If the total concentration of NSA is C , the stability constant

$$K_3 = \frac{[\text{MA}]}{[\text{M}][\text{A}]} \quad \dots \text{(A.2.2)}$$

and the effective extinction coefficient of the test solution is ϵ , then equation A.2.1 becomes

$$C\epsilon = \epsilon_{\text{MA}}[\text{MA}] + \epsilon_{\text{A}}[\text{A}] + \epsilon_{\text{HA}}[\text{HA}]$$

Substituting for $[\text{HA}]$ from equation 5.2.2 and rearranging

$$(\epsilon - \epsilon_{\text{A}})[\text{A}] + (\epsilon - \epsilon_{\text{HA}})K_1[\text{H}][\text{A}] + (\epsilon - \epsilon_{\text{MA}})[\text{MA}] = 0 \quad \dots \text{(A.2.3)}$$

Then substituting for $[\text{MA}]$ and multiplying by $C/[\text{A}]$ gives

$$C(\epsilon - \epsilon_{\text{A}}) + C(\epsilon - \epsilon_{\text{HA}})K_1[\text{H}] + C(\epsilon - \epsilon_{\text{MA}})K_3[\text{M}] = 0$$

or

$$\text{od} = C\epsilon_{\text{MA}} - \frac{1}{K_3[\text{M}]} [(\text{od} - C\epsilon_{\text{A}}) + (\text{od} - C\epsilon_{\text{HA}})K_1[\text{H}]]$$

so a plot of

$$\text{od vs. } \frac{1}{[\text{M}]} [(\text{od} - C\epsilon_{\text{A}}) + \text{od} - C\epsilon_{\text{HA}}]K_1[\text{H}]$$

gives a straight line of slope $-\frac{1}{K_3}$ and intercept $C\epsilon_{\text{MA}}$.

APPENDIX 5

pK determination from two solutions

From equation 5.2.3

$$od = \frac{(C_{\epsilon A} - od)}{K_1 [H]}$$

For two solutions (a) and (b)

$$od_a = \frac{(C_{\epsilon A} - od_a)}{K_1 [H]_a}$$

$$od_b = \frac{(C_{\epsilon A} - od_b)}{K_1 [H]_b}$$

Then subtracting

$$od_a - od_b = \frac{1}{K_1} \left(\frac{C_{\epsilon A} - od_a}{[H]_a} - \frac{C_{\epsilon A} - od_b}{[H]_b} \right)$$

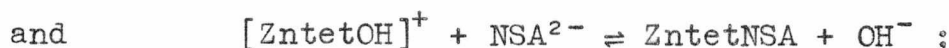
and thus

$$K_1 = \left[\frac{(C_{\epsilon A} - od_a)}{[H]_a} - \frac{(C_{\epsilon A} - od_b)}{[H]_b} \right] / (od_a - od_b)$$

APPENDIX 6

Optical density expression for the stability constant of
[ZntetOH]⁺ with NSA²⁻

Assuming that under the conditions used the reaction between Zntet and NSA can be ignored (i.e. [ZntetOH]⁺ >> [Zntet]²⁺) then the equilibria in solution may be represented by



$$K_2 = \frac{[\text{ZntetNSA}][\text{OH}^-]}{[\text{ZntetOH}]^+[\text{NSA}^{2-}]}$$

Let the total concentration of NSA be C and the extinction coefficients of MNSA, NSA²⁻, HNSA and the effective extinction coefficient of the test solution be ϵ_{ML} , ϵ_{L} , ϵ_{HL} and ϵ , respectively.

Then $\text{od} = C_{\epsilon} = \epsilon_{\text{ML}}[\text{ML}] + \epsilon_{\text{L}}[\text{L}] + \epsilon_{\text{HL}}[\text{HL}]$

Substituting for [HL] and rearranging gives

$$(\epsilon - \epsilon_{\text{ML}})[\text{ML}] + (\epsilon - \epsilon_{\text{L}})[\text{L}] + (\epsilon - \epsilon_{\text{HL}})K_1[\text{H}][\text{L}] = 0$$

and multiplying by C/[L] and substituting for ML gives

$$(C_{\epsilon} - C_{\epsilon_{\text{ML}}}) \frac{K_2[\text{M}]}{[\text{OH}]} + (C_{\epsilon} - C_{\epsilon_{\text{L}}}) + (C_{\epsilon} - C_{\epsilon_{\text{HL}}})K_1[\text{H}] = 0$$

and rearranging gives

$$\text{od} = C_{\epsilon_{\text{ML}}} - \frac{1}{K_2} \frac{[\text{OH}]}{[\text{M}]} ((\text{od} - C_{\epsilon_{\text{L}}}) + (\text{od} - C_{\epsilon_{\text{HL}}})K_1[\text{H}])$$

so a plot of

$$\text{od vs. } \frac{[\text{OH}]}{[\text{M}]} ((\text{od} - C_{\epsilon_{\text{L}}}) + (\text{od} - C_{\epsilon_{\text{HL}}})K_1[\text{H}])$$

gives a straight line of slope $-\frac{1}{K_2}$ and intercept $C_{\epsilon_{\text{ML}}}$.

APPENDIX 7

PROGRAM GRC5 - Least squares for kinetic data NSA.

This program is shown overleaf.

The identifiers used in the data and printout are as follows:

K1 is the first proton stability constant of NSA;

M is the total metal concentration;

Y[C] and V[C] are the reciprocal relaxation time and pH of the Cth solution;

N is the number of sets of data;

F is a multiplication factor for Y;

KF, KB, ERRKF and ERRKB are as for program GR2

(Appendix 3).

The program uses the pH values to compute the values of $[M]/(1 + K_1[H])$ and then using a least squares procedure "plots" τ^{-1} vs. $[M]/(1 + K_1[H])$ and prints out values of k_f , k_b and the standard deviations in these values.

PROGRAM GRC5

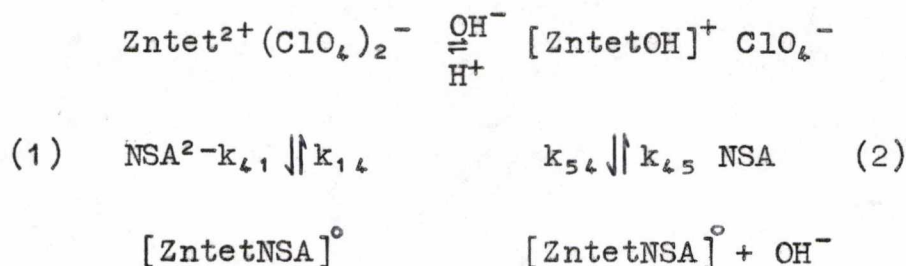
```
LEAST SQUARES FOR KINETIC DATA NSA;
"BEGIN" "REAL" SX,SY,SXY,S2X,S2D,DENOM,KF,KB ,ERRKF,ERRKB,K1,F,M,H;
"INTEGER" C,N;
"ARRAY"Y,X,V[1:100];
"READ"N,F,M,K1;
SPECIAL(5);
"FOR" C:=1 "STEP" 1 "UNTIL" N "DO"
"READ"V[C],Y[C];
"PRINT"'SYSTEM IS'L2'';
"PRINT"'HIGH PH PLOT'L2S5'T'S9'M/(1+K1*H)';
  SX:=SY:=SXY:=S2X:=S2D:=0;
  "FOR"C:=1"STEP"1"UNTIL"N"DO"
    "BEGIN"H:=EXP(-V[C]*2.3026);
    X[C]:=M/(1+K1*H);
    Y[C]:=Y[C]*F;
    SX:=SX+X[C];
    SY:=SY+Y[C];
    S2X:=S2X+X[C]*2;
    SXY:=SXY+X[C]*Y[C];
    "PRINT" SCALED(4),Y[C],SAMELINE,'S4',SCALED(4),X[C];
  "END";
  DENOM:=N*S2X-SX*2;

KF:=(N*SXY-SX*SY)/DENOM;
KB:=(SY*S2X-SXY*SX)/DENOM;
"FOR" C:=1 "STEP" 1 "UNTIL" N "DO"
S2D:=S2D+(Y[C]-KF*X[C]-KB)*2;
ERRKF:=SQRT((N*S2D)/((N-2)*DENOM));
ERRKB:=SQRT((S2X*S2D)/((N-2)*DENOM));
"PRINT" 'L3'SLOPE =',SAMELINE,SCALED(4),KF,SAMELINE,
'S3'STD. DEV. IN SLOPE =',SCALED(4),ERRKF,'L1',
SAMELINE,'INTERCEPT=',SCALED(4),KB,
'S3'STD. DEV. IN INTERCEPT=',SCALED(4),ERRKB;
"END";
```

APPENDIX 8

Relaxation expression for the reaction of $Zntet^{2+}$
with NSA^{2-}

At high pH NSA^{2-} can react either with $Zntet^{2+}$ or $[ZntetOH]^+$.



The formation of $[ZntetOH]^+$ from $Zntet^{2+}$ is very fast in comparison with the other rate constant.

Let $[ZnOH]$ represent $[ZntetOH]^+$ and L represent NSA^{2-} (ignoring changes for the sake of clarity).

For pathway (1) the relaxation expression is identical to the simplified expression for the reaction of metal ions with NSA^{2-} , i.e.

$$-\frac{d\Delta[ZnL]}{dt} = \frac{k_{14}[Zn]\Delta[ZnL]}{1+K_1[H]} + k_{14}\Delta[ZnL]$$

For pathway (2), at equilibrium

$$\frac{d[ZnL]}{dt} = k_{54}[ZnOH][L] - k_{45}[ZnL][OH]$$

at time t ,

$$\frac{d([ZnL] + \Delta[ZnL])}{dt} = k_{54}([ZnOH] + \Delta[ZnOH])([L] + \Delta[L]) - k_{45}([ZnL] + \Delta[ZnL])([OH] + \Delta[OH])$$

Subtracting and neglecting second order terms

$$\Delta[ZnOH] = 0 \text{ as } [ZnOH] \gg L \text{ and } \Delta[OH] = 0$$

because solution is buffered.

$$\text{Then } \frac{d(\Delta[ZnL])}{dt} = k_{54}[ZnOH]\Delta[L] - k_{45}\Delta[ZnL][OH] .$$

From $K_1 = \frac{[HL]}{[H][L]}$ by a similar process to above, it can be shown that

$$\Delta L = \frac{-\Delta[ZnL]}{(1 + K_1[H])}$$

and using the stoichiometric relationship

$$\Delta[ZnL] + \Delta[L] + \Delta[HL] = 0$$

$$-\frac{d\Delta[ZnL]}{dt} = \frac{k_{54}[ZnOH]}{1 + K_1[H]} \Delta[ZnL] + k_b \Delta[ZnL][OH]$$

Thus combining pathways (1) and (2)

$$-\frac{d\Delta[ZnL]}{dt} = \frac{k_{41}[Zn]\Delta[ZnL]}{1 + K_1[H]} + k_{14}\Delta[ZnL] + \frac{k_{54}[ZnOH]\Delta[ZnL]}{1 + K_1[H]} + k_b \Delta[ZnL][OH]$$

This is the equation of an exponential and

$$\tau^{-1} = \frac{k_{41}[Zn]}{1+K_1[H]} + k_{14} + \frac{k_{54}[ZnOH]}{1+K_1[H]} + k_{45}[OH]$$

But $K_2 = \frac{[ZnOH]}{[Zn][OH]}$ and $[ZnOH] + [Zn] = [Zn]_{total}$

So the relaxation expression becomes

$$\tau^{-1} = \frac{k_{41}[Zn]^t}{(1+K_1[H])(1+K_2[OH])} + k_{14} + \frac{k_{54}K_2[OH][Zn]^t}{(1+K_1[H])(1+K_2[OH])} + k_{45}[OH]$$

where $[Zn]^t$ is the total concentration of Zntet.

Under the experimental conditions used

$$K_2[OH] \gg 1 \quad \text{and} \quad k_{54} > k_{41}$$

so the relaxation expression simplifies to

$$\tau^{-1} = k_{14} + k_{45}[OH] + \frac{k_{54}[Zn]^t}{1+K_1[H]}$$

REFERENCES

1. M. Florkin and E.H. Stotz, Comprehensive Biochemistry, Vol. 12 (Pub. Elsevier, 1964).
2. M.E. Riepe and J.H. Wang, J. Biol. Chem., 1968, 243, 2779.
3. J.M. Brewer and G. Weber, J. Biol. Chem., 1966, 241, 2550.
4. J.A. Hartsruck and W.N. Lipscomb, The Enzymes, Vol. III, 3rd ed., P.D. Boyer, ed. (Academic Press, N.Y. 1971), p.1.
5. R.C. Bray, R. Petterson and A. Ehrenberg, Biochem. J., 1961, 81, 178.
6. e.g. C.S.G. Phillips and R.J.P. Williams, Inorganic Chemistry (Oxford Univ. Press 1966), Vol. 2.
7. B.L. Vallee and R.J.P. Williams, Chem. in Brit., 1968, 4, 389.
8. E. Breslow and A.W. Girrotti, J. Biol. Chem., 1960, 241, 5651.
9. L.G. Sillén and A.E. Martell, Stability Constants of Metal Ion Complexes (Chem. Soc., London 1964 and 1971).
10. M. Eigen and G.G. Hammes, Adv. in Enzymology, 1963, 25, 1.
11. H. Irving and R.J.P. Williams, J. Chem. Soc., 1953, 3192.
12. A.E. Dennard and R.J.P. Williams, Transition Metal Chemistry (Arnold, London 1966), 2.
13. B.L. Vallee and R.J.P. Williams, Proc. Nat. Acad. Sci., 1968, 59, 498.
14. S. Lindskog, Structure and Bonding, Vol. 8, 153.
15. S. Chaberek, Jnr., R.C. Courtney and A.E. Martell, J. Amer. Chem. Soc., 1952, 74, 5057.
16. A. Thorslund and S. Lindskog, Eur. J. Biochem., 1967, 3, 117.
17. S. Lindskog and B.G. Malmström, J. Biol. Chem., 1962, 237, 1129.
18. R.G. Wilkins, Acc. Chem. Res., 1970, 3, 408.
19. M. Eigen, Advances in the chemistry of the coordination compounds, Kirschner ed. (Macmillan, New York 1961), p.371.
20. M. Eigen, Proceedings of the Robert A. Welch Foundation Conferences on Chemical Research, III. Molecular Structure, Houston, Texas, 1959, p.161.
21. H. Hoffmann and U. Nickel, Ber. Bunsenges. Phys. Chem., 1968, 72, 1096.
22. U. Nickel, H. Hoffmann and W. Jaenicke, Ber. Bunsenges. Phys. Chem., 1968, 72, 526.

23. K. Kustin, R.F. Pasternack and E.M. Weinstock, J. Amer. Chem. Soc., 1966, 88, 4610.
24. R.F. Pasternack, P.R. Huber, U.M. Huber and H. Sigel, Inorg. Chem., 1972, 11, 276.
25. D.J. Hewkin and R.H. Prince, Coord. Chem. Rev., 1970, 5, 45.
26. J.P. Hunt, Coord. Chem. Rev., 1971, 7, 1.
27. R.M. Fuoss, J. Amer. Chem. Soc., 1958, 80, 5059.
28. M. Eigen, W. Kruse, G. Maass and L.C. de Maeyer, Prog. Reaction Kinetics, 1964, 2, 287.
29. P. Hemmes, J. Amer. Chem. Soc., 1972, 94, 75.
30. K. Kustin and J. Swinehart, Prog. Reaction Kinetics, 1970, 13, 107.
- 30a. D.B. Rorabacher, Inorg. Chem., 1966, 5, 1891.
31. E.F. Caldin, Fast Reactions in Solution (Blackwell, 1964).
32. D.N. Hague, Fast Reactions (Wiley, 1971).
33. M. Eigen and L.C. de Maeyer, Techniques of Organic Chemistry, Vol. VIII, Part II, S.L. Friess, E.S. Lewis and A. Weissberger, eds. (Interscience, New York, 1963), Ch. XVIII.
34. H. Strehlow, Adv. Molec. Relaxn. Proc., 1972, 2, 235.
35. G.H. Czerlinski, Chemical Relaxation (Arnold, London, 1966).
36. L.J. Wilson and N.J. Rose, J. Amer. Chem. Soc., 1968, 90, 6041.
37. H.B. Jonassen, R.B. LeBlanc, A.W. Meibohm and R.M. Rogan, J. Amer. Chem. Soc., 1950, 72, 2430.
38. G. Schwarzenbach, Helv. Chim. Acta, 1950, 33, 974.
39. J.E. Prue and G. Schwarzenbach, Helv. Chim. Acta, 1950, 33, 985.
40. D.C. Weatherburn, E.J. Billo, J.P. Jones and D.W. Margerum, Inorg. Chem., 1970, 9, 1557.
41. A.I. Vogel, Quantitative Inorganic Analysis (Longmans, London, 1961), p.55.
42. A.I. Vogel, Quantitative Inorganic Analysis (Longmans, London, 1961), p.433.
43. C.B. Monk, J. Chem. Soc., 1949, 427.
44. P. Bonneman-Bemia, Ann. Chim., 1941, 16, 395.
45. S. Chaberek, Jr., and A.E. Martell, J. Amer. Chem. Soc., 1952, 74, 6228.
46. E.F. Caldin and J.E. Crooks, J. Sci. Inst., 1967, 44, 449.

47. J.E. Crooks and B.H. Robinson, Trans. Faraday Soc., 1970, 66, 1436.
48. J.E. Crooks, M.S. Zetter and P.A. Tregloan, J. Phys. (E), 1970, 3, 73.
49. S.J. Glasstone, K.J. Laidler and H. Eyring, The Theory of Rate Processes (McGraw-Hill, London, 1941), Ch. 1.
50. A.E. Martell, in Metal Binding in Medicine Symposium (Philadelphia 1959), M.J. Seven, ed.
51. A. Ferrari, A. Braibanti, A.M.M. Lanfredi and A. Tiripicchio, Acta. Cryst., 1967, 22, 240.
52. J.E. Colman and B.L. Vallee, J. Biol. Chem., 1960, 235, 390.
53. S. Lindskog, J. Biol. Chem., 1963, 243, 945.
54. R.T. Simpson and B.L. Vallee, Biochemistry, 1969, 8, 3776.
55. G.L. Cottam and R.L. Ward, Arch. Biochem. Biophys., 1970, 141, 768.
56. R.L. Ward, Biochemistry, 1969, 8, 1879, 2447.
57. M. Ciampolini, P. Paoletti and L. Sacconi, J. Chem. Soc., 1960, 4553.
58. G.R. Cayley and D.N. Hague, Trans. Faraday Soc., 1971, 67, 2896.
59. K. Krishnan and R.A. Plane, Inorg. Chem., 1966, 5, 1150.
60. J. Takemoto and K. Nakamoto, J. Chem. Soc. (D), 1970, 17, 1017.
61. R.J.H. Clark, Spectrochim. Acta, 1965, 21, 955.
62. G.A. Barclay and A.K. Barnard, J. Chem. Soc., 1958, 2540.
63. M. Ciampolini and N. Nardi, Inorg. Chem., 1966, 5, 1150.
64. D.A. MacInnes, The Principles of Electrochemistry (Dover Publications, New York, 1961), p.381.
65. E.D. Eastman, J. Amer. Chem. Soc., 1920, 42, 1648.
66. J.A. Hull, R.H. Davies and L.A.K. Staveley, J. Chem. Soc., 1964, 5422.
67. G. Degischer and G.H. Nancollas, J. Chem. Soc. (A), 1970, 1125.
68. P.C. Jain, E.C. Lingafelter and P. Paoletti, J. Amer. Chem. Soc., 1968, 90, 519.
69. G.D. Andreeti, P.C. Jain and E.C. Lingafelter, J. Amer. Chem. Soc., 1969, 91, 4112.
70. M.M. DiVaira and P.L. Orioli, Acta. Cryst., 1968, B24, 1269.
71. L.V. Interrante, Inorg. Chem., 1968, 7, 943.
72. P. Paoletti, M. Ciampolini and L. Sacconi, J. Chem. Soc., 1963, 3589.

73. S.E. Rasmussen, Acta. Chem. Scand., 1959, 13, 2009.
74. C.K. Jørgenson, Acta. Chem. Scand., 1956, 10, 887.
75. M. Ciampolini and P. Paoletti, Inorg. Chem., 1967, 6, 1261.
76. D.P. Rablen, H.W. Dodgen and J.P. Hunt, J. Amer. Chem. Soc., 1972, 94, 1772.
77. P.L. Peczok and J. Bjerrum, Acta. Chem. Scand., 1957, 11, 1419.
78. M. Ciampolini, P. Paoletti and L. Sacconi, J. Chem. Soc., 1961, 2994.
79. L. Sacconi, P. Paoletti and M. Ciampolini, J. Chem. Soc., 1961, 5115.
80. C.K. Jørgenson, Acta. Chem. Scand., 1957, 11, 399.
81. R.A. Horne, J. Phys. Chem., 1957, 61, 1651.
82. R.A. Horne, R.H. Holm and M.D. Meyers, J. Phys. Chem., 1957, 61, 1655, 1661.
83. D.C. Weatherburn, E.J. Billo, J.P. Jones and D.W. Margerum, Inorg. Chem., 1970, 9, 1557.
84. Y. Tomita and K. Ueno, Bull. Chem. Soc. Jap., 1963, 36, 1069.
85. M.A. Cobb and D.N. Hague, J.C.S. Faraday I, 1972, 68, 1.
86. D. Hopgood and R.J. Angelici, J. Amer. Chem. Soc., 1968, 90, 2508.
87. M.A. Cobb and D.N. Hague, Trans. Faraday Soc., 1971, 67, 3069.
88. F.G. Mann and W.J. Pope, Proc. Roy. Soc., 1925, A109, 444;
J. Chem. Soc., 1926, 482.
89. G. Anderegg, Helv. Chim. Acta, 1964, 47, 1801.
90. G. Degischer and G.H. Nancollas, Inorg. Chem., 1970, 9, 1259.
91. N.C. Li and R.A. Manning, J. Amer. Chem. Soc., 1955, 77, 5225.
92. G. Anderegg, Helv. Chim. Acta, 1965, 48, 1712.
93. M.A. Cobb, Ph.D. Thesis, University of Kent, 1972.
94. J.R. van Wazer, Phosphorus and its compounds, Vol. I, (Interscience, New York, 1966), p.658.
95. G.R. Cayley and D.N. Hague, Trans. Faraday Soc., 1971, 67, 786.
96. I.M. Klotz and W.C. Loh Ming, J. Amer. Chem. Soc., 1953, 75, 4159; 1954, 76, 805.
97. R.G. Wilkins, Inorg. Chem., 1964, 3, 520.
98. G.S.D. Weir, Private communication, 1972.
99. R.H. Holyer, C.D. Hubbard, S.F.A. Kettle and R.G. Wilkins, Inorg. Chem., 1965, 4, 929; 1966, 5, 622.

100. F. Fittipaldi and S. Petrucci, J. Phys. Chem., 1967, 71, 3414.
101. G.G. Hammes and J.I. Steinfeld, J. Amer. Chem. Soc., 1962, 84, 4639.
102. T.J. Swift, Inorg. Chem., 1964, 3, 526.
103. P.V. Khadikar, R.L. Ameria and W.V. Bhagwat, Science and Culture, 1970, 36, 482.
104. Z.L. Ernst and J. Menashi, Trans. Faraday Soc., 1963, 59, 230.
105. L.G. Bray, J.F.J. Dippy, S.R.C. Hughes and L.W. Laxton, J. Chem. Soc., 1957, 2405.
106. A. Ågren, Svensk. Kem. Tidskr., 1956, 68, 181, 185, 189.
107. S.J. Ashcroft and C.T. Mortimer, Thermochemistry of Transition Metal Complexes, (Academic Press, London, 1970).
108. M.S. Zetter, Ph.D. Thesis, University of Kent, 1970.
109. H. Sternlicht, D.E. Jones and K. Kustin, J. Amer. Chem. Soc., 1968, 90, 7110.
110. D.N. Hague and M. Eigen, Trans. Faraday Soc., 1966, 62, 1236.
111. D.N. Hague, S.R. Martin and M.S. Zetter, J.C.S. Faraday I, 1972, 68, 37.
112. R.A. Alberty, G. Yagil, W.F. Diven and M. Takahashi, Acta. Chem. Scand., 1963, 17, S34.
113. D.E. Fenton, J. Chem. Soc. (A), 1971, 3481.
114. H. Irving and J.J.R.F. Da Silva, J. Chem. Soc., 1963, 458.
115. Y. Tomita, T. Ando and K. Ueno, J. Phys. Chem., 1965, 69, 404.
116. M. Cohn and T.R. Hughes, J. Biol. Chem., 1962, 237, 176.
117. M.E. Heyde and L. Rimai, Biochem. Biophys. Res. Comm., 1970, 41, 313.
118. H. Sternlicht, R.G. Shulman and E.W. Anderson, J. Chem. Phys., 1965, 43, 3123, 3133.
119. P.W. Schneider, H. Brintzinger and H. Erlenmeyer, Helv. Chim. Acta, 1964, 47, 992.
120. J. Neely and R. Connick, J. Amer. Chem. Soc., 1970, 92, 3476.
121. G.R. Cayley and D.N. Hague, J.C.S. Faraday I, in press.
122. D.W. Margerum, in Mechanisms of Inorganic Reactions, R.F. Gould, ed., Adv. Chem. Series No. 49 (Amer. Chem. Soc., Washington D.C., 1965), p.75.
123. M. Yasuda, K. Yamasaki and H. Ohtaki, Bull. Chem. Soc. Jap., 1960, 33, 1067.
124. M. Bobtelsky, Bull. Soc. Chim. France, 1955, 328.

125. J.L. Hall, J.A. Swisher, D.G. Brannon and T.M. Liden, Inorg. Chem., 1962, 1, 409.
126. D.E. Allen, D.J. Baker and R.D. Gillard, Nature, 1967, 214, 906.
127. K.S. Bai and A.E. Martell, J. Inorg. Nucl. Chem., 1969, 31, 1697.
128. F.G. Zharovskii, Trudy Komissii Analit Khim Akad Nauk SSSR, 1951, 3, 101.
129. W.E. Hatfield and J.T. Yoke, Inorg. Chem., 1962, 1, 463.
130. J.W. Collat, Analyt. Chem., 1958, 30, 1726.
131. P. Paoletti and M. Ciampolini, La Ricerca Scientifica, 1963, 3, 399.
132. A. Vacca, D. Arenare and P. Paoletti, Inorg. Chem., 1966, 5, 1384.
133. S.R. Martin, Private communication, 1972.
134. K. Kinley and S. Peats, Private communication, 1972.
135. S.L. Bradbury, J. Biol. Chem., 1969, 244, 2002.
136. R.C. Courtney, R.L. Gustafson and A.E. Martell, J. Amer. Chem. Soc., 1958, 80, 2121.
137. G.R. Lenz and A.E. Martell, Inorg. Chem., 1965, 4, 378.
138. H. Brintzinger, Helv. Chim. Acta, 1961, 44, 935, 1199.
139. M.M. Taqui Khan and A.E. Martell, J. Amer. Chem. Soc., 1967, 89, 5585.
140. G. Schwarzenbach, A. Anderegg, W. Schneider and H. Senn, Helv. Chim. Acta, 1955, 38, 1147.
141. G. Schwarzenbach and R. Bauer, Helv. Chim. Acta, 1956, 39, 722.
142. A. Agren and G. Schwarzenbach, Helv. Chim. Acta, 1955, 38, 1920.
143. R.J. Kula, Analyt. Chem., 1965, 37, 989.
144. L. Pauling, J. Chem. Soc., 1948, 1461.
145. D.W. Margerum and H.M. Rosen, J. Amer. Chem. Soc., 1967, 89, 1088.
146. J.P. Jones, E.J. Billo and D.W. Margerum, J. Amer. Chem. Soc., 1970, 92, 1875.
147. R.K. Steinhaus and D.W. Margerum, J. Amer. Chem. Soc., 1966, 87, 441.

